X-RAY CRYSTAL STRUCTURES, THERMAL ANALYSIS AND COMPUTATIONS OF CONFORMATIONAL POLYMORPHS

A Thesis
Submitted for the Degree of
Doctor of Philosophy

By

SAIKAT ROY

School of Chemistry
University of Hyderabad
Hyderabad 500 046
India

July 2007

I dedicate this thesis

To

My Parents

STATEMENT

I hereby declare that the matter embodied in this thesis entitled **"X-ray Crystal Structures, Thermal Analysis and Computations of Conformational Polymorphs"** is the result of investigations carried out by me in the School of Chemistry, University of Hyderabad under the supervision of Prof. Ashwini Nangia.

In keeping with the general practice of reporting scientific observations due acknowledgements have been made wherever the work described is based on the findings of other investigators.

Hyderabad   Saikat Roy

July 2007

CERTIFICATE

Certified that the work **"X-ray Crystal Structures, Thermal Analysis and Computations of Conformational Polymorphs"** has been carried out by **Saikat Roy** under my supervision and that the same has not been submitted elsewhere for a degree.

Dean   Prof. Ashwini Nangia

School of Chemistry   Thesis Supervisor

ACKNOWLEDGEMENT

SYNOPSIS

This thesis entitled "**X-RAY CRYSTAL STRUCTURES, THERMAL ANALYSIS AND COMPUTATIONS OF CONFORMATIONAL POLYMORPHS**" consists of seven chapters.

CHAPTER ONE

INTRODUCTION

Polymorphism is defined as the ability of a compound to exist in more than one crystalline modifications. The presence of different conformers of the same molecule in different crystal structures is termed as conformational polymorphism, whereas conformational isomorphism is the occurrence of more than one conformer of the same molecule in the same crystal structure. There is renewed interest in understanding why more than one molecule or conformation (i.e. $Z' > 1$) occur in the crystal lattice. Conformational polymorphs often crystallize as concomitant polymorphs, in practice, because their energy differences are very small and there is dynamic equilibrium of conformers in solution. Selected examples of conformational polymorphs will be discussed in this chapter.

Polymorphism is very common in pharmaceutical solids, with estimates of 30-50% in drug-like molecules, compared to 4-5% polymorphic compounds in organic crystals[5] in the Cambridge Structural Database. Polymorphs have different crystal structures, molecular arrangement and/or hydrogen bonding and hence, each polymoph is a unique material with its own physical and chemical properties. It is therefore important to know the correct crystalline modification in active pharmaceutical ingredients (APIs) to enable formulation of drug substances. Among the various analytical methods used for the characterization of polymorphs, thermal analysis (*i.e.* differential scanning calorimetry, thermogravimetry, hot stage microscopy) and *in-situ* variable temperature powder X-ray diffraction have received considerable attention. Thermal relation among kinetic/thermodynamic polymorphs, such as enantiotropic or monotropic, and their stability must be understood.

The issue of conformation energy (intramolecular) and lattice energy (intermolecular) compensation in conformational polymorphs is examined in this thesis. Energy differences between conformational polymorphs (kinetic and thermodynamic)

are very small (0.5-3 kcal mol^{-1}) because intra- and intermolecular energies may cancel each other. A metastable conformation may be stabilized by stronger hydrogen bonds in the crystal structure to make up for the intramolecular energy penalty. Alternatively, a stable conformer may not able to form very strong hydrogen bonds, leading to a balance of energy in these inter-related events during self assembly and crystallization.

Ab initio crystal structure prediction (CSP) is one of the main challenges in crystal engineering. The task becomes even more difficult for conformationally flexible molecules. Since various conformers exist in dynamic equilibrium with in a few kcal per molecule energy difference, the question is which conformer will be present in the crystal structure. Conformers residing in local minima or the global minimum starting model give very different prediction results. We observed that if conformational energy (E_{conf}) is accounted with lattice energy (U_{latt}) to re-rank predicted crystal structure frames, the predicted lowest energy structure matches with experimental structure. Understanding the evolution from molecule → conformation → crystal is analyzed in some conformational polymorphic systems.

CHAPTER TWO

CONFORMATION AND LATTICE ENERGY COMPENSATION IN KINETIC AND THERMODYNAMIC POLYMORPHS OF 4,4-DIPHENYL-2,5-CYCLOHEXADIENONE

4,4-Diphenyl-2,5-cyclohexadienone **1** (Figure 1a) crystallized as four conformational polymorphs and a record number of 19 crystallographic independent molecules characterized by low-temperature X-ray diffraction: form A ($P2_1$, $Z' = 1$), form B ($P\overline{1}$, $Z' = 4$), form C ($P\overline{1}$, $Z' = 12$), and form D (*Pbca*, $Z' = 2$). Tetramorphic crystal structure of **1** are stabilized by different C−H···O hydrogen bonding motifs. High Z' structures have drawn a great interest from crystallographers in recent times, but the exact reasons for the crystallization of more than one molecule in the asymmetric unit are still not properly understood. We noted that the strength of C−H···O interaction in a particular form of **1** correlates with Z', i.e. high Z' structures have shorter C−H···O interactions. Whereas strong O−H···O hydrogen bonds have been ascribed to multiple Z'

in monoalcohols, phenols and cholesterol, we show that even weak C–H···O hydrogen bonds follow similar trend.
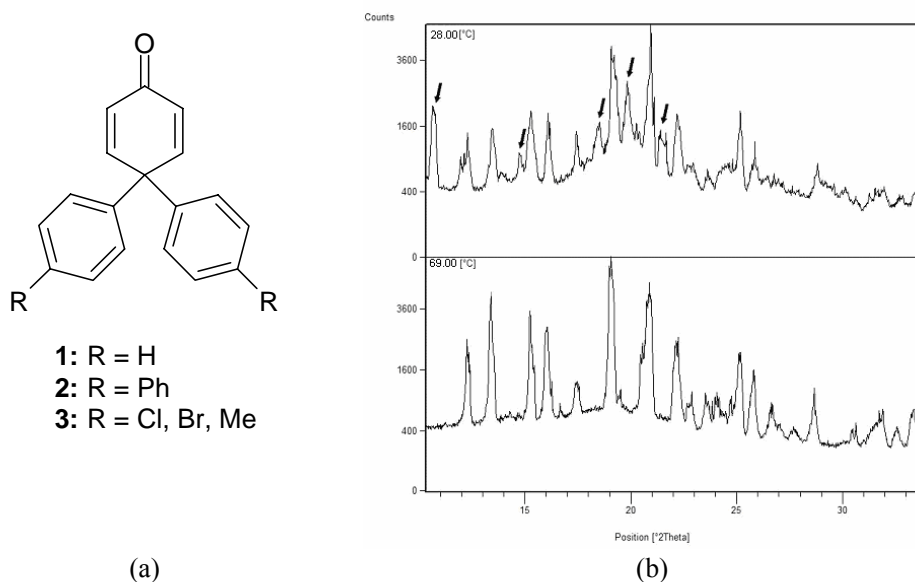
Figure 1. (a) Molecular structure 4,4-Diphenyl-2,5-cyclohexadienone **1** and derivative discussed in this chapter. (b) Powder XRD of **1** at 28 °C (top) and 69 °C (bottom). The peaks that disappear upon heating are marked with an arrow. Peak profile at 69 °C nicely matches with form A.

Crystallization of compound **1** from EtOAc/*n*-hexane afforded a concomitant mixture of forms A-D. Kinetic and thermodynamic forms were identified by variable temperature powder X-ray diffraction (VT-PXRD) and lattice energy computation. When PXRD was recorded on a normal crystallization batch of compound **1**, it showed form A is ~40%, forms B+C are ~50%, and form D is ~10% at room temperature. The concomitant mixture transformed to form A upon heating to ~70 °C (Figure 1b). Least squares refinement of the observed PXRD at 69 °C with the simulated PXRD of crystal structure matches perfectly. Melt crystallization of the mixture at 115 °C afforded form B. Molecular conformer energy (E_{conf}) and lattice energy (U_{latt}) were calculated for forms A, B and D. Compensation of E_{conf} and U_{latt} gave E_{total} of stable form A = 1.22 kcal mol^{-1},

metastable form B = 1.49 kcal mol^{-1}, and form D = 1.98 kcal mol^{-1} respectively. VT-PXRD and computation suggest that form A is the thermodynamic stable form, form B is the kinetic form, and form D is metastable.

Reproduction of stable form A was carried out in *Cerius*^{2} using COMPASS force field. The 3rd rank lowest energy predicted frame in flexible body lattice energy minimization is ranked as the lowest energy frame in rigid body minimization method using the experimental conformer and taking E_{conf} into account. By considering U_{latt} and E_{conf} contributions, the predicted structure of form A matches with global minimum frame #1. Re-ranking of predicted frames using this iterative method is new in the CSP literature.

CHAPTER 3

VARIABLE TEMPERATURE POWDER X-RAY DIFFRACTION AND CRYSTAL STRUCTURE REPRODUCTION OF 2,6-DIMETHYL-4-(α,α-DIPHENYLMETHYLENE)-1,4-BENZOQUINONE

A conformational polymorphic system, 2,6-dimethyl-4-(α,α-diphenylmethylene)-1,4-benzoquinone **4** was reported in 1980 by Paul and Curtin.[11] Three crystalline modifications α, β and γ forms in space group $P2_1/c$, $P2_12_12_1$ and $Pna2_1$ having one molecule each in the asymmetric unit are known.

4
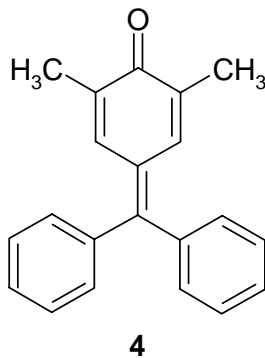
Lattice energy and conformational energy computation of these three crystal structure showed that α form is the most stable among them. The β form is less stable by

~1 kcal mol^{-1} and γ form by ~9 kcal mol^{-1} relative to the α form. Room temperature crystallization afforded concomitant polymorphs mixture of dominant α (80%), minor β (18%) and trace amount of γ form (2%). Variable temperature powder diffraction confirmed that the concomitant mixture transforms to β form at ~170 ºC. Phase transformation of α and γ to β at high temperature in this enantiotropic cluster and the presence of β phase until melting means that it is the stable polymorph at high temperature.

Ab initio prediction with the Gaussian optimized conformer in *Cerius*^{2}, using COMPASS force field resulted in all the three forms predicted correctly in the lowest energy frame of their respective space group ($P2_1/c$, $P2_12_12_1$, $Pna2_1$) on flexible body lattice energy minimization. In terms of U_{latt}, β form is predicted in 3rd frame, γ form in 6th frame and α form in 7th frame compared to global energy minimum. By applying the iterative method of chapter 2, taking E_{conf} and re-ranking of frames based on E_{total} gave experimental crystal structure γ, β and α forms as 1st, 2nd and 3rd lowest energy structure.

CHAPTER 4

STABLE POLYMORPH OF VENLAFAXINE HYDROCHLORIDE BY SOLID TO SOLID PHASE TRANSITION AT HIGH TEMPERATURE

The anti-depressant drug Venlafaxine {(±)-1-[2(dimethylamino)-1-(4-methoxyphenyl)-ethyl]-cyclohexane-1-ol} hydrochloride **5** (VenHCl) is a serotonin−norepinephrine reuptake inhibitor having sales of US $ 3.8 billion per annum (Effexor®, Wyeth). Single crystal structures of two polymorphs (forms 1 and 2), melt form (form 3), hydrate (form 4) are known in the literature. Thermal relationships of these forms were established by DSC, HSM and a novel amorphous semi-solid form was characterized by sublimation (form 5) in our laboratory. Continuing studies on phase transitions of VenHCl, solid crystalline material (form 2) was heated on the hot stage

microscope. The fine needle morphology transformed to thin plates at ~180 ºC (Figure 2b and 2c). These plate-like crystals were characterized by single crystal X-ray diffraction, DSC, FT-IR and shown to be a new polymorph of VenHCl, termed as form 6. The unit cell parameters of form 6 ($P2_1/n$, $Z' = 2$) are significantly different from those of forms 1 and 2 ($Pca2_1$, $Z' = 1$; $P2_1/n$, $Z' = 1$). All three crystal structure have the common V-shaped acceptor-bifurcated O–H···Cl⁻ and N⁺–H···Cl⁻ hydrogen bond synthon. The presences of two molecules in the asymmetric unit of form 6 provides efficient packing compared to form 1 and form 2 and also explain the 10 ºC higher melting point.
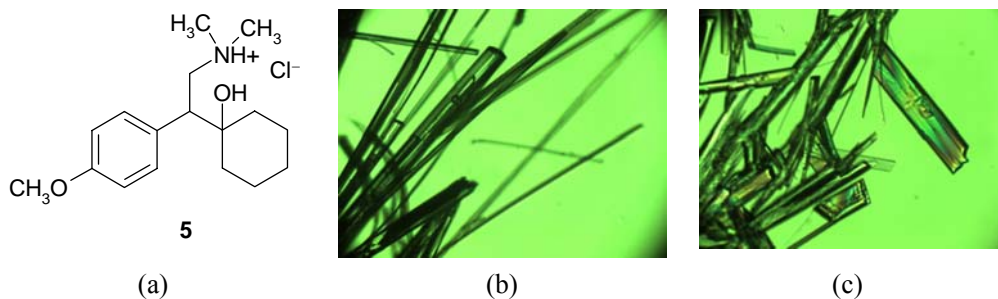
Figure 2. (a) Venlafaxine hydrochloride structure. (b) Needle shape crystals of form 2 at room temperature (c) Conversion to the new form at ~185 ºC.

The transformation of form 1 and 2 to form 6 was examined by variable-temperature powder X-ray diffraction (VT-PXRD). The powder peak profile at ~180 ºC matches with the simulated peaks of crystal structure of form 6. Highest melting novel form 6 is the most stable polymorph of VenHCl.

CHAPTER 5

KINETIC AND THERMODYNAMIC CONFORMATIONAL POLYMORPHS OF BIS(*P*-TOLYL)KETONE *P*-TOSYLHYDRAZONE

Two conformational polymorphs of acetone tosyl hydrazone are reported. Phenylogue-extended series of polymorphs were recently reported from our group. We studied bis(*p*-tolyl)ketone *p*-tosylhydrazone **6** to discover new phenylogue series in

polymorph clusters. This molecular engineering approach gave three conformational polymorphs of compound **6**. Form 1 has strong N–H···O=S dimer synthon but forms 2 and 3 have no hydrogen bonds up to 3.0 Å, even though the molecule contains SO$_2$NH group. Energy calculations of these three forms suggest that close-packed structure form 3 is the thermodynamic polymorph and more stable than hydrogen-bonded form 1, whereas form 2 is metastable. The melting point of form 3 is 17 ºC higher than form 1 in DSC. Polymorph 1 and 3 are assigned as kinetic and thermodynamic forms.

6: R = Me
7: R = H
8: R = F
9: R = Cl
10: R = Br
11: R = I

(a)   (b)
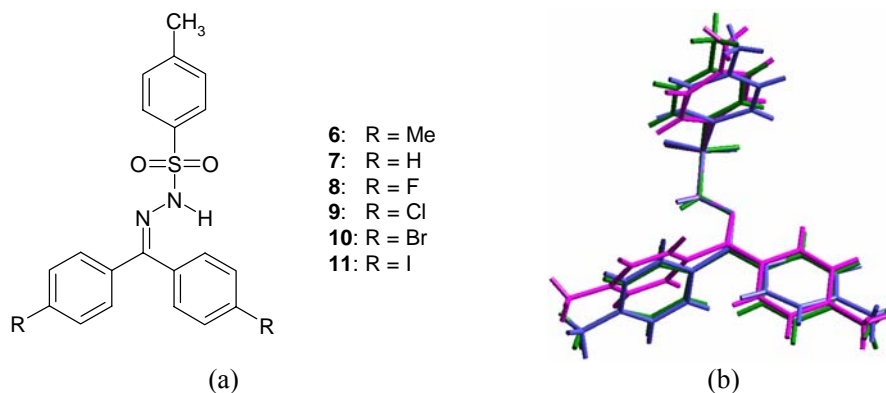
Figure 3. (a) Molecular structure studied in this chapter. (b) Overlay of molecular conformation of **6**. Magenta = form 1, green = form 2, blue = form 3.

Compound **6** is a rare example where strong hydrogen bond synthon leads to the kinetic form and close packing gave the thermodynamic modification. CSD survey shows only two genuine examples of dimorphs showing a similar phenomenon, but thermodynamic and kinetic state was not assigned in these cases. Curtin–Hammett reaction kinetics states that if reaction intermediates (or conformer) of kinetic and thermodynamic products are in equilibrium, the product ratio depends on the free energy of the respective transition states. Curtin–Hammett energy profile for the crystallization of conformational polymorphs 1 and 3 is proposed. Reproduction of crystal structure for compound **6** starting from the observed conformer present in the three crystal forms were predicted with good r.m.s.d in lowest energy frame for all three polymorphs. The starting conformer is important in generating the final crystal structure and small changes in

conformation can change the crystal packing from hydrogen bonded structure to the close packed form.

Other derivative **7-11** have the expected N–H···O=S dimer synthon and we have not found polymorphs in course of our studies despite considerable effort. Pseudopolymorph[17] of compound **6** (CH_2Cl_2 solvate), chloro (**9**) and bromo (**10**) derivatives (benzene solvate) are also discussed in this chapter.

CHAPTER 6

CONCLUSIONS AND FUTURE PROSPECTS

Polymorphs are ideal systems to study molecular structure–crystal structure–crystal energy relationships with a minimum number of variables, because differences arise due to molecular conformations, hydrogen bonding and crystal packing effects and not due to a different chemical species. It is very important to identify the kinetic and thermodynamic form in a polymorphic system. For compounds **1**, **4** and **6** we were able to calculate the energy difference and isolate kinetic and thermodynamic forms. Re-ranking of frames in crystal structure reproduction by taking only non-bonded contribution of lattice energy (U_{latt}) summing up with conformational energy (E_{conf}) gave the correct prediction for molecule **1** and **4**.

Transformation of polymorphs is very important in drug substances where metastable soluble form can transform to the stable modification during manufacture, formulation and/or storage e.g. ritonavir. We were able to correlate the thermochemical relation among polymorphs of a leading anti-depressant drug venlafaxine hydrochloride and phase transformation to a new polymorph was identified through thermal analysis. It would not have been possible to characterize new polymorphs unambiguously and assign the kinetic/thermodynamic phase without the use of thermal methods, e.g. DSC, TGA, hot stage microscopy. *In-situ* variable temperature powder X-ray diffraction gave valuable structural and physical information about polymorphic phases.

Nucleation and crystallization from solution to solid-state is a very complex phenomenon and still not properly understood.[19] So far no theory or experiment is developed to completely delineate the sequence of events during crystallization. For

flexible molecules different conformations equilibrate in solution, which can produce kinetic and thermodynamic conformational forms. The self assembly of conformational polymorphs is proposed *via* Curtin–Hammett principle of reaction kinetics. For tosyl hydrazone (**6**) strong hydrogen bonding leads to the kinetic form, and the less stable conformation gave thermodynamically stable close-packed crystal structure.

Salient crystallographic details of the crystal structures discussed in this thesis have been given in an appendix at the end of the thesis. A full list of atomic coordinates has been deposited with the University of Hyderabad and is available upon request from Prof. Ashwini Nangia (ashwini_nangia@rediffmail.com).

xx

CONTENTS

CHAPTER 1

INTRODUCTION

1.1 Polymorphism: Background, Definition and Importance

Structural diversity exists in every aspect of Nature. Structural chemistry is no exception. Crystal polymorphism is one manifestation of diversity. The word '*Polymorphism*' originally comes from the Greek literature (*poly* = many, *morph* = form). Mitscherlich (1822) first documented polymorphism in the context of crystallography.[1] He noticed that arsenates and phosphates can exist as different crystal forms. Ostwald's work[2] on the relative stability of different crystal structures of the same compound was a major development in polymorphism. Buerger and McCrone's work[3] concerning the change in properties like melting point, solubility of different crystal forms of the same chemical compound gave the subject of polymorphism a major uplift. Historical developments in polymorphism chronologically listed in Table 1.[4]

Berzelius first described the existence of different crystal structures for the same element as allotrope.[5] Allotropes and polymorphs are closely related. Polymorphism is used in general to refer to structural diversity of molecular compounds whereas allotropy is the structural diversity of elements.[6] McCrone defined polymorph as "*a solid crystalline phase of a given compound resulting from the possibility of at least two crystalline arrangements of the molecules of that compound in the solid state*".[7] Burger tried to simplify it as "*if these (solids composed of only one component) can exist in different crystal lattices, then we speak of polymorphism*".[8] In modern chemistry, a crystal is described as a 'supermolecule par excellence' by Dunitz.[9] In his view polymorphic modifications are 'superisomers' and polymorphism is a kind of 'superisomerism'.

Table 1 Important milestones in polymorphism research over the last 200 years.[4]

Year	Name	Event
1822	Mitscherlich	Identified different crystal structure of arsenate and phosphate.
1844	Amici	Discovered polarizing microscope for visual characterization of solids.
1876	Millard	Geometrical and structural basis in growing different form of same substance.
1891	Lahman	Phase transformation in crystal form.
1897	Ostwald	Famous 'Rule of Steps' on relative stability of polymorph.
1906-19	Groth	Summarization of organic crystal polymorphism in five volume collection.
1926	Tammann	Thermodynamic stability and relationship between different polymorphic modifications.
1937	Bloom and Buerger	Pointed out about the fundamental property change and its importance in polymorphs.
1956-69	McCrone	Worked on pharmaceutical importance on drug polymophism.
1973	Corradini	Coined the term conformational polymorphism; polymorphism arises due to torsional degree of freedom of molecular conformers.
1996	– – – –	Glaxo vs. Novopharm litigation on form I and form II of ranitidine hydrochloride.
1998	– – – –	Unexpected formation of stable and less soluble polymorph of Ritonavir (Norvir) at Abbott laboratory
2000-present	– – – –	1. Book 'Polymorphism in molecular crystals' by Bernstein. 2. Two theme issues of *Crystal Growth & Design*. 3. Several special issues of journals, monographs and reviews on polymorphism and its industrial significance.

Polymorphism in organic solids is of fundamental importance because of its ability to alter physical and chemical properties in different crystal structures, such as melting point, density, compressibility, solubility, hardness, dipole moment and bioavailability.[10] Polymorphism has received particular attention in the recent literature because of its importance in drug substances and pharmaceutical formulation.[10,11] Molecular recognition, crystal nucleation, crystallization, and phase relationship between solids can be inferred through studies on polymorphism.[12] Polymorphs present special opportunities to analyze structure–property relationships[13] because the conformation, hydrogen bonding and lattice energy of the same molecule in different crystalline environments may be compared in polymorphic structures. One of the challenges in crystal engineering is our ability to understand and control polymorphism.

Polymorphism can be both beneficial and problematic. It is often serendipitous and there exists no general methodology for producing new forms of a given compound. Understanding the origin of polymorphism and controlling the outcome of crystallization process to avoid undesired forms is a current goal in crystal engineering. Patent litigation associated with Ranitidine hydrochloride[14] and formation of less soluble stable polymorph of Ritonavir[4j,14b] during manufacturing highlighted the significance of polymorph selection and screening before marketing stage. Getting the right polymorph is not only important for drugs and pharmaceuticals but also for speciality chemicals like explosives, dyes, pigments, flavors and confectionery products.[15] For example, oxotitanium phthalocyanine exists in four polymorphic forms. Among the four forms, one form is used as photosensitive charge generation material while other forms are inactive.[16] Current approaches of the discovery and selection of polymorphic forms include methods, such as varying solvent of crystallization, temperature, and extent of supersaturation. soluble additives,[17] epitaxial growth,[18] laser induced nucleation,[19] crystallization in capillaries,[20] confinement within porous materials,[21] functionalized polymer heteronuclei,[22] cross nucleation, *in-situ* flash cooling.[23] A wide range of crystallization conditions are applied in combinatorial approach to generate new polymorphs in high-throughput crystallization screens.[24] This approach enables emerging strategies to speed-up pharmaceutical development and capture solid form diversity of pharmaceutical substances.[25]
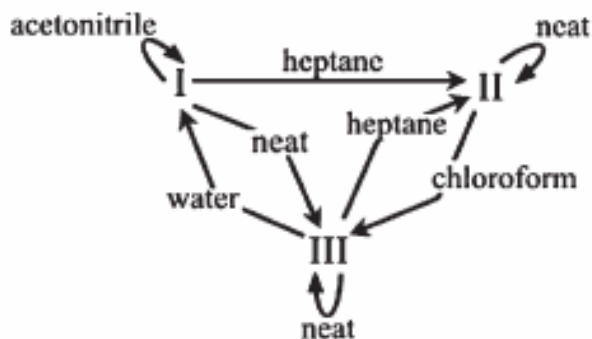
Scheme 1. Observed polymorph transformations among three anthranilic acid crystal forms *via* solvent-drop grinding.[28]

Co-crystallization extended the crystal engineering prototype for discovering new polymorphs in active pharmaceutical ingredients (APIs)[26] and exploitation of supramolecular robust synthons.[27] Mechanochemistry methods such as solid-state grinding and solvent drop grinding is a useful tool to obtain new forms of a polymorphic compound. Jones *et al* demonstrated selective conversion of particular polymorphs of anthranilic acid (Scheme 1) and succinic acid through solid state solvent drop grinding.[28] The increasing awareness among chemists of the phenomenon polymorphism and its frequent occurrences in the last decade has made this subject a mature topic in modern solid-state research.[4k]

1.2 Polymorphic Compounds in the Cambridge Structural Database

McCrone's statement[7] four decade ago "*the number of forms known for a given compound is proportional to the time and money spent in research on that compound*" is strongly validated in last few years. Many papers[29] and reviews[30a,b] are being reported on polymorphs, and two theme issues of *Crystal Growth & Design*[4l,m] devoted to polymorphism highlight its wide scope and the challenges in understanding this important phenomenon. Different groups carried out database analyses to estimate the percentage of compounds that are polymorphic reported in Cambridge Structural Database (CSD).[31] It was found that about 4-5% of organic compounds,[31b,c] 5.5% organometallics, and 2.1% of coordination compounds

are shown to exhibit polymorphism.[31d] There is a considerable growth in the reported structures and papers on polymorphism. To show the increase in polymorph literature a search was carried out to find three or more polymorphs reported in the CSD (Conquest 1.9, MAY 2007, 426722 entries). Table 2 illustrates the database search results obtained in the previous (Gavezotti and Filippini[32], Yu et. al.[29c,33] and V. S. S. Kumar[34]) and present studies. During last decade number of trimorphs has increased 10 fold indications use of sophisticated instrument and growing scientific interest in polymorphism. Polymorphism is more widespread in pharmaceutical solids, with estimates of 30-50% in drug-like molecules[11,15c] compared to CSD percentage of 4-5% in organic compounds. However drug molecules are often not archived in the CSD for proprietary reasons.

Table 2. Database search results on polymorphic occurrence.

	No. of clusters identified by Gavezotti and Filipini[32] 1995	No. of clusters identified by Yu et. al.,[33] 2000	No. of clusters identified Kumar[34] 2002	No. of clusters identified by Yu et. al. in,[29c] 2005	No. of clusters identified in the present study 2007
three forms	13	27	42	102	124
four forms	3	3	3	14	20
five forms	none	none	one	one	3
six forms	none	none	one	one	none
seven forms	none	none	none	none	one

The search criteria was similar to that reported by L. Yu *et al*,[29c] on all organic compounds with "form", "polymorph", "modification" or "phase" in the qualifier, excluding the entries for which 3D coordinates are unavailable. Refcodes of trimorph, tetramorph, pentamorph and heptamorph found in the search are tabulated in Appendix I.

Polymorphs are classified, such as concomitant polymorphs, configurational polymorphs, conformational isomorphs, conformational polymorphs or tautomeric polymorphs based on their structural similarity, visual inspection and occurrence.[4k] Among

various types of polymorphs, conformational and concomitant are more common. Some examples are discussed in the next section. Apart from polymorphs, pseudopolymorphs[35] are as important as polymorphs in pharmaceutical industry, because of their influence on change of physical properties in solid state formulation. *Pseudopolymorphs* are defined as crystalline forms of a compound that differ in the nature or stoichiometry of included solvent molecules.[36]

1.3 Concomitant, Conformational Polymorphism and Conformational Isomorphism

Different types of polymorphs and crystals are schematically represented in Scheme 2. When polymorphs crystallize simultaneously in the same flask under identical crystal growth conditions from the same solvent, they are termed as *concomitant polymorphs*.[37] This phenomenon occurs when there are many metastable forms with almost similar energies that crystallize together. Concomitant polymorphism in benzamide is the first example of a polymorphic organic substance reported by Wöhler and Liebig in 1832.[38a] Davey and co-workers were able to determine crystal structure of the metastable form of benzamide by in situ synchrotron powder X-ray diffraction after almost 200 years.[38b,c] Some recent examples of concomitant polymorphs are shown in Scheme 3.[17,38,39]

The presence of multiple functional groups capable of forming various hydrogen bonding motifs increases the scope of polymorphism engaging *via* different kind of hydrogen bonding synthons[40] in the crystal structures. Polymorphs with different kind of hydrogen bonding pattern in different forms is termed as *synthon polymorphism*.[41] Recently Viseshwar and co-workers reported[42] polymorphism in a 2:1 co-crystal (multi component system) of 4-hydroxybenzoic acid and 2,3,5,6-tetramethylpyrazine due to formation of homo- and heterosynthons in form 1 and 2. Sometimes polymorphism may arise because of different packing arrangement of molecule with presence of same synthon or conformation. This represents the case of *packing polymorphism*.[43]
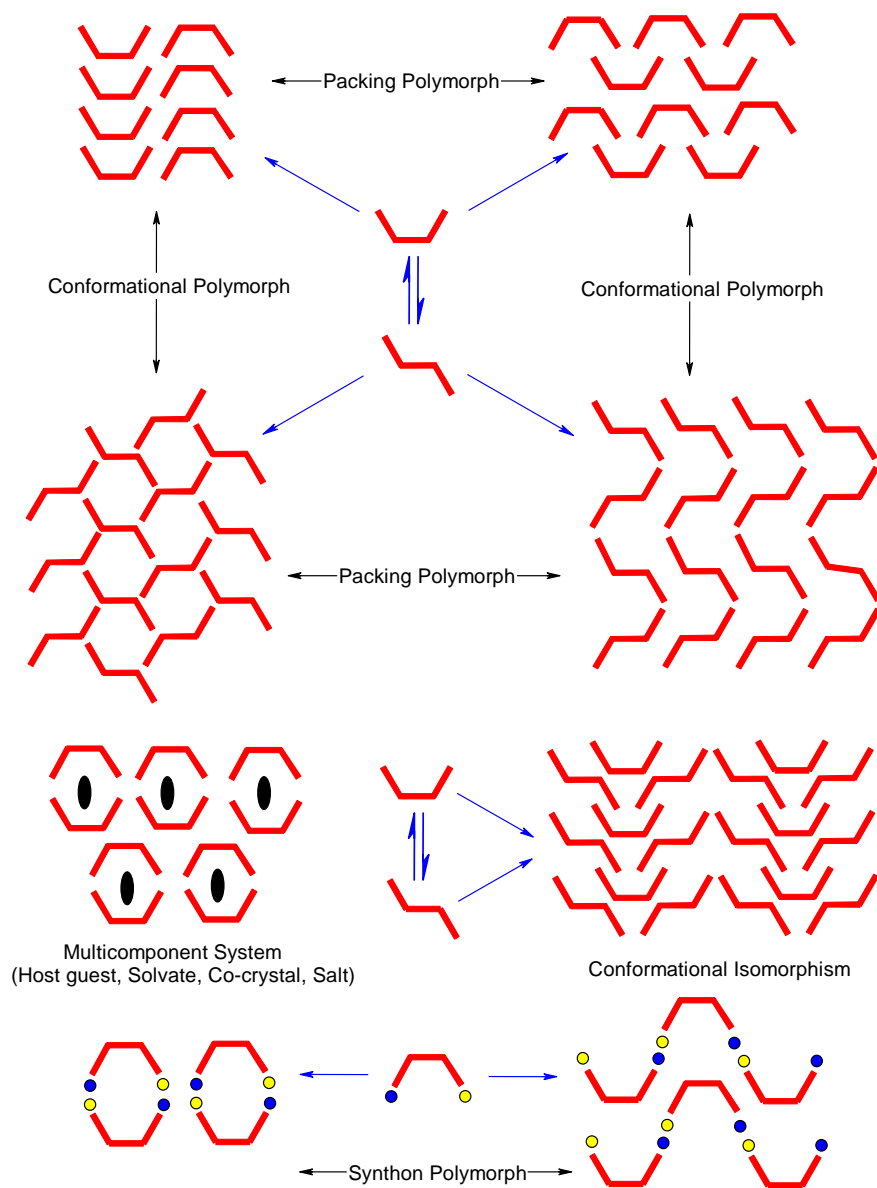
Scheme 2. Schematic illustration of different arrangement of conformers and packing of molecule in the crystal lattice leading to different kind of polymorphism.

(38)   **(39a)**   **(39b)**   **(39c)**

(39d)   **(39e)**   **(39f)**
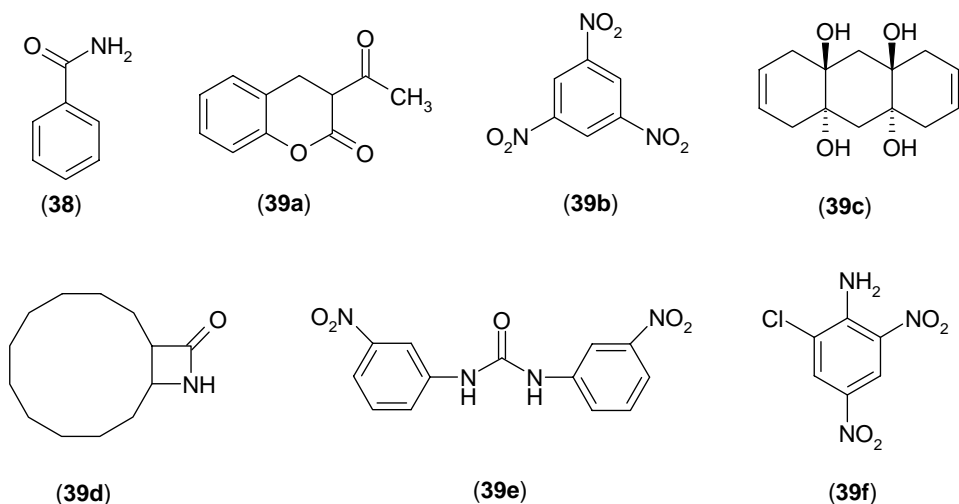
Scheme 3. Some recent examples for concomitant polymorphs. (Reference in parenthesis)

Conformational polymorphism is defined as the existence of different conformers of the same molecule in different polymorphic modifications.[29b,44] Conformationally flexible molecules have greater scopes for their polymorphic occurrence because of greater degree of freedom than rigid molecule. Energy differences between conformational polymorphs (kinetic and thermodynamic) are very small (0.5-3 kcal mol^{-1}) because intra- and intermolecular energies may cancel each other. A metastable conformation may be stabilized by stronger hydrogen bonds in the crystal structure to make up for the intramolecular energy penalty. Alternatively, a stable conformer may not be able to form very strong hydrogen bonds, leading to a balance of energy in these inter-related events during self assembly and crystallization. Hence, to measure the stability among the polymorph, conformation energy should be accounted along with lattice energy.

A study by Yu and co-workers showed that 5-Methyl-2-[(2-nitrophenyl)amino]-3-thiophenacarbonitrile (**ROY**),[29c] has a record number of seven polymorphs that result from the rotation of thiophene ring. **ROY** is the "most polymorphic" organic compound in the Cambridge Structural Database (CSD, January 2007) for which X-ray structures are determined. Recently Andrew and co-workers[45a] reported conformational polymorphism of N-(4'-methoxyphenyl)-3-bromothiobenzamide due to difference in planarity of the thioamide

group with respect to the Br-substituted phenyl group. Some recent examples of conformational polymorphs are shown in Scheme 4. [29c,45]

(29b)   **(29c)**   **(45a)**   **(45b)**

(45c)   **(45d)**   **(45e)**

(45f)   **(45g)**   **(45h)**
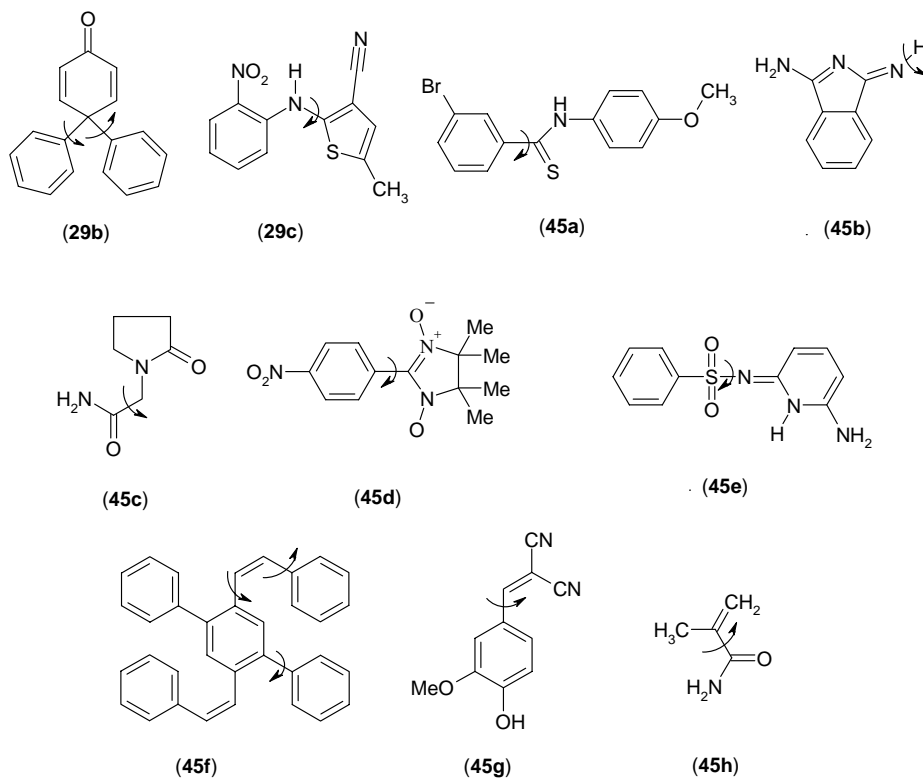
Scheme 4. Some examples of the recently reported molecules with conformational polymorphism. The arrows show the sites for conformational polymorphism. (Reference in parenthesis)

The existence of different conformers of the same molecule in the same crystal structure represents *conformational isomorphism*.[4k] This situation arises when there is more than one molecule in the asymmetric unit ($Z'>1$).

1.4 Multiple Molecules in the Asymmetric unit (Z')

The number of symmetry-independent or crystallographic unique molecules in a crystal lattice is *Z'*. Alternatively, *Z'* may be defined in relation to the number of molecules in the unit cell: $Z = Z' \times$ number of lattice points $\times$ number of symmetry operations.[46] There is renewed interest on why molecules crystallize with *Z'* > 1 from a fundamental viewpoint, because the factors leading to its occurrence are still not properly understood.[47] Structures that exhibit *Z'*>1 is against the rule of close packing. However it is often observed that molecule crystallizes with *Z'*>1 for polymorphic compounds. A study by Gavezzotti and Filippni showed that polymorph with one partner having *Z'*=1 and at least one partner with *Z'*> 1 is 28% compare to overall percentage in the CSD, which is 8.3%.[32]

Many groups have tried to correlate the occurrence of *Z'*>1 with close packing frustration and optimization of intermolecular interactions.[48] Presence of irregular molecular shape and strong hydrogen bonds associate in nucleosides and nucleotides, steroids, and alcohols is one of the reason of higher *Z'*.[48,49] Brock and Craven have noted that monoalcohols have a greater tendency to form high *Z'* structures: 40% of monoalcohols[48b] 33% of *vic*-diols[48e] and ~50% of cholesterol[48f] have *Z'*>1. Our recent study shows that sublimation and melt crystallization,[50] which are kinetic methods of crystallization, gave higher probability of occurrence with *Z'*>1 (18 %) in the crystal structure, compared to crystallization from solution.

Clegg and co-workers recently studied salt of 1,8-bis(dimethylamino)naphthalene systems and reported the importance of weak interaction like C–H⋯O and π–π stacking in the formation of *Z'*>1.[51] Steed *et al* showed that weak interaction C–H⋯X or C–H⋯π (where X=halogen) and π–π stacking can influence molecule in crystallization with more than one molecule in asymmetric unit for the triaryl derivative of group 14 elements and oxo-anion structures.[52] In present study we showed the weak C–H⋯O hydrogen bonds follow similar trend like O–H⋯O hydrogen bonds have been ascribed to multiple *Z'* in monoalcohols, phenols and cholesterol.

1.5 Thermodynamic and Kinetic Interplay in Crystallization

Crystallization process can be considered as two-step process *viz.* nucleation, or multiple selection processes on different length and timescales, and crystal growth, involving subsequent growth of nascent nuclei. Nucleation is the primary stage of crystallization. Crystal growth from those nuclei or crystallization starts after that. Various groups studied crystal growth aspect as it is in macroscopic scale.[54] Two recent papers by Davey *et al* and Desiraju *et al* on crystal formation pathway of tetrolic acid and Na(saccharinate).nH$_2$O systems advance our understanding of primary stage of crystallization *i.e.* nucleation.[55]
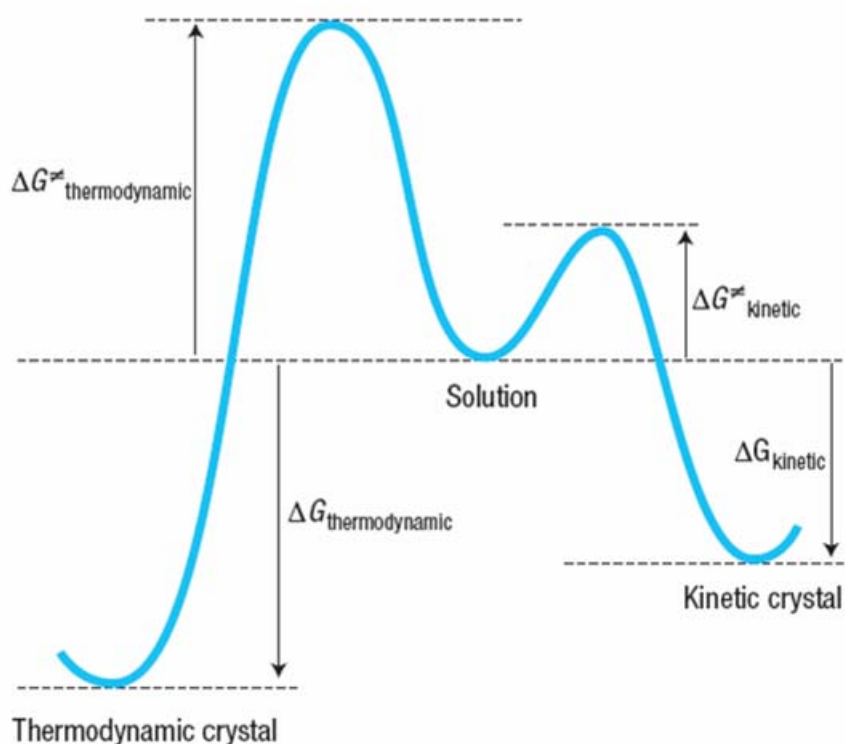
Scheme 5. Schematic diagram for a hypothetical transition from solution to thermodynamic and kinetic crystals. Note that if the thermodynamic crystal also has a low $\Delta G^{\neq}$, it is also the kinetic crystal and polymorphism would be unlikely.

Crystallization is like a supramolecular reaction, which is dictated by thermodynamics and kinetics, how stable and how fast. In contrast to all the supramolecular reactions, which take place in solution in a thermodynamically controlled manner,[56] crystallization is generally a kinetic phenomenon that follow.[57] The Curtin-Hammett principle states that if reaction intermediates (or conformer) of kinetic and thermodynamic products are in equilibrium, the product ratio depends on the free energy of the respective transition states. The free energy-reaction progress diagram (Scheme 5) illustrates the balance between kinetic and thermodynamic factors. This diagram shows that kinetically favored crystal would form faster, because the activation energy barrier ($\Delta G^{\neq}$) is lower. The thermodynamically driven crystal would take a longer time to form as its ($\Delta G^{\neq}$) is higher. However, it would be more stable because its final energy state is lowest. Nucleation can be considered as the transition state of the crystallization where long range interaction (H-bond) predominant over short range interaction (van der Waals). Different thermodynamic and kinetic forms can be observed if there is a clash between the short-range and long-range interactions and there will be a possibility of polymorphism. In this circumstance, the case of concomitant polymorphism will arise if $\Delta G^{\neq}_{kinetic} \approx \Delta G^{\neq}_{thermodynamic}$, whereas in general, $\Delta G^{\neq}_{thermodynamic} > \Delta G^{\neq}_{kinetic}$ will lead to different kinetic and thermodynamic form. However, conditions e.g. high temperature and highly polar solvents that will lower $\Delta G^{\neq}_{thermodynamic}$, may lead to change in energy order. If short-range and long-range interactions both favor same crystal structure then the thermodynamic and kinetic forms are same and polymorphism is less likely.

Kinetic and thermodynamic polymorphs generally have different conformer in crystal structures for conformationally flexible molecules. Conformationally flexible molecules have more degree of freedom in solution and can exist with different conformers in dynamic equilibrium. These conformers can interconvert among each other with very small energy barrier. Stable conformer can give kinetic form and metastable can end with thermodynamically stable form. Desiraju likened crystallization to a supramolecular reaction leading to kinetic and thermodynamic products (polymorphs) through Curtin–Hammett like reaction kinetics.[53] Recent papers[46e,50,58] suggest the following model of crystallization for polymorphs: the kinetic crystal nucleates faster because of stronger hydrogen bond clusters (long range interaction) and lower activation energy compared to the thermodynamic form

which could be more stable due to better close packing (van der Waals force) but it should cross over a high energy barrier.

Kinetic and thermodynamic product may convert to each other on variation of external condition like temperature, pressure or addition of foreign additive. In practice, kinetic forms transform into thermodynamic form upon increasing the temperature of the substance which provide the energy required to cross the energy barrier. Thermal analysis can provide valuable data to detect this kind of phase transition and quantify the stability of polymorphs.

1.6 Enantiotropic and Monotropic Polymorphs

Polymorphic system can be represented in pressure-temperature or energy-temperature phase diagram. Among these two, energy-temperature diagrams is common for organic substances due to available data. Energy-temperature diagrams are helpful for the characterizing and understanding of polymorphic behavior of a substance. Tammann[4f] developed many 'rules' from these diagrams which was later expanded by Burger and Ramberger[59a] and by Grunenberg.[59b] The two polymorphic modifications are said to be enantiotropic when the transition point between the two phases is found at a temperature below the melting point of either of them (Figure 1a). When there is no transition point below the melting point of the two polymorphs then the two forms are monotropically related (Figure 1b). This is known as *heat-of-transition rule*.[4k]

The *heat-of-fusion rule* states that in an enantiotropic system higher melting polymorph will have the lower heat of fusion. If the higher melting polymorph has a higher heat of fusion the two are related monotropically. Solid and liquid will be in equilibrium at melting point and Gibbs free energy will be zero for two phases. The entropy of fusion can be expressed as,

$$\Delta S_f = \Delta H_f / T_f$$

Entropy of fusion rule states that two modifications are enantiotropically related if polymorph with higher melting point has the lower entropy of fusion and monotropically related if lower melting polymorph has lower entropy of fusion. [4k]

(a)   (b)
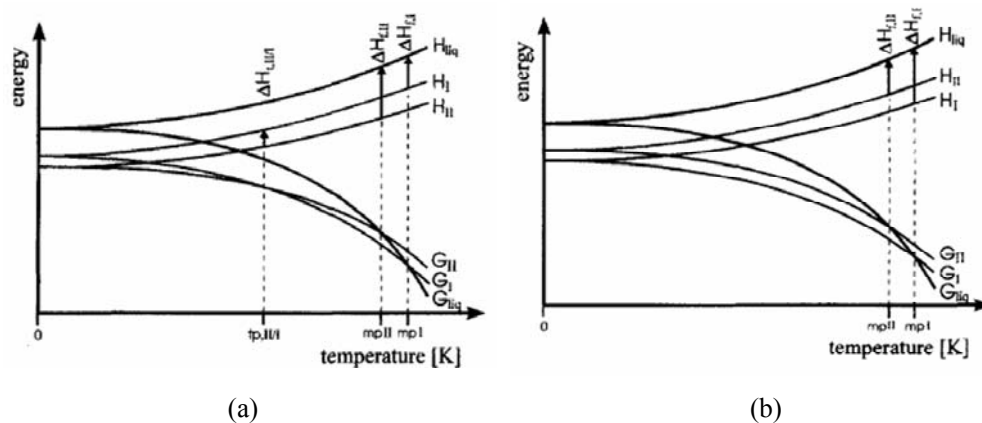
Figure 1. (a) Fundamental E/T diagram for dimorphic enantiotropic system. Form I is stable below transition point. Above transition point Form II is stable. (b) Fundamental E/T diagram for dimorphic monotropic system. Form I is more stable at all temperature below melting point than form II.

1.7 Thermal Analysis and Variable Temperature Powder XRD

The proper characterization of polymorphs is very important in pharmaceutical and other specialty chemicals and thermodynamics of their relationship should be studied to understand the phase transformation. Various analytical methods are being currently used to characterize the crystalline forms of these solids. Single crystal X-ray diffraction, powder XRD, variable temperature powder XRD, solid-state NMR, thermal analysis are some well known methods. Of these methods thermal analysis like differential scanning calorimetry (DSC), thermogravimetric analysis (TGA), hot stage microscopy (HSM) have special significance in characterization of polymorphs.[61] TG is a reliable method to obtain accurate host-guest ratios and the temperature for guest release. It is also very useful method in analyzing sublimation of solid forms. DSC provides valuable data for elucidating the stability relationships between polymorphs. For example, whether polymorphs are related as enantiotropic or monotropic can be inferred from heats and entropy of fusion.[4k] However, DSC can be misleading in cases where sample sublimation/decomposition occur during heating, because decomposition product sometimes can recrystallize or alter the melting point of the pure compound. The online combination of a TGA with a Fourier Transform Infrared

Spectrometer (FT-IR) enables both gravimetric (TGA) and spectroscopic (FT-IR)[4k,61] analysis can effectively solve this problem. TG-IR offers the analysis of evolved vapour from sublimation and decomposition of solid form. So it is very useful method to distinguish between sublimation and decomposition upon heating of a polymorphic compound. HSM can also provide valuable information for phase transition of polymorphic compounds. Melting/recrystallization or solid to solid state transformation of compounds can be observed through a microscope, often through crossed polarizers by varying the temperature of the substance.[4k] This technique also allows to confirms the thermal event visually recorded on DSC and TG experiments visually.

In situ variable temperature powder X-ray diffraction (VT-PXRD) has gained considerable attention for its finger print proofs of structural and physical changes of polymorphic phase. Sometimes DSC may not show the phase transition due to faster heating. In such cases VT-PXRD is very useful to detect the phase behavior changes. Many pharmaceutically important compounds have been studied by VT-PXRD to understand the phase relation.[62] This technique is also useful for the study of solvent loss of host-guest compounds and pseudopolymorphs.[62d] Grant and co-workers studied polymorphic transformation of three forms of Piroxicam.[62a] Recently de Villiers and co-workers reported that transformation of the pharmaceutically preferred polymorph C of mebendazole.[62b]

1.8 Crystal Structure Prediction

Polymorphism and crystal structure prediction are related aspects of crystal engineering.[9,53,62] *Ab intio* crystal structures simulation starting from the molecular diagram through computations popularly known as *crystal structure prediction* (CSP). Most methods of CSP are based on a search for the crystal structure that corresponds to the global minimum in the lattice energy. Although the techniques and details vary, all methods of CSP involve three general steps:

- Building a molecular structure from the chemical bonding diagram.
- Searching for plausible packing arrangements of the molecule.
- Ranking the generated structures by some criteria, usually lowest lattice energy.

The basic problem with lattice energy based methods is that many structures are found within a few kcal/mol of the global minimum and ranking of structure is based only on account of the thermodynamic (enthalpic) factors. But crystallization is governed by both thermodynamic and kinetic factors and the latter is more important in polymorphic systems. The lattice energy of molecular crystals is composed of the following terms:

$$U = U_{vdw} + U_{elec} + U_{intra} + U_{other}$$

where, U_{vdw} and U_{elec} refer to intermolecular repulsion-dispersion (van der Waals) and electrostatic interactions respectively. U_{intra} is the difference in intramolecular energy between the conformation of the molecule(s) in the asymmetric unit of the crystal and that in the gas phase. For rigid molecules the term U_{intra} will vanish. U_{intra} plays significant contribution in re-ranking of crystal structure of conformational flexible molecule. A flexible molecule can distort away from the optimal (gas phase) conformation if the resulting intermolecular interactions in the solid-state crystal structure give rise to a sufficiently low lattice energy to compensate for the intramolecular energy penalty associated with the suboptimal conformer. Re-ranking of crystal structure frame based on E_{total} for conformationally flexible molecule is advisable for correct prediction.[64] Total energy of system can be expressed as:

$$\Delta E_{total} = \Delta E_{lattice} + \Delta E_{conf}$$

A major concern in the computational study of a flexible molecule is the selection of the starting conformation. Since various conformers exist in dynamic equilibrium within a few kcal mol^{-1} energy difference, the question is which conformer will be present in the crystal structure. Conformers residing in local minima or the global minimum starting model give very different prediction results. Price and co-workers recently studied aspirin[64a] and piracetam,[64b] to illustrate these issues. Structure prediction is relatively easier when gas phase and the crystal conformations are similar. In aspirin, it was assumed (correctly) that the gas phase conformer is present in the crystal structure. Piracetam represents a higher level of difficulty in that the gas phase conformation is different from what is obtained in the (at the time) three known crystal forms of the compound.

Reproduction of crystal structure *i.e.* CSP for the molecule of which crystal structure already determined experimentally[65] is beneficial for the improvement and refinement of

computational methodologies. In the present case we have studied reproduction of crystal structure on dieneone and fuchsone systems, which have various molecular conformations within few kcal mol^{-1} energy. The importance of conformational energy balance with lattice energy and conformation picking from flexible body CSP (molecule is allowed to minimize freely in lattice energy minimization stage) is reported for the first time in this thesis. The present study is an example of the evolution from molecule $\rightarrow$ conformation $\rightarrow$ crystal along the supramolecular reaction pathways.

1.9 Theme of the Present Work

This thesis deals with the X-ray structural analysis of conformational polymorphs and uses of thermal analysis to determine stability and kinetic/thermodynamic states. Lattice and conformational energy compensation among conformational polymorphs are studied to understand the delicate energy balance between stable and metastable forms. Crystal structure prediction taking into account both lattice and conformational energy gave excellent match with the experimental crystal structure of two polymorphic systems, which are discussed in chapter 2 and 3. The uses of *in situ* variable temperature powder diffraction in understanding thermal relation among kinetic and thermodynamic forms is discussed for three polymorphic systems. Discovery, characterization and screening of all the possible solid forms of a drug substance are important for drug development formulation and marketing. The novel 6th polymorph of a leading anti-depressant drug Venlafaxine.HCl and phase relations among the different forms is established in chapter 4. Crystal engineering strategy in development of new conformational polymorph is demonstrated through phenylogue series approach in chapter 5. A Curtin–Hammett energy profile for kinetic and thermodynamic crystallization products of conformational polymorphs is proposed.

1.10 References

1. E. Mitscherlich, *Abhl. Akad. Berlin*, **1822–1823**, 43.
2. W. F. Ostwald, *Z. Phys. Chem.*, **1897**, *22*, 289.
3. (a) M. J. Buerger and M. C. Bloom, *Z. Krristallogr.*, **1937**, *96*, 182; (b) J. Haleblian and W. C McCrone, *J. Pharma. Sci.*, **1969**, *58*, 911.

4. Historical development on polymorphism (Table 1) (a) ref 1 (b) G. B. Amici, *Ann. Chim. Phys., Ser. 3*, **1844**, *12*, 114. (c) E. Mallard, *Annales Mines*, **1876**, *10*, 60. (d) O. Lehmann, *Die Krystallanalyse oder die chemische Analyse durch Beobachtung der Krystallbildung mit Hülfe des Mikroskps*, Wilhelm Engelmann, Liepzig, **1891**. (e) ref 2. (d) P. H. R. Groth, *volume 1-5*, W. Engelmann, Liepzig, **1906-1919**. (f) G. Tammann, *The States of Aggregation* (trans. F. F. Mehl) Constable and Company, Ltd., London, **1926**, pp-116-57. (g) ref 3a. (h) ref 3b. (i) P. Corradini, Chem. Ind. (Milan), **1973**, *55*, 122. (j) S. R. Chemburkar, J. Bauer, K. Deming, H. Spiwek, K. Patel, J. Morris, R. Henry, S. Spanton, W. Dziki, W. Porter, J. Quick, P. Bauer, J. Donaubauer, B. A. Narayanan, M. Soldani, D. Riley and K. McFarland, *Org. Process Res. Dev.*, **2000**, *4*, 413. (k) J. Bernstein, *Polymorphism in Molecular Crystals*, Clarendon, Oxford, **2002**. (l) *Cryst. Growth Des.*, **2003**, *3*, 867-1040. (m) *Cryst. Growth Des.*, **2004**, *4*, 1087-1441.

5. J. Berzelius , *Jahresbericht*, **1844**, *23*, 44.

6. W. B. Jensen, *J. Chem. Educ.*, **1998**, *75*, 817.

7. W. C. McCrone, in *Physics and Chemistry of the Organic Solid State*, Vol. *2*, eds. D. Fox, M. M. Labes and A. Weissberger, Wiley Interscience, New York, **1965**, pp. 725-767.

8. A. Burger, in *Topics in pharmaceutical science*, eds D. D. Breimer and P. Speiser, Elsevier, Lausanne, **1983**, pp 347-358.

9. J. D. Dunitz, in *The crystal as a supramolecular entity*. Perspective in supramolecular chemistry, Vol. *2*, ed. G. R. Desiraju, Wiley, Chichester, **1996**, pp 1-30.

10. (a) S. L. Morissette, Ö. Almarsson, M. L. Peterson, J. F. Remenar, M. J. Read, A. V. Lemmo, S. Ellis, M. J. Cima and C. R. Gardner, *Adv. Drug Delivery Rev.*, **2004**, *56*, 275. (b) Ö. Almarsson and M. J. Zaworotko, *Chem. Commun.,* **2004**, 1889. (c) C. R. Gardner, C. T. Walsh and Ö. Almarsson, *Nat. Rev.*, **2004**, *3*, 926. (d) S. Datta and D. J. W. Grant, *Nat. Rev.*, **2004**, *3*, 42.

11. R. Hilfiker, F. Blatter and M. von Raumer, in *Polymorphism in the Pharmaceutical Industry*, ed. R. Hilfiker, Wiley–VCH, Weinheim, **2006**, pp. 1-19.

12. (a) J. D. Dunitz and J. Bernstein, *Acc. Chem. Res.*, **1995**, *28*, 193. (b) D. Braga and F. Grepioni, *Chem. Soc. Rev.*, **2000**, *4*, 229. (c) N. Blagden and R. J. Davey, *Cryst. Growth Des.*, **2003**, *3*, 873. (d) R. J. Davey, K. Allen, N. Blagden, W. I. Cross, F. H. Lieberman, M.J. Quayle, S. Righini, L. Seton and G.J.T. Tiddy, *CrystEngComm*, **2002**, *4*, 257.

13. (a) C. P. Brock, W. B. Schweizer and J. D. Dunitz, *J. Am. Chem. Soc.*, **1991**, *113*, 9811. (b) J. D. Dunitz, *Acta Cryst.*, **1995**, *B51*, 619.

14. (a) J. Bernstein, *Polymorphism in Molecular Crystals*, Clarendon, Oxford, **2002**, pp 298-301. (b) S. L. Morissette, S. Soukasene, D. Levinson, M. J. Cima and Ö. Almarsson, *Proc. Nat. Acad. Sci (USA).*, **2003**, *100*, 2180.

15. (a) G. Klebe, F. Graser, E. Hädicke and J. Berndt, *Acta Cryst.*, **1989**, *B45*, 69. (b) I. Bar and J. Bernstein, *J. Pharm. Sci.*, **1985**, *74*, 255. (c) S. R. Byrn, R. R. Pfeiffer and J. G. Stowell, *Solid-State Chemistry of Drugs*; SSCI: West Lafayette, IN, **1999**. (d) J. Bernstein, R. J. Davey and J. -O. Henck, *Angew. Chem. Int. Ed.*, **1999**, *38*, 3440. (e) R. J. Davey, *Chem. Commun.*, **2003**, 1463.

16. O. Okada and M. L. Klein, *J. Chem. Soc., Faraday Trans.*, **1996**, *92*, 2463.

17. P. K. Thallapally, R. K. R. Jetti, A. K. Katz, H. L. Carrell, K. Singh, K. Lahiri, S. Kotha, R. Boese and G. R. Desiraju, *Angew. Chem. Int. Ed.*, **2004**, *43*, 1149.

18. (a) S. J. Bonafede and M. D. Ward, *J. Am. Chem. Soc.*, **1995**, *117*, 7853. (b) C. A. Mitchell, L. Yu and M. D. Ward, *J. Am. Chem. Soc.*, **2001**, *123*, 10830.

19. J. Zaccaro, J. Matic, A. S. Myerson and B. A. Garetz, *Cryst. Growth Des.*, **2001**, *1*, 5.

20. (a) L. J. Chyall, J. M. Tower, D. A. Coates, T. L. Houston and S. L. Childs, *Cryst. Growth Des.*, **2002**, *2*, 505. (b) J. L. Hilden, C. E. Reyes, M. J. Kelm, J. S. Tan, J. G. Stowell and K. R. Morris, *Cryst. Growth Des.*, **2003**, *3*, 921.

21. J. M. Ha, J. H. Wolf, M. A. Hillmyer and M. D. Ward, *J. Am. Chem. Soc.*, **2004**, *126*, 3382.

22. (a) M. D. Lang, A. L. Grzesiak and A. J. Matzger, *J. Am. Chem. Soc.*, **2002**, *124*, 14834. (b) C. P. Price, A. L. Grzesiak and A. J. Matzger, *J. Am. Chem. Soc.*, **2005**, *127*, 5512.

23. W. I. F. David, K. Shankland, C. R. Pulham, N. Bladgen, R. J. Davey and M. Song, *Angew. Chem. Int. Ed.*, **2005**, *44*, 7032.

24. (a) M. L. Peterson, S. L. Morissette, C. McNulty, A. Goldsweig, P. Shaw, M. LeQuesne, J. Monagle, N. Encina, J. Marchionna, A. Johnson, M. J. Cima and Ö. Almarsson, *J. Am. Chem. Soc.*, **2002**, *124*, 10958. (b) Ö. Almarsson, M. B. Hickey, M. L. Peterson, S. L. Morissette, S. Soukasene, C. McNulty, M. Tawa, J. M. MacPhee and J. F. Remenar, *Cryst. Growth Des.*, **2003**, *3*, 927.

25. S. L. Morissette, Ö. Almarsson, M. L. Peterson, J. F. Remenar, M. J. Read, A. V. Lemmo, S. Ellis, M. J. Cima and C. L. Gardner, *Adv. Drug Deliv. Rev.*, **2004**, *56*, 275.

26. (a) Ö. Almarsson and M. J. Zaworotko, *Chem. Commun.*, **2004**, 1889. (b) P. Vishweshwar, J. A. McMahon, M. Oliveira, M. L. Peterson and M. J. Zaworotko, *J. Am. Chem. Soc.*, **2005**, *127*, 16802. (c) M. Rafilovich and J. Bernstein, *J. Am. Chem. Soc.*, **2006**, *128*, 12189. (d) G. M. Day, A. V. Trask, W. D. S. Motherwell, and W. Jones, *Chem. Commun.*, **2006**, 54. (e) S. Ahn, F. Goo, B. M. Kariuki and K. D. M. Harris, *J. Am. Chem. Soc.*, **2006**, *128*, 8441.

27. L. S. Reddy, N. J. Babu and A. Nangia, *Chem. Commun.*, **2006**, 1369.

28. A. V. Trask, N. Shan, W. D. S. Motherwell, W. Jones, S. Feng, R. B. H. Tan and K. J. Carpenter, *Chem. Commun.*, **2005**, 880.

29. (a) C. Bilton, J. A. K. Howard, N. N. L. Madhavi, A. Nangia, G. R. Desiraju, F. H. Allen and C. C. Wilson, *Chem. Commun.*, **1999**, 1675. (b) V. S. S. Kumar, A. Anthony, A. Nangia, W. T. Robinson, C. K. Broder, R. Mondal, I. R. Evans, J. A. K. Howard and F. H. Allen, *Angew. Chem. Int. Ed.*, **2002**, *41*, 3848. (c) S. Chen, I. A. Guzei and L. Yu, *J. Am. Chem. Soc.*, **2005**, *127*, 9881. (d) Z.-Q. Zhang, J. M. Njus, D. J. Sandman, C. Guo, B. M. Foxman, P. Erk and R. V. Gelder, *Chem. Commun.*, **2004**, 886.

30. (a) N. Blagden and R. J. Davey, *Cryst. Growth Des.*, **2003**, *3*, 873. (b) P. Erk, H. Hengelsberg, M. F. Haddow and R. van Gelder, *CrystEngComm*, **2004**, *6*, 474.

31. (a) F. H. Allen and R. Taylor, *Chem. Soc. Rev.*, **2004**, *33*, 463. www.ccdc.cam.ac.uk. (b) J. Van de Streek and S. Motherwell, *Acta Cryst.*, **2005**, *B61*, 504. (c) J. A. R. P.

Sarma and G. R. Desiraju, *Crystal Engineering: The Design and Application of Functional Solids*; eds. M. J. Zaworotko and K. R. Seddon, Kluwer: Dordrecht, **1999**, 325. (d) D. Braga and F. Grepioni, *Chem. Soc. Rev.*, **2000**, *29*, 229.

32. A. Gavezzotti and G. Filippini, *J. Am. Chem. Soc.*, **1995**, *117*, 12299.

33. L. Yu, G. A. Stephenson, C. A. Mitchell, C. A. Bunnell, S. V. Snorek, J. J. Bowyer, T. B. Borchardt, J. G. Stowell and S. R. Byrn, *J. Am. Chem. Soc.*, **2000**, *122*, 585.

34. V. S. S. Kumar, *PhD Thesis*, University of Hyderabad, **2002**.

35. A. Nangia, *Cryst. Growth Des.*, **2006**, *6*, 2.

36. (a) T. L. Threlfall, *Analyst*, **1995**, *120*, 2435. (b) A. Nangia and G. R. Desiraju, *Chem. Commun.*, **1999**, 605.

37. J. Bernstein, R. J. Davey and J. -O. Henck, *Angew. Chem. Int. Ed.*, **1999**, *38*, 3440.

38. (a) F. Wöhler and J. Liebig, *Annal. Pharm.*, **1832**, *3*, 249. (b) W. I. F. David, K. Shankland, C. R. Pulham, N. Blagden, R. J. Davey and M. Song, *Angew. Chem. Int. Ed.*, **2005**, *43*, 7032. (c) N. Blagden, R. Davey, G. Dent, M. Song, W. I. F. David, C. R. Pulham and K. Shankland, *Cryst. Growth Des.*, **2005**, *5*, 2218.

39. (a) R. G. Gonnade, M. M. Bhadbhade and M. S. Shashidhar, *Chem. Commun.*, **2004**, 2530. (b) G. Mehta, S. Sen and K. Venkatesan, *CrystEngComm*, **2005**, *7*, 398. (c) L. Fábián, A. Kálmán, G. Argay, G. Bernáth and Z. C. Gyarmati, *Chem. Commun.*, **2004**, 2114. (d) M. Rafilovich, J. Bernstein, R. K. Harris, D. C. Apperley, P. G. Karamertzanis and S. L. Price, *Cryst. Growth Des.*, **2005**, *5*, 2197. (e) C. M. Reddy, S. Basavoju and G. R. Desiraju, *Chem. Commun.*, **2005**, 2439.

40. (a) G. R. Desiraju, *Angew. Chem. Int. Ed. Engl.*, **1995**, *34*, 2311. (b) A. Nangia and G. R. Desiraju, *Top. Curr. Chem.*, **1998**, *198*, 57.

41. G. R. Desiraju, *Science*, **1997**, *278*, 404.

42. B. R. Sreekanth, P. Vishweshwar and K. Vyas, *Chem. Commun.*, **2007**, DOI: 10.1039/b700082k.

43. S. R. Vippagunta , H. G. Brittain and D. J. W. Grant, *Adv. Drug Deliv. Rev.*, **2001**, *48*, 3.

44. J. Bernstein, *Organic Solid State Chemistry* (Ed. G. R. Desiraju), Elsevier, Amsterdam, **1987**, pp 471-518.

45. (a) A. Bashkirava, P. C. Andrews, P. C. Junk, E. G. Robertson, L. Spiccia and N. Vanderhoek, *Chem. Asian J.*, **2007**, *2*, 530. (b) Z. -Q. Zhang, J. M. Njus, D. J. Sandman, C. Guo, B. M. Foxman, P. Erk and R. V. Gelder, *Chem. Commun.*, **2004**, 886. (c) F. P. A. Fabbiani, D. R. Allan, S. Parsons and C. R. Pulham, *CrystEngComm*, **2005**, *7*, 179. (d) M. Tamura, Y. Hosokoshi, D. Shiomi, M. Kinoshita, Y. Nakasawa, M. Ishikawa, H. Sawa, T. Kitazawa, A. Eguchi, Y. Nishio and K. Kajita, *J. Phys. Soc. Jpn.*, **2003**, *72*, 1735. (e) R. K. R. Jetti, R. Boese, J. A. R. P. Sarma, L. S. Reddy, P. Vishweshwar and G. R. Desiraju, *Angew. Chem. Int. Ed.*, **2003**, *42*, 1963.(f) Z. Xie, L. Liu, B. Yang, G. Yang, L. Ye, M. LI and Y. Ma, *Cryst. Growth Des.*, **2005**, *5*, 1959. (g) T. V. Timofeeva, G. H. Kuhn, V. V. Nesterov, Vladimir N. Nesterov, D. O. Frazier, B. G. Penn and M. Y. Antipin, *Cryst. Growth Des.*, **2003**, *3*, 383. (h) C. Guo, M. B. Hickey, E. R. Guggenheim, V. Enkelmann and B. M. Foxman, *Chem. Commun.*, **2005**, 2220.

46. J.W. Steed, *CrystEngComm*, **2002**, *5*, 169.

47. (a) K. Kim and A.J. Matzger, *J. Am. Chem. Soc.*, **2002**, *124*, 8772. (b) K. E. Plass, K. Kim and A. J. Matzger, *J. Am. Chem. Soc.*, **2004**, *126*, 9042.

48. (a) A. Gavezzotti and G. Filippini, *J. Phys. Chem.*, **1994**, *98*, 4831. (b) C. P. Brock and L. L. Duncan, *Chem. Mater.*, **1994**, *6*, 1307.(c) J. W. Steed, E. Sakellariou, P. C. Junk and M. K. Smith, *Chem. Eur. J.,* **2001**, *7*, 1240. (d) H. J. Lehmler, L. W. Robertson, S. Parkin and C. P. Brock, *Acta Cryst.*, **2002**, *B58*, 140. (e) C. P Brock, *Acta Cryst.*, **2002**, *B58*, 1025. (f) S. E. Gibson, H. Ibrahim and J. W. Steed, *J. Am. Chem. Soc.*, **2002**, *124*, 5109.(g) B. M. Craven, *Acta Cryst.*, **1979**, *B35*, 1123.

49. T. Steiner, *Acta Cryst.*, **2000**, *B56*, 673.

50. B. Sarma, S. Roy, A. Nangia, *Chem. Commun.*, **2006**, 4918;

51. G. S. Nichol and W. Clegg, *Cryst. Growth Des.*, **2006**, 6, 451.

52. (a) P. D. Prince, G. S. McGrady and J. W. Steed, *New J. Chem.*, **2002**, *26*, 457. (b) K. M. Anderson, A. E. Goeta, K. S. B. Hancock and J. W. Steed *Chem. Commun.*, **2006**, 2138.

53. G. R. Desiraju, *Nat. Mater.*, **2002**, *1*, 77.

54. (a) J. Hulligar, *Angew. Chem. Int. Ed.*, **1994**, *33*, 143. (b) S. X. M. Boerrigter, F. F. A. Hollander, J. van de Streek, P. Bennem and H. Meekes, *Cryst. Growth Des.*, **2002**, *2,* 51. (e) J. Lu, X. –J. Wang, C. -B. Ching, *Cryst. Growth Des.*, **2003**, *3*, 83. (f) A. L. Rohl, *Current Opinion in Solid State and Materials Science*, **2003**, *7*, 21. (g) H. M. Cuppen, G. M. Day, P. Verwer and H. Meekes, *Cryst. Growth Des.*, **2004, 4**, 1341. (h) R. Hiremath, S. W. Varney and J. A. Swift, *Chem. Commun.*, **2004**, 2676.

55. (a) S. Parveen, R. J. Davey, G. Dent and R. G. Pritchard, *Chem. Commun.*, **2005**, 1531. (b) R. J. Davey, G. Dent, R. K. Mughal and S. Parveen, *Cryst. Growth Des.,* **2006**, *6*, 1788. (c) R. Banerjee, P. M. Bhatt, M. T. Kirchner and G. R. Desiraju, *Angew. Chem. Int. Ed.*, **2005**, *44*, 2515.

56. S. J. Rowan, S. J. Cantrill, G. R. L. Cousins, J. K. M. Sanders and J. F. Stoddart, **2002** *Angew. Chem. Int. Ed.*, **2002**, *41***,** 898.

57. (a) D. Y. Curtin, *Rec. Chem. Prog.*, **1954**, *15*, 111 (b) J. L. Seeman, *Chem. Rev.* **1983**, *83*, 83. (c) F. A. Carey and R. J. Sandberg, *Advanced Organic Chemistry*, *Part A – Structure and Mechanisms*, 4th Ed., Plenum Press, New York, pp. 220-222

58. (a) J. W. Chew, S. N. Black, P. S. Chow, R. B. H. Tan, K. J. Carpenter, *CrystEngComm*, **2007**, *9*, 128.

59. (a) A. Burger and R. Ramberger, *Mikrochim. Acta, II*, **1979**, 259. (b) A Grunenberg, B. Keil, J, -O, Henck and H. W. Sisler, *Int. J. Pharm.*, **1996**, *129*, 147.

60. a) L. R. Nassimbeni, *Acc. Chem. Res.*, **2003**, *36*, 631. (b) L. R. Nassimbeni, in *Encyclopedia of Supramolecular Chemistry*; Vol. *1*, eds. J.L. Atwood and J.W. Steed, Marcel Dekker, New York, **2004**, pp. 696-704.

61. G. W .V. Cave, J. Antesberger, L. J. Barbour, R. M. McKinlay and J. L. Atwood, *Angew. Chem. Int. Ed.*, **2004**, *43*, 5263.

62. (a) A. R. Sheth, S. Bates, F. X. Muller, and D. J. W. Grant, *Cryst. Growth Des.*, **2004**, *4*, 1091. (b) M. M. de Villiers, R. J. Terblanche, W. Liebenberg, E. Swanepoel, T. G. Dekker and M. Songa, *Journal of Pharmaceutical and Biomedical Analysis*, **2005**, *38*, 435. (c) I. Kushida and K. Ashizawa, *J. Pharm. Sci.*, **2002**, *91*, 2193. (d) O. Sumarna, J. Seidel, E. Weber, W. Seichter, B. T. Ibragimov and K. M. Beketov, *Cryst. Growth Des.*, **2003**, *3*, 541.

63. (a) J. D. Dunitz, *Chem. Commun.*, **2003**, 545. (b) A. Gavezzotti, *J. Am. Chem. Soc.*, **1991**, *113*, 4622. (c) A. Gavezzotti, *Acc. Chem. Res.*, **1994**, *27*, 309-14.

64. (a) C. Ouvrard and S. L. Price, *Cryst. Growth & Des.*, **2004**, *4*, 1119. (b) H. Nowell and S. L. Price, *Acta Cryst.*, **2005**, *B61*, 558.

65. P. Nimmanpipug, K. Tashiro and O. Rangsiman, *J. Phys. Chem. B*, **2003**, *107*, 8343.

CONFORMATION AND LATTICE ENERGY COMPENSATION IN KINETIC AND THERMODYNAMIC FORMS OF 4,4-DIPHENYL-2,5-CYCLOHEXADIENONE

2.1 Introduction:

Polymorph screening is now recognized as an important step in the development of drugs and other specialty chemicals.[1] Understanding polymorphism, growing new crystal forms, controlling the selective growth of one form, transformations between polymorphs are of great current interest. Studies on polymorphs provide fundamental information on molecular recognition, crystal nucleation, crystallization, and the relationship between solid phases. The existence of polymorphism implies that free energy differences between various forms are small (< 3 kcal mol^{-1}) and that kinetic factors are important during crystal nucleation and growth. Molecular conformations, hydrogen bonding, packing arrangements, and lattice energies of the same molecule in different supramolecular environments may be compared in polymorphic structures.[2] Polymorph interconversion upon heating, grinding or by ultrasound is reported in the literature.[3] As different polymorphs have different physical and chemical properties, the selective growing of one or another form is major goal for the chemist. This led to an increased interest on developing methods to control the outcome of crystallization in producing desired polymorphs. High-throughput crystallization for screening of polymorphs has become a very popular method in exploring solid forms of pharmaceutical compounds.[4] Crystallization conditions play a direct role on the crystal products, kinetic or thermodynamic. A kinetic form which appears in normal condition at room temperature may be converted to the stable thermodynamic form upon heating or grinding. Recently Groof and co-workers[5] reported the polymorphic transformation of nifidipine, a drug for calcium channel blocker, by thermal analysis and variable temperature powder X-ray diffraction (VT-PXRD) study. They have shown that the

kinetically obtained forms are converted to thermodynamically stable one upon heating above 110 °C.

The occurrence of polymorphs is common in conformationally flexible molecules because of more degrees of freedom due to presence of several equi-energetic conformations in solution, which may lead to different crystal structures.[6] Energy differences between conformers are typically of the same order of magnitude as lattice energy differences,[6] i.e. $\Delta E_{conf} \approx \Delta U_{latt} = 0\text{-}2$ kcal mol^{-1}, which means that the energy penalty in molecular conformation can be compensated by the lattice energy gained through intermolecular interactions and close packing, and vice versa, depending on local enthalpy effects in each crystal structure. Bernstein[7] reviewed some early examples of intra- and intermolecular energy compensation in conformational polymorphs several years ago Price[8] recently examined intra- and intermolecular energy compensation in conformational polymorphs of some drugs, e.g. aspirin, barbituric acid, piracetam. However there is one exception in the above mentioned energy compensation among conformational polymorphs of 5-methyl-2-[(2-nitrophenyl)amino]-3-thiophenecarbonitrile, (common name ROY because of its red, orange and yellow colored polymorphic forms) which has record seven polymorphs.[9] In ROY the stable perpendicular conformation is present in the thermodynamic yellow crystal form. Concomitant conformational polymorphism of 4,4-diphenyl-2,5-cyclohexadienone was studied to understand quantitative energy balance in conformational polymorph.
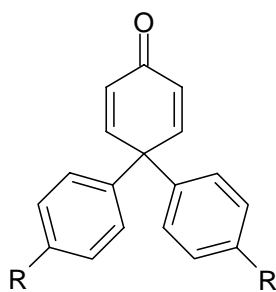
1: R = H
2: R = Ph
3: R = Cl, Br, Me

Polymorphism of 4,4-Diphenyl-2,5-cyclohexadienone **1** was studied recently in our group. It crystallizes as a tetramorphic cluster of A-D.[10] Crystallographic data of conformational polymorphs A-D of diphenyl benzoquinone **1** are listed in Table 1. Diphenyl quinone **1** has several acidic activated donor hydrogens of the sp^2 and phenyl C–H type whereas there is only one carbonyl acceptor in the molecule. Depending on the molecular conformation one or more of the several possible C–H⋯O interactions[11] are optimized in the crystal structures. Form A has linear zigzag chains of C–H⋯O hydrogen bonds from distinct C–H donors to the O-atom of quinone ring of graph set notation[12] $C(8)$ (Figure 1a). In form B two symmetry independent molecules form centrosymmetric C–H⋯O dimer synthon **I** [graph set $R_2^2(8)$] with the quinone moiety (2.33 Å, 169.2º; 2.49 Å, 123.5º), while the other two molecules form centrosymmetric C–H⋯O synthon, **II** [graphset $R_2^2(20)$] through the *para*-hydrogens (2.64 Å, 138.0º; 2.74 Å, 121.6º). Triclinic form B ($P\bar{1}$, $Z = 8$) and form C ($P\bar{1}$, $Z= 24$) have almost same packing arrangement and engaged in similar kind of C–H⋯O synthon **I** and **II.** Powder X-ray diffraction pattern is also very close for these two triclinic forms which indicates the similarity of these structures (Figure 2). Form D has $C(10)$ chains that connect to form cyclic $R_4^3(32)$ pattern (2.36 Å, 137.9º; 2.54 Å, 166.9º) and *o*-phenyl C–H⋯O synthon **III** of $R_2^2(16)$ ring (2.57 Å, 144.5º; 2.47 Å, 165.1º). Metrics of C–H⋯O geometries are listed alongside the packing diagrams in Figure 1. Study of analogous compounds bis(biphenylyl) ketone **2** and substituted phenyl derivatives **3** (4-Cl/Br/Me) did not afford any polymorph after considerable effort. Chloro and bromo derivative of cyclohexanone found to be isomorphous and chloro methyl-exchange was not observed in this family.[13a] In contrast to polymorphs of phenyl extended compound **2** gave isostructural host-guest compounds (Figure 3).[13]

Table 1. Crystallographic data on polymorphs A-D of diphenyl quinone **1**.[10]

	Form A	Form B	Form C	Form D
CSD refcode	HEYHUO	HEYHUO01	HEYHUO02	HEYHUO03
Space group	$P2_1$	$P\bar{1}$	$P\bar{1}$	*Pbca*
Z', Z	1, 2	4, 8	12, 24	2, 16
a [Å]	7.9170(6)	10.0939(2)	18.3788(4)	10.7921(6)
b [Å]	8.4455(6)	16.2592(3)	19.9701(4)	17.4749(12)
c [Å]	10.3086(9)	16.2921(4)	24.4423(5)	27.9344(19)
α [deg]	90	88.2570(10)	95.008(1)	90
β [deg]	105.758(2)	85.3380(10)	111.688(1)	90
γ [deg]	90	83.6450(10)	105.218(1)	90
V [Å^3]	663.36(9)	2648.00(10)	7871.8(3)	5268.2(6)
R-factor	0.050	0.068	0.112	0.059
ρ_{calcd} [g cm^{-3}]	1.233	1.236	1.247	1.242
T [K]	160(2)	150(2)	140(2)	100(2)

The number of symmetry-independent or crystallographic unique molecules in a crystal lattice is Z'. The large number and wide range of Z' values in polymorphs A-D is a record among crystal structures: $\Sigma\ Z' = 19$ and $\Delta\ Z'_{max} = 11$. A high Z' of 12 in form C is a record in polymorph clusters and as such rare in the CSD (Scheme 1).[16] Very few compounds have high number of polymorphs and high Z', which are shown in scheme 2. Compound **1** has high Z' in form C and form B.

(a)

(b)

(c)

(d)
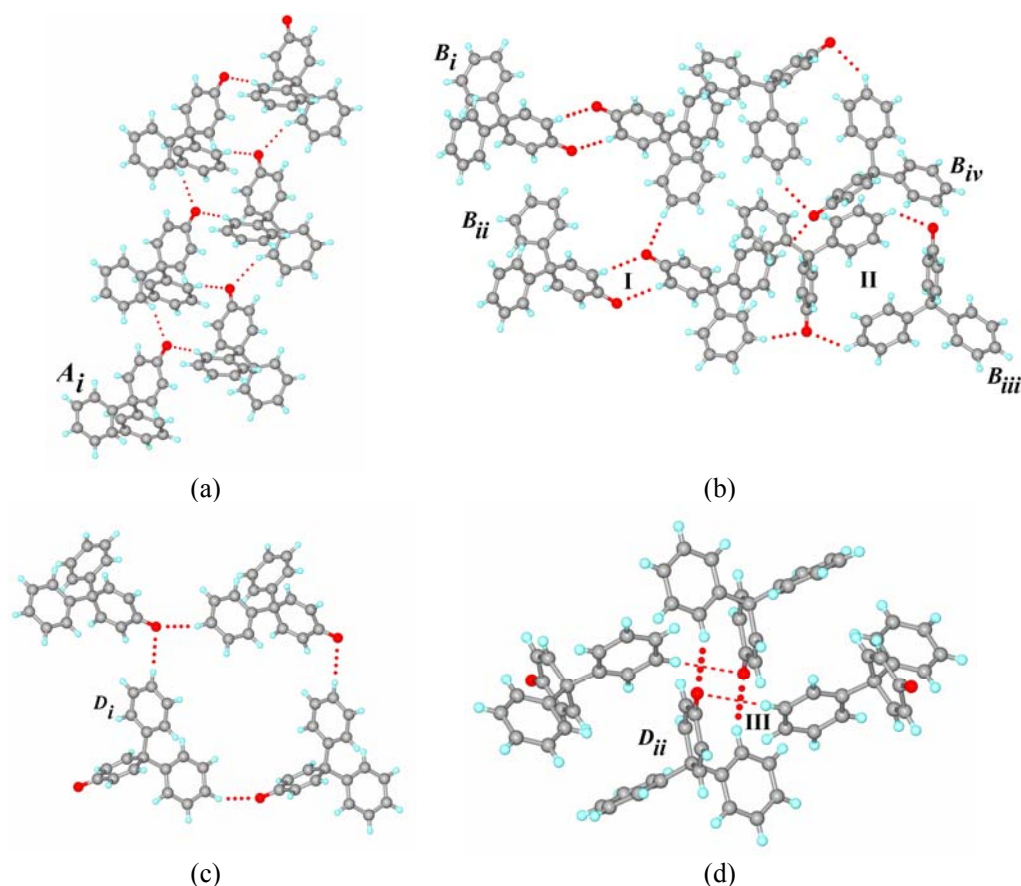
Figure 1. (a) Helices of C–H···O hydrogen bonds between 2_1 screw related molecules in form **A** [graph set $C(8)$]. (b) Centrosymmetric C–H···O synthon **I** between B_i, B_{ii} molecules of $R_2^2(8)$ pattern and synthon **II** between B_{iii}, B_{iv} molecules of $R_2^2(20)$ notation in form **B**. Crystal structure of form C is similar to B. (c) C–H···O interactions between translation and screw axis related D_i molecules in form **D** of graph set $R_4^3(32)$. (d) Centrosymmetric C–H···O synthon **III** between D_{ii} molecules ($R_2^2(16)$ pattern) and C–H···O interaction. Neutron-normalized distances are quoted. Note that different C–H donors participate in C–H···O interactions in different crystal forms. Cyclic C–H···O synthons **I-III** are labeled.

(a)   (b)
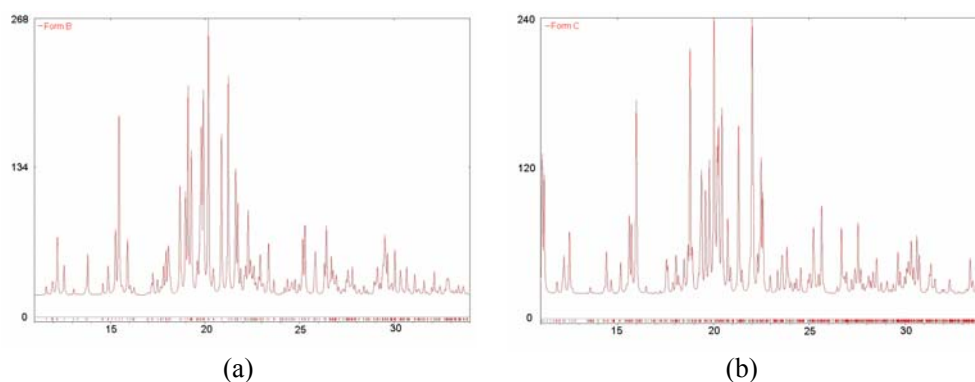
Figure 2. Calculated powder X-ray diffraction (Powder Cell 2.3) of forms B (a) and C (b) of diphenyl quinone **1**. They are indistinguishable from powder XRD revealed the similarity in the two triclinic forms.
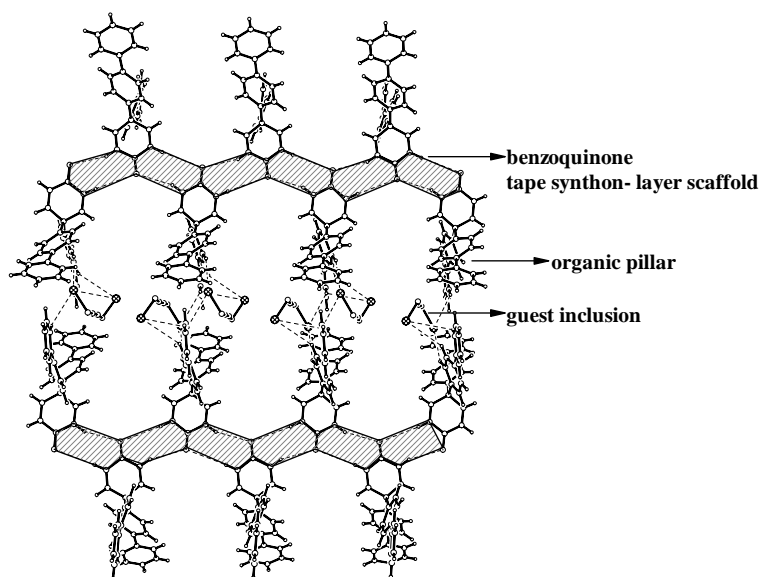
Figure 3. The clay mimic structure observed in **2**.dibromobutane and with other guests. Figure taken from ref 13b.

QAXMEH (n= 7, *Z'*= 1)

SUTHAZ (n= 5, *Z'*= 2)

BEWKUJ (n= 4, *Z'*= 2)

BIXGIY (n= 4, *Z'*= 1)

HEYHUO (n= 4, *Z'*= 12)

KAXHAS (n= 4, *Z'*= 1)

MABZNA (n= 4, Z'= 4)

RUWYIR (n= 4, *Z'*= 2)

Conformational polymorphs (4 forms or more)

PUBMUU (n= 3, *Z'*= 16)

IFULUQ (n= 4, *Z'*= 8)

DUVZOJ (n= 3, *Z'*= 6)

ZZZVTY (n= 3, *Z'*= 5)

THIOUR (n= 3, *Z'*= 4.5)
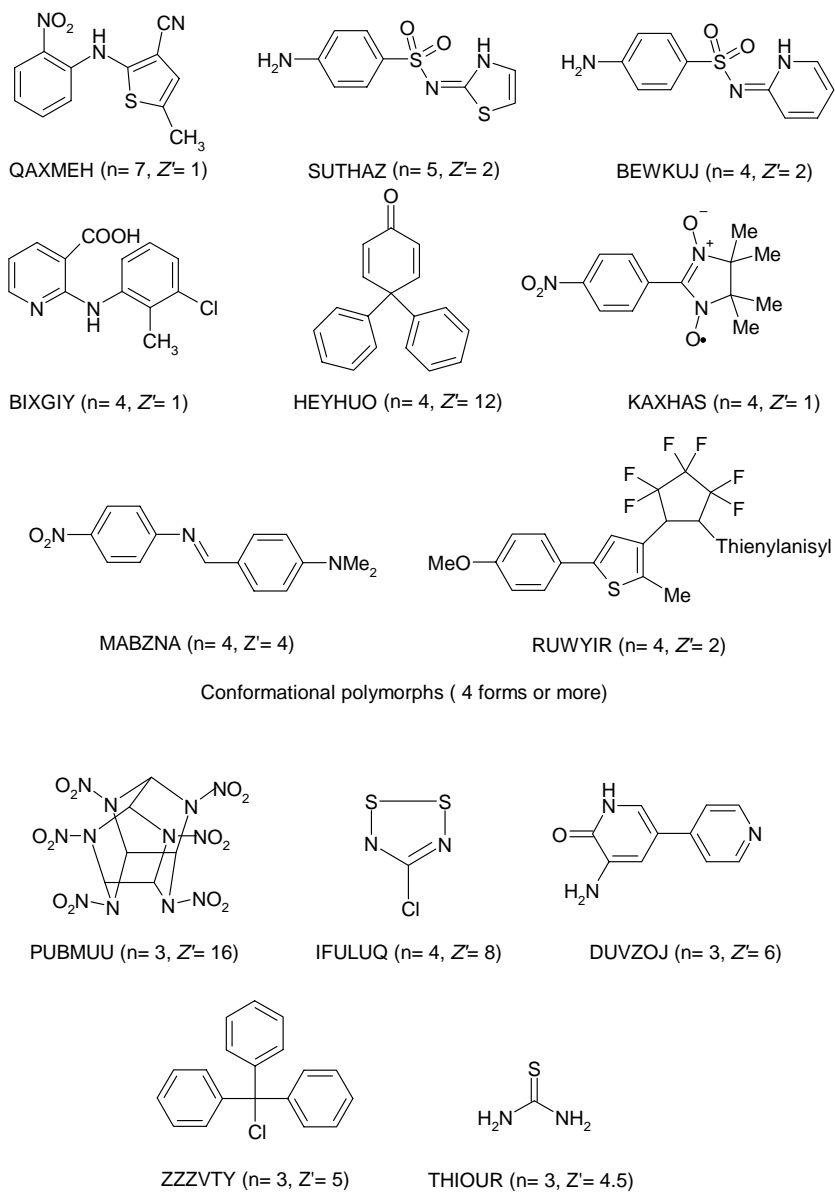
Multiple molecules in asymmetric unit (Z'>4)

Scheme 1. Some polymorphic systems with ≥ 3 forms in organic crystal structures and multiple molecules in the asymmetric unit.[9a,10,14,15] n = number of reported polymorph, *Z'*= number of molecule in asymmetric unit.

2.2 High *Z'* and C–H···O Strength

Why certain categories of compounds crystallizes with *Z'* > 1 is not properly understood. Steed[17] has critically reviewed the reasons for high *Z'* in crystal structures. Alcohols, phenols, steroids, nucleotides, nucleosides show higher frequency of *Z'* > 1 because of awkward shape of the molecule and the enthalpic advantage from σ-cooperative chains *via* forming strong O–H···O hydrogen bonds.[18] There are several low-lying molecular conformations present in solution which can inter-convert during crystallization. Concomitant-conformational polymorphism of molecule **1** belongs to this class.
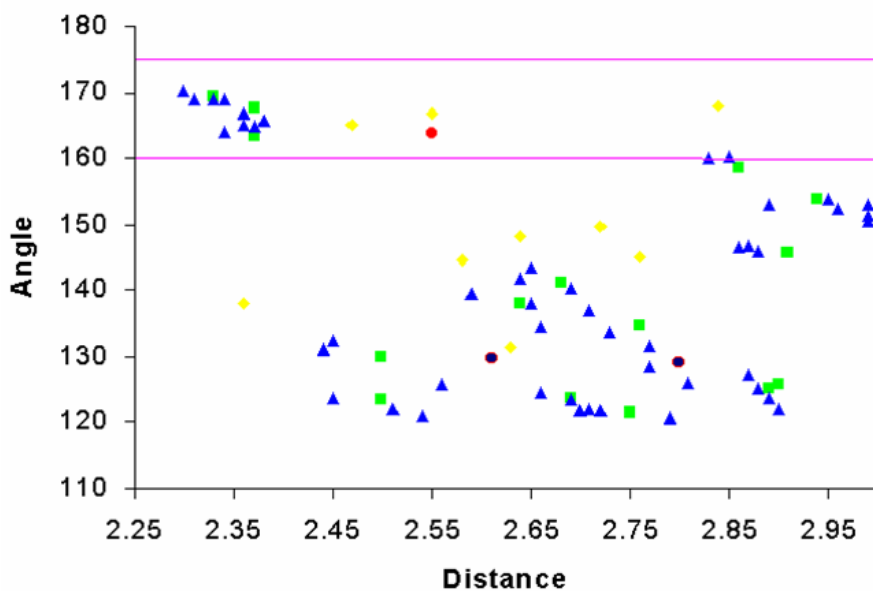
Figure 4. H···O distance (2.2-3.0 Å) vs. C–H···O angle (120-180°) scatter plot of interactions in tetramorphs A-D. A = ● (*Z'* = 1), B = ■ (*Z'* = 4), C = ▲ (*Z'* = 12), D = ◆ (*Z'* = 2). The shortest H···O distance (marked with an arrow in the linear band) is inversely related to *Z'* (number of symmetry-independent conformations) in this polymorphs family.

Cholesterol ($Z' = 8,16$) is a prototype example of strong O–H···O hydrogen bonds being associated with unusually high Z'. There are a few example in literature where weak hydrogen bonding like C–H···O and C–H···Cl interactions play a role in giving high Z' structures.[19] Similar interesting trend in C–H···O bond strength/ distance and the number of conformations in a particular structural (Z') polymorph of **1** has been noticed. Distance–angle scatter plot of C–H···O interactions for forms A-D (Figure 4) show C–H···O contacts in form C are, in general, shorter than those in forms B and D and longer in form A. Only short-linear interactions between $\theta = 160\text{-}175°$ are taken in to consideration. The shortest H···O distance in form C is 2.30 Å and it has the highest Z' value of 12, whereas form B has H···O = 2.33 Å and $Z' = 4$, forms D and A have even longer H···O distances of 2.47 and 2.55 Å and smaller Z' value of 2 and 1 respectively. This result nicely correlates with C–H···O interaction in a particular form being inversely related to the Z' value of that crystal structure.

High Z' polymorphs and C–H···O strength correlation suggests about the importance of kinetic factors during crystallization. Subsequent experiments were aimed to identify the kinetic form and thermodynamic form among concomitant polymorphs A-D, and phase transitions among these forms.

2.3 Variable Temperature Powder X-ray Diffraction of 1

In preliminary batches single crystals of all four forms of compound **1** was obtained, though normal crystallization afforded forms A and B in later experiments. Unit cell check of several single crystals confirmed that form A and form B are the dominant forms. However powder X-ray diffraction shows all four forms in the concomitant mixture at room temperature (Figure 5). A typical solid upon crystallization from EtOAc/*n*-hexane contains form A (~40%), forms B+C (~50%), and form D (~10%) as shown in Figure 5. The ratios were determined by least square refinement of observed powder XRD with simulated peaks of each crystal structure (Powder Cell 2.3).[20] As triclinic forms B and C have similar structure, it is not possible to distinguish between

these closely related structure by their overlapping diffraction patterns (Figure 2). Percentages of polymorphic forms in different batches vary within 5%.
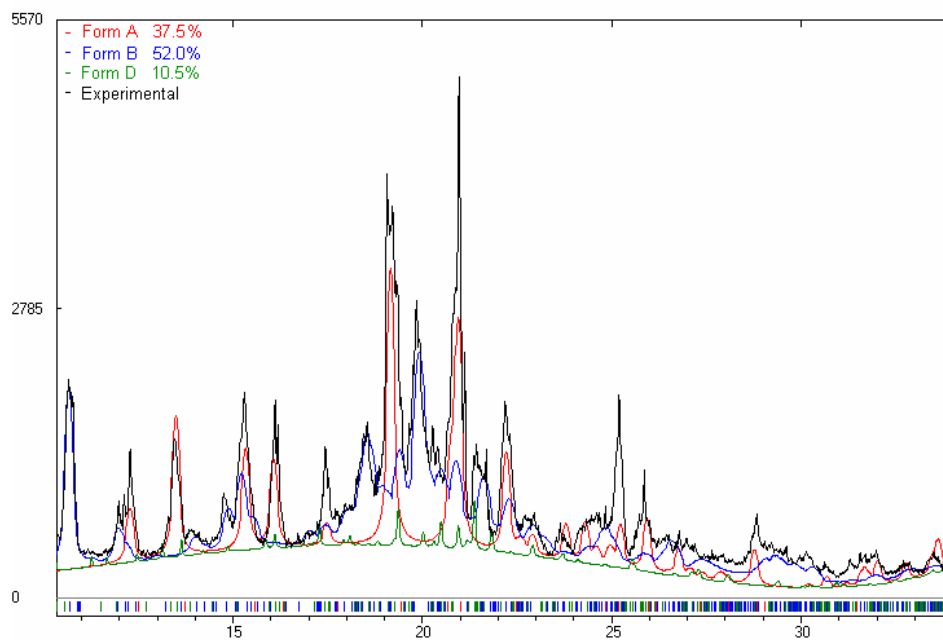
Figure 5. Powder X-ray diffraction of solid **1** at room temperature: black = experimentally observed powder pattern; red, blue and green = calculated powder pattern of form A (37.5%), B (52.0%), and D (10.5%), respectively. Least square refinement in Powder Cell 2.3[20]: R_p = 14.82, R_{wp} = 19.32.

Differential scanning calorimetry (DSC) of the polymorphic mixture **1** showed a single endotherm peak at 120.45 °C (Figure 6), corresponding to the melting point of **1**. This means that the four forms melt at the same temperature, which is surprising because they have very different crystal packing arrangements.
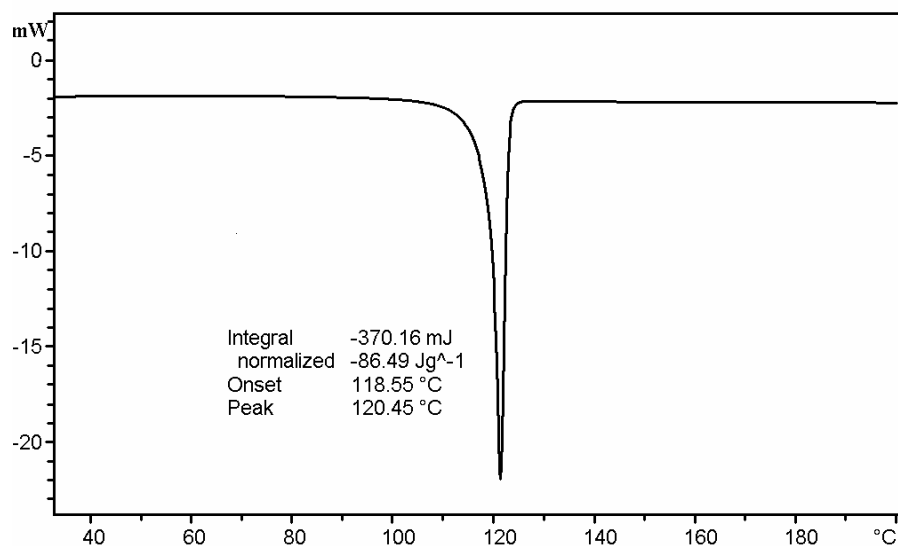
Figure 6. DSC of diphenyl quinone **1** recorded at scan rate of 10 °C min^{-1}. All four forms A-D melt at the same temperature (T_{endo} = 120-121 °C).

To study the exact behavior of phase transition the mixture of forms at room temperature was heated in the variable powder x-ray diffractometer bench (VT-PXRD). The peak profile is relatively invariant in the temperature range 30-60 °C. Notable changes were observed as the temperature reached to 70 °C (Figure 7a): certain peaks disappeared and the overall pattern becomes significantly sharper with fewer but more intense lines. The peak profile remains unchanged on further heating of the sample. after which the material becomes amorphous and then semi-solid/melt at 105-115 °C. There are no reflections except the peak from the sample holder at 2θ = 25.2° (Figure 7). Heating to 70 °C completely converts the mixture of polymorphs A-D to form A.

(a)   (b)
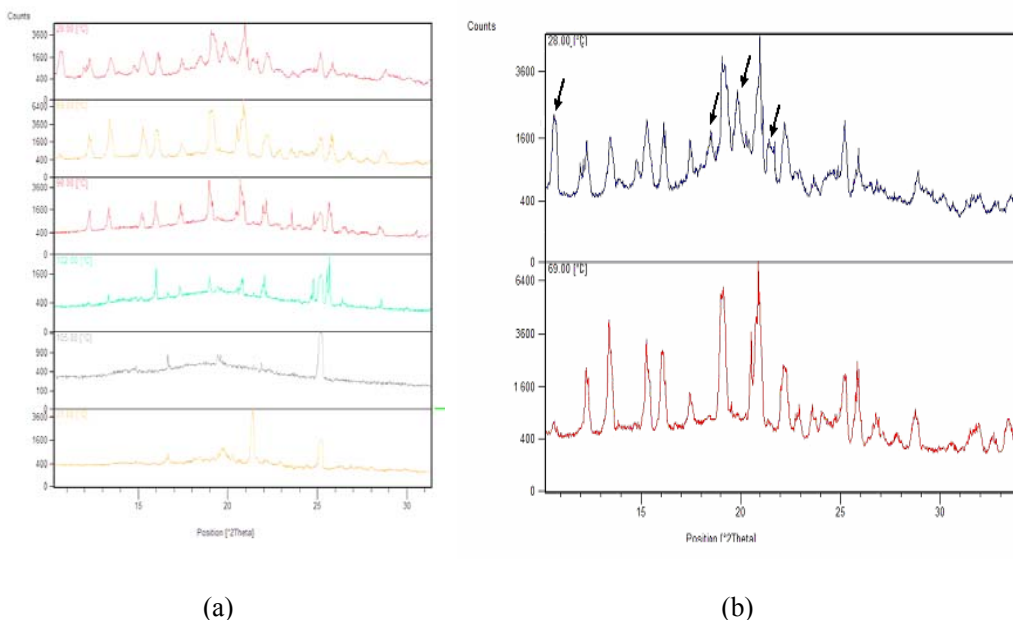
Figure 7. (a) Powder X-ray diffraction patterns of **1** recorded at different temperatures during a heating experiment. (b) Powder XRD of **1** at 28 °C (top) and 69 °C (bottom). The peaks that disappear upon heating are marked with an arrow.

VT-PXRD shows that upon heating of polymorphs A-D to a pre-melting temperature of 70 °C transforms the mixture to form A (Figure 8a) in good polymorph purity (>95%). Monoclinic polymorph A therefore is the thermodynamic modification in the enantiotropic system of polymorphs of **1** between 30-80 °C. Melt crystallization generally gives kinetic forms upon solidification. Kinetic form B was prepared by heating the polymorphic mixture to a melt phase in the powder X-ray diffractometer pan at ~115 °C. Cooling the sample to room temperature afforded reasonably pure polymorph B (Figure 8b). The observed powder diffractions patterns were matched with the calculated profiles from the respective single crystal structures in Powder Cell 2.3. This was also confirmed by unit cell checking of randomly picked crystals from the melt crystallization batch.

Thus stable form A and metastable form B has been isolated from the polymorphic mixture in pure state (>95%) under optimized experimental conditions

derived from VT-PXRD study. This study highlights the utility and information obtained from powder XRD measurements in a polymorphic system that does not exhibit phase transitions in thermal techniques like DSC.

Chiral form A was prepared in high purity and shown to have a non-linear optical signal equal to that of urea when irradiated with Nd^{+3}-YAG laser (1.06 μm); the mixture of polymorphs from a typical solution crystallization is SHG inactive. Controlled crystallization by heating of the material for getting pure form A is preferred over solution crystallization to avoid contamination from other polymorphs. There always chance of accidental seeding of laboratory space, which may result in mixture of forms.[2c,21] Ostwald's rule[22] of stages states "When leaving a metastable state, a given chemical system does not seek out the most stable state, rather the nearest metastable one that can be reached with minimum loss of free energy." Our observations indicate that polymorphs of **1** do not follow Ostwald's rule of stages, with stable form A having appeared first from solution crystallization followed by metastable forms B and C. Simultaneous nucleation of more than one form from solution, inter-conversion among polymorphs, appearance in order of stability, and heterogeneous cross nucleation may also result in concomitant appearance of polymorphs.[23] Different batches of crystallization yield almost same concomitant mixture of forms confirmed by PXRD data. Polymorphs A-D crystallize concomitantly from solution suggests that more than one C–H···O synthon and close packing motif is optimized during the early stages of molecular recognition and crystal nucleation.

2.4 Conformation and Lattice Energy Compensation

Interplay of intra- and intermolecular energies in conformational polymorphic systems plays a role in kinetic and thermodynamic stability and their concomitant appearance. Many conformers which are in dynamic equilibrium in solution can end up with very different crystal structures. In this sense compound **1** having 19 crystallographic distinct molecular conformations present in four forms is a ideal system for the study of kinetic and thermodynamic influence in formation of different molecular packing arrangement during crystallization.

(a)   (b)
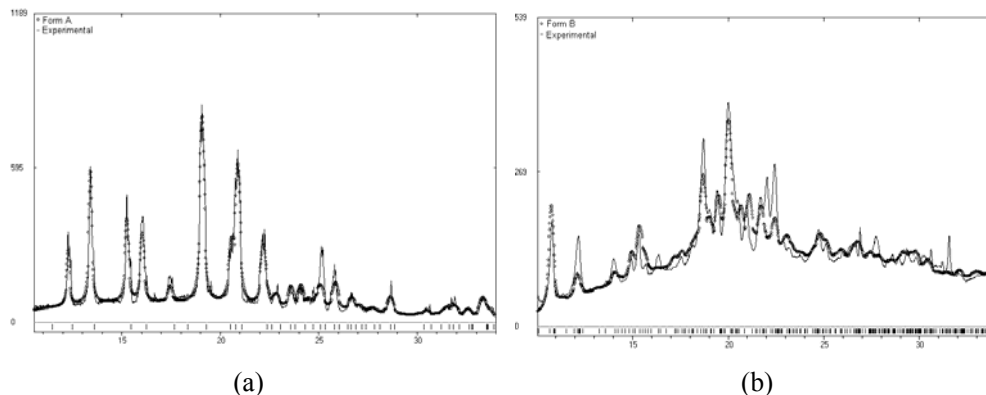
Figure 8. (a) Experimental powder XRD of **1** at 69 °C (black line) matches with the calculated powder pattern of polymorph A (dotted line). (b) Experimental powder XRD of **1** from melt crystallization (black line) shows good agreement with the calculated powder pattern of polymorph B (dotted line).

2.4.1 Conformation Analysis

The 19 crystallographically independent molecules of **1** differ in the rotation about the C–C bonds between the quinone and the phenyl rings. These different conformations may be defined through eight possible torsion angles parameters. Among 8-dimensional torsion angle space τ_1 and τ_2, taken from a single asymmetric unit having minimum value and are selected to represent conformational surface map in these 19 molecules (Table 2). These torsion angles lie in the range τ_1 = 8-22° and τ_2 = 12-38° along the scatter plot diagonal (Figure 9a). Overlay of nineteen conformations show the geared rotation of phenyl rings (Figure 9b).

(a)   (b)
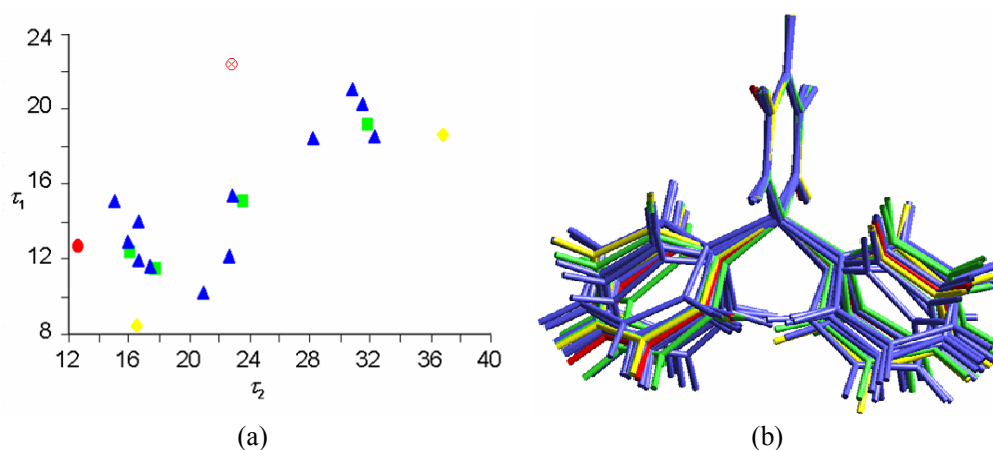
Figure 9. (a) Conformational map (τ_1 *vs* τ_2) of nineteen crystallographic independent conformations of **1** lie along the diagonal. A = ● ($Z' = 1$), B = ■ ($Z' = 4$), C = ▲ ($Z' = 12$), D = ♦ ($Z' = 2$), gas phase rotamer = ⊗ ($\tau_1 = \tau_2 = 22.3°$). (b) Overlay of all the conformations. Red = form A, Green= form B, Blue= form C, Yellow = form D.

Conformation energy (E_{conf}) and dipole moment (μ) were calculated in Spartan 04[24] (Table 3). The molecule was extracted from the crystal structure and energy minimized (HF/6-31G**) keeping the conformation fixed (heavy C and O atoms invariant) following the method of Yu et al.[9a] In the X-ray crystal structure position of hydrogen atom is not precise as heavy atom and for the reduce error in energy calculation H atoms were allowed to relax to reasonable geometries. Among the nineteen conformer B_i has the most stable conformation with energy value E_{conf} = –479813.50 kcal mol^{-1} which arbitrarily fixed to 0 for the comparison. Energies of conformers in forms A, B and D (E_{conf}) lie within 1.3 kcal mol^{-1} of B_i. Conformers C_i-C_{xii} are higher in energy (E_{conf} = 2-9 kcal mol^{-1}) may be due to the error in experimental X-ray geometry co-ordinates, because the *R*-factor of form C is high (11.1%). Different conformers can readily inter convert through geared (correlated) rotation of phenyl rings[10] about τ_1, τ_2. The energy barrier is in the range accessible through thermal motion of atoms (RT ~0.5 kcal mol^{-1} at 298 K) in the crystallization regime of –5 to 100 ºC.

Table 2. Energy and dipole moment of 19 conformers of **1** calculated in Spartan 04.

Crystal polymorph label	Molecular conformation label[a]	Phenyl torsion angles		HF/6-31G**	
		τ_1 [°]	τ_2 [°]	E_{conf}[b] [kcal mol^{-1}]	μ [D]
Form A	A_i	12.5	12.6	1.22	5.15
Form B	B_i	12.3	16.0	0.00	5.22
	B_{ii}	14.9	23.6	0.06	5.20
	B_{iii}	19.1	31.8	0.66	5.34
	B_{iv}	11.5	17.7	1.12	5.24
Form C	C_i	12.8	16.0	2.81	5.20
	C_{ii}	11.9	16.7	3.94	5.40
	C_{iii}	18.4	32.3	4.16	5.06
	C_{iv}	12.1	22.7	4.76	5.30
	C_v	15.2	22.0	5.19	5.40
	C_{vi}	10.2	21.0	5.51	5.24
	C_{vii}	11.5	17.4	7.99	5.50
	C_{viii}	18.3	28.2	8.14	5.08
	C_{ix}	20.9	30.8	8.15	5.21
	C_x	14.0	16.7	8.31	5.15
	C_{xi}	14.9	15.1	8.54	5.23
	C_{xii}	20.1	31.5	8.90	5.39
Form D	D_i	18.5	36.8	1.08	5.21
	D_{ii}	8.4	16.5	1.25	5.17
---	Energy minimized	22.3	22.3	−2.78	4.87

[a] Conformers in different polymorph are numbered in the order of increasing energy.
[b] Relative to the most stable conformation B_i = −479813.50 kcal mol^{-1}, a value that is arbitrarily fixed at 0.00 for comparison of conformation energies.
Energy minimized: The molecular conformer was drawn and optimized to the stable gas-phase rotamer.

2.4.2 Lattice Energy

Crystal lattice energies, U_{latt}, of tetramorphs A-D were computed in COMPASS and DREIDING 2.21 force fields (Table 3, *Cerius*^{2})[25] by energy minimization of the experimental crystal structures. COMPASS force field is better parameterized and gives more accurate energies of organic molecules,[26] which are typically stabilized by

hydrogen bonds, intermolecular interactions, and van der Waals forces. COMPASS[27] is better suited for molecule **1** because electrostatic stabilization from C–H···O hydrogen bonds and edge-to-face aromatic interactions is included in the Coulomb term. COMPASS value has been considered for the stability ranking of the different forms of **1.** Form A has the most stable crystal structure (U_{latt} = −32.69 kcal mol^{-1}) and forms B, C, D are less stable by 1.03, 1.06, 0.82 kcal mol^{-1}, respectively. According U_{latt} value stability order of the tetramorph is form A < form D < form B. Form C was not considered in the stability ranking because of its refinement problem as discussed earlier. This energy order shows that form B is the least stable which is kinetic form and obtained from melt crystallization.

Table 3. Lattice energies [U_{latt}, kcal mol^{-1}] of forms A-D computed in *Cerius*^{2}, corrected to per molecule of **1**.

	Form A		Form B		Form C		Form D	
U_{latt}	COM PASS	DREI DING 2.21	COM PASS	DREI DING 2.21	COM PASS	DREI DING 2.21	COM PASS	DREI DING 2.21
Total	−32.69	−42.12	−31.66	−39.66	−31.63	−39.71	−31.87	−42.42
van der Waals	−28.01	−27.78	−28.19	−27.22	−28.18	−27.23	−27.80	−27.19
Colum bic	−4.68	−12.50	−3.47	−10.43	−3.45	−10.49	−4.07	−12.49
Hydro gen bond[a]	---	−1.84	---	−2.01	---	−1.99	---	−2.74

[a] Hydrogen bond energy is partitioned in DREIDING 2.21 but it is part of the Coulomb component in COMPASS force field.

Lattice and conformation energy calculation show a compensation among the polymorphs. Either the molecular conformer or the lattice energy is at the minimum, but both intra- and intermolecular energies are not the lowest in any structure. Molecular conformations B$_i$-B$_{iv}$ are lower in energy (E_{conf} = 0.00, 0.06, 0.66, 1.12 kcal mol^{-1}) but crystal lattice B is metastable (U_{latt} = −31.66 kcal mol^{-1}), whereas lattice energy supports

the stability of form A (U_{latt}=−32.69 kcal mol^{-1}) by 1.03 kcal mol^{-1} than form B. In increasing order of E_{total} (COMPASS): form A (thermodynamic, most stable) < B (kinetic, intermediate stable) < D (least stable). This energy order is consistent with the thermodynamic stability of form A in VT-PXRD experiments and crystallization from the melt to give kinetic from B.

Table 4. Relative energies[a] [per molecule, kcal mol^{-1}] of crystal forms A, B and D.[b]

Polymorph	U_{latt}		E_{conf} HF/6-31G**[c]	$E_{total} = U_{latt} + E_{conf}$	
	COMPASS	DREIDING 2.21		COMPASS	DREIDING 2.21
A	0.00	0.30	1.22	1.22	1.52
B	1.03	2.76	0.46	1.49	3.22
D	0.82	0.00	1.16	1.98	1.16

[a] Values are taken from Tables 2 and 3. Both U_{latt} and E_{conf} are relative energies.
[b] Form C is excluded because the errors are too large.
[c] Average E_{conf} value is estimated for multiple conformers as $\Sigma E_{conf} \div Z'$.

The 12 high-energy conformers in crystal structure C may be viewed as metastable relic of relatively stable 4 conformers in form B. Both form B and C crystal are packed via C–H···O synthons **I** and **II**, and near identical powder XRD peaks (Figure 2). High Z' (=12) polymorph C represents a "snap shot picture of an evolving crystal nucleus" on the way to form B ($Z' = 4$) wherein the molecules have aggregated to form the crystal lattice but the periodicity is yet to reach the highest possible crystal symmetry. Presence of stronger C–H···O interactions in higher energy conformers of form C help to gear up the kinetic factors in the nucleation step. In short, high Z' structures are not just a crystallographic oddity but open a window to "see" crystal nucleation and growth.[17,28]

An oft-repeated question in conformational polymorphic systems is: does molecular conformation determine crystal packing or does favorable crystal packing trap a metastable molecular conformation. It is difficult to quantify the inter- and intramolecular energy interplay when they are almost similar in terms of contribution. In the different polymorphs of compound **1** it was observed that one particular conformation is associated with a specific C–H···O synthon. For example, B_{iv} and C_{vii}

rotamers have near identical conformations and they engage in synthon **II** in crystal structures of polymorphs B and C. Form A have a metastable conformer in the crystal though it has the stable crystal packing arrangement. To understand this phenomenon, reproduction of the crystal structure of form A by computations was performed.

2.5. Crystal Structure Reproduction of Form A

Ab initio prediction of the crystal structures of organic molecules now posses great importance and major challenge in crystal engineering field.[29] Although there have been cases where the crystal structure of a molecule was genuinely predicted just from the chemical diagram, it is certainly may not possible to predict the crystal structures molecule with $Z' > 1$ or molecule with conformational flexibility by *ab initio* calculations. Particularly prediction of conformationally flexible molecule is very difficult because;

- Stable crystal structure may result from a metastable conformation. The stable conformation may result in higher packing energy than the predicted global minimum structure.

- Many conformations residing in local minima along with the global minimum in energy landscape can result in different crystal structures. Which metastable conformation out of several low lying rotamers is to be selected for simulation?

- Both conformation and lattice energy contribution to crystal structure stabilization must be accounted.

- Will the most stable or higher energy crystal structure be observed and which ones to select?

Some success is been achieved in recent years in crystal structure prediction (CSP) of conformationally flexible molecule based on the approach to *ab initio* calculations by Price *et al*.[8] Zaworotko and coworkers[1c] reported X-ray crystal structure of Form II of aspirin, a comformationally flexible molecule, which was computationally predicted by Ouvrard and Price.[8b] Recently Jones and coworkers[30] have reported a new polymorph of maleic acid after 124 years of the first polymorph reported which was

formed during cocrystallization experiment with caffeine. After obtaining the second form they have performed crystal structure reproduction computationally and found that the new form is the global minimum in lattice energy.
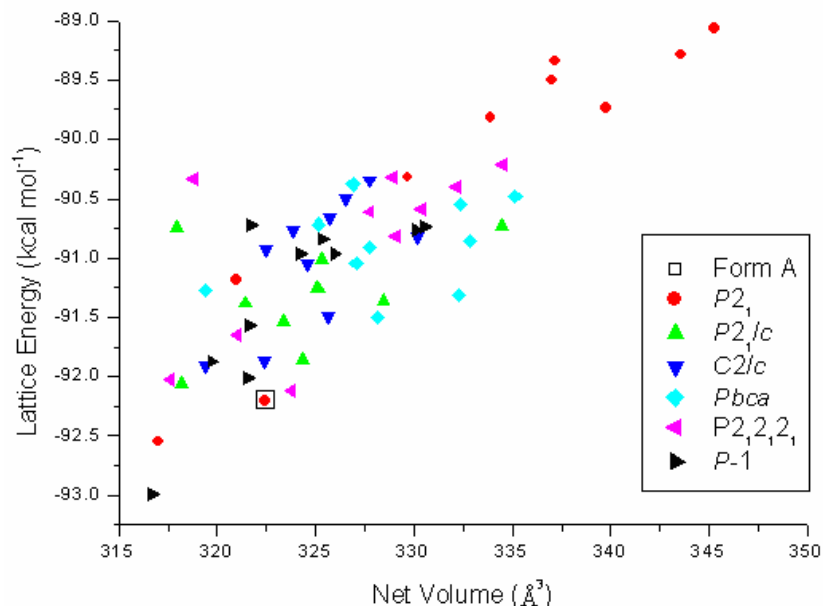
Figure 10. Lattice energy vs. cell volume for structures of molecule **1** generated in six common space groups using full body minimization in Polymorph Predictor. Experimental crystal structure A matches with the 3rd rank predicted structure based on U_{latt}.

The present work is a possible solution for predicting and ranking structure frames of a conformationally flexible molecule. Thermodynamic polymorph A is the target in crystal structure prediction because it is having one molecule in asymmetric unit. The objective of our simulations is to reproduce the known stable polymorph A and to find out closely energetic structures as guide for future crystallization experiments. Polymorph Predictor (*Cerius*^{2}) (PP) computations using COMPASS force field was used to generate several putative crystal structures of **1** from the stable molecular conformation in Gaussian 03.[31] Crystal structure frames were generated in six common

space groups, $P2_1/c$, $P\bar{1}$, $C2/c$, $Pbca$, $P2_1$ and $P2_12_12_1$. Conformation in the predicted structures was allowed to vary during energy minimization of frames (defined as full body minimization) to cover the complete landscape of crystal structures in flexible molecules. Ten unique low energy frames within 4 kcal mol^{-1} from the global minimum are plotted for each space group in Figure 10 (see Appendix II for predicted frames). Experimental structure A is the 3rd rank frame based on U_{latt}. Cell parameters, torsion angles and lattice energy of CSP frame #3 match with experimental structure remarkably well (Table 5). Crystal packing in the simulated structure is identical to the observed form and their powder XRD profiles overlap well (Figure 11). Refinement of powder XRD patterns of frames 1-15 with form A do not match except with predicted structure #3. Frame #3 matching with the observed structure is short of the correct answer, yet our reproduction of a large and flexible molecule **1** is quite good in term of successful example. Frame #1 is defined as the lowest energy predicted structure.

Table 5. Comparison of predicted[a] and experimental structure[b] parameters.

Form	a [Å]	b [Å]	c [Å]	β [°]	V [Å^3]	ι_1, ι_2 [°]	U_{latt} [kcal mol^{-1}]
Full body minimization							
Frame #3	7.712	8.286	10.415	104.32	322.45	14.6, 15.9	−92.201
Form A	7.713	8.286	10.415	104.32	322.46	14.6, 15.9	−92.196
Rigid body minimization							
Frame #1	7.699	8.133	10.165	104.96	307.51	12.6, 12.7	−32.697
Form A	7.701	8.139	10.160	105.00	307.54	12.6, 12.7	−32.695
Crystallographic parameters from Table 1[c]							
Form A	7.917	8.445	10.308	105.75	331.68	12.5, 12.6	---

[a] Predicted structure in *Cerius*^{2} (PP) using COMPASS force field.
[b] Experimental form A minimized in *Cerius*^{2} with COMPASS force field.
[c] Deviation in cell parameters compared to the full body minimized structure #3 is <3%.

(a)

(b)

(c)

(d)
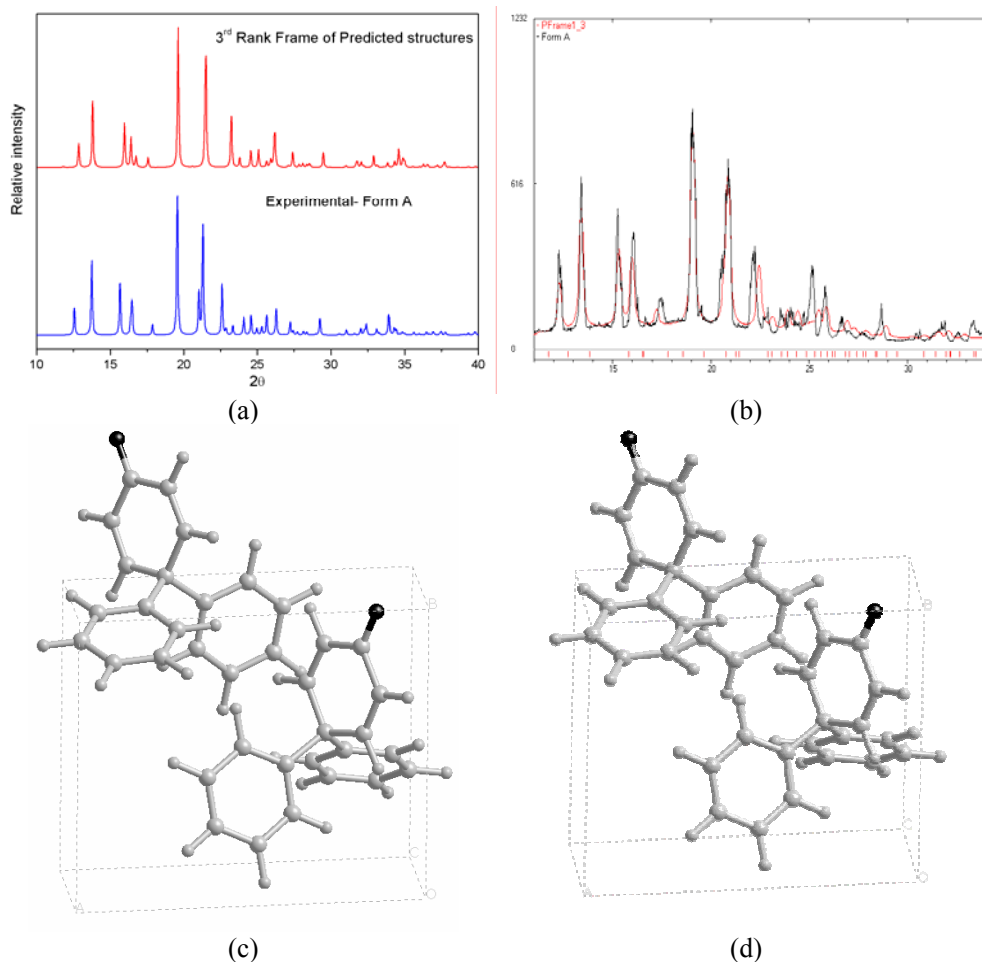
Figure 11. (a) Powder XRD of predicted and experimental crystal structure (b) Least square refinement of powder XRD of PP frame #3 (red line) to the experimental form A (black line) in Powder Cell 2.3. R_p = 25.60, R_{wp} = 37.14..(c) Unit cell packing in form A, (d) Unit cell packing in predicted frame #3

Reproduction of crystal structure was carried out starting from rotamer A_i using rigid body minimization after structure generation step. Given the correct molecular conformation, C−H···O synthon and crystal packing of form A predicted lowest energy structure #1 (Table 5). This highlights how important starting conformation is in determining the crystal structure of conformationally flexible molecule. To further attest the significance of metastable conformations in generating structures of **1**, the gas-phase

conformation, which is not observed in any known polymorph so far, was used in CSP. Predicted structures from the stable Gaussian 03[32] rotamer ($\tau_1 = \tau_2 = 23.8°$) are less stable (U_{latt} −28 to −30 kcal mol^{-1}, Table 6) than observed crystal structures (U_{latt} −31 to −33 kcal mol^{-1}, Table 3) of metastable conformations. The contribution of molecular conformation to crystal structure stabilization is significant and so one should accurately compute both intramolecular and intermolecular energy terms. Predicted structures in full body minimization adopt the best molecular conformation for a stable crystal structure in that space group because the conformation is allowed to adjust during the simulation.

Table 6. Rigid body minimization in polymorph predictor from the stable conformation (Gaussian 03) of **1** in different space groups. The lowest energy frame is listed.

Space Group	U_{latt} [kcal mol^{-1}]	V [Å^3]	ρ_{calcd} [g cm^{-3}]	Cell dimensions [Å, °]
$P2_1$	−29.45	332.831	1.251	7.744, 8.485, 10.396, 106.87
$P\overline{1}$	−29.84	318.780	1.283	6.806, 14.561, 6.808, 102.19, 91.99, 103.89
Pbca	−28.91	330.561	1.237	8.298, 31.737, 10.042
$P2_1/c$	−28.76	326.402	1.253	6.638, 7.049, 29.290, 72.29
$C2/c$	−29.13	324.725	1.260	7.124, 12.724, 12.385, 74.31
$P2_12_12_1$	−28.31	335.887	1.218	9.490, 15.572, 9.091

Global minimum conformer: The stable gas-phase conformation in Gaussian 03 ($\tau_1 = \tau_2 = 23.8°$) is similar to the global minimized rotamer in Spartan 04 ($\tau_1 = \tau_2 = 22.3°$).

Lattice energy (U_{latt}) of minimized crystal structures after full body minimization is much lower (ca. −92 kcal mol^{-1}) than rigid body minimized structures (ca. −32 kcal mol^{-1}). The contribution from valence terms (bonds, angles, torsions, cross-terms) is ca. −60 kcal mol^{-1} in full body minimization for molecule **1** but valence terms are not considered in rigid body minimization (fixed to zero). This contribution of valence terms in flexible body lattice energy is not as accurate as the rigid lattice energy, which quantifies the intermolecular component arising from hydrogen bonds, electrostatic

interactions and van der Waals forces. Instead of taking into account valence term from force field calculation, conformation energy may be calculated by quantum mechanical methods. The gain/penalty from molecular conformation must be added/subtracted to accurately calculate the total crystal energy. To implement this method U_{latt} component was calculated by rigid body minimization and E_{conf} was determined in Spartan 04. The starting 10 rotamers were extracted from the full body minimization frame and the generated structures were minimized by the rigid body method. The minimum energy structure in rigid body method matches with the full body reference frame in all respects: cell parameters, crystal packing, and simulated PXRD (Table 7). Frame numbers 1-10 of flexible body method were re-ranked based on the total energy, $E_{total} = E_{conf} + U_{latt}$, of rigid body minimized frames (Table 8). There is significant reorganization of predicted structures rankings when accurately calculated conformation and lattice energies are considered together to prioritize the simulated frames using increasing E_{total} as the criterion instead of U_{latt} energy. Frame #3 of flexible body minimization is now the global minimum frame #1 and it perfectly matches with stable form A.

The advantage of both flexible body and rigid body minimization methods in *Cerius*[2] Polymorph Predictor has been taken to simulate crystal structures of a molecule with several low-energy conformations. The best conformation for generating stable crystal packing is determined by allowing torsion angles to vary. Then U_{latt} and E_{conf} are accurately calculated for this ideal conformation and their sum is taken to finalize the lowest energy structure. The above iterative method for deriving the correct metastable conformation and then re-ranking predicted crystal structure frames is not reported in the literature to our knowledge. It is suited for structure prediction of flexible drug molecules, in which conformation and lattice energy contributions must be properly quantified. This matching of the observed crystal structure of form A with the global minimum simulated structure reinforces the importance of both intra- and intermolecular energies to crystal structure stabilization in conformationally flexible molecules.

Table 7. Unit cell dimensions and angles of frames #1-10 in full body minimization are compared with the cell parameters after rigid body method. The global minimum frame #1 based on E_{total} matches with the structure of experimental form A.

New rank from Table 7	Starting rank from Appendix II	Space Group	Full body method Cell dimensions [Å, º] and net volume [Å^3]	Rigid body method Cell dimensions [Å, º] and net volume [Å^3]
1	3	$P2_1$	7.712, 8.286, 10.415, 75.68, 322.45	7.713, 8.289, 10.412, 75.65, 322.44
2	1	$P\bar{1}$	6.805, 14.599, 6.800, 76.46, 86.06, 74.68, 316.69	6.805, 14.598, 6.800, 74.46, 86.06, 74.68, 316.68
3	6	$P2_12_12_1$	15.140, 8.626, 9.728. 317.63	15.140, 8.627, 9.729, 317.61
4	10	$C2/c$	17.700, 8.986, 17.640, 66.80, 322.37	17.701, 8.986, 17.640, 66.79, 322.35
5	7	$P\bar{1}$ [a]	9.819, 9.054, 8.941, 107.65, 99.55, 115.33, 321.49	10.199, 9.054, 8.941, 107.66, 116.59, 102.12, 321.49
6	8	$C2/c$	12.253, 12.895, 16.892, 73.19, 319.37	12.253, 12.895, 16.892, 73.19, 319.37
7	5	$P2_1/c$	8.499, 18.756, 9.034, 117.90, 318.19	8.499, 18.755, 9.034, 117.88, 318.18
8	4	$P2_12_12_1$	9.514, 13.794, 9.869, 323.78	9.512, 13.798, 9.869, 323.82
9	2	$P2_1$	14.823, 6.617, 6.640, 103.21, 316.98	14.823, 6.613, 6.642, 103.22, 316.97
10	9	$P\bar{1}$ [a]	6.573,12.284, 8.702, 113.63, 94.07, 93.13, 319.69	6.573, 12.931, 8.701, 114.13, 94.07, 104.84, 319.69

The molecular conformation for rigid body simulation is taken from predicted frames (Appendix II)

[a] The variation in cell parameters is high for triclinic crystal systems. The structures are determined to be identical by matching simulated powder XRD patterns and molecular packing diagrams.

Table 8. U_{latt} of lowest energy frame by rigid body method starting from the molecular conformation in full body minimized frames #1-10. E_{conf} is calculated in Spartan 04. The simulated structures of **1** are re-ranked based on intra- and intermolecular energy sum, E_{total} [kcal mol^{-1}].

Frame # in full body method[a]	Space group[b]	U_{latt} in rigid body method [kcal mol^{-1}]	E_{conf}[c] [kcal mol^{-1}]	$E_{\text{total}} = U_{\text{latt}} + E_{\text{conf}}$ [kcal mol^{-1}]	Re-ranking of frames based on E_{total}
3	$P2_1$[d]	−30.93	1.38	−29.55	1
1	$P\bar{1}$	−30.83	2.03	−28.80	2
6	$P2_12_12_1$	−30.91	2.25	−28.66	3
10	$C2/c$	−30.42	1.82	−28.60	4
7	$P\bar{1}$	−30.88	2.59	−28.29	5
8	$C2/c$	−30.06	1.82	−28.24	6
5	$P2_1/c$	−30.85	2.79	−28.06	7
4	$P2_12_12_1$	−30.01	2.14	−27.87	8
2	$P2_1$	−31.03	3.27	−27.76	9
9	$P\bar{1}$	−29.88	2.37	−27.51	10

[a] Taken from Appendix II.
[b] See Table S3 for matching cell parameters.
[c] Relative to the stable gas-phase rotamer, E_{conf} = −479812.98 kcal mol^{-1}.
[d] Unit cell in full body/rigid body minimized structure: 7.712/7.713 Å, 8.286/8.289 Å, 10.415/10.412 Å, 75.68/76.65º, 322.45/322.44 Å^3.

2.6 Conclusions

In the present study it has been shown that selective growth of kinetic and thermodynamic form can be achieved from a concomitant polymorphic system where different forms lie in shallow energy profile and very close energy differences. Our experimental and computational results on tetramorphic cluster A-D of diphenyl quinone **1** are summarized as:

❖ Thermodynamic form A is enatiotopically related with other forms in the temperature range 30-80 °C. Pure form A can be obtained heating of the concomitant mixture above 70 °C. Form B is the kinetic form prepared by melting of the sample at 115 °C. These data were verified by VT-PXRD experiment which is a useful tool for monitoring phase transformations.

❖ Computation of energy for conformational polymorph A-D support the thermodynamic relation and enatiotopic transformation of different form to stable form A. Different modification lie in the 0.3 kcal mol^{-1} (~1.3 kJ mol^{-1}) energy window range. This value serves as a benchmark for future work on concomitant polymorphs; crystal structures that usually lie in a shallow potential energy well.

❖ Importance of weak but directional C–H⋯O interactions promote multiple molecules in the asymmetric unit for the compound **1**. High Z' forms stabilized by shorter H⋯O distance, whereas stable form A have longer H⋯O distance. This study show that even weak C–H⋯O hydrogen bonds follow similar trend like what strong O–H⋯O interaction do for the high Z' structures of monoalcohols, phenols and cholesterol.

❖ Lattice and conformational energy computation support the interplay of minimization of intramolecular (rotamer) and intermolecular (interaction) energies for the occurrence of conformational polymorphism in **1**. Stable form can be obtained from a metastable conformation, where better packing make up the intramolecular energy penalty.

❖ Re-production of thermodynamic form A computationally by full body minimization of lattice energy predicts as in frame #3 based on U_{latt}. Ra-ranking of predicted frame based on consideration of E_{conf} contribution and U_{latt} (rigid component) gives global minimum structure #1 matching with form A.

This present exercise validate the kinetic and thermodynamic occurrence of conformational polymorphs separated by < 0.3 kcal mol^{-1}.

2.7 Experimental Section
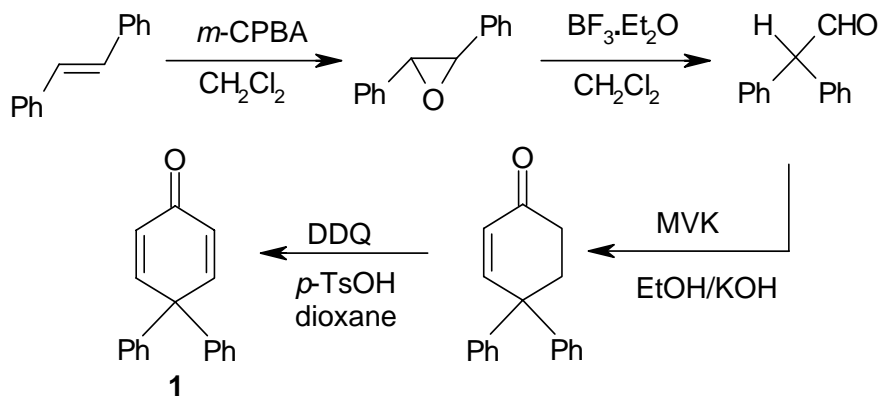
Compound **1** is prepared in four steps as shown in Scheme above.[32]

To a stirred solution of *m*-CPBA (1.14 g, 6.6 mmol) in 15 ml of dry CH_2Cl_2 was added *trans*-stilbene (1.1 g, 6.0 mmol) in CH_2Cl_2 solution (60 ml) drop wise at 0 °C. The reaction was continued for 30 h. The mixture was washed with $NaHCO_3$ solution and cold water. The resulting epoxide was extracted with CH_2Cl_2 solvent and evaporated *in vaccuo* to give pure *trans*-stilbene oxide (1.2 g, 95%).

To a stirred solution of *trans*-stilbene oxide (1.20 g, 6.0 mmol) in dry CH_2Cl_2 (60 ml) with $BF_3.Et_2O$ (0.5 ml, 225 mg, 3.0 mmol) was added drop wise for 5 min then stirring continues for 30 min at 0 °C. The reaction mixture was washed with 50 ml water twice and the solvent evaporated to obtain diphenyl acetaldehyde (960 mg, 80%).

To a mixture of diphenyl acetaldehyde (700 mg, 3.6 mmol) and methyl vinyl ketone (MVK, 0.3 ml, 3.7 mmol) in 30 ml dry THF was added 0.5 ml of 3N ethanolic KOH drop wise over a period of 5 min at 0 °C. The mixture was stirred for 2 h at 0 °C and then for 2 h at room temperature. Reaction mixture neutralized with 20% HCl and extracted with EtOAc to obtain crude product. Purification by column chromatography yielded pure 4,4'-diphenyl-2-cyclohexenone (440 mg, 50%).

To a solution of the above cyclohexenone (248 mg, 1.0 mmol) in 40 ml of 1,4-dioxane was added DDQ (908 mg, 4.0 mmol) and a catalytic amount of *p*-TsOH (15 mg,

0.1 mmol) and the solution was refluxed for 72 h. After cooling, the reaction mixture was filtered through celite and the filtrate was diluted with CH_2Cl_2, washed thrice with 30 ml 10% NaOH solution. Work up gave the crude product which was purified on silica gel column to obtain pure 4,4-diphenyl-2,5-cyclohexadienone **1** (100 mg, 40%). M.P. 120° C, ^{1}H NMR [400 MHz, δ, $CDCl_3$]: 6.38 (d, J = 10 Hz, 2H, α-enone Hs), 7.25-8.15 (m, 12H, Ph + β-enone Hs). IR [KBr]: 3028, 1655, 1620, 1487, 1446, 1400, 1267, 1226 cm^{-1}.

Crystallization of Polymorphs A-D

The pure solid **1** after column chromatography was analyzed by powder XRD. The bulk material (100 mg of the solid) shows all four forms A-D in the concomitant crystallization batch (Figure 5): monoclinic form A 37.5%, triclinic forms B + C 52.0%; orthorhombic form D 10.5%.

Polymorphic forms A, B and C were crystallized by slow evaporation of a solution of **1** in 5% EtOAc/*n*-hexane at ambient temperature. Three types of morphologies were observed: needle, block, plate. Needle type crystals correspond to form A and block/plate crystals correspond to form B as confirmed by random cell checking of different crystals. Crystallization by slow evaporation at –5 ºC in domestic refrigerator yielded form A whereas crystal growth from saturated solution by fast evaporation at ambient temperature yielded form B predominantly. Crystals of form D were obtained from CH_2Cl_2/EtOAc/*n*-hexane solvent mixture. In recent batches crystal corresponding to form C was not found of random cell checking on the CCD diffractometer.

Pure Form A: 100 mg of the polymorphic mixture **1** was taken in a test tube and heated at ~70 °C for 30 min in an oil bath and cooled slowly to room temperature. The mixture converted to form A in >95% purity as confirmed by powder XRD (Figure 8a).

Pure Form B: 100 mg of the polymorphic mixture **1** was heated in the aluminum pan of powder X-ray diffractometer until the compound melts (~120 °C). The cooled solid is form B (powder XRD in Figure 8b).

Differential Scanning Calorimetry

DSC was performed on Mettler Toledo 822e module. Samples (4-6 mg) were placed in crimped but vented aluminum pans and heated @ 10 °C min⁻¹ from 30-200 °C. The instrument was purged with a stream of dry nitrogen @ 150 ml min⁻¹.

Spartan 04, Gaussian 03 and *Cerius*² Computations

*Cerius*² simulations and crystal energy:[25] All simulations were carried out in version 4.8 of *Cerius*² molecular modeling environment running on Silicon Graphics workstation. Geometry optimization was carried out using density functional theory (DFT) at the B3LYP/6-31G (d,p) level in Gaussian 03.[31] The global minimized rotamer of **1** from Gaussian 03 was entered as the input for Polymorph Predictor. Crystal structure prediction was carried out in six common space groups ($P2_1$, $P2_1/c$, $C2/c$, $Pbca$, $P2_12_12_1$, $P\overline{1}$). Cell parameters of predicted frames in $C2/c$ were compared with reduced cell parameters to confirm that they represent different structures. Reduced cell parameters are used for comparison. Atom point charges were assigned in COMPASS force field. Default options were used throughout with fine search option in Monte Carlo simulation and for clustering of frames to get unique structures. Lattice energy minimization of predicted structures was carried out without any modifications except for the use of Ewald summation of van der Waals interactions at a cut-off of 6.0 Å. All calculations were carried out either by relaxing the molecular conformation during the minimization, referred to as full body method, or by keeping the conformation fixed during minimization, the so-called rigid body method. Full body lattice energy minimizations were carried out even though these calculations take ~5-fold longer computer-time because this method gives more accurate results for flexible molecules, such as **1**. Lattice energies were computed for experimental polymorphs of **1** in *Cerius*² program by energy minimization of crystal structures in DREIDING 2.21 and COMPASS. Force field charges were assigned in COMPASS and charge equilibrium method was used in DREIDING 2.21. COMPASS is better parameterized for structure prediction and energy of organic molecules. Crystal lattice energies are calibrated for the number of molecules in the unit cell (per molecule).

Energy of all 19 conformers were calculated in Spartan 04[24] using crystallographic coordinates as the input; hydrogen atom positions were re-optimized at the HF/6-31G** level while keeping the heavy atoms fixed. The gas-phase conformation of **1** was obtained by global energy minimization. The gas phase rotamer of **1** calculated in Spartan 04 ($\tau_1 = \tau_2 = 22.3°$) is very similar to the minimized conformation in Gaussian 03[31] ($\tau_1 = \tau_2 = 23.8°$).

Variable Temperature Powder X-ray Diffraction

Powder data were collected on PANlytical X'Pert PRO X-ray powder diffractometer using a parallel beam of monochromated Cu-K$_\alpha$ radiation ($\lambda = 1.54056$ Å) and an X'celerator detector at 40 kV and 40 mA. Diffraction patterns were collected over the 2θ range 5-50º. Samples were loaded in an 18-mm alumina holder for variable temperature powder X-ray diffraction data collection and an aluminum sample holder with a 10 mm diameter sample cavity for room temperature data. The program X'Pert High Score was used for the processing and comparison of powder patterns. Powder Cell 2.3[20] was used for calculating PXRD patterns and for profile fitting and least square refinement of unit cell parameters, a displacement parameter, a background polynomial function, peak shape asymmetry terms, and an overall temperature factor using the known single-crystal structures of polymorphs A, B and D as the model. Temperature settings for the variable temperature powder X-ray diffraction data were set at T = 28, 39, 49, 59, 69, 79, 89, 94, 98, 102, and 105 °C. The sample was cooled to room temperature (31 °C) and data were recollected. Powder XRD profiles are plotted in the range $2\theta = 10$-34° for all samples. There are no significant peaks below 10° and only minor peaks between 35-50°. There are wide peaks at 25.2° and 34.8° from the sample holder.

2.8 References

1. (a) J. Bernstein, *Polymorphism in Molecular Crystals*, Clarendon, Oxford, **2002**.
    (b) H. G. Brittain, *J. Pharm. Sci.*, **2007**, *96*, 705. (c) P. Vishweshwar, J. A.

McMahon, M. Oliveira, M. L. Peterson and M. J. Zaworotko, *J. Am. Chem. Soc.*, **2005**, *127*, 16802. (d) Ö. Almarsson and M. J. Zaworotko, *Chem. Commun.*, **2004**, 1889.

2. (a) A. Kálmán, L. Fábián, G. Argay, G. BernPth and Z. Gyarmati, *J. Am. Chem. Soc.*, **2003**, *125*, 34. (b) I. Weissbuch, V. Y. Torbeev and L. Leiserowitz, M. Lahav, *Angew. Chem. Int. Ed.*, **2005**, *44*, *3226*. (c) J. D. Dunitz and J. Bernstein, *Acc. Chem. Res.*, **1995**, *28*, 193. (d) H. Chow, P. A. W. Dean, D. C. Craig, N. T. Lucas, M. L. Scudder and I. G. Dance, *New J. Chem.*, **2003**, *27*, 704. (e) M. Morimoto, S. Kobatake and M. Irie, *Chem. Eur. J.*, **2003**, *9*, 621.

3. (a) M. M. de Villiers, R. J. Terblanche, W. Liebenberg, E. Swanepoel, T. G. Dekker and M. Songa, *Journal of Pharmaceutical and Biomedical Analysis*, **2005**, *38*, 435. (b) A. V. Trask, N. Shan, W. D. S. Motherwell, W. Jones, S. Feng, R. B. H. Tan and K. J. Carpenter, *Chem. Commun.,* **2005**, 880. (c) S. Gracin, M. Uusi-Penttilä and Å. C. Rasmuson, *Cryst. Growth Des.*, **2005**, *5*, 1787.

4.   (a) Ö. Almarsson, M. B. Hickey, M. L. Peterson, S. L. Morissette, S. Soukasene, C. McNulty, M. Tawa, J. M. MacPhee and J. F. Remenar, *Cryst. Growth Des.*, **2003**, *3*, 927. (b) M. L. Peterson, S. L. Morissette, C. McNulty, A. Goldsweig, P. Shaw, M. LeQuesne, J. Monagle, N. Encina, J. Marchionna, A. Johnson, M. J. Cima and Ö. Almarsson, *J. Am. Chem. Soc.*, **2002**, *124*, 10958.

5. D. Grooff, M. M. De Villiers and W. Liebenberg, *Thermochimica Acta*, **2007**, *454*, 33.

6. T. V. Timofeeva, G. H. Kuhn, V. V. Nesterov, Vladimir N. Nesterov, D. O. Frazier, B. G. Penn and M. Y. Antipin, *Cryst. Growth Des.*, **2003**, *3*, 383.

7. J. Bernstein, in *Organic Solid State Chemistry*, Ed. G. R. Desiraju , Elsevier, Amsterdam, **1987**, pp. 471-518.

8. (a) T. C. Lewis, D. A. Tocher and S. L. Price, *Cryst. Growth Des.*, **2004**, *4*, 979. (b) C. Ouvard and S. L. Price, *Cryst. Growth Des.*, **2004**, *4*, 1119. (c) H. Nowell and S. L. Price, *Acta Cryst.*, **2005**, *B61*, 558.

9.   (a) L. Yu, G. A. Stephenson, C. A. Mitchell, C. A. Bunnell, S. V. Snorek, J. J. Bowyer, T. B. Borchardt, J. G. Stowell and S. R. Byrn, *J. Am. Chem. Soc.*, **2000**, *122*, 585. (b) S. Chen, I. A. Guzei and L. Yu, *J. Am. Chem. Soc.*, **2005**, *127*, 9881.

10. V. S. S. Kumar, A. Addlagatta, A. Nangia, W. T. Robinson, C. K. Broder, R. Mondal, I. R. Evans, J. A. K. Howard and F. H. Allen, *Angew. Chem. Int. Ed.*, **2002**, *41*, 3848.

11. G. R. Desiraju, *Acc. Chem. Res.*, **2002**, *35*, 565.

12. J. Bernstein, R. E. Davis, L. Shimoni and N.-L. Chang, *Angew. Chem. Int. Ed. Engl.*, **1995**, *34*, 1555.

13. (a) V. S. S. Kumar and A. Nangia, *Chem. Commun.*, **2001**, 2392.(b) V. S. S. Kumar, *PhD Thesis*, University of Hyderabad, **2002**.

14.   (a) N. Blagden, R. J. Davey, H. F. Lieberman, L. Williams, R. Payne, R. Roberts, R. Rowe and R. Docherty, *J. Chem. Soc.*, *Faraday Trans.*, **1998,** *94*, 1035. (b) I. Bar and J. Bernstein, *J. Pharm. Sci.*, **1985**, *74*, 255. (c) M. Takasuka, H. Nakai and M. Shiro, *J. Chem. Soc., Perkin Trans. 2*, **1982,** 1061 (d) M. Tamura, Y. Hosokoshi, D. Shiomi, M. Kinoshita, Y. Nakasawa, M. Ishikawa, H. Sawa, T. Kitazawa, A. Eguchi, Y. Nishio and K. Kajita, *J. Phys. Soc. Jpn.*, **2003** *72*, 1735. (e) H. Nakai, K. Ezumi and M. Shiro *Acta Cryst.*, **1981**, *B37*, 193. (f) M. Morimoto, S. Kobatake and M. Irie, *Chem. Eur. J.*, **2003**, *9*, 621.

15. (a) N. I. Golovina, A. V. Raevsky, N. V. Chukanov, B. L. Korsunsky, L. O. Atovmyan and S. M. Aldoshin, *Ross. Khim. Zhurnal*, **2004**, *48*, 41. (b) A. D. Bond, D. A. Haynes, C. M. Pask and J. M. Rawson, *J. Chem. Soc., Dalton Trans.*, **2002**, 2522. (c) G. Reck, V. Hagen and E.Hohne, *Pharmazie*, **1986**, *41*, 181. (d) B. Kahr and R. L. Carter, *Mol. Cryst. Liq. Cryst. Sci. Technol.*, **1992**, *219*, 79. (e) S. Tanisaki, H. Mashiyama and K. Hasebe, *Acta Cryst.*, **1988**, B*44*, 441.

16. F. H. Allen and R. Taylor, *Chem. Soc. Re*v., **2004**, *33*, 463. www.ccdc.cam.ac.uk.

17. J. W. Steed, *CrystEngComm*, **2003**, *5*, 169.

18. (a) C. P. Brock and L. L. Duncan, *Chem. Mater.*, **1994**, *6*, 1307. (b) C. P. Brock, *Acta Cryst.*, **2002**, *B58*, 1025. (c) A. Gavezzotti and G. Fillippini, *J. Phys. Chem.*, **1994**, *98*, 4831.

19. (a) H. Jacobsen, H. W. Schmalle, A. Messmer and H. Berke, *Inorg. Chem. Acta*, **2000**, *306*, 153. (b) G. S. Nichol and W. Clegg, *Cryst. Growth Des.*, **2006**, *6*, 451.

20. Least square refinement was carried out using Powder Cell 2.3. N. Krauss, G. Nolze, Federal Institute for Materials Research and Testing, Berlin, Germany, **2000**.

21. J.-O. Henck, J. Bernstein, A. Ellern and R. Boese, *J. Am. Chem. Soc.*, **2001**, *123*, 1834.

22. W. Ostwald, *Z. Phys. Chem.*, **1897**, *22*, 289.

23. L. Yu, *J. Am. Chem. Soc.*, **2003**, *125*, 6380.

24. Spartan 04, Irvine, CA. www.wavefun.com.

25. *Cerius*[2] suite of software for crystal lattice energy calculation and crystal structure prediction are crystal packer and polymorph predictor. www.accelrys.com.

26. A. Dey, M. T. Kirchner, V. R. Vangala, G. R. Desiraju, R. Mondal and J. A. K. Howard, *J. Am. Chem. Soc.*, **2005**, *127*, 10545.

27. H. Sun, *J. Phys. Chem.* **1998**, *102*, 7338.

28. D. Das, R. Banerjee, R. Mondal, J. A. K. Howard, R. Boese and G. R. Desiraju, *Chem. Commun.*, **2006**, 555.

29. (a) W. D. S. Motherwell, H. L. Ammon, J. D. Dunitz, A. Dzyabchenko, P. Erk, A. Gavezzotti, D. W. M. Hofmann, F. J. J. Leusen, J. P. M. Lommerse, W. T. M. Mooij, S. L. Price, H. Scheraga, B. Schweizer, M. U. Schmidt, B. P. van Eijck, P. Verwer, D. E. Williams, *Acta Cryst.*, **2002**, *B58*, 647. (b) G. M. Day, W. D. S. Motherwell, H. Ammon, S. X. M. Boerrigter, R. G. Della Valle, E. Venuta, A. Dzyabchenko, J. D. Dunitz, B. Schweizer, B. P. van Eijck, P. Erk, J. C. Facelli, V. E. Bazterra, M. B. Ferraro, D. W. M. Hofmann, F. J. J. Leusen, C. Liang, C. C. Pantelides, P. G. Karamertzanis, S. L. Price, T. C. Lewis, H. Nowell, A.

Torrisi, H. A. Scheraga, Y. A. Arnautova, M. U. Schmidt, P. Verwer, *Acta Cryst.*, **2005**, *B61*, 511.

30. G. M. Day, A. V. Trask, W. D. S. Motherwell and W. Jones, *Chem. Commun.*, **2006**, 54.

31. M. J. Frisch *et al*, Gaussian 03, Revision B.05. www.gaussian.com.

32. (a) D. J. Reif and H. O. House, *Org. Syn.*, **1963**, *Coll. Vol. IV*, 860. (b) D. J. Reif, H. O. House, *Org. Syn.*, **1963**, *Coll. Vol. IV*, 375. (c) A. C. Cope, P. A. Trumbell, E. R. Trumbell, *J. Am. Chem. Soc.*, **1958**, *80*, 2844. (d) H. E. Zimmerman, K. G. Hancock, G. C. Licke, *J. Am. Chem. Soc.*, **1968**, *90*, 4892. (e) K.-B. Chai, P. Sampson, *J. Org. Chem.*, **1993**, *58*, 6807.

VARIABLE TEMPERATURE POWDER X-RAY DIFFRACTION AND CRYSTAL STRUCTURE REPRODUCTION OF 2,6-DIMETHYL-4-(α,α-DIPHENYLMETHYLENE)-1,4-BENZOQUINONE

3.1 Introduction

The occurrence of polymorphism in flexible systems continues to be reported regularly, with conformational changes being highlighted.[1] Conformationally flexible molecules can exhibit various packing arrangements because of changes in soft torsion parameter of almost similar conformer energy.[2] As discussed in chapter 2, the difference in lattice energies observed between polymorphic forms is comparable with the energy range required to bring about changes in molecular torsional parameters of single bonds. The present work focuses on the polymorphs transition of dimethyl fuchsone [2,6-dimethyl-4-(α,α-diphenylmethylene)-1,4-benzoquinone] **4**, which is known exist as three conformational polymorphs.[3] Compound **4** may be viewed as a derivative of methylene extended homologue of compound **1**. Predicting crystal structure from molecular skeleton using the previous knowledge on crystal packing is important to improve computational methodology. Reproduction of crystal structure of **4** was done with the iterative method described in previous chapter to further validate the method of evolution from molecule → conformation → crystal.

4
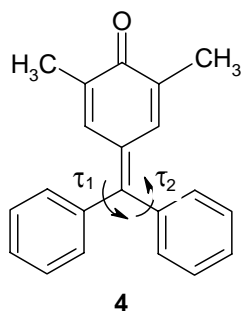
Scheme 1. 2,6-dimethyl-4-(α,α-diphenylmethylene)-1,4-benzoquinone

3.2 Dimethyl Fuchsone Polymorphs: An overview

Structural study of conformational polymorphs of 2,6-dimethyl-4-(α,α-diphenylmethylene)-1,4-benzoquinone **4** was done by Paul and Curtin in the 1980's.[3] Three crystalline modifications α, β and γ forms in space group $P2_1/c$, $P2_12_12_1$ and $Pna2_1$ having one molecule each in the asymmetric unit (Table 1).[3,4] Phase transition of achiral α form to chiral β form and their structural relationship was discussed. Molecule **4** has only one acceptor carbonyl group with several phenyl and methyl C–H donors. Crystal structures of all the three forms are stabilized by C–H⋯O interactions (Table 2). In α-form screw related molecule propagate along [010] plane to form form a 2D polar layer (Figure 1a). Alternate 2D layers are arranged in opposite directions. Crystal structure of β-form also have similar 2D layers arrangement of molecule with meta hydrogen of one of the phenyl ring engaged in C–H⋯O interaction with carbonyl acceptor in same layer (Figure 1b). Interestingly in α-form orientation of neighboring molecules are positioned 120° with respect to the quinone like ring with molecule of adjacent layer (Figure 1c), whereas in β-form corresponding angle is 180° (Figure 1d).[3] The packing in γ form is completely different from α and β-forms. Two para hydrogens of phenyl ring are involved in bifurcated C–H⋯O interaction with translation and glide related molecules to form square channels (Figure 1e). A two fold interpenetration complets the close packing (Figure 1f).

(a)

(b)

(c)

(d)

(c)

(d)
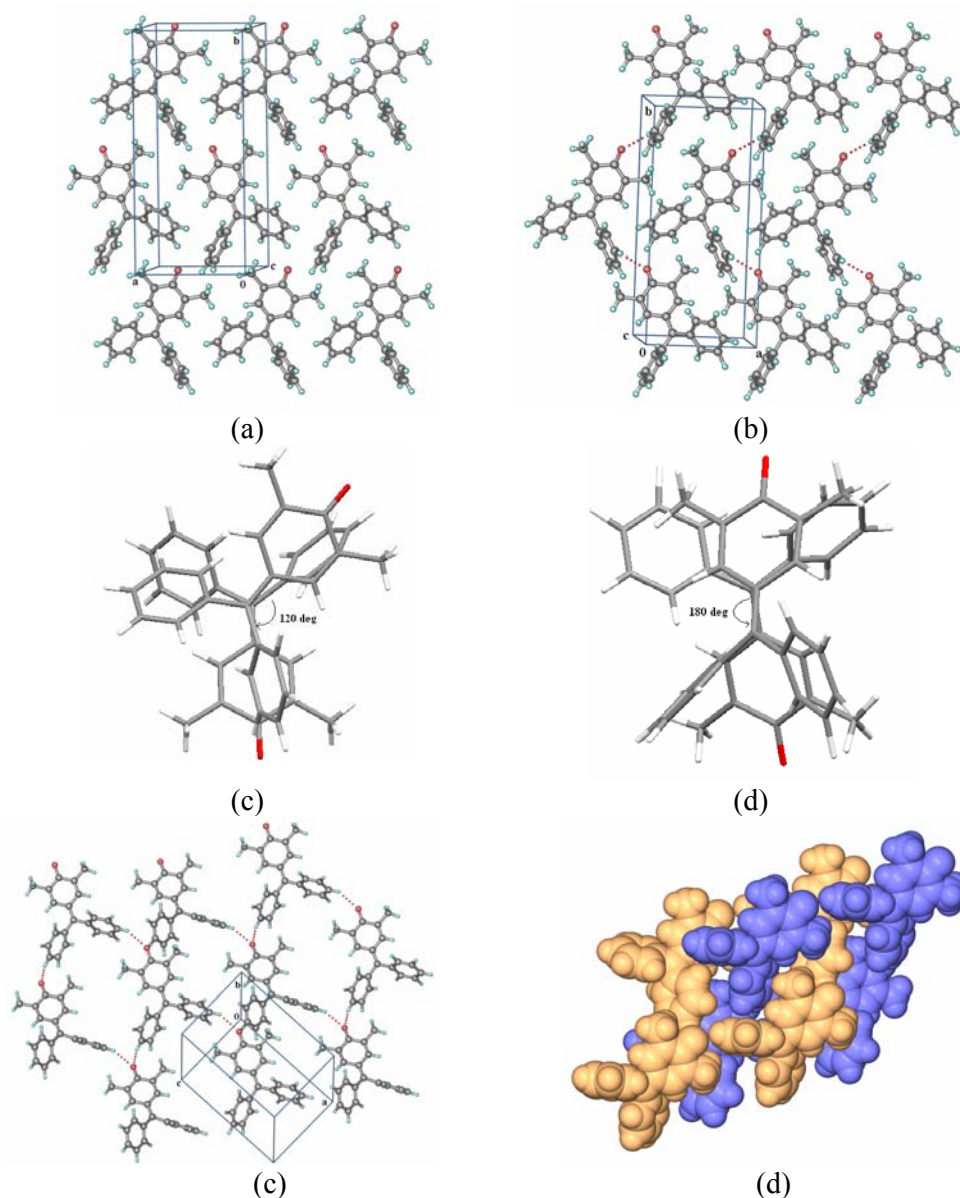
Figure 1. (a) In α-form of **4** the molecules form a 2D polar layer. Two adjacent layer stabilized through C–H···O hydrogen bonding. (b) C-H···O hydrogen bonded chains zig-zag pattern in the crystal structure of the β-form of **4** forming one direction 2D polar layer. Orientation of neighboring molecules in adjacent layer for (c) α-form and (d) β-form (e) Bifurcated C–H···O hydrogen bonded network in the crystal structure of the γ-form. (f) Presence of two fold interpenetration between square channel.

We revisited phase transition in polymorphs of **4** using variable temperature powder X-ray diffraction (VT-PXRD).

3.3 Variable Powder X-ray Diffraction Study

Routine crystallization of **4** afforded mostly single crystals of α and β forms from various solvents like ethyl acetate, benzene, toluene, 1,4-dioxane, chloroform as confirmed by single crystal cell checking. However a typical crystallization of dimethyl fuchsone **4** from EtOAc showed the presence of α form (~80%), β form (~18%), and γ form (~2%) in the bulk solid (Figure 2)**.** These ratios were determined by least squares refinement of the observed powder XRD with simulated peaks of each crystal structure.[5]
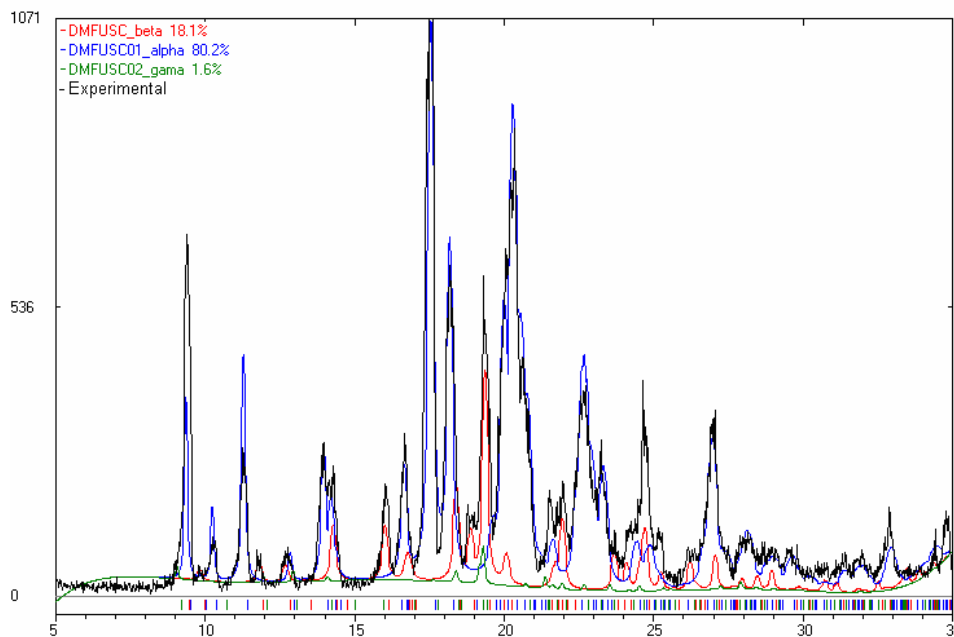
Figure 2. Powder X-ray diffraction of solid **4** at room temperature shows alpha form (~80%), beta form (~18%), and D (~2%) present as concomitant mixture.

Differential scanning calorimetry (DSC) of the polymorphic mixture **4** obtained from EtOAc solvent showed a single endotherm peak at 202.53 °C (Figure 3), corresponding to the melting point of **4**. There were peaks indicating phase transition prior to melting. The flat base line in DSC profile imply there may be enthalpy changes,

but those are too weak to be detected in routine DSC. We observed similar single peak melting endotherm DSC in **1** having 4 polymorphs.

Integral   -478.76 mJ
  normalized -112.38 Jg^-1
Onset   201.24 °C
Peak   202.53 °C
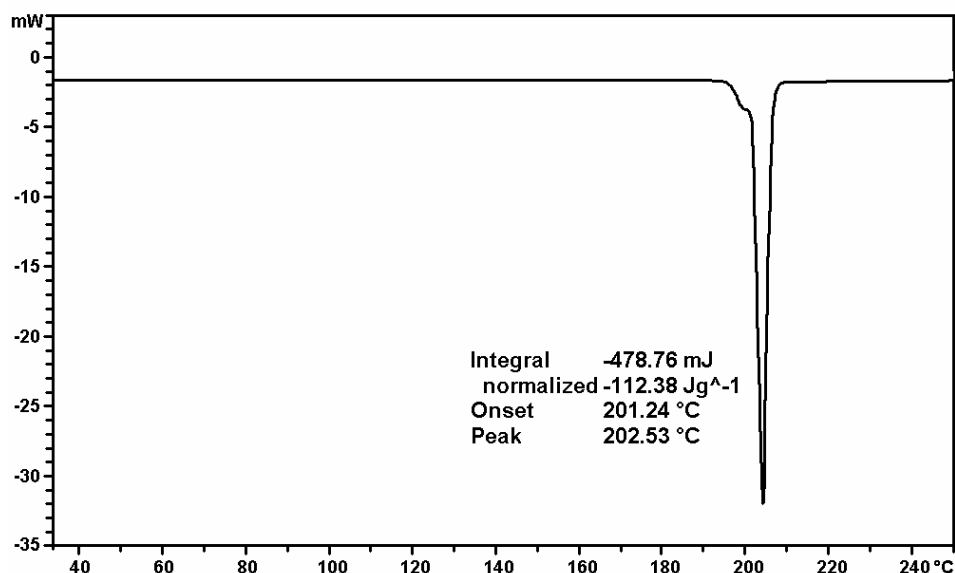
Figure 3. DSC of dimethyl fuchsone **4** recorded at scan rate of 2 °C min^{-1}. All three polymorphs melt at the same temperature (T_{endo} = 201-202 °C). There is a small shoulder endotherm at 200 °C.

        The concomitant mixture of three forms at room temperature was heated in variable powder X-ray diffraction (VT-PXRD) experiments to understand phase transition behavior. The peak profile is relatively invariant between 30-100 °C (Figure 4). Major changes in the powder line are observed as the sample was heated to 168 °C. Certain peaks disappeared and the overall pattern becomes significantly sharper. Further heating of the sample does not show changes in peak profile upto ~180 °C. After this temperature material becomes amorphous and then semi-solid/melt at 190-200 °C. VT-PXRD shows that upon heating concomitant mixture of polymorphs α, β and γ to a pre-melting temperature of 168 °C transforms the mixture to β-form (Figure 5) in good polymorphic purity (>97%). Orthorhombic polymorph β is perhaps the thermodynamic modification in the enantiotropic system of polymorphs of **4** between 30-180 °C.

Experimental conditions are optimized to crystallize thermodynamic stable β-form of the enantiotropic cluster.
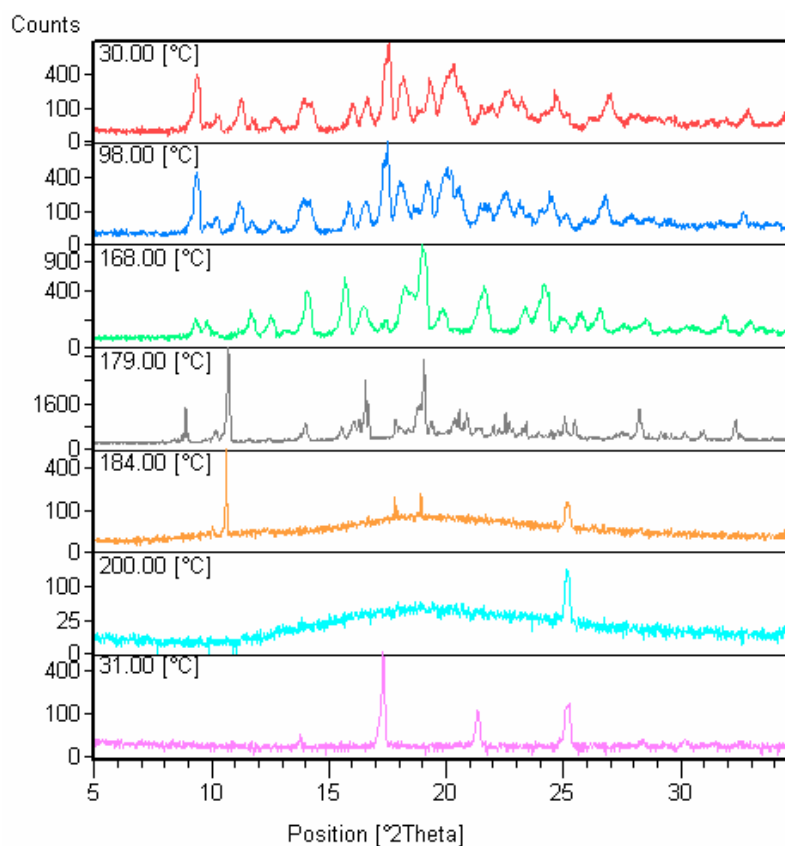
Figure 4. Powder X-ray diffraction patterns of **4** recorded at different temperatures during a heating experiment.
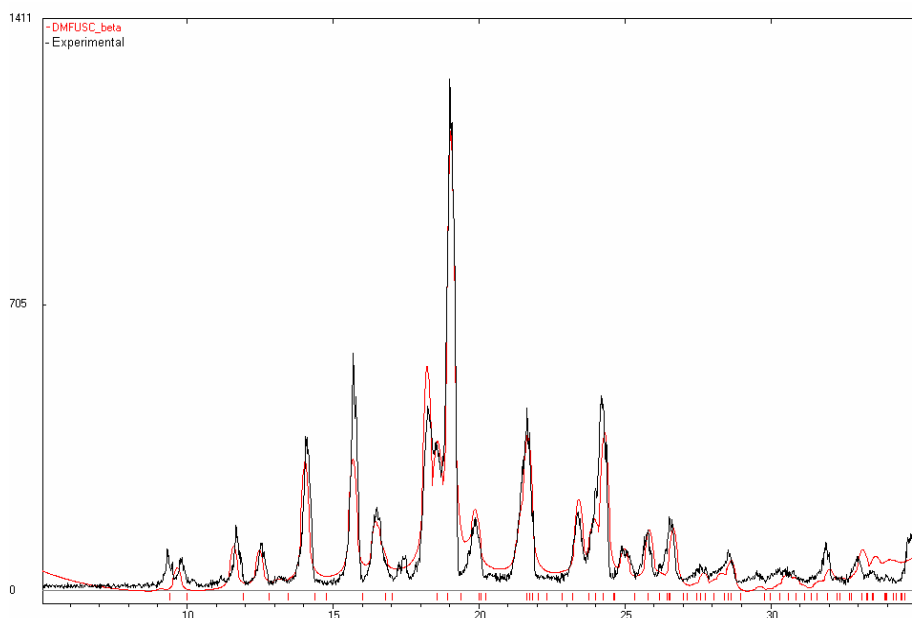
Figure 5. Experimental powder XRD of **4** at 168 °C (black line) matches nicely with the calculated powder pattern of β form (red line)

3.4 Lattice and Conformation Energy

Crystal lattice energies, U_{latt}, of three conformational polymorph of **4** were computed in COMPASS and DREIDING 2.21 force fields (Table 3, *Cerius*[2])[6] by energy minimization of the experimental crystal structures. COMPASS[7] is better suited for molecule **4** like molecule **1** described in chapter 2, because electrostatic stabilization from C−H···O hydrogen bonds and aromatic interactions is included. COMPASS values were considered for the stability ranking of the three forms of **4.** Crystal structure of α-form has the most stable lattice ($U_{latt} = -37.17$ kcal mol^{-1}) and forms β, γ are less stable by 0.45 and 0.43 kcal mol^{-1}, respectively. According to U_{latt} value the stability order of the trimorphs is α < γ < β. This lattice energy value show β is the least stable form.

Table 3. Lattice energies [U_{latt}, kcal mol^{-1}] of three polymorphs computed in *Cerius*^{2}, corrected to per molecule of **4**.

U_{latt}	α Form (*P*21/*c*)		β Form (*P*2₁2₁2₁)		γ Form (*P*na21)	
	COM PASS	DREIDING 2.21	COM PASS	DREIDING 2.21	COM PASS	DREIDING 2.21
Total	−37.17	−41.44	−36.72	−40.49	−36.74	−40.82
van der Waals	−34.19	−32.84	−33.55	−32.08	−33.46	−32.03
Electrostatic	−2.98	−8.60	−3.17	−8.41	−3.28	−8.79
Hydrogen bond[a]	-----	0.00	-----	0.00	-----	0.00

[a] Hydrogen bond energy is partitioned in DREIDING 2.21 but it is part of the Coulomb component in COMPASS force field.

Three symmetry-independent molecular conformers exist in the asymmetric unit of three forms of compound **4** differ only in phenyl ring torsion (Figure 6). However α and β forms have very similar conformations, whereas in γ form phenyl ring position is little outward directed. These different conformations may be represented through minimum four possible torsion angles (τ_1, τ_2, τ_3 and τ_4) for the molecule **4** (Scheme 2). Torsional angle vary within 3-5 ° for the different conformation of **4** in three different polymorphs (Table 4). Conformation energy (E_{conf}) was calculated in Spartan 04[8] (Table 5). The molecule was extracted from the crystal structure[3] and energy minimized (HF/6-31G**) keeping the conformation fixed (heavy C and O atoms invariant) and H atoms were allowed to relax to reasonable geometries.[9] Among the three conformers α form has the most stable conformation with energy value E_{conf} = −5,52,575.44 kcal mol^{-1} and forms β, γ are less stable by 0.61 and 9.48 kcal mol^{-1}, respectively. Lattice and conformation energy calculation show α form is stable in both ways to have a win-win situation. Taking into account intra- and intermolecular the energies (E_{total}): α form < β form < γ form (Table 5). Crystal structure of β form is thermodynamically stable in experiments but it is 1 kcal mol^{-1} higher in energy than α form. The variation between computation and experiments is difficult to explain with the available data.

τ_1= C3-C4-C7-C8
τ_2= C3-C4-C7-C14
τ_3= C4-C7-C14-C15
τ_4= C4-C7-C8-C9
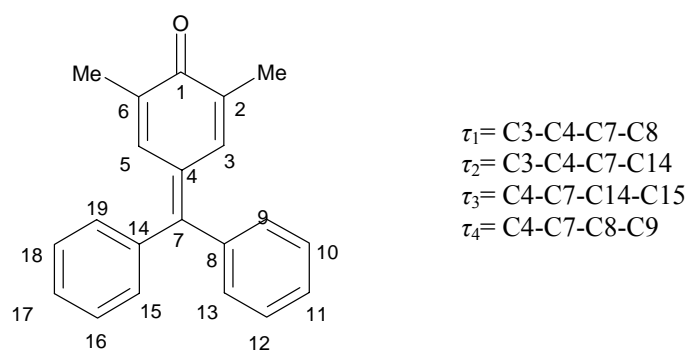
Scheme 2. Torsion angle definition τ_1- τ_4.

Table 4. Torsion angle values for three conformational polymorphs of **4**.

Torsion angle	α Form (°)	β Form (°)	γ Form (°)
τ_1	20.1	17.3	17.1
τ_2	20.0	18.7	19.3
τ_3	41.1	40.1	43.3
τ_4	48.9	47.8	54.3
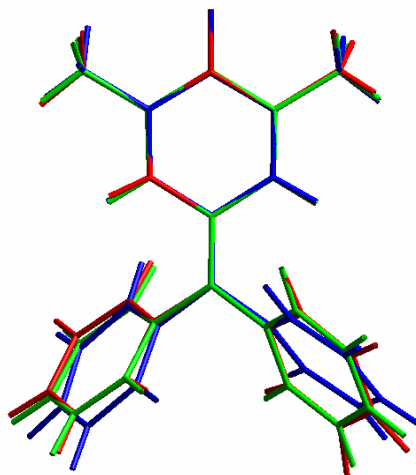
Figure 6. Overlay of symmetry-independent dimethyl fuchsone molecules. α-form (red), β-form (green), γ-form (blue).

Table 5 Lattice energy (U_{latt}, *Cerius*[2], COMPASS, kcal mol–1), conformation energy (E_{conf} *SPARTAN*, HF/6-31G**, kcal mol–1) and total energy ($\Delta E_{total} = \Delta U_{latt} + \Delta E_{conf}$)

Polymorph	U_{latt}	ΔU_{latt}	E_{conf}	ΔE_{conf}	ΔE_{total}
α Form $P2_1/c$	−37.17	0.00	−5,52,575.44	0.00	0.00
β Form $P2_12_12_1$	−36.72	+0.45	−5,52,574.83	0.61	1.06
γ Form $Pna2_1$	−36.74	+0.43	−5,52,565.96	9.48	+9.91

3.5 Crystal Structure reproduction

Crystal structure reproduction is done to find out whether the hypothetical energy minimized structures matches with the known polymorphs and to evaluate the efficacy of existing programs and force fields for crystal structure prediction (CSP). The *ab initio* energy minimized molecular conformation of **4** calculated in Gaussian 03[10] was taken as the starting geometry to generate hypothetical crystal structural in the *Cerius*[2] PP module. Crystal structure prediction (CSP) was carried out in six common space groups including observed space group ($P2_1/c$, $P\overline{1}$, $C2/c$, $P2_1$, $P2_12_12_1$ and $Pna2_1$) using the COMPASS force field. Conformation in the predicted structures allowed to vary during energy minimization of frames (full body minimization) to cover the complete landscape of crystal structures of compound **4**. Ten unique low energy frames (Table 6) within 4 kcal mol^{-1} from the global minimum are plotted for each space group in Figure 7. Experimental structure α, β and γ form found 6th, 3rd and 7th rank frame based on U_{latt}. Cell parameters, torsion angles and lattice energy of CSP matches with experimental structure remarkably well (Table 7). Prediction of three conformational polymorphs of **4** in lowest 10 frames of U_{latt} is quite good in term of success. Thermodynamically stable β form found among the 3rd lowest energy frame and predicted β form has lower energy compare to α and γ polymorphs. It is likely that the difference in co-ordinates and atomic positions of experimental structure are not faithfully energy minimized by the force field as a possible reason for the disagreement in previous computation. This study also highlights the importance of force field selections for the correct predictions in CSP.

Table 6. 10 lowest energy predicted frames of crystal structures **4** simulated using full body minimization method (*Cerius*[2], COMPASS)

Ranking based on U_{latt}	Space Group	Cell Volume[a] [Å^3]	Lattice energy[a] [kcal mol^{-1}]
1	*P*-1	383.90	−54.967
2	*P*-1	386.09	−54.682
3	**P2$_1$2$_1$2$_1$**	**384.76**	**−54.622**
4	*P*-1	386.34	−54.537
5	*P*212121	388.66	−54.389
6	**Pna2$_1$**	**380.59**	**−54.252**
7	**P2$_1$/c**	**379.76**	**−54.250**
8	*C*2/*c*	389.18	−54.051
9	*P*-1	387.84	−53.608
10	*P*-1	385.19	−53.585

[a] Normalized to per molecule of fuchsone.
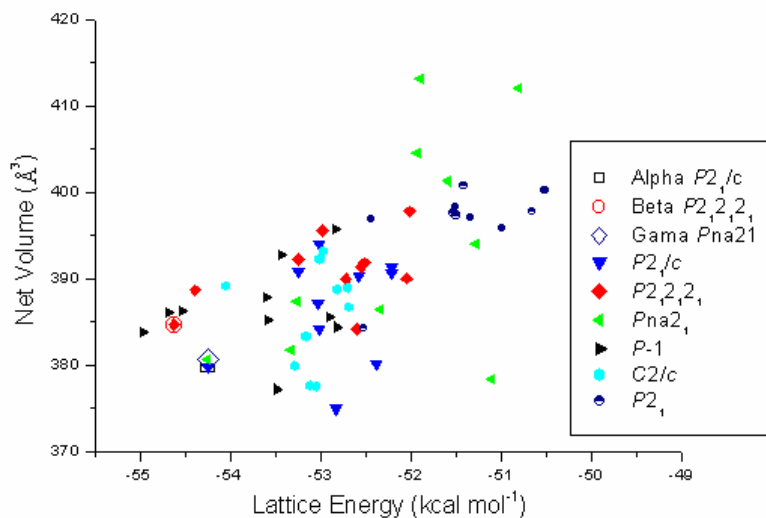
Figure 7. Lattice energy vs. cell volume for structures of molecule **4** generated in six common space groups using full body minimization in Polymorph Predictor. Experimental crystal structures α, β and γ forms matches with the 7th, 3rd and 6th rank predicted structure based on U_{latt}.

Table 7 Experimental crystal structures and minimum lattice energy structure predicted using *Cerius²* polymorph predictor in the fullbody minimization method.

Polymorph	a [Å]	b [Å]	c [Å]	β [°]	V/Z [Å³]	U_{latt} [kcal mol⁻¹]
α Form, $P2_1/c$						
Frame #7[a] Predicted	8.465	18.173	9.882	92.25	379.76	−54.250
α Form [b] ExptMin	8.458	18.188	9.888	92.07	379.75	−54.249
Form Expt	8.531	18.677	10.021	90.87	399.00	---
β Form, $P2_12_12_1$						
Frame #3[a] Predicted	7.846	17.384	11.284		384.76	−54.622
β Form[b] ExptMin	7.855	17.391	11.261		384.69	−54.620
β Form Expt	8.156	17.761	10.959		397.00	---
β Form, $Pna2_1$						
Frame #6[a] Predicted	11.852	15.992	8.033		380.59	−54.250
γ Form[b] ExptMin	11.851	15.993	8.032		380.60	−54.250
γ Form Expt	11.820	16.487	8.150		397.00	---

[a] Predicted structure in Cerius² (COMPASS force field, fullbody minimization).
[b] Experimental crystal structure was minimized in *Cerius²*

Frame numbers 1-10 of flexible body method (Table 6) were re-ranked based on the total energy, $E_{total} = E_{conf} + U_{latt}$, of rigid body minimized frames. A comparison of these new energy values is listed in Table 8. The out come of re-ranking does not support experimental results and it is difficult to interpret why metastable γ form rank lower in energy than stable β form.

Table 8. U_{latt} of lowest energy frame by rigid body method starting from the molecular conformation in full body minimized frames #1-10. E_{conf} is calculated in Spartan 04. The simulated structures of **4** are re-ranked based on intra- and intermolecular energy sum, E_{total} [kcal mol^{-1}].

Frame # in Full Body Method	Space group	U_{latt} in rigid body method [kcal mol–1]	E_{conf} [kcal mol–1]	$E_{total} = U_{latt} + E_{conf}$ [kcal mol–1]	Re-ranking of frames based on E_{total}
6	**γ form Pna2₁**	**–35.24**	**0.66**	**–34.58**	**1**
3	**β form P2₁2₁2₁**	**–34.85**	**0.36**	**–34.49**	**2**
7	**α form P2₁/c**	**–35.26**	**0.94**	**–34.32**	**3**
2	*P*-1	–35.37	1.26	–34.11	4
5	*P*2₁2₁2₁	–34.49	0.50	–33.99	5
4	*P*-1	–34.37	0.64	–33.73	6
8	*C*2/*c*	–33.78	0.19	–33.59	7
10	*P*-1	–33.51	0.02	–33.49	8
9	*P*-1	–33.40	0.00	–33.40	9
1	*P*-1	–36.27	2.95	–33.32	10

3.6 Conclusion

In the present study polymorphic transformation of kinetic α form to thermodynamic β form is confirmed through VT-PXRD study. Thermodynamically stable β form is enatiotopically related with other forms in the temperature range 30-180 °C and pure β form can be obtained by heating of the concomitant mixture above 160 °C. VT-PXRD experiment is very useful for the monitoring phase transformation when DSC does not show small enthalpic changes. Crystal structure of α form has win-win molecular and lattice energy combination and stable in room temperature. However at higher temperature β form is thermodynamically stable and α, γ convert to β form in phase transition. Re-production of all the three polymorphs computationally by full body minimization of lattice energy predicts as in frame #6, #3 and #7 based on U_{latt}. Thermodynamically stable β form matching frame is lower energy frame than α, γ form

predicted structure. This is a remarkable success in term of hypothetical structure generation by computation. Re-ranking of structures using rigid lattice energy component and conformation energy does not agree with experimental findings. However, all the three forms ranked in three lowest energy frames.

3.7 Experimental Section
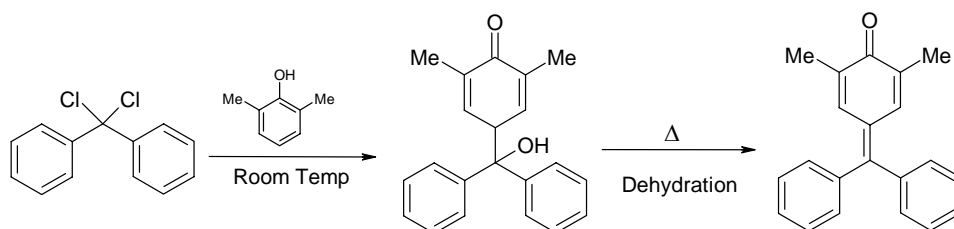
Compound **4** is prepared in two steps as shown in Scheme above.[11]

Dimethyl phenol (4.0 g, 0.034 mols) was stirred with 2.6 g (0.011 mols) of benzophenone dichloride for 10 h in a round bottomed flask. Excess phenol was removed from reaction mixture by steam distillation. Mixture was digested with 5% NaOH solution and extracted with ether. After filtration (3,5-dimethyl-4-hydroxypheny1) diphenyl methanol precipited by adding solid NH_4Cl. Product was recrystallized from benzene to obtain pure (3,5-dimethyl-4-hydroxypheny1) diphenyl methanol.

(3,5-dimethyl-4-hydroxypheny1) diphenyl methanol was heated in round bottom flask to dehydrate for 3-4 hr. Orange-red solid obtained as product which was recrystallized with benzene to obtain pure 2,6-dimethyl-4-(α,α-diphenylmethylene)-1,4-benzoquinone **4** (2.6 gm, 90%). M.P. 202 °C, ^{1}H NMR [400 MHz, δ, $CDCl_3$]: 2.43 (s, 6H), 6.84 (s, 2H), 6.84 (s, 2H).7.30 (10H, m). IR [KBr]: 2916, 1628, 1601, 1508, 1442, 1334, 1028, 918 cm^{-1}.

Variable Temperature Powder X-ray Diffraction

Powder data were collected on PANlytical X'Pert PRO X-ray powder diffractometer using a parallel beam of monochromated Cu-K$_\alpha$ radiation (λ = 1.54056 Å) and an X'celerator detector at 40 kV and 40 mA. Diffraction patterns were collected over the 2θ range 5-50º. Samples were loaded in an 18-mm alumina holder for variable temperature powder X-ray diffraction data collection and an aluminum sample holder with a 10 mm diameter sample cavity for room temperature data. The program X'Pert High Score was used for the processing and comparison of powder patterns. Powder Cell 2.3[5] was used for calculating PXRD patterns and for profile fitting and least square refinement of unit cell parameters, a displacement parameter, a background polynomial function, peak shape asymmetry terms, and an overall temperature factor using the known single-crystal structures of polymorphs A, B and D as the model. Temperature settings for the variable temperature powder X-ray diffraction data were set at T = 28, 39, 49, 59, 69, 79, 89, 94, 98, 102, and 105 °C. The sample was cooled to room temperature (31 °C) and data were recollected. Powder XRD profiles are plotted in the range 2θ = 10-34° for all samples. There are no significant peaks below 10° and only minor peaks between 35-50°. There are wide peaks at 25.2° and 34.8° from the sample holder.

Differential Scanning Calorimetry

DSC was performed on Mettler Toledo 822e module. Samples (4-6 mg) were placed in crimped but vented aluminum pans and heated @ 2 °C min^{-1} from 30-250 °C. The instrument was purged with a stream of dry nitrogen @ 150 ml min^{-1}.

Spartan 04, Gaussian 03 and *Cerius*² Computations

*Cerius*² simulations and crystal energy:[6] All simulations were carried out in version 4.8 of *Cerius*² molecular modeling environment running on Silicon Graphics workstation. Geometry optimization was carried out using density functional theory (DFT) at the B3LYP/6-31G (d,p) level in Gaussian 03.[10] The global minimized

conformer of **4** from Gaussian 03 was entered as the input for Polymorph Predictor. Crystal structure prediction was carried out in six common space groups which include the observed space groups ($P2_1$, $P2_1/c$, $C2/c$, $Pbca$, $P2_12_12_1$, $P\bar{1}$). Cell parameters of predicted frames in $C2/c$ were compared with reduced cell parameters to confirm that they represent different structures. Reduced cell parameters are used for comparison. Atom point charges were assigned in COMPASS force field. Default options were used throughout with fine search option in Monte Carlo simulation and for clustering of frames to get unique structures. Lattice energy minimization of predicted structures was carried out without any modifications except for the use of Ewald summation of van der Waals interactions at a cut-off of 6.0 Å. All calculations were carried out either by relaxing the molecular conformation during the minimization, referred to as full body method, or by keeping the conformation fixed during minimization, the so-called rigid body method. Lattice energies were computed for experimental polymorphs of **4** in *Cerius*[2] program by energy minimization of crystal structures in DREIDING 2.21 and COMPASS. Force field charges were assigned in COMPASS and charge equilibrium method was used in DREIDING 2.21. COMPASS is better parameterized for structure prediction and energy of organic molecules. Crystal lattice energies are calibrated for the number of molecules in the unit cell (per molecule).

Energy of three conformers were calculated in Spartan 04[8] using crystallographic coordinates as the input; hydrogen atom positions were re-optimized at the HF/6-31G** level while keeping the heavy atoms fixed. The gas-phase conformation of **4** was obtained by global energy minimization.

3.8 References

1. (a) P. Thuéry, M. Nierlich, R. Calemczuk, M. Saadioui, Z. Asfari and J. Vicens, *Acta Cryst.*, **1999**, *B55*, 95. (b) I. Bensemann, M. Gdaniec and T. Połoński, *New. J. Chem.*, **2002**, *26*, 448. (c) Z.-Q. Zhang, J. M. Njus, D. J. Sandman, C. Guo, B. M. Foxman, P. Erk and R. V. Gelder, *Chem. Commun.*, **2004**, 886. (d) F. P. A. Fabbiani, D. R. Allan, S. Parsons and C.R. Pulham, *CrystEngComm*, **2005**, *7*, 179.

2. (a) J. Starbuck, R. Docherty, M. H. Charlton and D. Buttar, *J. Chem. Soc.*, *Parkin Trans.*, *2*. **1999**, *94*, 677. (b) B.-Q Ma and P. Coppens, *Cryst. Growth Des.*, **2004**, *4*, 1377.

3. (a) T. W. Lewis, I. C. Paul and D. Y. Curtin, *Acta Cryst.,* **1980**, B*36*, 70. (b) E. N. Duesler, T. W. Lewis, I. C. Paul and D. Y. Curtin, *Acta Cryst.*, **1980**, B*36* 166.

4. F. H. Allen and R. Taylor, *Chem. Soc. Rev.*, **2004**, *33*, 463. www.ccdc.cam.ac.uk.

5. Powder Cell 2.3. N. Krauss, G. Nolze, Federal Institute for Materials Research and Testing, Berlin, Germany, **2000**.

6. *Cerius*[2] suite of software for crystal lattice energy calculation and crystal structure prediction are crystal packer and polymorph predictor. www.accelrys.com.

7. H. Sun, *J. Phys. Chem. B*, **1998**, *102*, 7338.

8. Spartan 04, Irvine, CA. www.wavefun.com.

9. (a) L. Yu, G. A. Stephenson, C. A. Mitchell, C. A. Bunnell, S. V. Snorek, J. J. Bowyer, T. B. Borchardt, J. G. Stowell and S. R. Byrn, *J. Am. Chem. Soc.*, **2000**, *122*, 585.

10. M. J. Frisch *et al*, Gaussian 03, Revision B.05. www.gaussian.com.

11. T.W. Lewis, D. Y. Curtin and I. C. Paul, *J. Am. Chem. Soc.*, **1979,** *101*, 5717.

STABLE POLYMORPH OF VENLAFAXINE HYDROCHLORIDE BY SOLID TO SOLID PHASE TRANSITION AT HIGH TEMPERATURE

4.1 Introduction

McCrone's statement[1] postulated almost 40 years ago that "the number of polymorphs of a material is proportional to the time and money spent on research on the compound," is increasingly proving to be correct. Literature values shows on the occurrence of polymorphism range from 5% in small organic molecules to 30-50% in drug substances of <600 g mol^{-1} molecular weight.[2] The greater occurrence of polymorphism in drugs is due to more attention and effort employed on studies for such molecules. Polymorphism study emerged in a significant way in the last decade, for pharmaceutical formulation because of its ability to change the properties like stability, solubility, density, bio-availability. Pharmaceutical compounds may typically be isolated in a variety of different crystalline forms, including polymorphs and salts. Thus, pharmaceutical development relies upon finding the crystal form having the best possible combination of properties. Once a solid form has been selected for development and clinical trials, a substantial cost is incurred if it becomes necessary to switch to a different crystal form, either due to unforeseen difficulties or the appearance of a previously unknown form. New forms can cause changes in a manufacturing process, and affect the intellectual property associated with the marketed form. Rolf Hilfiker[2] emphasizes in his authoritative book on pharmaceutical polymorphism that, "Although in hindsight everything may appear to be easy and straightforward, crystalline molecular solid-state forms are non-obvious, novel and require inventiveness." Appearance of a more stable form at late stages in drug development or commercial production is a nemesis in the pharmaceutical industry, publicized by the infamous accident at Abbott laboratories.[3] The sudden appearance of more stable polymorph of HIV protease inhibitor, Ritonavir (Norvir®) which is less soluble forced the removal of the oral capsule formulation from the market. After Ritonavir incident pharmaceutical industry gave

much attention in discovering *the most stable polymorph of a commercial drug*, which attracts much scientific attention in present time. For all these reasons, a complete set of characterization data on all the forms of interest that contain the active pharmaceutical ingredient (API) is desired, as early in the development process as possible.

Venlafaxine {(±)-1-[2(dimethylamino)-1-(4-methoxyphenyl)-ethyl]-cyclohexane -1-ol} hydrochloride (VenHCl) is an anti-depressant drug that act by inhibiting the reuptake of norepinephrine and serotonin in the brain (SNRI, serotonin–norepinephrine reuptake inhibitor).[4,5a] VenHCl sold under the trade name Effexor XR® (Wyeth) and widely prescribed anti-depressant drug with sales of over US $ 3.8 billion per annum. This extended release capsule is indicated in the treatment of GAD (generalized anxiety disorder). The present study aims to establish the accurate thermochemical relation and determine the stability of the marketed forms of leading anti-depressant drug venlafaxine hydrochloride (VenHCl, Scheme 1). The focus of the present work was on screening of all the possible polymorphs that can exist for this blockbuster drug. Single crystal structures of two polymorphs (forms 1 and 2),[6] melt form (form 3), hydrate (form 4) are known in the literature.[5] Thermal relationships of these forms were established by DSC, HSM and a novel amorphous semi-solid form was characterized by sublimation (form 5) in our laboratory. In this present study, a novel, stable polymorph of VenHCl obtained by the solid–to–solid phase transition, termed as form 6 is disscussed.

5
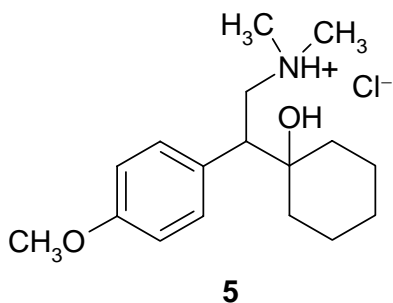
Scheme 1. Molecular diagram of Venlafaxine hydrochloride salt, VenHCl.

4.2 Venlafaxine Hydrochloride (VenHCl): Background of Form 1-4 and Transient Form 5

Racemic VenHCl (**5**) is known to exist in at least five different polymorphic/ pseudopolymorphic forms, which were characterized in the different patents.[5] Two crystalline polymorphic modifications form 1 ($Pca2_1$)[6a] and form 2 ($P2_1/n$)[6b] are widely studied. The solid state modification contains with hydrate/alcoholate forms (H_2O/MeOH/EtOH/*i*-PrOH), DMF/DMSO solvated forms and a phase from the melt are reported in the literature. The drug is marketed in forms 1 and 2 although form 2 is preferred in the formulation because of higher particle size with better filtration and drying characteristics.[7] The five polymorphs of VenHCl are classified according to their main melting endotherm in DSC: form 1 (210-212 °C), form 2 (209-211 °C), form 3 (202-204 °C, phase from melting), form 4 (219-220 °C, hydrate/alcohol solvate). Five polymorphs of VenHCl have been numbered as forms 1-6 in the present study, where form 5 new amorphous, transient glassy (semisolid) phase that is obtained by sublimation under vacuum.

4.2.1 Form 1-4

VenHCl form 1 and 2 were crystallized from hot *i*-PrOH as reported in literature[5a] and experimental conditions for the preparation of various forms are described in Section 4.9. Purity of phases 1 and 2 has been confirmed by experimental powder X-ray diffraction (XRD) of the samples with their simulated powder XRDs (Figure 1).[6,8] DSC thermograms shows forms 1 and 2 both having almost same melting temperature of 210-212 °C (Figure 2a). Both the forms undergoes phase transition after melting. Phase from melt (form 3) prepared by gradually heating of form 1 and 2 to 215 °C over 30 min to melt the solid, then cooling the material to room temperature. Melting of form 3 shows lower melting point (202-204 °C) then form 1 and 2 (Figure 2b). A hydrate form of VenHCl (form 4) is obtained upon crystallization from MeOH/EtOH, shows loss of water/alcohol at 70-80 °C and melts at 219-220 °C (Figure 2b). The powder XRD and DSC profile of form 3 and 4 matched nicely with the literature reported pattern.

(a)   (b)
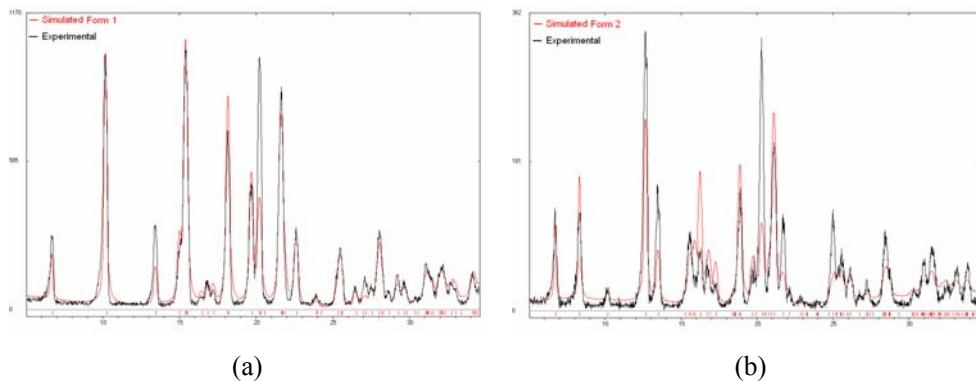
Figure 1. Match of the experimental and simulated X-ray powder diffraction pattern of VenHCl in Powder Cell 2.3. (a) Form 1, (b) Form 2.

(a)   (b)
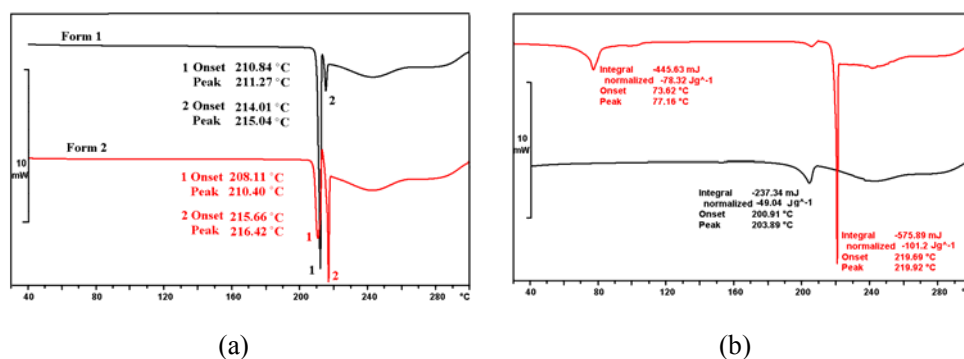
Figure 2. DSC thermograms of powder samples (a) form 1 (black) and form 2 (red) (b) phase from melt (black) and hydrate phase (red).

4.2.2 Form 5

Sublimation of VenHCl form 1 and 2 under reduced pressure (0.2 Torr, 160 °C) in sublimation apparatus gave an amorphous, semi-solid material hangs from the cold finger (Figure 3a). This glassy mass of liquid-like droplets is unstable under ambient condition (Figure 3b). DSC trace of this semi-solid form is very much different from that of forms 1-4. This semi-solid shows crystallization at 95-100 °C (exotherm) followed by melting at 216-218 °C (endotherm) and a broad endotherm at 220-260 °C for vaporization/ sublimation (Figure 3d). This new form of VenHCl which obtained under

very different experimental conditions is named as form 5. Form 5 is unstable and it transforms to form 1 under inert N_2 atmosphere in a few hours to a day. If sublimed material is left in an open air for 1 day (25-30 °C, RH 40-50%), it turns to hydrate form 4 (Figure 3e). DSC heat-cool-heat experiments show that after melting form 2 is transformed to phase 5. However similar heat-cool-heat experiment on form 1 leads to form 3 (phase from melt).

(a)   (b)   (c)

(d)   (e)
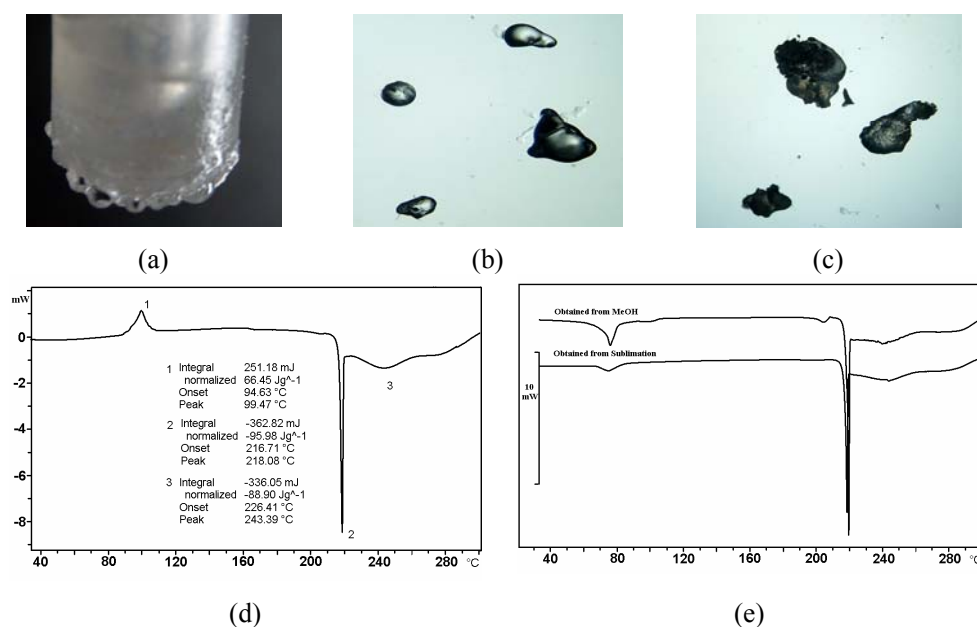
Figure 3. Transient semi-solid, glassy phase on the cold finger of the sublimation apparatus (a) and droplets immediately placed on a glass plate (b). The sublimed material (form 5) transforms to hydrate form 4 (c) after 1 day in Hyderabad climate (25-30 °C, RH 40-50%). (d) DSC of form 5, obtained from sublimation, recorded immediately. The exotherm at 100 °C is due to solidification of the glassy mass, the endotherm at 217-218 °C from melting, and vapor loss occurs at 220-260 °C. (e) DSC of VenHCl hydrate obtained from form 5 after 1 day in open air (below) and hydrate form 4 prepared by crystallization from MeOH (above). The endotherm at 80 °C is loss of solvent/water.

Phase changes in form 1 and 2 and the thermal events leading to sublimation of form 5 were studied by Hot stage Microscopy (HSM). HSM experiments further confirm the proposed interpretations drawn from DSC thermograms. In addition to the formation

of form 5, it was noticed that there is phase transition just before melting for both the formation if the heating rate is very slow. Detailed analysis of HSM study is discussed in the next section.

4.3 Hot stage Microscopy (HSM) Experiment

To understand accurate phase relation among different form of VenHCl visually, thermal events were monitored through HSM. Single crystals of form 2 (5-6 mg), which are obtained from EtOAc/MeOH solvent, have been used for the experiment. These long needles of form 2 crystals were examined on HSM. There was no change in morphology upto 150 ºC. After 160 ºC fine crystal started appearing on the hot plate. Transformation of long needle morphology crystals to thin plates visually observed on isotherm heating at ~180 ºC (Figure 4). Crystals of both morphology (needle and thin plate) were present for the temperature range 10-15 ºC range in the HSM frames. Further heating to 190 ºC and then cooling to room temperature (25-30 ºC) showed complete conversion to the plate-like crystals. Form 1 crystals, which are block in shape, also examined on similar way which also shows transformation to plate like crystal in the temperature range 160-180 ºC (Figure 5).

A suitable single crystal was selected from HSM experiment batch (form 6, plate like crystal) for single crystal X-ray diffraction data collection (Figure 6a). Single crystal data collected at 100 K and 298 K gave same cell measurements with usual variation with temperature. Structure solution was carried out on the crystal data set of better reflections. The unit cell parameters of form 6 solved in monoclinic space group $P2_1/n$ with two molecule in asymmetric unit ($Z' = 2$). This novel form 6 structure (Figure 6b) is different from the reported form 1 and 2 ($Pca2_1$, $Z' = 1$; $P2_1/n$, $Z' = 1$).[6] Crystallographic data of three crystalline polymorphs of VenHCl (**5**) is listed in Table 1.

Room Temp(30 °C)   150 °C   170 °C   173 °C

176 °C   182 °C   184 °C   187 °C

188 °C   189 °C   Crystals under polarized light   Crystals after cooling to room temp
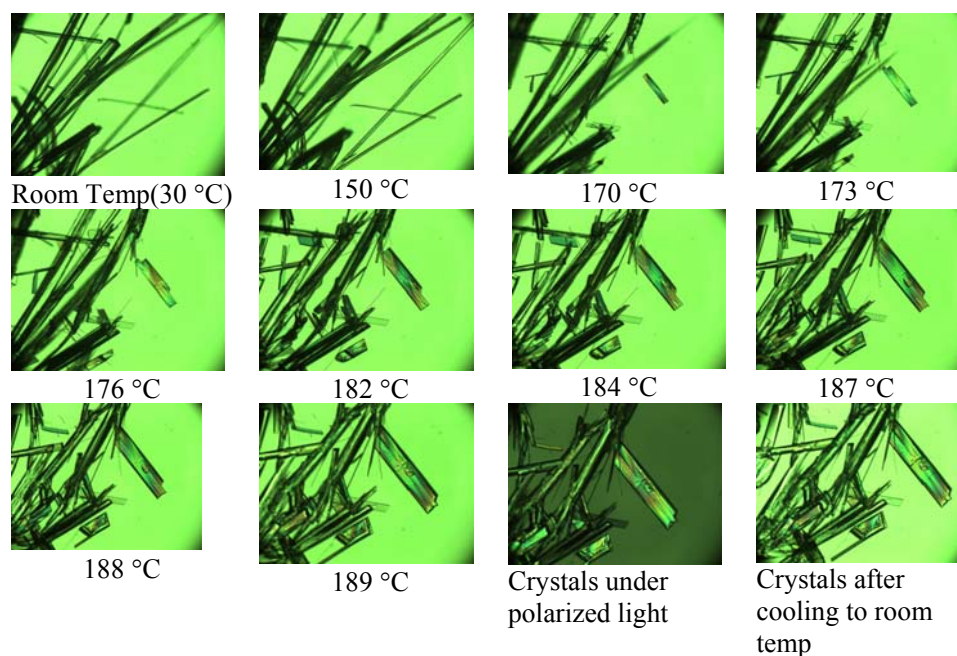
Figure 4. Hot Stage Microscopy on VenHCl form 2 crystals. It shows upon heating form 2 needle crystals (30 °C) slowly transform to produce plate like form 6 crystals (189 °C).

Room Temp(30 °C)   182 °C

189 °C   Crystals after cooling to room temp
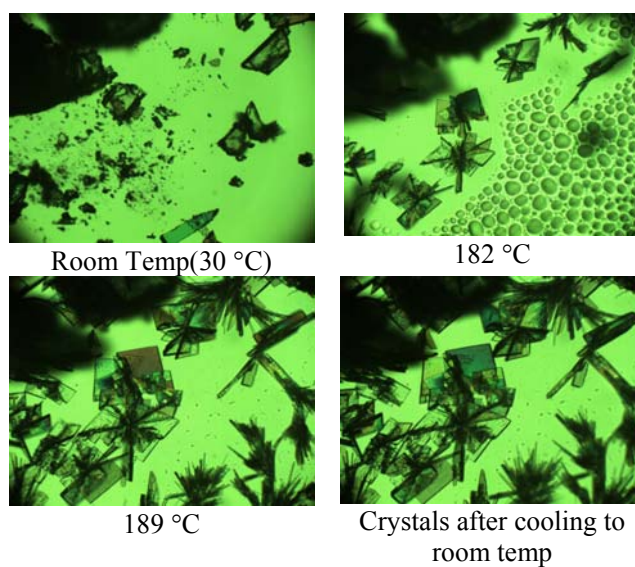
Figure 5. Hot Stage Microscopy on VenHCl form 1 crystals. Form 1 block shape crystals (30 °C) completely converted to a plate like form 6 (189 °C).

(a)   (b)
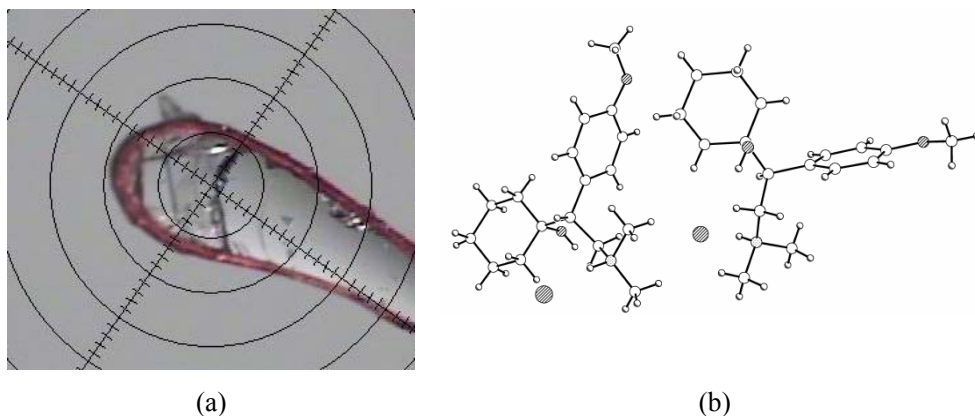
Figure 6. (a) Single crystal of VenHCl form 6 selected for X-ray diffraction. (b) Assymetric unit of novel form 6.

Table 1. Crystallographic data on form 1, 2 and 6 of VenHCl **5**.

	Form 1 (WOBMUV)	Form 2 (WOBMUV01)	Form 6 This study
Empirical formula	$C_{17}H_{28}NO_2^+.Cl^-$	$C_{17}H_{28}NO_2^+.Cl^-$	$C_{17}H_{28}NO_2^+.Cl^-$
Formula wt.	313.85	313.85	313.85
Crystal system	Orthorhombic	Monoclinic	Monoclinic
Space group	Pca2_1	$P2_1$/n	$P2_1$/n
T [K]	293	298.2	100
a [Å]	26.230	5.797	5.887(10)
b [Å]	5.8810	26.074	19.37(3)
c [Å]	11.448	11.722	31.41(5)
α [deg]	90.00	90.00	90.00
β [deg]	90.00	100.72	92.16(3)
γ [deg]	90.00	90.00	90.00
Z	4	4	8
Volume [Å^3]	1766	1741	3579(10)
D_{calc} [g/cm^3]	1.180	1.197	1.165

4.4 Variable Temperature Powder X-ray Diffraction of 5

The transformation of form 1 and 2 to form 6 was examined by variable-temperature powder X-ray diffraction (VT-PXRD). Pure powder material of form 1 and 2 (Figure 1) used for the experiments. For both the forms the powder diffraction profile

is relatively invariant from 25 to 170 ºC (Figure 7). Notable changes have been observed in peak profile in the temperature range 170-180 ºC. The intense peaks at 2θ = 12.0-13.5º and 20.0-22.0º disappear, which are replaced by new peaks at 14.0-15.0º and ~19.0º. For form 2 this change in to new peak profile pattern is clear and fast compared to form 1. However when material cooled to ~30 ºC after heating both form 1 and 2 show same powder profile (Figure 8).

(a)   (b)
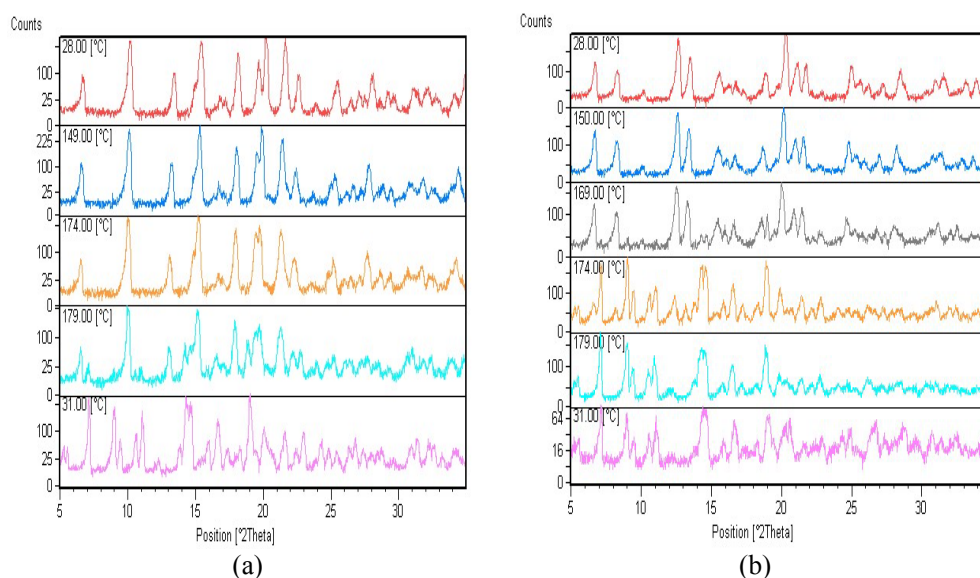
Figure 7. (a) Variable-temperature powder X-ray diffraction profile for (a) form 1 and (b) form 2. Form 1 transform to form 6 when heated upto ~180 ºC for 30 min and cooled back to room temperature. However form 2 to form 6 transformation is fast and complete when sample heated to ~180 ºC.

This new high temperature phase obtained from form 1 and 2 from the phase transformation at high temperature, which is stable upon cooling. So this formation of high T phase is thermodynamically stable form and phase transition is irreversible in nature. Least-squares refinement of the powder pattern at 179 ºC obtained from form 2 shows good match with the calculated diffraction peaks from the crystal structure of form 6 in Powder Cell 2.3[7] (Figure 8). As the single crystal data collected in much low

temperature than powder experiments, unit cell parameters of the crystal structure were adjusted to the temperature of the PXRD measurement for diffraction profile simulation. The slight discrepancy between the relative peak intensity arises due to the preferred orientation of microcrystalline particles in the sample. Moreover the single crystals obtained by solid–solid transformation at higher temperature and *R*-factor of 0.1073 is slightly high.

$2\theta / °$
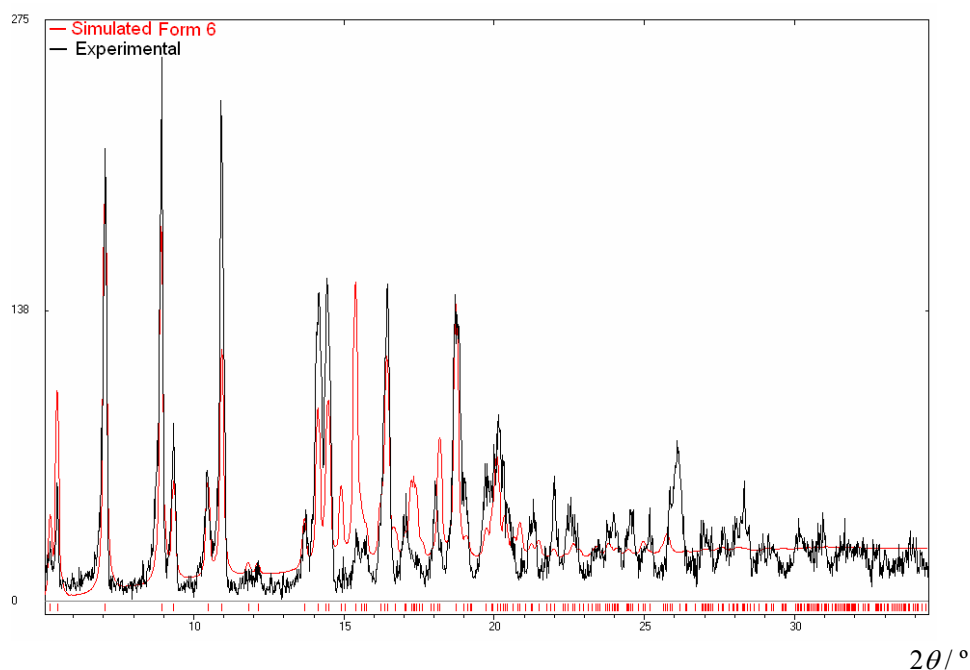
Figure 8. Match of the experimental powder trace at 179 ˚C (black) with calculated peaks of form 6 from the single crystal diffraction data (red) is good. Similar matching in peak profile observed with the material cooled to room temperature after heating for both form 1 and 2.

The observation in HSM experiments indicated solid–solid transformation which further verified by the VT-PXRD experiments. Change in crystals morphology were visualized in a 10-15 ºC range, at 175-190 ºC in the HSM frames and the evolution of new peaks in the PXRD profile at 170-180 ºC. The transformation of form 2 (and form 1) to form 6 is a solid–solid phase transition based on the appearance of diffraction

intensities in the VT-PXRD plots through the entire experiment as well as visual observation of HSM frames. Heating at the usual ramp rate of 5-10 ºC min^{-1} (DSC condition) up to 220 ºC and cooling of form 1 and 2, gave the melt (form 3) and sublimation polymorphs (form 5) of VenHCl upon cooling as discussed in section 4.2. DSC trace of form 1 and 2 does not show any phase transition in the temperature range 170-190 ºC (Figure 9). However this phase transition occurs only when the temperature is raised slowly or maintained isothermally for a while akin to thermodynamic conditions, e.g. @ 1-3 ºC min^{-1} as in HSM, or @ 10 ºC min^{-1} and standing at ~180 ºC for ~30 min in VT-PXRD. DSC trace of novel form 6 showed single melting endotherm at higher T_{onset} of 219 ºC (Figure 9). The melting point of form 6 (T_m = 219-220 ºC) is ~10 ºC higher than that of form 1 or 2 and does not show phase transition like form 1 and 2 (form 1 $\rightarrow$ 3; form 2 $\rightarrow$ 5). The phase relationships among VenHCl polymorphs are summarized in Table 2. A qualitative E vs. T phase diagram of the three crystalline form of VenHCl is schematized in Figure 10. Form 1 and 2 are monotropic but they readily interconvert to stable form 6 in the temperature range studied (enantiotropic).
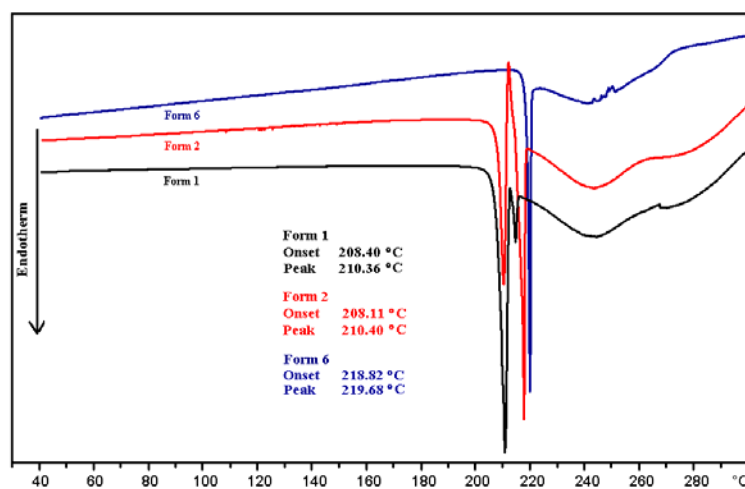
Figure 9. DSC of form 1 (black), form 2 (red) and form 6 (blue) at a heating rate of 2 ºC min^{-1}. Form 6 has the highest melting point of 219-220 ºC compared to form 1 and 2 of 208-210 ºC. In both forms 1 and 2, the lower T endotherm is due to melting and the higher T peak is a phase transition.

Table 2. Phase relationships, monotropic and enantiotropic system, in VenHCl polymorphs.

Polymorph	T range (°C)[a]	Phase relation	Remarks
1, 2	30-210[b]	monotropic	no change
1, 2, 3, 5	210-220[b]	enantiotropic	$1 \rightarrow 3, 2 \rightarrow 5$
1, 2, 6	30-180[c]	enantiotropic	$1, 2 \rightarrow 6$

[a] T values are ±5 °C.
[b] Heat @ 2-5 °C min^{-1} (DSC conditions).
[c] Heat @ 10 °C min^{-1} and isothermal at ~180 °C for 30 min (VT-PXRD conditions).
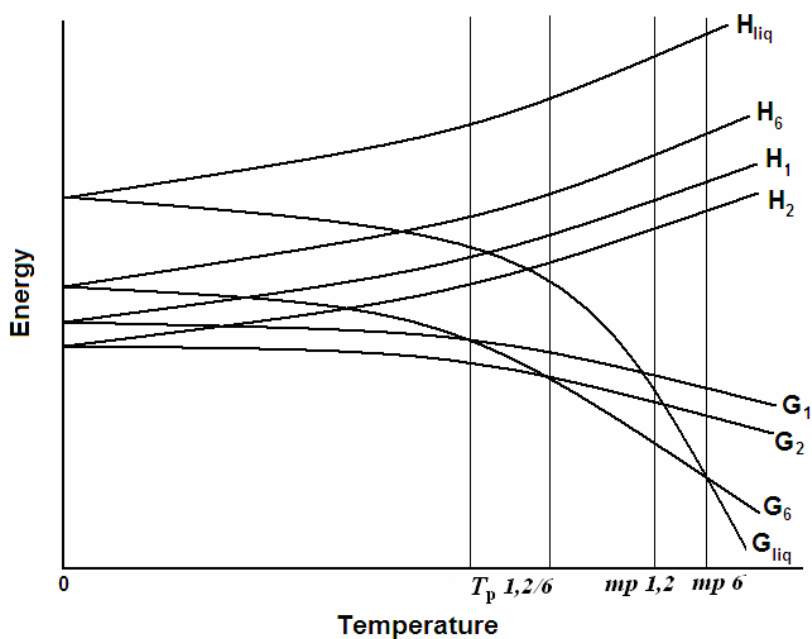
Figure 10. Energy vs. temperature diagram of VenHCl polymorphs 1, 2 and 6. Form 2 is more stable than form 1 and there is no inter-conversion between them. This diagram represents the enantiotropic system in which form 1 and 2 undergo phase transition to form 6 at ~180 °C. Melting point of form 6 is ~10 °C higher than forms 1 and 2.

4.5 Crystal structure of Form 6

Crystal structure of form 6 has two symmetry-independent molecules (i and ii) in the asymmetric unit, which have identical molecular conformation except that the orientation of –OCH$_3$ group is in opposite orientation (Figure 11). Interestingly,

molecular conformers of form 1 and 2 overlay nicely with the two conformations of form 6. Conformational energy calculation using density functional theory (DFT) at the B3LYP/6-31G (d,p) level in Gaussian03 shows conformer i is more stable than ii by 0.18 kcal mol^{-1}.[9] All the three forms have common V-shaped acceptor-bifurcated O–H···Cl$^-$ and N$^+$–H···Cl$^-$ hydrogen bond synthon motif between translation-related molecules except that this motif is along [010] in form 1 and along [100] in form 2 and form 6 (Figure 10). These O–H···Cl$^-$ and N$^+$–H···Cl$^-$ hydrogen bonds forming helical assembly in form 6 are longer than those in forms 1 and 2 (Table 3). Two symmetry independent molecules in form 6 form a self Host-guest structure, where inversion related molecule forms a dimer sitting inside channel as host (Figure 12c and 13). Form 6 with multiple molecules in the asymmetric unit can be viewed as an example of conformational isomorphism, whereas Forms 1, 2 and 6 of VenHCl are conformational polymorphs.[10]
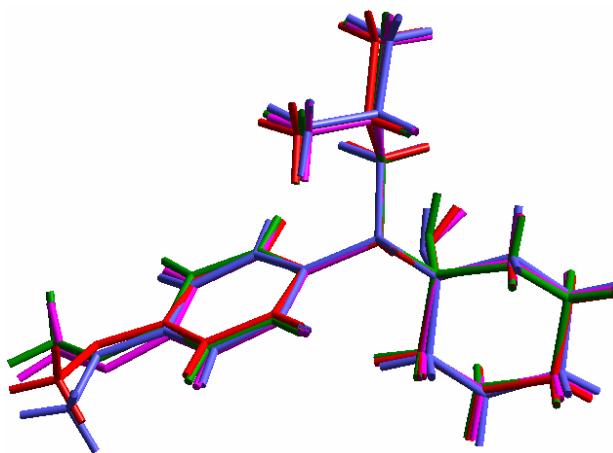
Figure 11. Overlay of symmetry-independent venlafaxine molecules. Form 1 (red), form 2 (magenta), form 6: molecule i (blue), molecule ii (green). Chloride counter ion is omitted.

(a)

(b)

(c)
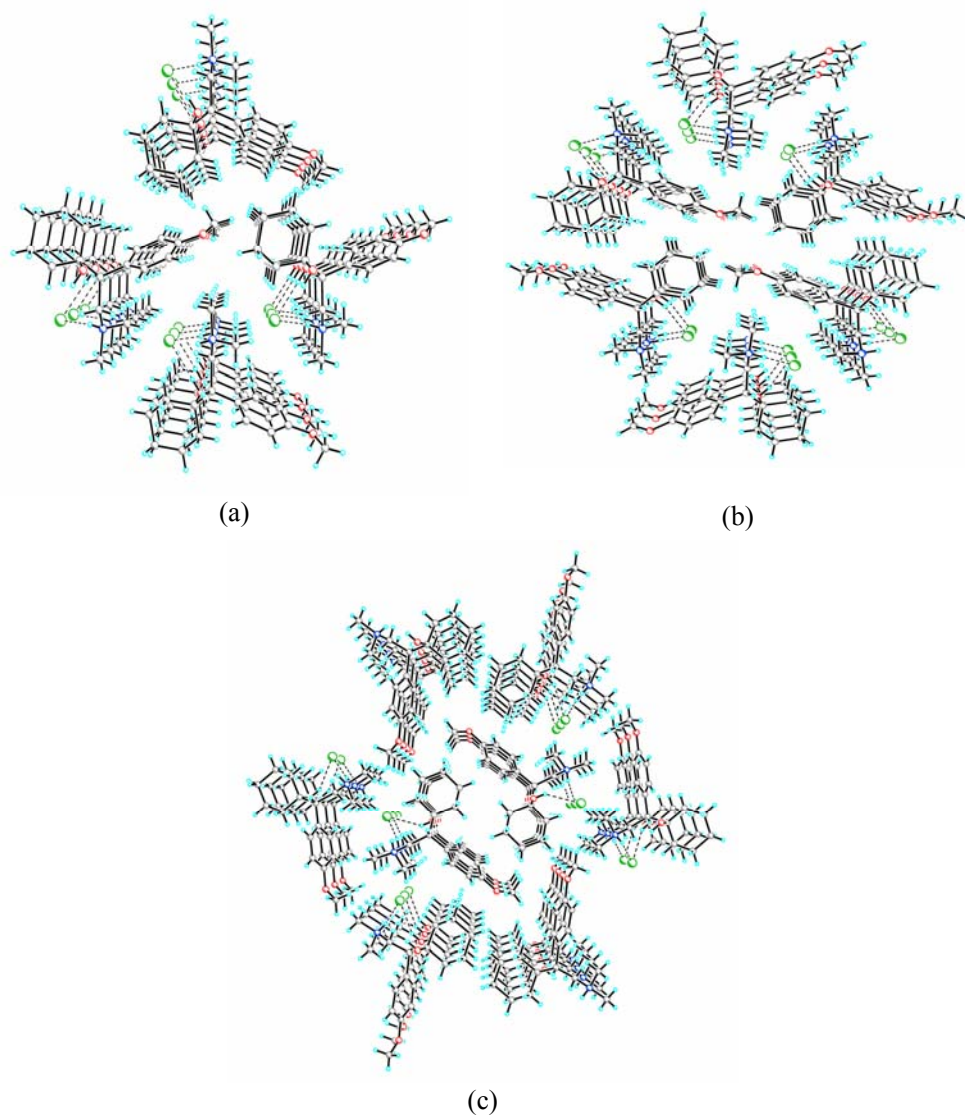
Figure 12. Close packing of the helical chains of molecules organized via the V-shaped O–H⋯Cl⁻ and N⁺–H⋯Cl⁻ hydrogen bond synthon. (a) form 1 down [010], (b) form 2 down [100], (c) form 6 down [100].

Table 3. Hydrogen bond distances in polymorphs of VenHCl (neutron normalized).

Compound	D–H···A	H···A / Å	D···A / Å	D–H···A / º
Form 1	O2–H28···Cl1⁻	2.19	3.181(3)	179.9
	N1⁺–H27···Cl1⁻	2.04	3.047(4)	172.7
Form 2	O2–H27···Cl1⁻	2.26	3.213(5)	163.6
	N1⁺–H28···Cl1	2.04	3.040(5)	168.7
Form 6	O1–H36···Cl1⁻	2.36	3.179(12)	141
	N2⁺–H2···Cl1⁻	2.13	3.127(13)	169
	O3–H3···Cl2⁻	2.42	3.272(11)	145
	N1⁺–H35···Cl2⁻	2.12	3.119(13)	169
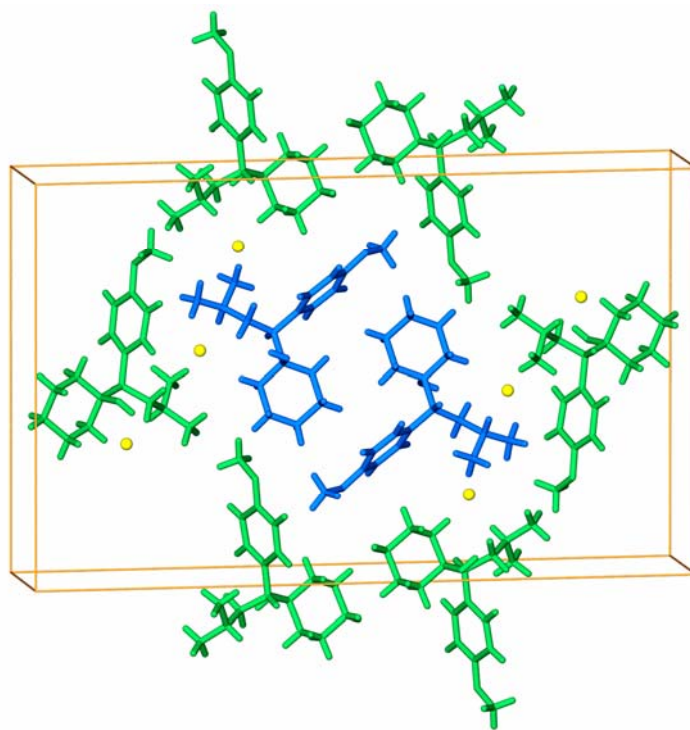
Figure 13. Symmetry-independent molecules i (blue) and ii (green) of form 6 results a self host-guest complex.

4.6 Stability of Polymorphs

Forms 1 and 2 of VenHCl are used in drug formulations currently.[7] However third crystalline modification form 6 have higher melting point and stable in room temparature. It is important to identify the kinetic form and the thermodynamic one. Thermal analysis confirmed the melting point of form 6 (T_m = 219-220 ºC) is ~10 ºC higher than that of form 1 or 2. It is believed that this last appearing and highest melting novel form 6 is the most stable thermodynamic polymorph of VenHCl, consistent with the Ostwald's law of stages.[11]

Stability of form 6 structure can be inferred from its better packing arrangements in the crystal lattice. The flexible VenH$^+$ cation has an approximate Y-shape in all three structures. Polymorphs 1, 2 and 6 have the same V-shaped H bond synthon and layered structures (Figures 14a-c) and so it is possible to dissect them in terms of the differences between the 2D layer structures. The inter-layer packing is largely van der Waals and C–H···O interactions (~2.7 Å) in all three polymorphs. Ladder like arrangement of VenH$^+$ molecules with the Cl$^-$ counter ions sandwiched between the rungs[12] in form 1 and 2. However form 6 has very different and compact arrangement of molecules forming a cage like structure where 0D dimer sitting inside the cavity (figure 14c). The parallel-aligned 1D ladders of form 2 reorganize to the 2D brick wall grid[13] of form 6 at higher temperature (at 180-190 ºC), the result is a better packing of hydrophobic layers and inter-locked molecules (Figure 14b,c). This makes conversion of form 2 to form 6 easier compare to form 1, which may have more complex transformation pathway revealed from structure relationship among the polymorph.

(a)

(b)

(c)
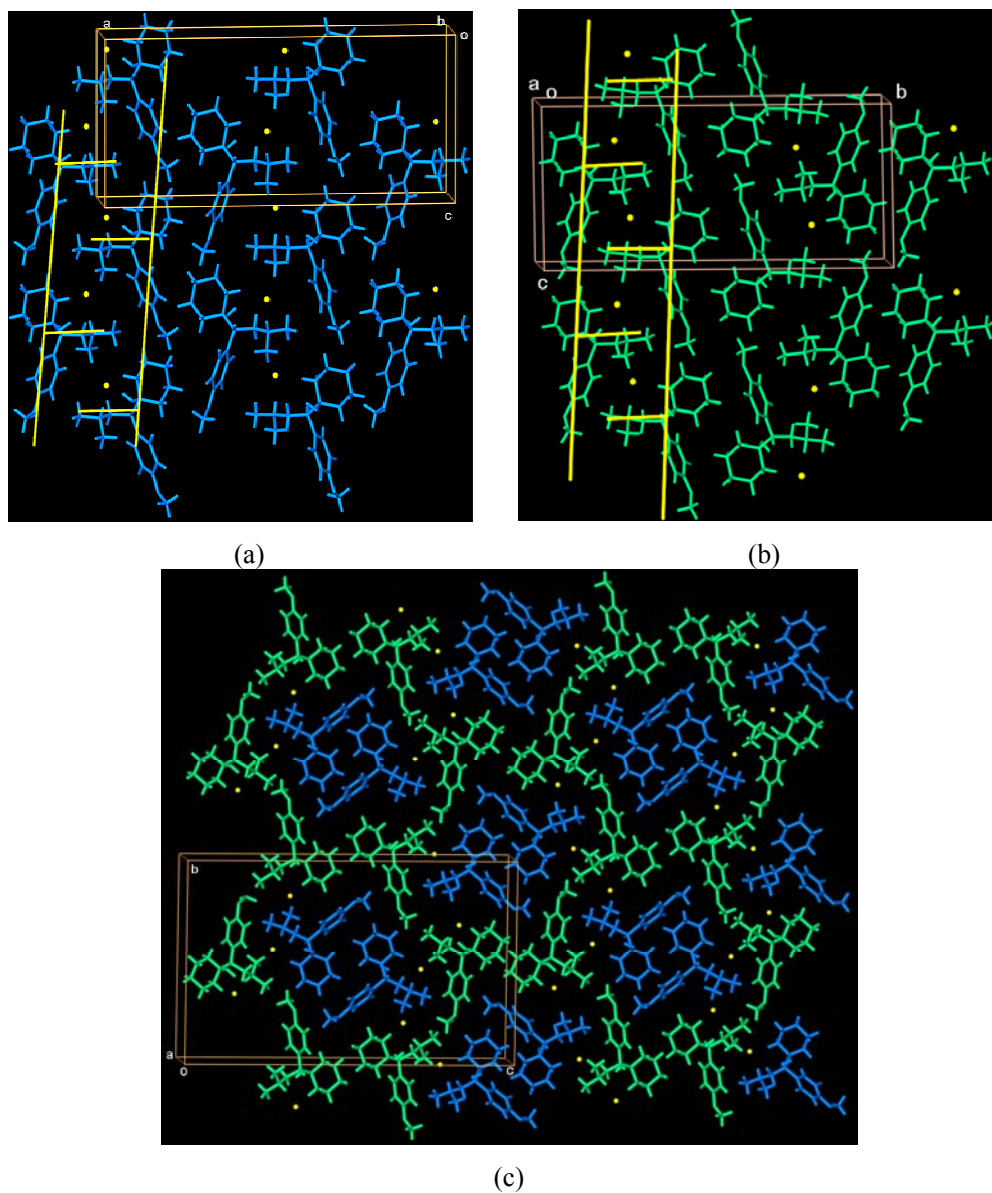
Figure 14. Chloride ions as guests in the 1D ladder network of VenH$^+$ form 1 (a), shown more clearly for form 2 (b) as yellow lines. There are hydrophobic interface between the adjacent ladders of form 1and 2. (c) Reorganization of the parallel-aligned 1D ladders to give the 2D brick wall network of form 6 is visualized clearly for color-coded symmetry-independent molecules.

The "infrared rule"[14] says that in hydrogen-bonded polymorphic structures (with similar hydrogen bond motifs) with higher frequency in bond stretching modes may be assumed to have the larger entropy. The highest v_s in the IR spectrum of form 1 is at 3323 cm^{-1}, form 2 at 3350 cm^{-1} and in form 6 at 3368 cm^{-1} (Table 4). This means that form 6 has larger entropy or weaker intermolecular hydrogen bonds. Form 1 and form 2 have stronger O−H···Cl$^-$ and N$^+$−H···Cl$^-$ hydrogen bonds in accordance with its lower bond stretch vibration than form 6. Form 6 having lower entropy of fusion (T$_m$ = ΔH/ΔS) contribute to the ~10 ºC higher melting point. At high temperature it is likely that the disk-like 0D dimers of blue molecules start lubricating much before the 2D grid of green molecules (Figure 14c) just prior to the melting transition, thereby increasing the melting point. For form 6 molecules are already close to the fluid-like state. The molecular movement is higher in the pre-melt state and as a result the entropy change for melting will be small. The lower ΔS is perhaps quite significant for the higher T$_m$ of form 6 because its density is lower than that of forms 1 and 2 (ρ_{calc} = 1.165 vs. 1.180, 1.197 g cm^{-3}).[6]

"Are High Z' polymorphs are metastable relative to their low Z' crystal structures?" is still not clear and is a debate.[15] Form 6 obtained in high temperature indicate the thermodynamic preference over other form. At high temperature several molecules with various conformations will be in dynamic equilibrium. This conformation can interchange using thermal energy of atoms (RT ~ 0.6, 0.8, 1.0 kcal mol^{-1} at 300, 400, 500 K), which is comparable to the rotation barrier of methyl group and torsions about C–C single bonds in the molecule (0.5-3.0 kcal mol^{-1}).[10] As there is only ~0.2 kcal mol^{-1} energy difference between two conformers which can give stable packing arrangements crystal nucleation occurs with multiple molecules in the unit cell (Z' = 2) at high temperature.

Table 4. FT-IR absorption maxima (cm^{-1}) of VenHCl polymorphs (KBr pellet).

Form 1	Form 2	Form 6
3323.65	3350.65	3368.02
2943.94	2935.92	2934.00
1612.64	1614.56	1612.64
1581.77	1581.77	1581.77
1512.73	1514.26	1514.26
1473.75	1471.82	1473.75
1242.27	1246.13	1248.06
1178.61	1178.61	1178.61
1039.73	1041.65	1041.65
970.28	972.21	-
927.84	-	927.84
908.55	908.55	908.55
829.47	837.18	837.18
769.67	767.74	767.74
733.02	-	736.87
663.57	655.86	-
-	580.63	580.63
528.54	522.76	520.83

4.7 Conclusion

Several patents literature disclosed different polymorphs of VenHCl, but their interrelationships, phase transitions, and relative stability are not established. In present study, reported forms 1-4 of VenHCl are better characterized by using DSC, TGA, HSM, FT-IR, single crystal XRD and VT-PXRD. Their phase relationship also confirmed though the discovery of a new phase, form 5, obtained by sublimation. In conclusion, a new, more stable, higher melting polymorph of venlafaxine hydrochloride is characterized by single crystal and powder XRD. The discovery of a new thermodynamic polymorph (form 6) of VenHCl by solid–solid phase transition is significant; because it can not be obtained from automated solution crystallization technique applies through high-throughput polymorph screens[16] in pharmaceutical industry. Moreover crystal structure prediction of form 6 by is quite unlikely due to lack of proper advance in methodology in crystal structure prediction[17] for conformationally

flexible molecules/salts and having $Z' > 1$. Finally, in pharmaceutical industry discovering *the most stable polymorph of a commercial drug* has great significance in the post-Ritonavir® (Abbott) era.[3] An exhaustive search of polymorph screening carried out by different methodology and techniques to discover all the possible polymorph of VenHCl and their phase relation quantified through coupling of different experiments outcome.

4.8 Experimental Section

Thermal Analysis

HSM was performed on a PolythermA hot stage and Heiztisch microscope supplied by Wagner & Munz. A Moticam 1000 (1.3 MP) camera supported by software Motic Image Plus 2.0ML is used to record images and videos. About 1-2 mg of the sample was heated @ 5 K/min up to 205 °C and then @ 2 K/min from 205 to 230 °C.

DSC was performed on a Mettler Toledo DSC 822e module and TGA was performed on a Mettler Toledo TGA/SDTA 851e module. Samples (9-10 mg) were placed in open alumina pans for the TG experiments and in crimped but vented aluminum sample pans (4-6 mg) for DSC experiments. Temperature range was 30-300 °C @ 2 K/min. Samples were purged by a stream of nitrogen flowing at 150 mL/min for DSC and 50 mL/min for TGA. The TGA instrument is coupled to a Bruker Tensor FT-IR spectrometer for evolved gas analysis. The evolved vapors from TGA instruments were passed through a coupled heated transfer line at 120 °C. For TGA-IR analysis, the sample size is 10-12 mg, the heating rate is 10 K/min, and the N_2 flow @ 50 mL/min.

Variable Temperature Powder X-ray Diffraction

Powder data were collected on PANlytical X'Pert PRO X-ray powder diffractometer using a parallel beam of monochromated Cu-K$_\alpha$ radiation (λ = 1.54056 Å) and an X'celerator detector at 40 kV and 40 mA. Diffraction patterns were collected over the 2θ range 5-50º. Samples were loaded in an 18-mm alumina holder for variable

temperature powder X-ray diffraction data collection and an aluminum sample holder with a 10 mm diameter sample cavity for room temperature data. The program X'Pert High Score was used for the processing and comparison of powder patterns. Powder Cell 2.3[7] was used for calculating PXRD patterns and for profile fitting and least square refinement of unit cell parameters, a displacement parameter, a background polynomial function, peak shape asymmetry terms, and an overall temperature factor using the known single-crystal structures of polymorphs A, B and D as the model. The sample was heated @ 10º min^{-1} and temperature settings for the variable temperature powder X-ray diffraction data were set at T = 28, 39, 49, 59, 69, 79, 89, 149, 159, 169, and 179 °C. The sample was cooled to room temperature (31 °C) and data were recollected. Powder XRD profiles are plotted in the range 2θ = 10-34° for all samples. There are only minor peaks between 35-50°.

Crystallization Experiments

Venlafaxine hydrochloride was prepared using the procedure of Yardley.[5,6a]

Pure form 1: VenHCl was dissolved in 8 times *i*-PrOH at 65 °C. The clear solution was seeded with 10% form 1 crystal and cooled to 25 °C over 5-6 h. The product was filtered and dried under reduced pressure to get form 1 (form 2 of US 2003/0109585 Al[6g]).Single Crystals of form 1 (orthorhombic) were obtained from MeCN/DMF solvent mixture at ambient temperature.

Pure form 2: VenHCl was dissolved in 16 times *i*-PrOH at 65 °C to get a clear solution and then cooled to 5 °C in 1 h. The product was filtered and dried under reduced pressure to get pure form 2 (form 1 of US 2003/0109585 A1[6g]).

Phase from melting (form 3): 100 mg of VenHCl was taken in a test tube and heated to 215 °C in an oil bath until the compound melted (~30 min). Upon slow cooling, the melt phase was obtained.

Hydrate form 4: 100 mg of VenHCl was dissolved in 5 mL of MeOH or EtOH and left at ambient temperature. The precipitated solid material after 3 days is form 4. The hydrated form is also obtained from the sublimed material when it is left in open air for 1 day.

Phase from sublimation (form 5): 100 mg of VenHCl was taken in a sublimation apparatus and heated to 140-160 °C at reduced pressure (0.2 Torr) for 1 h. The sublimed material was obtained as a glassy, amorphous mass. The semi-solid compound was collected and stored in inert N_2 atmosphere. The sublimed material is unstable and transforms to hydrate form 4 after 1 day in open atmosphere (25-30 °C, RH 40-50%).

Form 6 (High temperature phase) : 5-6 mg of VenHCl (form 2) was taken in a cover slide and heated upto 180 °C and continued for ~30 min to complete solid–solid transformation. On cooling down to room temperature pure crystalline material of form 6 was obtained. Attempted crystallization of form 6 (with and without seeding) from several solvents, such as ethylene glycol, DMSO, DMF, *i*-PrOH, MeOH, EtOH-EtOAc, MeOH-EtOAc, MeCN-DMF, at temperatures varying from 25-100 ºC afforded only form 1 or 2 crystals by unit cell checking or ill-defined powders.

X-ray Diffraction

X-ray reflections were collected on Bruker SMART-APEX CCD area detector with graphite-monochromated (Mo-Kα radiation, λ = 0.71073 Å) with 10 sec exposure time. Crystal structures were solved by direct methods and refined on F^2 in SHELX-TL. H atoms were refined isotropically. The reported crystal structure data is the best solution that could be derive from multiple experiments. Crystal data on polymorphs 1 and 2 are taken from the Cambridge Structural Database (CSD refcodes WOBMUV, WOBMUV01)[18]. Crystallographic data for VenHCl form 6 is provided at the end of this thesis in Appendix III.

Conformation Energy

Energy of conformers of form 1 and 2 calculated using density functional theory (DFT) in B3LYP/6-31G (d,p) level in Gaussian 03.[9] Crystallographic coordinates use as the input; hydrogen atom positions were re-optimized keeping the heavy atoms fixed.

4.9 References

1. W. C. McCrone, in *Physics and Chemistry of the Organic Solid State*, Vol. 2, D. Fox, M. M. Labes and A. Weissberger, (Eds.), Wiley Interscience, New York, **1965**, pp. 725-767.

2. R. Hilfiker, F. Blatter and M. von Raumer, in *Polymorphism in the Pharmaceutical Industry*, Ed., R. Hilfiker, Wiley–VCH, Weinheim, **2006**, pp. 1-19.

3. (a) S. L. Morissette, S. Soukasene, D. Levinson, M. J. Cima and Ö. Almarsson, *Proc. Nat. Acad. Sci. (USA)*, **2003**, *100*, 2180. (b) S. R. Chemburkar, J. Bauer, K. Deming, H. Spiwek, K. Patel, J. Morris, R. Henry, S. Spanton, W. Dziki, W. Porter, J. Quick, P. Bauer, J. Donaubauer, B. A. Narayanan, M. Soldani, D. Riley and K. McFarland, *Org. Process Res. Dev.*, **2000**, *4*, 413.

4. J. P. Yardley, G. E. M. Husbands, G. Stack, J. Butch, J. Bicksler, J. A. Moyer, E. A. Muth, T. Andree, H. Fletcher III, M. N. G. James and A. R. Sieleck, *J. Med. Chem.*, **1990**, *33*, 2899.

5. Patent literature on VenHCl: (a) G. E. M. Husbands, J. P. Yardley and A. E. Muth, American Home Products, U.S. Patent 4,535,186, **1985**. (b) S. M. Rao, K. Vyas, A. S. L. Devi and G. O. Reddy, Dr. Reddy's Research Foundation, WO 02/46140 A1, **2002**. (c) B.-Z. Dolltzky, J. Aronhime, S. Wizel and G. A. Nlsnevlch, Teva Pharmaceuticals, U.S. Patent 2002/0183553, **2002**. (d) B. József, K. N. Peter, S. Gyula, H. Károly, S. K. Zsuzsa, F. Béla, G. Tamás, N. Kálmán and K. György, Egis Gyógyszergyárrt, WO 03/042161 A1, **2003**. (e) P. A. V. D. Shaaf, C. Marcolli, M. Szelagiewicz and B. Freiermuth, Ciba Specialty Chemicals, U.S. 2003/0105359 A1, **2003**. (f) B. -Z. Dolltzky, J. Aronhime and G. A. Nlsnevich, Teva Pharmaceuticals, WO 03/048082 A2, **2003**. (g) K. A. N. All, J. Han and Y. J. Lee, Wyeth, U.S. 2003/0109585 A1, **2003**. (h) J. Han and Y. J. Lee, Wyeth, U.S. 2003/0114536 A1, **2003**. (i) R. S. Bhavin, P. M. Shankarbhal, P. G. Balkrushna, R. N. Venkata, M. S. Champaklal, A. V. Kumar, P. Kanwal and P. P. Ramanbhai, Cadila Healthcare, WO 03/050074 A1, **2003**.

6. (a) D. Vega, D. Fernández and G. Echeverria, *Acta Cryst.*, **2000**, *C56*, 1009. (b) A. Sivalakshmidevi, K. Vyas, S. M. Rao and G. O. Reddy, *Acta Cryst.*, **2002**, *E58*, o1072.

7. Information collected from PriorArt database. www.priorartdatabase.com/IPCOM/000029066

8. Least square refinement was carried out using Powder Cell 2.3. N. Krauss, G. Nolze, Federal Institute for Materials Research and Testing, Berlin, Germany, **2000**.

9. M. J. Frisch *et al*, Gaussian 03, Revision B.05. www.gaussian.com.

10. J. Bernstein, *Organic Solid State Chemistry* Ed., G. R. Desiraju, Elsevier, Amsterdam, **1987**, pp. 471-518.

11. W. Ostwald, *Z. Phys. Chem.*, **1897**, *22*, 289.

12. A. D. Bond, *Chem. Eur. J.*, **2004**, *10*, 1885.

13. B. Moulton and M. J. Zaworotko, *Chem. Rev.*, **2001**, *101*, 1629.

14. (a) A. Burger and R. Ramberger, *Mikrochim. Acta, II*, **1979**, 259. (b) J. Bernstein, *Polymorphism in Molecular Crystals*; Clarendon: Oxford, **2002**, pp 41-42.

15. D. Das, R. Banerjee, R. Mondal, J. A. K. Howard, R. Boese and G. R. Desiraju, *Chem. Commun.*, **2006**, 555.

16. S. L. Morissette, Ö. Almarsson, M. L. Peterson, J. F. Remenar, M. J. Read, A. V. Lemmo, S. Ellis, M. J. Cima and C. L. Gardner, *Adv. Drug Deliv. Rev.*, **2004**, *56*, 275.

17. G. M. Day, W. D. S. Motherwell, H. Ammon, S. X. M. Boerrigter, R. G. Della Valle, E. Venuta, A. Dzyabchenko, J. D. Dunitz, B. Schweizer, B. P. van Eijck, P. Erk, J. C. Facelli, V. E. Bazterra, M. B. Ferraro, D. W. M. Hofmann, F. J. J. Leusen, C. Liang, C. C. Pantelides, P. G. Karamertzanis, S. L. Price, T. C. Nowell, H. Lewis, A. Torrisi, H. A. Scheraga, Y. A. Arnautova, M. U. Schmidt and P. Verwer, *Acta Crys.*, **2005**, B*61*, 511.

18. F. H. Allen and R. Taylor, *Chem. Soc. Rev.*, **2004**, *33*, 463. www.ccdc.cam.ac.uk

CHAPTER 5

KINETIC AND THERMODYNAMIC CONFORMATIONAL POLYMORPHS OF BIS(*P*-TOLYL)KETONE *P*-TOSYLHYDRAZONE

5.1 Introduction

Hydrogen bonding functional group not using their acceptor or donor site is very rare and attract special attention to the chemist.[1] Etter proposed hydrogen bonding rule to explain how molecules can organize via energetically favored patterns of strong hydrogen bonds.[2] Desiraju introduced supramolecular synthon concept to describe solid state self assembly of molecules during crystallization.[3] Supramolecular 'robust synthon' have a dominant role in determining preferred packing motifs during self assembly and crystal nucleation.[4] Molecular organization in organic crystal structures is predominantly directed by strong, directional hydrogen bonds even though their contribution to crystal lattice energy is no more than 20-30%. The major stabilization is from numerous weak, isotropic van der Waals and dispersion interactions. Kitaigorodskii suggested in "*The theory of close packing of molecules*" in 1955,[5] that organic molecules in crystals tend to close pack to fill space as tightly as possible and that packing coefficients of molecular crystals are about 0.65-0.77. For aromatic and hydrocarbon-like molecules the average packing coefficient is ~0.72. Close packing motifs are structure-determining in Kitaigorodskii's model. Kitaigorodskii considered that for a given molecule, the actual crystal structure is the one that corresponds to the most densely packed arrangement of all possible structures. On the other hand, Etter and Desiraju's proposed model is quite reliable in predicting crystal structure synthons when H bonding dominates.

Desiraju[6] linked crystallization to a supramolecular reaction leading to kinetic and thermodynamic products (polymorphs) through Curtin–Hammett like reaction kinetics. Because of strong hydrogen bonding, kinetic forms nucleate faster over thermodynamic one and polymorphism is highly unlikely if the kinetically favored form is also the more stable one. Polymorphs that differ in the nature of H bond synthon or molecular conformation or overall packing features are well documented[7] but it is quite

rare to find a hydrogen-bonded crystal structure and another close-packed polymorph without strong H bonds. Gavezzotti and Fillippini[8] analyzed crystal structures and thermodynamic stability of organic polymorph clusters over a decade ago, but there were no examples of H-bonded vs. non-H-bonded pairs reported at that time. To understand the delicate balance between kinetic and thermodynamic factor those polymorph clusters are ideal candidates, in which one structure a hydrogen-bonded form and another close-packed, dense polymorph are present. To find such forms the Cambridge Structural Database (CSD)[9] was searched.

5.2 Literature Occurrence of H-bonded vs. Non-H-bonded Pairs

The Cambridge Structural Database (CSD 5.28-Nov 2006) was searched for polymorphic clusters having the qualifier polymorph, form, phase, or modification excluding organometallic compound and 3-D coordinate not determined gave 5882 hits. This subset was searched for molecules with O–H/ N–H group present but ionic, polymeric and disorderd structures having R factor > 0.1 were discarded to give 1868 hits. These 1868 structures were searched such that there is no strong O–H···O, O–H···N, N–H···O, N–H···N hydrogen bond (D–H···A) in the structure (contact criteria: H···A 1.5–2.5 Å, D–H···A 120–180º, D···A 2.5–3.5 Å). 93 polymorphic refcodes from this subset were extracted that have no strong H bonds but contain OH/ NH groups (see Appendix IV for CSD refocdes). These 93 clusters were manually analyzed to give 4 clusters in which there is no strong H bond in one polymoprh but another reported form has conventional H bonds (Scheme 1). These four refcodes are KUVWON,[10a] MAMGUD,[10b,c] UCUGOP,[10d] WEFKEY.[10e] Structure analysis of these four polymorphic pairs reveal KUVWON and UCUGOP have O–H···O or N–H···N hydrogen bond in one structure, whereas another form being stabilized by a weaker O–H···π[10a] or N–H···π[10d] interaction. In other two molecule (MAMGUD and WEFKEY) O–H···N/ N–H···O H bond are present in one structure but absent in the second form.[10b,c,e] However kinetic-thermodynamic relationship and crystal lattice energy relation of H-bonded and close-packed polymorph pairs were not discussed by their authors.[10b,c,e]
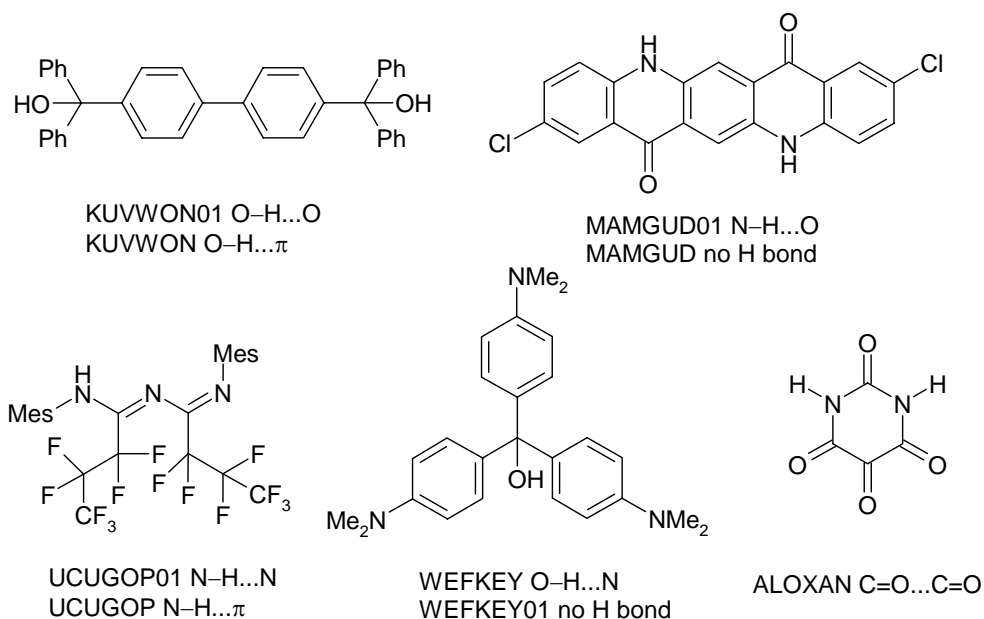
Scheme 1. Four polymorph pairs in the CSD in which there is strong H bonding in one crystal structure and weaker or no H bonding in the other form, as indicated against their refcodes. The crystal structure of alloxan is stabilized by dipolar interactions. No H bonded polymorph is known for alloxan.

Price and coworkers[11] have studied crystal structures of alloxan experimentally and computationally. Experimental structure is stabilized by strong dipolar C=O···C=O interactions and dense packing with no conventional N–H···O hydrogen bonds. They have also shown that this non-H bonded structure lies at the global lattice energy minimum in crystal structure prediction frames. No experimental H-bonded polymorph of alloxan is known till date. The work presented in this chapter is the study of polymorphic system bis(*p*-tolyl)ketone *p*-tosylhydrazone **6** (Scheme 2), where kinetic forms have expected N–H···O=S hydrogen bond dimer synthon and thermodynamic, higher melting form 3 is stabilized by close packing to the exclusion of conventional H bonds such as O–H···O, N–H···O and N–H···N.
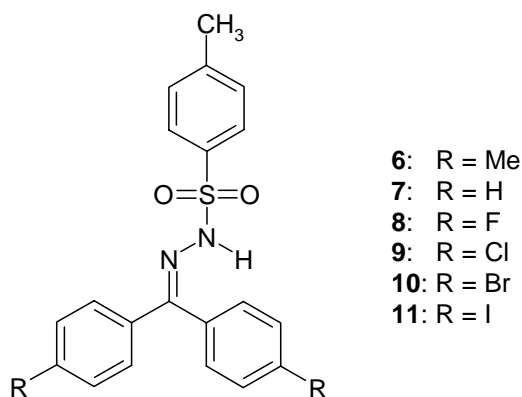
Scheme 2. Compounds studied in this Chapter.

5.3 Molecular Engineering Approach to Produce New Conformational Polymorph

In a recent thesis from our group, S. Aitipamula reported that hydroquinone and 4,4′-terphenyl diol make a phenylogue-extended series of polymorphs (Scheme 3a).[12] The fascinating rhombohedral structure of β-hydroquinone was reproduced in an another diphenolic compound through applying molecular engineering approach. To discover new conformational polymorphic system, similar molecular engineering approach applied to acetone tosyl hydrazone, for which two conformational polymorphs are reported.[13] Now molecule **6** has Ar–SO$_2$ and Ar–C–Ar portions (Scheme 3b), which can vary independently to several conformations. Interestingly, molecule **6** afforded three conformational polymorphs in the following sequence of experiments: it crystallized as form 1 (space group *C*2/*c*) with the expected SO$_2$NH···O=S dimer synthon and two additional polymorphs (forms 2, 3 in space group *C*2/*c*, *P*2$_1$/*c*) wherein the NH donor surprisingly does not engage in strong N–H···O hydrogen bonds with SO$_2$ acceptors.
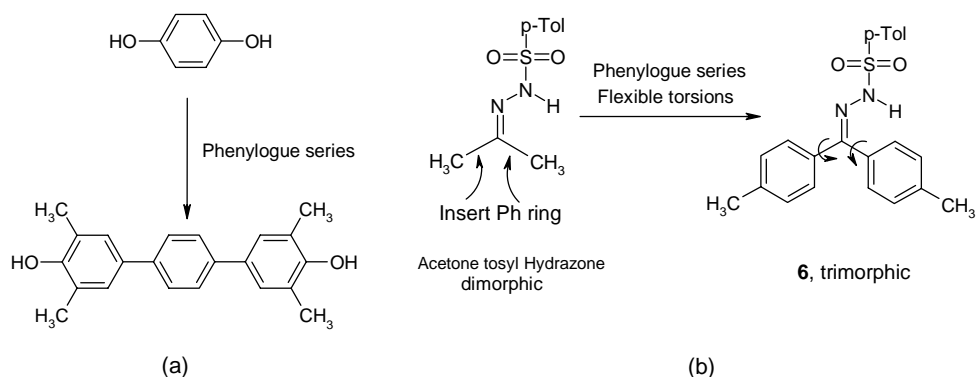
Scheme 3. Phenylogue series approach to polymorph clusters illustrated for hydroquinone [ref. 12]. (b) From dimorphs of acetone tosylhydrazone → trimorphs of tolyl tosylhydrazone **6**.

Polymorphism and pseudopolymorphism is very common in sulfonamide drug compounds. Almost 50% of sulfonamide functional group content molecule exhibits polymorphism.[14] Bingham *et al.* reported 100 solvates of sulfathiazole,[14c] which is an antimicrobial drug. Two self-complementary hydrogen bond synthons of SO_2NH are bimolecular dimer and extended catemer of graph set notation $R_2^2(8)$ and $C(4)$.[15] A CSD search on the occurrence probability of hydrogen bond synthons in SO_2NH group was carried out. The CSD (ConQuest 1.9, November 2006 update) was searched for sulfonamide compounds with the qualifiers: organic, $R < 0.10$, 3-D coordinates determined, no errors, not polymeric. The sub-database of 1266 hits was analyzed for hydrogen bond synthons shown in Scheme 4 in the distance/ angle range: H···A 1.5–2.5 Å, D–H···A 140–180º. Synthon probability is the number of hits containing a particular motif as a percentage of compounds that contain the required functional group, as reported by Allen et al.[4a] Among the 1266 hits of accurate organic crystal structures of sulfonamide in CSD, 16.1% and 18.5% of structures are stabilized by dimer and catemer synthon respectively (Scheme 4). NH donor approaching the S=O group or another competing acceptor, such as carbonyl C=O, ether/alcohol C–O or pyridine N can result synthon polymorphism.[7a] Alternatively, the molecules may be assembled *via* the same H bond synthon but they exist in different conformations to exhibit conformational polymorphism. There is no example found of a polymorphic sulfonamide molecule that

differs by the presence of strong N–H···O/N hydrogen bond in one crystal structure and the complete absence of strong H bonds in another form. There are 28 sulfonamides with no strong H bonds found in the search (see Appendix V for molecular diagram). They are all secondary amides and the C atom on the NH group side is secondary/ tertiary. Moreover absence of strong H bonding from the NH donor is not necessarily due to a deficiency of acceptor groups because some of these molecules have additional O/N acceptors (e.g. CSD refcodes AYEQEA, AYEQIE, IHEJEK, ODASAQ). There are several N–*sec* and even N–*tert* sulfonamides with normal N–H···O H bonds of 2.0-2.3 Å in the sub-database of 1266 crystal structures (e.g. CSD refcodes ATAMOX, PELZOV, VOTZOT, PSAHPP, TIDQUS, AXAGOV). Interestingly compound **6** formed dimer in form 1 and close pack structure in form 2 and 3 with no strong H bonding. There was no catemar H bonded polymorph produced in our experiments. Structural details of three conformational polymorphs are discussed.
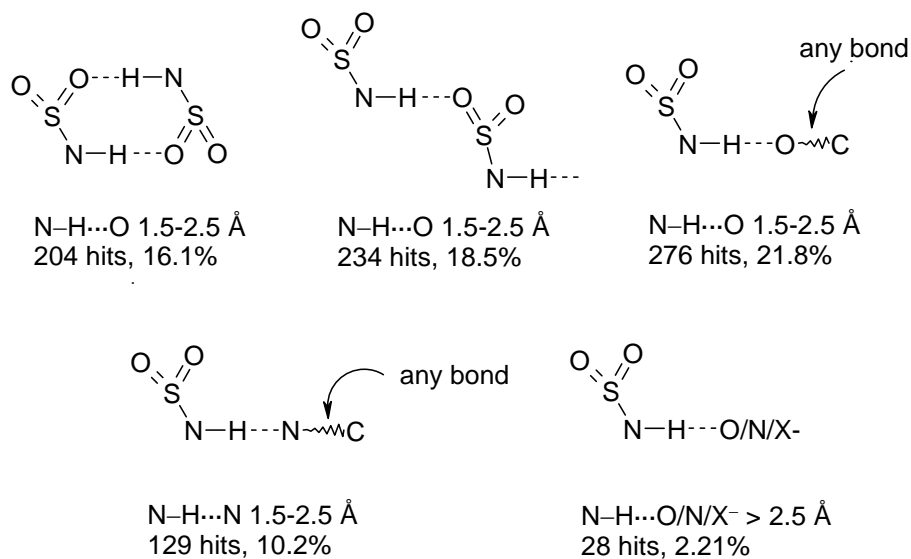
Scheme 4. Occurrence probability of hydrogen bond synthons of sulfonamide group in a sub-database of 1266 crystal structures (CSD).

5.4 Conformational Polymorphs of 6

Initially, recrystallization of **6** from EtOH/CH_2Cl_2 afforded hexagonal shape single crystals (Figure 1a) for X-ray diffraction, designated as form 1. Structure solution and refinement solved in monoclinic $C2/c$ space group. Solvent-drop grinding (or kneading) is a standard method in polymorph screens nowadays because it gives good success rate for finding new crystalline forms.[16] Microcrystalline powder of **6** was grinded with a few drops of CH_2Cl_2 and using this material as seed afforded plate type single crystals of form 2 (Figure 1b). Crystals were twinned despite several attempts and the best of these was mounted on the goniometer for X-ray data collection. Crystal structure solution proceeded using CELL_NOW and TWINABS program (see experimental section) and structure solved in monoclinic $C2/c$ space group. A third polymorph (form 3) of **6** obtained from EtOH solvent (Figure 1c) at ambient temperature, which solved in monoclinic $P2_1/c$ space group. The crystallographic details for the trimorphs of **6** are given in Table 1. The bulk purity of polymorphic solids 1 and 3 was confirmed by their experimental powder X-ray diffraction (XRD) pattern with their simulated powder XRDs from the X-ray structure (Figure 2).[17] Transient form 2 could not been recovered in many trials under different experimental conditions, such as several solvents, using new glassware, and change to a different laboratory, subsequent to the isolation of stable form 3. Form 2 belongs to the anecdotal category of disappearing polymorphs.[18]

| (a) | (b) | (c) |
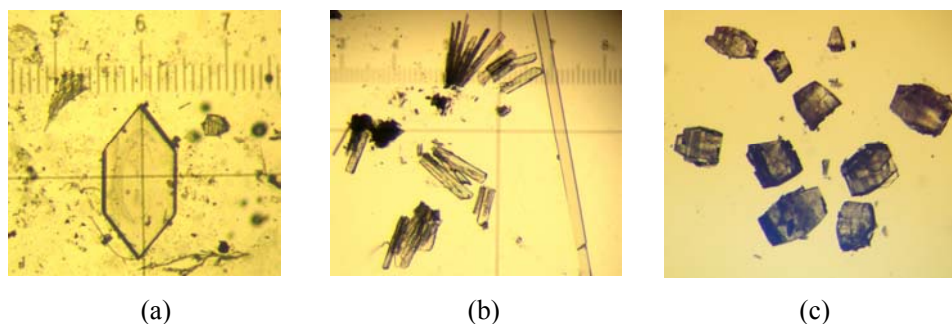
Figure 1. Single crystals of sulfonamide **6**. (a) Form 1 (crystallized from EtOH/CH_2Cl_2). (b) Form 2 (kneading followed by crystallization from CH_2Cl_2). (c) Form 3 (crystallized from EtOH).

Table 1. Crystal data of three conformational polymorphs obtained from sulfonamides **6**

	Form 1	Form 1 (low temp data)	Form 2	Form 3
Empirical formula	$C_{22}H_{22}N_2O_2S$	$C_{22}H_{22}N_2O_2S$	$C_{22}H_{22}N_2O_2S$	$C_{22}H_{22}N_2O_2S$
Formula wt.	378.48	378.48	378.48	378.48
Crystal system	Monoclinic	Monoclinic	Monoclinic	monoclinic
Space group	$C2/c$	$C2/c$	$C2/c$	$P2_1/c$
T [K]	100(2)	298(2)	298(2)	298(2)
a [Å]	22.0093(13)	22.250(3)	42.043(8)	8.2971(5)
b [Å]	11.9763(7)	12.1201(15)	8.0381(16)	39.758(3)
c [Å]	15.1853(9)	15.2891(19)	12.345(3)	5.9349(4)
α [deg]	90	90	90	90
β [deg]	100.937(1)	100.538(2)	104.08(3)	97.2940(10)
γ [deg]	90	90	90	90
Z	8	8	8	4
Volume [Å^3]	3930.0(4)	4053.5(9)	4046.5(14)	1942.0(2)
D_{calc} [g/cm^3]	1.279	1.240	1.242	1.295

2θ / °

(a)

2θ / °

(b)
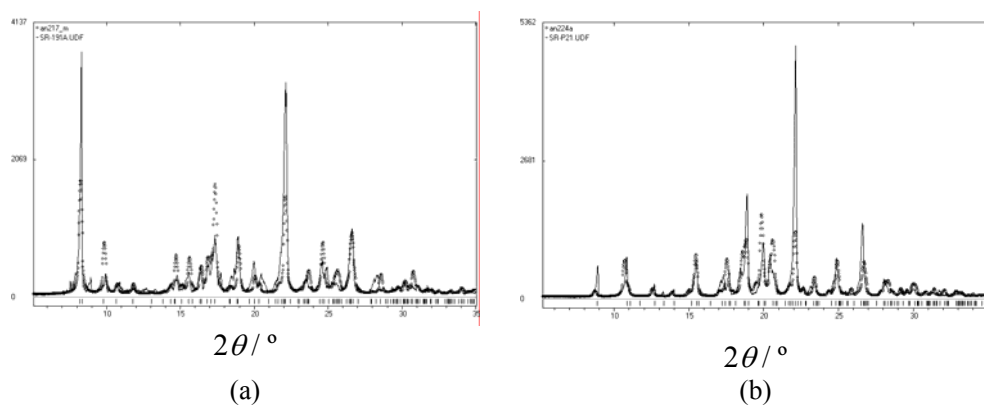
Figure 2. Least squares refinement of the experimental powder X-ray diffraction pattern (line) with the calculated profile (circles) in Powder Cell 2.3: (a) form 1; (b) form 3.

5.4.1 Crystal Structure of Form 1

Form 1 stabilized by SO_2NH expected centrosymmetric dimer synthon of N–H⋯O (1.99 Å, 159°) as shown in Figure 3a. Numerous phenyl CH donors involve in weak C–H⋯O interaction to connect molecular aggregates of dimer chains (Table 2). Ortho hydrogens of S-tolyl and one of N-tolyl ring involved in via C–H⋯O and C–H⋯π interactions (2.45 Å, 2.53 Å) with the 2_1 screw axis related molecule of next chain (Figure 3b). Another C–H⋯O interaction (2.44 Å, 173°) connect two glide related dimer chains.

(a)   (b)
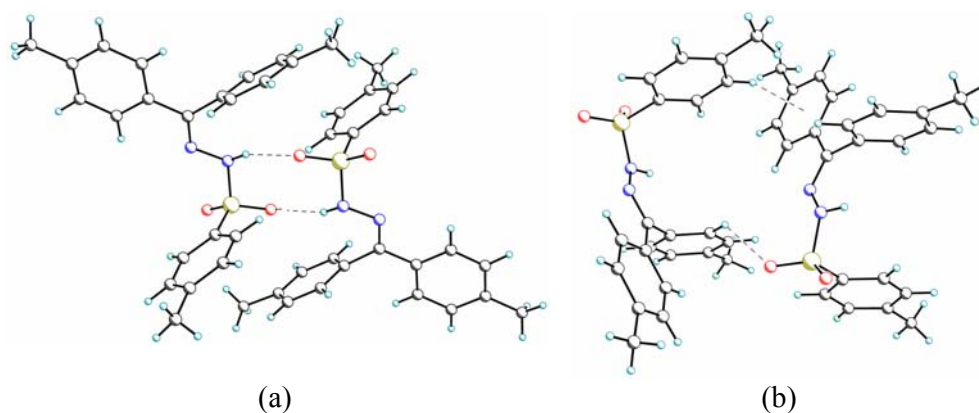
Figure 3. (a) Sulfonamide N–H⋯O dimer synthon of $R_2^2(8)$ graph set in the crystal structure of form 1 (*C2/c*) of molecule **2**. (b) Auxiliary C–H⋯O and C–H⋯π interactions from phenyl CH donors.

5.4.2 Crystal Structure of Form 2 and Form 3

Crystal forms 2 and 3 have similar molecular packing devoid of strong H bonds (Figure 4) The strong NH donor is not involved in H bonding up to H⋯O < 3.0 Å (Table 2). However there are several weak C–H⋯O interactions present between phenyl and methyl CH with the SO_2 acceptors in the distance range ~2.7 Å for form 2. SO_2 acceptors of form 3 are connected to two-point C–H⋯O motif from phenyl CH donors (~2.5 Å) but there are no short contacts between molecules aligned along the monoclinic *b*-axis (=39.76 Å).

(a)   (b)
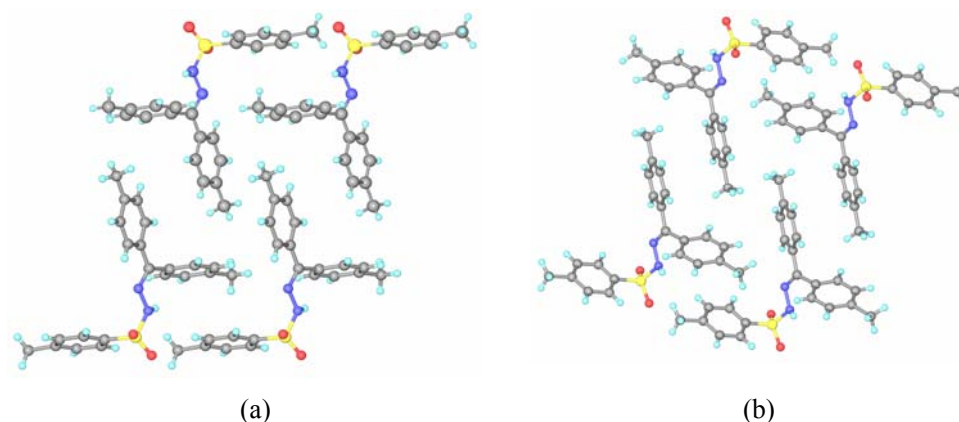
Figure 4. The sulfonamide NH donor does not participate in conventional hydrogen bond or N–H···π interaction in (a) form 1 (*C*2/c) and (b) form 3 (*P*2$_1$/*c*). Note the herringbone T-motif between tolyl groups.

The hydrogen bonded dimer structure of form 1 has crystal density of 1.240 g cm^{-3}, which is typical of molecular crystals. Whereas form 3 has good close packing and higher density but no strong H bonds (comparison of forms 1-3 at 298 K: packing fraction 64.6, 64.7, 67.9 %; density 1.240, 1.242, 1.295 g cm^{-3}). Close packing arrangement stabilized form 3 and compensate the energy comes from H-bonding interactions. On the other hand form 2 has no strong H bonds and also of lower density. It is also found to be a metastable polymorph in further experiments. The highest density and packing fraction of crystal form 3 is explained (Figure 5) by the better eclipsing of tolyl rings and more efficient close packing than form 2 structure.

(a)   (b)
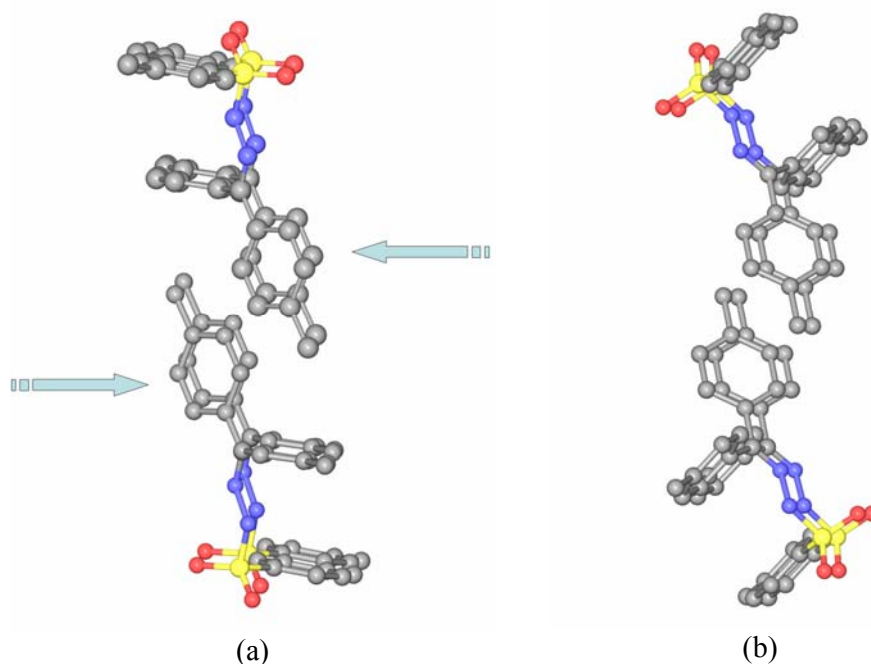
Figure 5. (a) The movement of form 2 molecules towards each other (marked by arrows) results in better eclipsing and more efficient close packing, as shown for dense form 3 (b). The inter-centroid ring separation between tolyl rings decreases from 6.2 to 4.9 Å and the *c*-axis contracts from 12.34 Å (*C2/c*, Z = 8) to 5.93 Å (*P2₁/c*, Z = 4).

5.4.3 Crystal Structure of 6.(CH₂Cl₂)₀.₅ Solvate

In addition to polymorphs 1-3 of compound **6**, a pseudopolymorph **6**.(CH$_2$Cl$_2$)$_{0.5}$ was isolated from *n*-hexane/CH$_2$Cl$_2$ in *P*-1 space group.[19] This structure stabilized by the centrosymmetric N–H···O hydrogen bond dimer synthon. The other O-atom of SO$_2$ involves in C–H···O interaction with phenyl CH doners (Table 2). Square channels of aromatic walls surround CH$_2$Cl$_2$ guest molecules in the hydrogen-bonded host structure of **6** as shown in Figure 6. CH$_2$Cl$_2$ guest resided in a 8.8 × 7.1 Å void surrounded by four dimers of molecule **6.**
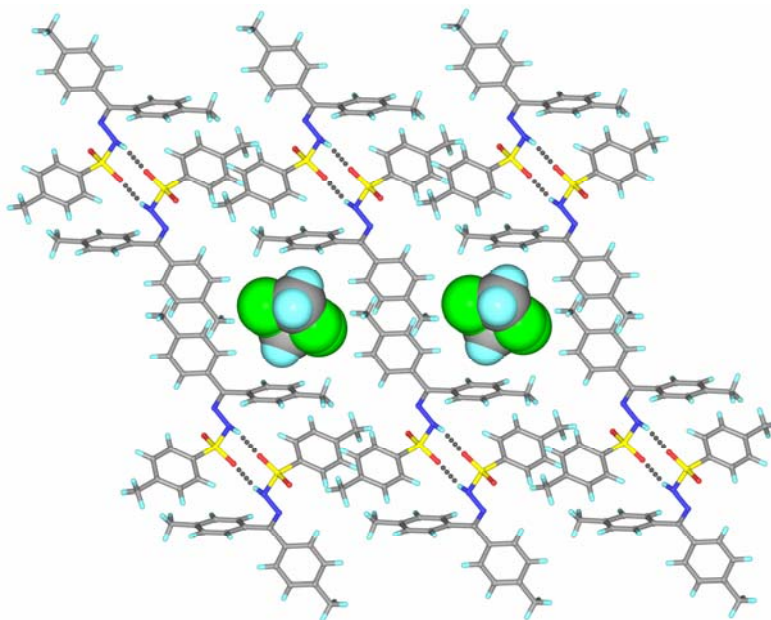
Figure 6. Sulfonamide N–H···O dimer synthon and CH_2Cl_2 molecules in the 8.8 × 7.1 Å voids created by the tolyl groups in **6**.$(CH_2Cl_2)_{0.5}$.

Table 2. Hydrogen bond geometry[a] for the three polymorphs of **6** and CH_2Cl_2 solvate.

Com pound	Interaction	H···A/ Å, d	D···A/Å D	∠D–H···A /° θ	N2-N1-S1-C5/° τ_1
6 form 1 (100 K)	N(1)–H(1)···O(1)	1.99	2.954(2)	159	65.9
	C(11)–H(11)···O(2)	2.44	3.520(2)	173	
	C(16)–H(16)···O(2)	2.45	3.205(2)	126	
	C(6)–H(6)···O(2) (intra)	2.47	2.886(2)	102	
	C(3)–H(3)···π	2.53		155	
6 form 2	C(4)–H(4)···O(2)(intra)	2.45	2.875(9)	102	70.3
6 form 3	C(16)–H(16)···O(2)	2.47	3.280(3)	140	62.4
	C(6)–H(6)···O(2) (intra)	2.52	2.913(2)	100	
6.CH_2Cl_2	N(1)–H(1)···O(1)	1.99	2.971(3)	162	60.3
	C(11)–H(11)···O(2)	2.43	3.359(4)	143	

[a] Neutron-normalized values.

5.5 Benzophenone Derivatives of *p*-Tosyl hydrazine

As a further extension to search for new polymorphic systems different benzophenone analogues were studied. The *para*-methyl group on the benzophenone moiety of **6** was replaced with other groups, such as H, F, Cl, Br (**7-10**). The iodo derivative **11** did not afford single crystals for X-ray diffraction. These compounds did not show any evidence of polymorphism under similar experimental conditions, such as crystallization from different solvents, solvent drop grinding, and using ball mill ground material as seeds. These structures are consistently stabilized by the sulfonamide N–H···O=S dimer (Figure 7).
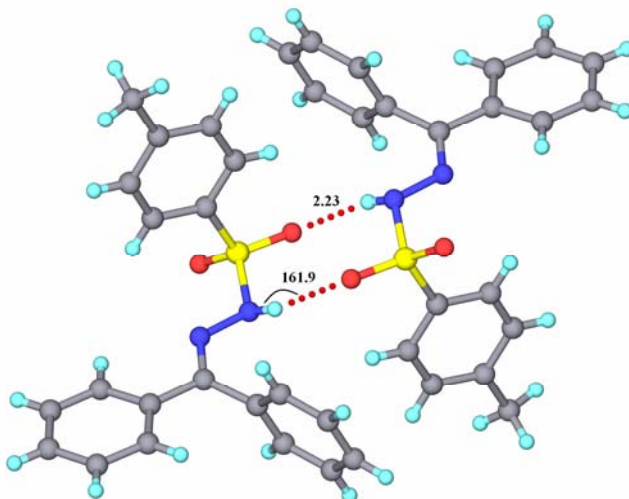
Figure 7. SO$_2$NH dimer synthon in phenyl derivate **7**. The distance and angle of N–H···O=S is indicated (Å, deg). Halogen derivatives **7-10** contain the same dimer synthon but have different overall crystal packing.

Phenyl and difluoro derivatives (**7** and **8**) were isolated from ethanol at ambient temperature and crystal structures were solved in triclinic *P* $\bar{1}$ and monoclinic *P*2$_1$/c space group respectively. The packing of both the crystal lattice mainly constitute through centrosymmetric dimer of N–H···O=S. (Table 3). Chloro and bromo sulfonamides (**9** and **10**) involved in many C–H···O interactions along with N–H···O=S

dimer synthon for the stabilization of crystal structure (Table 3). Chloro derivative also involved in Cl···Cl type 1 interaction[20] (Figure 8a) but bromo derivative does not show any halogen-halogen interactions. There is a degree of similarity expected when methyl group is exchanged with a halogen or among the halogen derivatives.[21] Form 1 of tolyl compound **6** and chloro structure **9** are isomorphous and isostructural (see Appendix III for crystal data). However, in the present series of structures the recurring motif is the sulfonamide dimer synthon but there is little similarity in the space group and/ or molecular arrangement and overall packing of crystal structures of **6-10.** The chloro and bromo sulfonamides **9** and **10** also crystallized as benzene solvates. Solvates **9.**(PhH)$_{0.5}$ and **10.**(PhH)$_{0.5}$ exhibit similar molecular packing in their isomorphous triclinic unit cells. These solvate structures stabilized by the centrosymmetric N–H···O hydrogen bond dimer synthon and guest occupied the square channel similar to the chloroform solvate of **6** structure (Figure 8b).

(a)   (b)
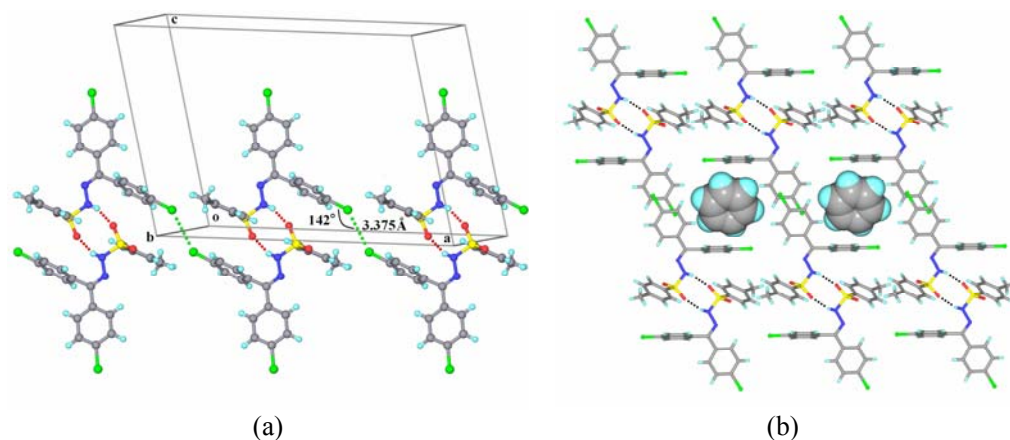
Figure 8. (a) Chloro sulfonamide **9** engage in N–H···O=S dimer synthon and type 1 halogen-halogen interaction in crystal packing arrangement. (b) Inclusion of benzene in the cavity of chloro sulfonamide **9**. Benzene solvate of bromo sulfonamide **10** also has similar structure.

Table 3. Hydrogen bond geometry in sulfonamide crystal structures **7-10**.[a]

Compound	Interaction	H···A/ Å d	D···A/ Å D	∠D–H···A /° θ	N2-N1-S1-C5 /° τ_1
7	N(1)–H(1)···O(1)	2.04	3.009(3)	160	62.6
	C(4)–H(4)···O(1) (intra)	2.48	2.902(4)	102	
8	N(1)–H(1)···O(1)	2.09	3.011(2)	151	66.5
	C(11)–H(11)···O(2)	2.36	3.335(3)	149	
	C(6)–H(6)···O(2) (intra)	2.50	2.900(2)	100	
9	N(1)–H(1)···O(1)	1.98	2.948(2)	160	64.9
	C(11)–H(11)···O(2)	2.46	3.5346(2)	173	
	C(16)–H(16)···O(2)	2.40	3.248(2)	134	
	C(6)–H(6)···Cl(2)	2.73	3.457(2)	124	
	C(6)–H(6)···O(2) (intra)	2.48	2.895(2)	101	
	C(18)–Cl(2)···Cl(2)–C(18)	---	3.375(1)	142	
10. PhH	N(1)–H(1)···O(1)	2.03	3.006(3)	162	59.9
	C(11)–H(11)···O(2)	2.47	3.356(3)	139	
10	N(1)–H(1)···O(1)	1.97	2.937(2)	161	65.8
	C(6)–H(6)···O(1)	2.47	3.455(3)	151	
	C(10)–H(10)···O(2)	2.48	3.320(2)	134	
	C(17)–H(17)···O(2)	2.46	3.536(3)	175	
	C(4)–H(4)···O(2) (intra)	2.48	2.899(2)	101	
10. PhH	N(1)–H(1)···O(1)	2.07	3.025(4)	157	60.2
	C(19)–H(19)···O(2)	2.43	3.333(5)	140	

[a] Neutron-normalized values.

5.6 Conformation Analysis and Lattice Energy

There is one symmetry-independent molecule in the unit cell of each polymorph but the flexible molecule adopts a different conformation in each of the crystal structures, i.e. forms 1-3 are conformational polymorphs (Figure 5). Molecular conformation energy (E_{conf}) of these three different conformations was computed in Gaussian 03 at the B3LYP/6-31G(d,p) level.[22a] E_{conf} value of form 1 have the stable

conformation, whereas form 2 and form 3 conformations are destabilized by 6.29 kcal mol^{-1} and 0.85 kcal mol^{-1} respectively. The energy difference between these possible conformers is comparable to the energy of hydrogen bonds and the cumulative energy from aromatic packing motifs, and so the molecule may adopt metastable conformer(s) in the crystal lattice.

Crystal lattice energies (U_{latt}) were calculated in *Cerius*^{2} using COMPASS force field.[22b] ΔU_{latt} follows the stability order form 3 < 2 < 1. Energy differences between molecular conformers and crystal lattice energy are of comparable magnitude within a few kcal mol^{-1} (Table 4) and so their cumulative effect must be taken to compute total crystal energies (E_{total}). The energy values in Table 4 are consistent with the observed kinetic, metastable and thermodynamic state of polymorphs 1-3. The sulfonamide molecule is flexible and has different torsion angles in the benzophenone and tosyl portions of the molecule (Figure 9). The necessity of taking molecular conformer stabilization (or destabilization) into account for computing crystal energy is underscored by the fact that ΔE_{total} ranking matches with thermal measurements and phase relation. Form 3 is the most stable polymorph (thermodynamic), form 1 is higher in energy by 2.54 kcal mol^{-1} (kinetic), and form 2 has very high energy of 7.86 kcal mol^{-1} (metastable, disappeared). Energy difference of ~2.5 kcal mol^{-1} between forms 1 and 3 is typical for polymorphs. On the other hand, ΔU_{latt} values suggest that form 1 is less stable than form 2 which does not agree with our experiments. The reason for the disappearing nature of crystal form 2 is not as much the lattice energy but its highly metastable molecular conformer in the crystal lattice.

Table 4 Lattice energy (U_{latt}, *Cerius*^{2}, COMPASS, kcal mol^{-1}), conformation energy (E_{conf}, Gaussian 03, B3LYP/6-31G(d,p), kcal mol^{-1}) and total energy ($\Delta E_{total} = \Delta U_{latt} + \Delta E_{conf}$).

Polymorph	U_{latt}	ΔU_{latt}	E_{conf}	ΔE_{conf}	ΔE_{total}
form 1	−41.13	3.39	−947322.05	0.00	3.39
form 2	−42.10	2.42	−947315.76	6.29[a]	8.71
form 3	−44.52	0.00	−947321.20	0.85	0.85

[a] The value may be over-estimated due to higher *R*-factor of 0.723 for form 2.
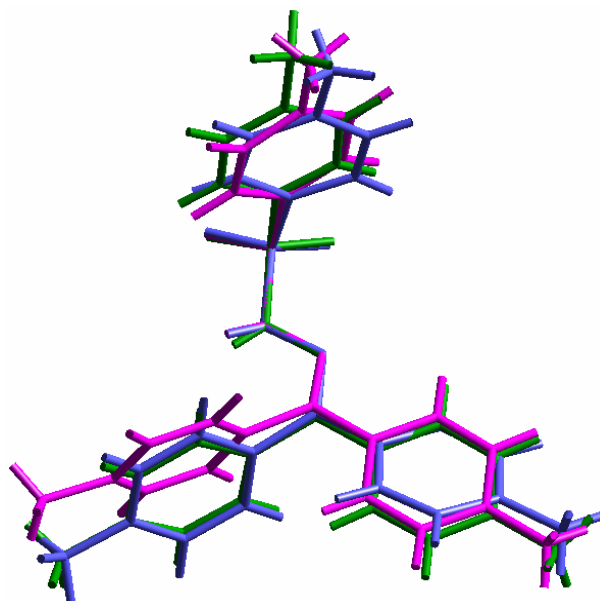
Figure 9. Molecular conformations of sulfonamide **6** in polymorphs 1-3. Magenta = form 1, Green = Form 2, Blue = Form 3. Note that the tolyl groups are oriented differently in the three forms.

Conformation analysis of compound **6** (as well as other derivatives) shows that the variation occurs in the $N–N–S–C_{phenyl}$ moiety ($\tau_1 = 60\text{-}70º$, Table 2,3); variation in $N–N–C–C_{phenyl}$ torsions is minimal ($\Delta\tau_2$, $\Delta\tau_3$ <4º) with respect to the global minimum rotamer. The conformer energy vs. torsion angle profile of **6** was therefore plotted by varying τ_1 while τ_2 and τ_3 were held constant (Figure 10a). The phenyl ring torsional variation and τ_2, τ_3, are ignored because that will make system complex for computations. Moreover, aryl group orientation around the SO_2NH functional group variation is more and that leads to main conformational difference among conformers of **6**. Molecular conformations in observed three polymorphs of **6** (Table 2) lie close to the global minimum rotamer at $\tau_1 = 60º$, i.e. within 10º torsion angle and 5 kcal mol^{-1} energy range. Higher energy conformers which reside on the 1-5 kcal mol^{-1} energy range can compensate energy penalty of this value easily by crystal structure stabilization due to stronger hydrogen bonds and better close packing. The significant torsion angle (τ_1) in

form 1 of tolyl compound **6** is similar to monoclinic form II of acetone hydrazone (65.9, 64.5° respectively),[13] showing similarity between these phenylogue-related crystal structures, as was anticipated at the beginning of this study (Scheme 3). Interestingly sulfonamide molecule is present in the stable rotamer ($\tau_1 \approx 60°$) in all the three solvates crystal lattice. The overlay of molecular conformers in these 10 crystal structures (Figure 10b; polymorphs of **6**, **7-10**, 3 solvates) shows that there is wide variation in the orientation of the three pendant tolyl groups if orientation of the central SO_2NH moiety kept as fixed in the 8 crystal structures containing the dimer synthon and the two polymorphs without strong H bonds.

(a)   (b)
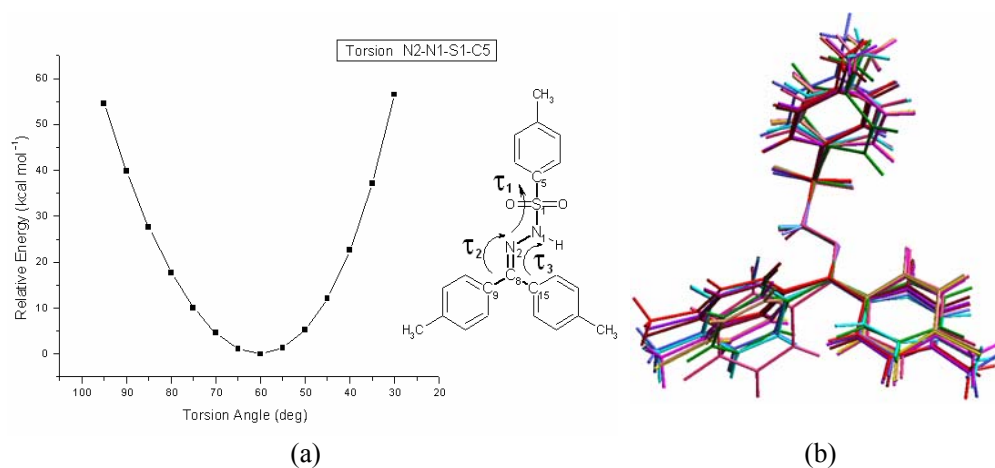
Figure 10. (a) Potential energy surface map for molecule **6** showing the deep curvature near the stable SO_2NH torsion angle, $\tau_1 = $ N2–N1–S1–C5 = 60°. Conformer energies were computed in Gaussian 03, B3LYP/6-31G(d,p) and scaled to the lowest value = 0.0. The observed conformers (Table 2) are within a 10° torsion angle and 5 kcal mol^{-1} energy range of the stable conformer. (b) Overlay of molecular conformers in crystal structures **6-10**. Tolyl **6**, form 1 = Red, Tolyl **6**, form 2 = Blue, Tolyl **6**, form 3 = Cyan, Tolyl **6**•(CH$_2$Cl$_2$)$_{0.5}$ = Magenta, Phenyl **7** = Green, Fluorophenyl **8** = Pink, Chlorophenyl **9** = Purple, Chlorophenyl **9**•(PhH)$_{0.5}$ = Brown, Bromophenyl **10** = Dark Red, Bromophenyl **10**•(PhH)$_{0.5}$ =Yellow.

5.7 Thermal Analysis

Inter-conversion and stability of forms 1-3 were examined by differential scanning calorimetry (Figure 11). Form 1 melts at 142-143 °C, the minor endotherm at 159 °C arising due to concomitantly growing form 3. Form 2 undergoes phase transition at ~140 °C followed by melting at 157-158 °C. Form 3 has a flat base line and melts in a clear endotherm at 159-160 °C with no evidence of any other phase change. Melting point of form 3 is higher than form 1 by 17 °C, it has highest density and packing fraction, and its crystal lattice energy is lower than that of form 1. To rationalize more accurate phase relation among different forms of **6** visually, thermal events were monitored through hot stage microscopy (Figure 12). Concomitant existence of form 1 along with minor amount of form 3 was confirmed by the visualization of two melting events (142 ºC and 156 ºC). Phase transformation of form 2 to form 3 going through melting is visualized at around 142-143 ºC, followed by melting of form 3 at 157-158 ºC. Form 3 has sharp melting at 158 ºC. The thermal transformations concluded from DSC experiments mentioned earlier are consistent with HSM results.
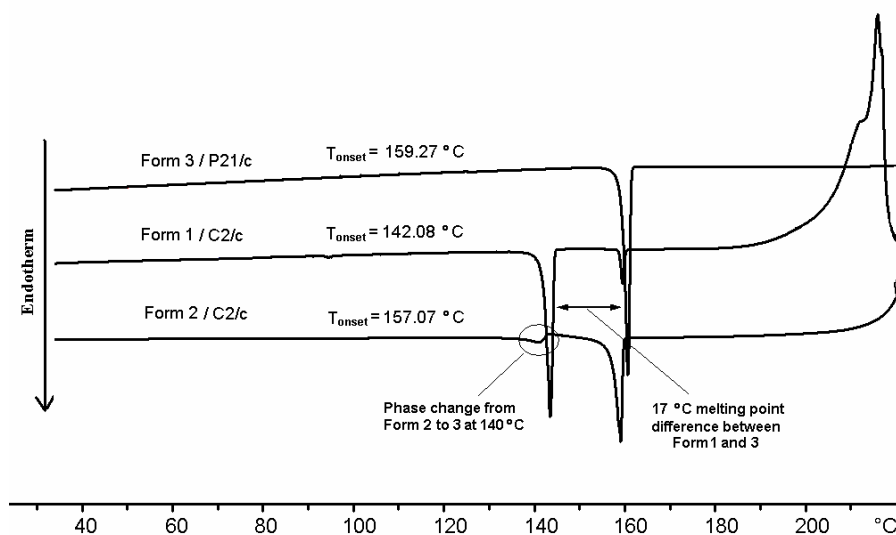
Figure 11. DSC trace of forms 1-3 of sulfonamide **6** polymorphs. Form 1 crystallized concomitantly with a minor amount of thermodynamic form 3. Form 2 undergoes phase transition to form 3 at 140 °C. Form 3 exhibits a sharp melting endotherm at 159 °C.

(a) 30 ºC   (b) 143 ºC   (c) 156 ºC

(d) 30 ºC   (e) 142-143 ºC   (f) 157-158 ºC

(g) 30 ºC   (h) 157 ºC   (i) 158 ºC
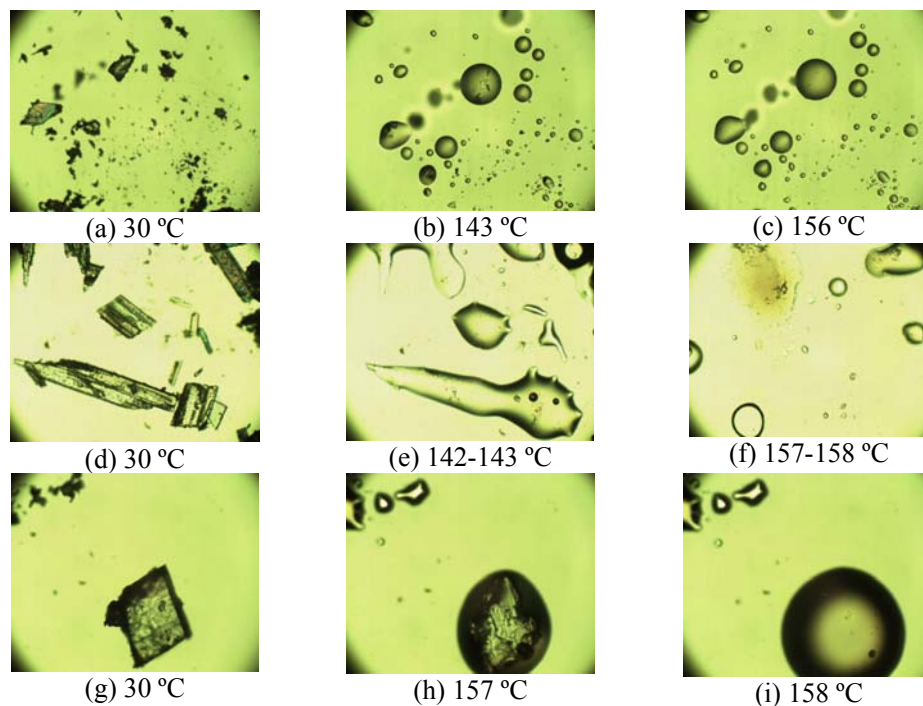
Figure 12. HSM frames. Form 1: As crystallized form 1 (a) melts at 142-143 ºC. A few crystallites of concomitant form 3 melt at 156-157 ºC. From 2: As crystallized form 2 (d) melts at 142-143 ºC (e), and form 3 (after phase transition) melts at 157-158 ºC (f). Form 3: Pure form 3 (g) starts to melt at 157 ºC (h) and this process completes at 158 ºC (i) Sample was heated @ 5 ºC min^{-1}.

Packing diagram of form 2 and form 3 reveals lot of similarity and the facile phase transition of form 2 to 3 is understood from the reorganization of molecule to better packing arrangement. Tolyl rings of a cluster of four molecules are arranged in a herringbone T-motif in both crystal structures (Figure 4,5). These inter-digitating tolyl groups are farther apart in form 2 and move closer to each other in the crystal lattice of 3 upon heating with a decrease in inter-ring distance and c-axis (Figure 5). Their cell edges follow simple numerical relation (Table 1): $a_{form3} \approx b_{form2}$ (8.29, 8.04 Å); $c_{form3} \approx 0.5 \times c_{form2}$ (5.93, 12.34 Å); $b_{form3} \approx a_{form2}$ (39.76, 42.04 Å). A molecular reorganization pathway for metastable form 2 to thermodynamic form 3 is explained. But

transformation of form 1 to 3 is very difficult to explain because their H bonding, molecular packing and crystal structures are very different and there was no transformation of form 1 to 3 observed in thermal analyses.

Thermal gravimetry analysis and DSC were done for the solvate structures reported in this chapter to confirm the host: guest stoichiometry. Solvent loss while heating of choloroform solvate of compound **6** (Figure 13a) and benzene solvate of **9** and **10** (Figure 13b, c) is consistent with 2:1 of host and guest ratio. First broader endotherm corresponds to solvent loss and then sharp endotherm is for melting of the desolvated material. For **6**.$(CH_2Cl_2)_{0.5}$, the higher melting endotherms at 141-143 °C and 158-160 °C are due to unsolvated form 1 and stable form 3. The loss of solvent from host: guest crystal gives unsolvated dimer form 1. The minor endotherm at 158 °C corresponding to 3 could be due to concomitantly growing stable phase in the bulk solid.

(a)

(b)   (c)
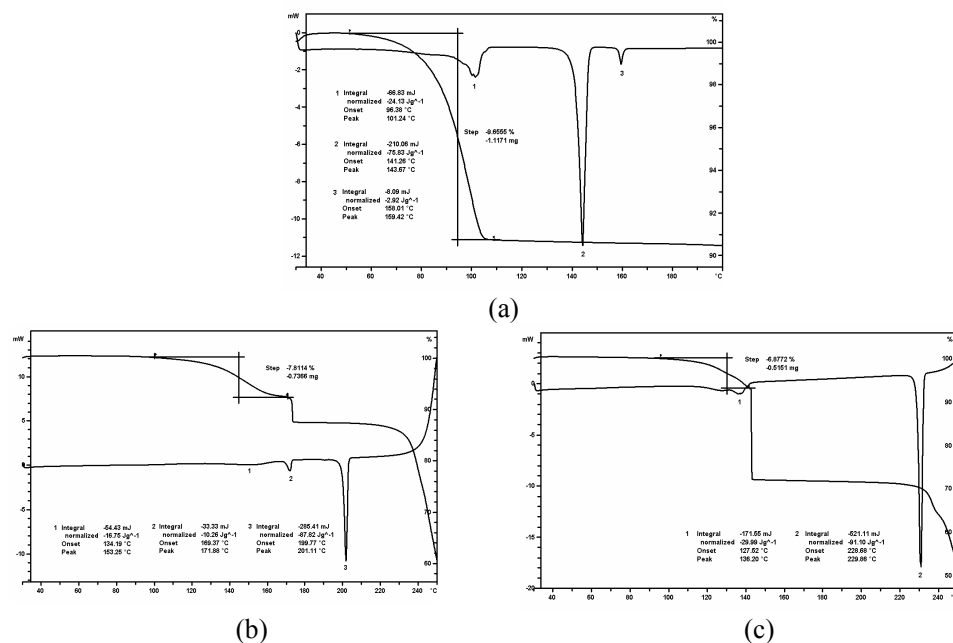
Figure 13. DSC and TGA trace of (a) **2**.$(CH_2Cl_2)_{0.5}$ (b) **5**.$(PhH)_{0.5}$ (c) **6**.$(PhH)_{0.5}$. Solvent loss is consistent with weight decrease for the given host:guest stoichiometry. Melting endotherms at 142 °C and 158 °C are assigned to form 1 (major) and form 3 (trace) polymorphs of **2** after desolvation.

5.8 Crystal Structure Reproduction

Why does molecule 2 not make strong H bonds in its stable polymorph despite the SO_2NH group? The reason for the presence of strong H-bonding, or lack of it, in different crystal forms of **6** could be related to the molecular conformation and to support this hypothesis crystal structure prediction (reproduction) was computed using the rigid body method starting from the experimental conformation as the input (*Cerius*^{2}, COMPASS).[22b] Conformation of the molecule was kept fixed during energy minimization to compare several putative structures for that particular conformer. To check whether one conformer leads to the hydrogen-bonded structure and another conformer to the close packed form as the lowest energy frame, crystal structures were predicted starting from experimental conformers 1-3 in six common space groups ($P2_1/c$, $P\bar{1}$, $C2/c$, $Pbca$, $P2_12_12_1$ and $P2_1$), which include the observed space groups. Ten lowest energy frames from each space group were analyzed (see Appendix VI for predicted frames). The most stable predicted frame in the observed space group was compared with the experimental crystal structure (Table 5). The starting molecular conformer appears to implant its signature in the crystal structure. Superposition of nearest-neighbor molecules in the experimental crystal structure and the lowest energy predicted frame in the appropriate space group show good similarity for all three polymorphs of **6** (Figure 14). The next best energy frames (2nd, 3rd, etc) have higher lattice energy by as much as 2 kcal mol^{-1} in each case (see Appendix VI for predicted frame energy difference). This means that a given conformation gives the observed crystal structure as a relatively stable predicted frame and alternative structures from the same conformer are unlikely.

To further ascertain that molecular conformation is important in giving stable H bonded clusters, the energy of N–H···O=S dimer were computed for rotamers of **6** in Spartan 04 (RHF/6-31G**):[22c] conformer 1 = –10.59 kcal mol^{-1}; conformer 2 = +6.31 kcal mol^{-1}; and conformer 3 = –6.99 kcal mol^{-1}. Thus, conformer 1 present in form 1, favors H bonded dimer as the nucleating aggregate compared to conformer 3 whereas conformer 2 is highly disfavored for dimer formation. The increasingly destabilizing nature of H bond dimer structures for conformer 3 and 2 was also revealed in polymorph predictor frames (see Appendix VI). There is no low energy H bond dimer structure

predicted for conformer 2 up to 5 kcal mol^{-1} and dimer type structures predicted with conformer 3 are ~4 kcal mol^{-1} higher in energy than the minimized close packed structure frame #1 listed in Table 5. These results also confirm the importance of right molecular conformation selection in predicting the correct crystal structure of conformationally flexible molecule.[23]

Table 5. Experimental crystal structures and minimum lattice energy structure predicted using *Cerius*^{2} polymorph predictor in the observed space group.

Polymorph	a [Å]	b [Å]	c [Å]	β [°]	V/Z [Å^3]	U_{latt} [kcal mol^{-1}]
Form 1, *C2/c*						
Frame #1[a]	21.605	11.734	15.027	101.01	467.39	−41.13
Predicted Form 1[b]	21.609	11.734	15.029	101.01	467.56	−41.13
ExptMin Form 1 Expt	22.009	11.976	15.185	100.94	491.25	---
Form 2, *C2/c*						
Frame #1[a]	42.327	7.846	11.874	108.63	467.05	−41.72
Predicted Form 2[b]	41.209	7.919	11.778	104.33	465.49	−42.10
ExptMin Form 2 Expt	42.043	8.038	12.345	104.08	505.81	---
Form 3, *P2$_1$/c*						
Frame #1[a]	8.070	39.466	5.836	95.91	462.18	−42.77
Predicted Form 3[b]	8.144	38.986	5.764	95.49	455.47	−44.52
ExptMin Form 3 Expt	8.297	39.758	5.935	97.29	485.50	---

[a] Predicted structure in *Cerius*^{2} (COMPASS force field, rigid body minimization).
[b] Experimental crystal structure was minimized in *Cerius*^{2}

(a)   (b)

(c)
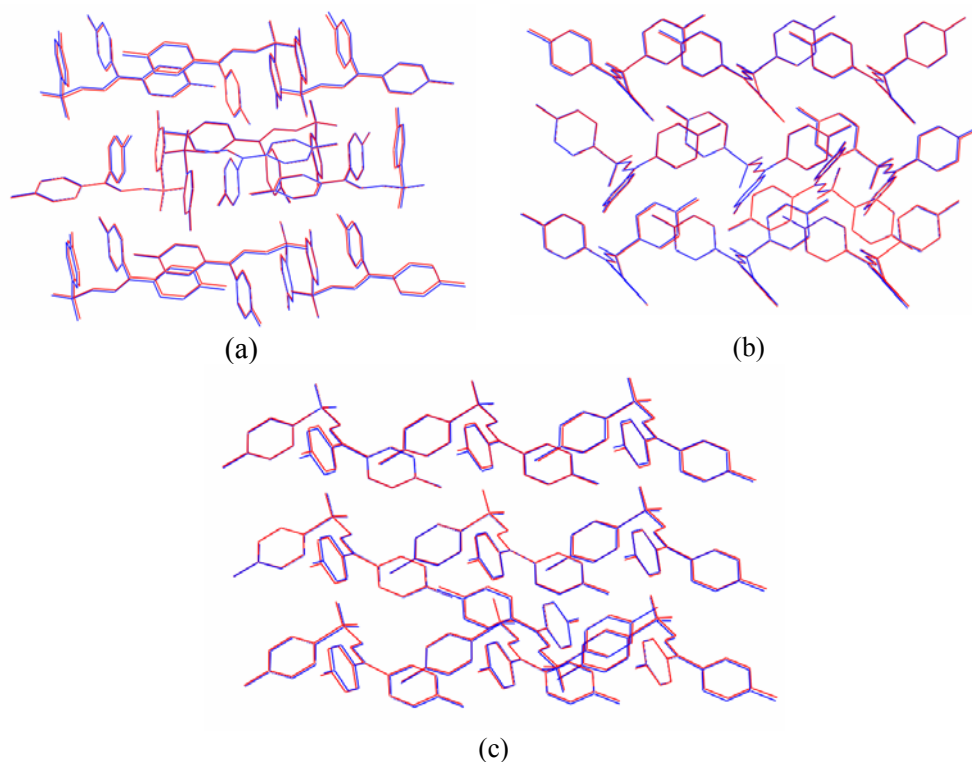
Figure 14. (a) A superposition of crystal form 1 and predicted frame #1 in *C*2/*c* space group. Rms deviation of 0.0019 indicates excellent match of molecular clusters. (b) A superposition of crystal form 2 and predicted frame #1 in *C*2/*c* space group. Rms deviation of 0.0824 indicates good match of molecular clusters. (c) An overlay of crystal form 3 and predicted frame #1 in *P*2$_1$/*c* space group. Rms deviation of 0.1388 indicates moderate match of molecular clusters. 10 neighboring molecules were superposed in each case.

Computations simulation from the *ab intio* structure of molecule **6** also done to examine if experimental crystal structure can be reproduced. Gaussian optimized conformers taken as starting model and structure simulated in six common space groups (*P*2$_1$/*c*, *P* $\bar{1}$, *C*2/*c*, *Pbca*, *P*2$_1$, *P*2$_1$2$_1$2$_1$) using Polymorph Predictor (PP) in DREIDING 2.21 force field and molecular conformation allowed to vary. Predicted frames did not give recognizable matching with the observed structures among the 10 lowest energy output for each space group. Pertinent to the present discussion it was noted that SO$_2$NH does not participate in conventional H bond up to 3.0 Å in majority of predicted

structures starting from gas phase minimized rotamers (49/60, see Appendix VII, Table 1 for predicted structures). The absence of conventional H bonds in predicted frames of **6** is surely related to its molecular structure, but the difficult question is: how are molecular and crystal structure related? A current challenge in crystal engineering is to understand molecular and crystal structure relations, and this problem is even more difficult when they influence each other in subtle ways, e.g. as in conformational polymorphs. On the other hand, PP on dimorphic acetone tosyl hydrazone gave 50/60 H bonded structures as the output and all 60 low energy frames have strong H bonds for sulfamethoxazole drug (see Appendix VII, Table 2 and 3 for predicted frames).

5.9 Curtin–Hammett Energy Profile

Curtin[24a] and Hammett stated that the product distribution in a reaction does not depend on the energy of the products but on how fast they form. Secondly, if a fast pre-equilibrium of conformers precedes a high energy step, then the product distribution does not depend on the relative amounts of conformations in solution but on the activation energy required to form the product. The Curtin–Hammett principle[27] has been widely applied to explain reactivity in stereoselective reactions, asymmetric catalysis, enzyme catalysis and photochemical transformations.[25]

Hydrogen bonding favors the kinetic crystal whereas close packing stabilizes the thermodynamic crystal, and rapid equilibrium between low energy conformers in solution is reminiscent of the Curtin–Hammett principle.[24] The chemical events from molecular conformers to polymorphs 1 and 3 are depicted in the free energy vs. crystallization pathway (Figure 15). Interplay of kinetic and thermodynamic factors in crystallization leads to polymorphism and it follows Curtin–Hammett like reaction kinetics.[6,7a] Computed energy (differences) are approximated as free energy (differences) because the contribution of entropy in crystallization is difficult to estimate ($\Delta G = H - T\Delta S$). A solution of molecule **6** at near-ambient temperature ($\sim RT = 0.6$ kcal mol^{-1} at 300 K) will have a higher concentration of conformer 1 compared to conformers 3 and 2, in inverse relation to their ΔE_{conf} values (Table 4), along with several other low-lying conformations in dynamic equilibrium. The hydrogen-bonded crystal 1 will nucleate

faster because there are more molecules in the required conformation and electrostatic stabilization to the H bonded aggregate at long-range (r^{-1}) will lower $\Delta G_1^{\ddagger}$ barrier. On the other hand, there are fewer molecules of higher energy conformer 3 and weak, van der Waals interactions provide stabilization only at short-range (r^{-6}).[25] So $\Delta G_3^{\ddagger}$ will be higher and form 3 will nucleate slowly. The final crystal structure of form 3 is more stable than H bonded form 1 by 3.39 kcal mol^{-1} (ΔU_{latt}, Table 4) because the loss of H bond energy is more than compensated by dispersion energy in the latter, dense modification. The present example of a H-bonded, kinetic form and a close-packed, thermodynamic polymorph illustrates two very different ways of crystal structure stabilization. Understanding the interplay of molecular conformation, H bonding and dense packing during self-assembly is a necessary step in understanding crystallization and polymorphism.
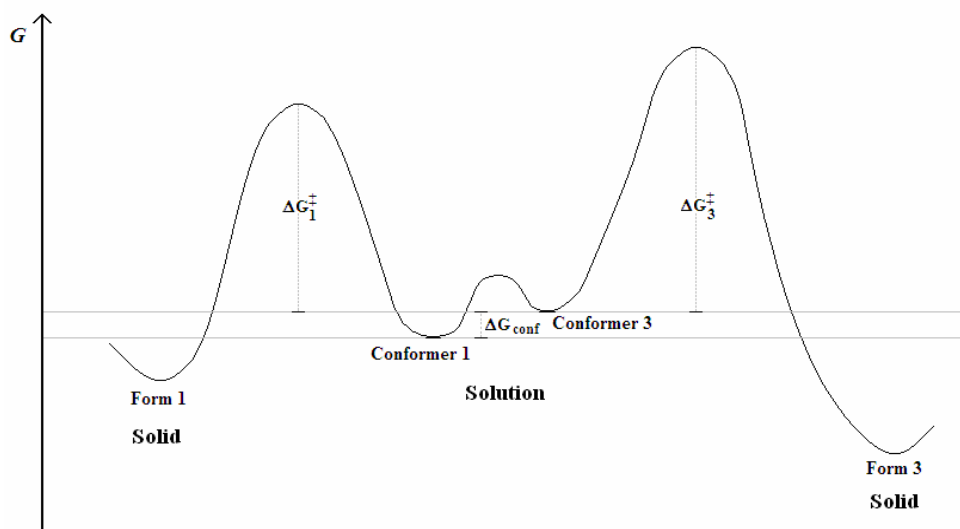
Figure 15. Curtin–Hammett principle in the crystallization of conformational polymorphs 1 and 3. Energy difference between conformers, $\Delta G_{conf} \sim$ 1-2 kcal mol^{-1}, is less than the activation energy barrier for crystallization, $\Delta G^{\ddagger}$, which involves breaking of solute–solvent aggregates and formation of solute–solute nuclei. Free energy differences are estimated from computed conformer and lattice energies.

5.10 Phenyl–Tolyl Exchange Polymorph Cluster

Study of 4,4-diphenyl-1,5-cyclohexadienonone described in chapter 2 shows that phenyl compound crystallize as tetramorph but tolyl derivative does not yield any polymorph. In the present study tolyl compound **6** is polymorphic whereas phenyl compound **7** is not. These observations encouraged us to examine the occurrence of polymorphism in phenyl/ tolyl pairs of crystal structures reported in literature. A CSD search on polymorphic pairs of phenyl/ tolyl exchange compound shows, there are 119 tolyl group containing and 958 phenyl-containing organic polymorph hits, which represent 35 and 284 different polymorphic compounds in each set. There are only 4 cases wherein polymorphs of both the phenyl and tolyl compounds pair is reported (Table 6). The exact reasons why tolyl sulfonamide **6** is trimorphic whereas phenyl compound **7** is not a polymorphic are difficult to explain. Remote *para*-substitution can bring very little effect on SO_2NH hydrogen bonding region. Steric factor may not be a reason, as found in frequent literature occurrence and also Cl derivative **9**, which have similar size as tolyl one does not crystallizes without H-bonded polymorphs. A possible reason for this could be the stable herringbone type packing of tolyl rings in form 3, which is also present in form 2 (Figure 4,5). In this close-packed arrangement the tolyl-SO_2 and N-tolyl form a dimer sandwich (circled). From size considerations, this specific motif would be stabilized only for the R = Me compound **6,** but not for other derivatives.

Table 6. Occurrence of polymorphism in phenyl/ tolyl crystal structures in the CSD (November 2006 update).

Tolyl group containing polymorphic structures = 119			
Both tolyl and phenyl are polymorphic	4		
Tolyl is polymorphic but phenyl is not polymorphic	12		
Tolyl is polymorphic but phenyl structure is not reported	19		
Phenyl group containing polymorphic structures = 958			
Both phenyl and tolyl are polymorphic	2		
Phenyl is polymorphic but tolyl is not polymorphic	31		
Phenyl is polymorphic but tolyl structure is not reported	249		
Refcodes of four phenyl–tolyl polymorph pairs			
PHENOL	UJIRIO	FEVNAV	NEDZEB
CRESOL	EBIDUP	BPHENO	NEDYUQ

5.11 Conclusion

Structural, thermodynamic and computational results on trimorphs of tolyl tosyl hydrazone **6** highlight the following interesting observations. (1) It is an unusual example of a molecule that contains the important SO_2NH functional group and exhibits H bonded and non-H bonded polymorphism as the kinetic and thermodynamic forms respectively. (2) The presence of H bonding in one polymorph and the complete absence in another form, and the fact their experimental energies may now be computed provides a benchmark for force fields in crystal structure computation programs. (3) It is generally believed that H-bonded structures are kinetic and close pack structures are thermodynamic in nature. Polymorphs 1 and 3 provide experimental proof in crystal structures of the *same* molecule that hydrogen bonding favors the kinetic crystal and close packing results in the thermodynamic phase. This result quantifies the crystallization model with experimental structures and optimized energies.

Finally in conclusion, crystallization of polymorphs 1 and 3 from inter-converting molecular conformers is shown to follow the Curtin–Hammett energy profile in a supramolecular reaction.

5.12 Experimental Section

Synthesis and Crystallization
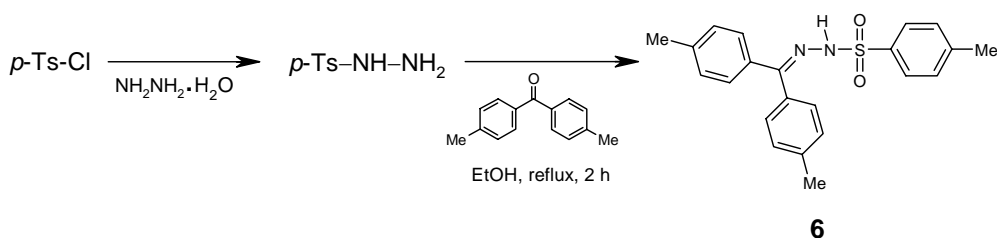
Scheme 5. Compound **6** was prepared by the condensation of *p*-tosylhydrazine with bis(*p*-tolyl)ketone. Derivatives **7-11** were prepared in a similar manner [ref. 26]

Bis(*p*-Tolyl)ketone *p*-tosylhydrazone **6** and benzophenone derivative **7-11** were synthesized[26] as shown in Scheme 4.

To a stirred solution of *p*-toluenesulfonyl chloride (5.0 g, 26 mmol) in 30 mL THF was added hydrazine hydrate (2.8 g, 55 mmol) drop wise at 0 °C. The reaction was continued for 30 min and the product extracted with ether to give *p*-toluenesulfonyl hydrazide (4.5 g, 90%). M.p. 108 ºC.

bis(*p*-Tolyl)ketone *p*-tosylhydrazone (6) To a well-stirred solution of *p*-toluenesulfonyl hydrazide (1.2 g, 6.6 mmol) in 10 mL ethanol was added equimolar amount of 4,4'-dimethyl benzophenone (1.5 g, 6.6 mmol). The reaction mixture was refluxed for 2 h. Cooling the reaction mixture afforded crystalline bis(*p*-tolyl)ketone *p*-tosylhydrazone as precipitate. The solid was collected by filtration and washed with cold ethanol. Recrystallization from hot ethanol gave pure **6** (1.9 g, 75%). M.p. 159 °C, ^{1}H NMR [400 MHz, δ, CDCl$_3$]: 2.33 (s, 3H), 2.42 (s, 6H), 6.97 (d, 8 Hz, 2H), 7.07 (d, 8 Hz, 2H), 7.28 (m, 6H), 7.50 (s, 1H), 7.82 (d, 8 Hz, 2H). IR [KBr]: 3287, 3030, 1597, 1510, 1385, 1315, 1165 cm^{-1}. LC/MS (R_I 0.68) *m/z* 379 [M + 1]$^+$.

Benzophenone *p*-tosylhydrazone (7) M.p. 180 °C, ^{1}H NMR [400 MHz, δ, CDCl$_3$]: 2.52 (s, 3H), 7.21 (s, 2H), 7.34 (m, 11H), (s, 1H), 7.93 (d, 8 Hz, 2H). IR [KBr]: 3202, 1595, 1491, 1444, 1377, 1168, 1055 cm^{-1}. LC/MS (R_I 0.69) *m/z* 351 [M + 1]$^+$.

bis(*p*-Fluorophenyl)ketone *p*-tosylhydrazone (8) M.p. 164 °C, ^{1}H NMR [400 MHz, δ, CDCl$_3$]: 2.44 (s, 3H), 6.96 (d, 8 Hz, 2H), 7.00 (m, 8H), 7.47 (s, 1H), 7.84 (d, 8 Hz, 2H). IR [KBr]: 3177, 2762, 1599, 1508, 1381, 1332, 1226, 1157, 1068 cm^{-1}. LC/MS (R_I 0.69) *m/z* 387 [M + 1]$^+$.

bis(*p*-Chlorophenyl)ketone *p*-tosylhydrazone (9) M.p. 202 °C, ^{1}H NMR [400 MHz, δ, CDCl$_3$]: 2.44 (s, 3H), 7.07 (d, 8 Hz, 2H), 7.25 (m, 6H), 7.48 (d, 8 Hz, 2H), 7.50 (d, 1H, 8Hz), 7.83 (d, 8 Hz, 2H). IR [KBr]: 3192, 1597, 1489, 1400, 1348, 1315, 1168, 1089, 1457 cm^{-1}. LC/MS (R_I 0.69) *m/z* 420 [M + 1]$^+$.

bis(*p*-Bromophenyl)ketone *p*-tosylhydrazone (10) M.p. 229 °C, ^{1}H NMR [400 MHz, δ, CDCl$_3$]: 2.44 (s, 3H), 7.00 (d, 8 Hz, 2H), 7.26 (d, 10 Hz, 2H), 7.41 (d, 10 Hz, 2H), 7.49 (s, 1H), 7.67 (d, 8 Hz, 2H), 7.83 (d, 8 Hz, 2H). IR [KBr]: 3190, 1597, 1489, 1394, 1340, 1167, 1068 cm^{-1}. LC/MS (R_I 0.69) *m/z* 509 [M + 1]$^+$.

bis(*p*-Iodophenyl)ketone *p*-tosylhydrazone (11) M.p. 201 °C (decompose), ^{1}H NMR [400 MHz, δ, CDCl$_3$]: 2.46 (s, 3H), 6.87 (d, 8 Hz, 2H), 7.14 (d, 10 Hz, 2H), 7.35 (d, 8 Hz, 2H), 7.50 (d, 1H), 7.64 (d, 8 Hz, 2H), 7.85 (m, 8 Hz, 4H). IR [KBr]: 3246, 1579, 1367, 1170, 1033, 1008 cm^{-1}.

Crystallization of **6** from EtOH/CH$_2$Cl$_2$ at −5 °C gave plate-like crystals of form 1 along with a few irregular blocks (Figure 1a). The plate morphology corresponds to form 1 as confirmed by unit cell checking. The irregular blocks are concomitantly growing form 3. There are also a few **6.**(CH$_2$Cl$_2$)$_{0.5}$ solvate crystals (see next) in the same batch.

Grinding compound **6** with a few drops of CH$_2$Cl$_2$ added (kneading), and using the microcrystalline powder as seeds for crystallization from the same solvent at ambient temperature afforded very thin crystals of form 2 along with block crystals of form 3 (Figure 1b).

Pure form 3 crystals of block and plate morphology crystallized by slow evaporation of a solution of compound **6** from EtOH at ambient temperature (Figure 1c).

Crystallization of **6** from CH$_2$Cl$_2$/*n*-hexane at ambient temperature gave plate-like unstable crystals that became opaque within one day. Immediate data collection on a single crystal showed it as **6.**(CH$_2$Cl$_2$)$_{0.5}$. The same solvated crystals were obtained concomitantly with form 1 also (unit cell check) but crystal quality is better in this experiment.

Crystallization of 7-11:

Compound **6-9** were crystallized from the EtOH at ambient temperature. Compound **10** was crystallized from MeCN at ambient temperature. Iodo compound **11** did not afford single crystals or material suitable for powder XRD.

Solvates **9.**(PhH)$_{0.5}$ and **10.**(PhH)$_{0.5}$ crystallized from 1:1 EtOH/ benzene mixture at ambient temperature.

X-ray Crystallography

Crystal structures were solved using direct methods and refined by full-matrix least-squares refinement on F^2 with anisotropic displacement parameters for non-H atoms in SHELX-TL (Bruker, SMART).[27] H atoms were refined isotropically. The structure of twinned form 2 crystal was solved using CELL_NOW[28] (for p4p file) and TWINABS[29] (for hkl files). A new p4p file was created after thresholding the frames. This new p4p file when executed in CELL_NOW gave two different p4p files. The 2nd file contains information about two orientation matrices. Data reduction were carried out in SAINT[30] using the 2nd p4p file as input. Absorption correction was done by TWINABS to get two sets of hkl files, hkl4 and hkl5. Structure solution was carried out in XPREP by using hkl4 file and refinement was executed on hkl5 file in SHELX-TL. Crystallographic parameters and final *R*-factor are acceptable for all structures.

Powder XRDs were recorded on a PANlytical 1830 diffractometer using Cu-Kα radiation 1.54056 Å and generator power of 35 kV and 25 mA. Reflections were collected in the 2θ range 5-50° at scan rate of 2° min^{-1}.

Thermal Analysis

DSC was performed on a Mettler Toledo DSC 822e module and TGA was performed on a Mettler Toledo TGA/SDTA 851e module. Samples (9-10 mg) were placed in open alumina pans for the TG experiments and in crimped but vented aluminum sample pans (4-6 mg) for DSC experiments. Temperature range was 30-200 °C @ 2 K/min. Samples were purged by a stream of nitrogen flowing at 150 mL/min for DSC and 50 mL/min for TG. The TG instrument is coupled to a Bruker Tensor FT-IR spectrometer for evolved gas analysis. The evolved vapors from TGA instruments were passed through a coupled heated transfer line at 120 °C. For TGA-IR analysis, the sample size is 10-12 mg, the heating rate is 10 K/min, and the N_2 flow @ 50 mL/min. Temperature range was 30-200 °C @ 10 K/min.

HSM was performed on a PolythermA hot stage and Heiztisch microscope supplied by Wagner & Munz. A Moticam 1000 (1.3 MP) camera supported by software

Motic Image Plus 2.0ML is used to record images and videos. About 1-2 mg of the sample was heated @ 5 K/min up to 200 °C.

Gaussian 03 and *Cerius*^{2} Computations

Conformational energy (E_{conf}) of the three polymophs **6** was calculated using density functional theory (DFT) at the B3LYP/6-31G (d,p) level in Gaussian 03 using crystallographic coordinates as the input. Hydrogen atom positions were re-optimized keeping the heavy atoms fixed. The gas phase rotamer of **6** was calculated and potential energy scan was carried out in 5° torsion angle intervals at the B3LYP/6-31G (d,p) level in Gaussian 03.

Lattice energies were computed for experimental polymorphs of **6** in *Cerius*^{2} program by energy minimization of crystal structures in COMPASS assigned with force field charges. COMPASS is better parameterized for structure prediction and energy minimization for a broad range of organic molecules. Crystal lattice energies are calibrated for the number of molecules in the unit cell (per molecule).

All simulations were carried out in version 4.8 of *Cerius*^{2} molecular modeling environment running on Silicon Graphics workstation. Crystal structure prediction of **6** was carried out in six common space groups ($P2_1$, $P2_1/c$, $C2/c$, *Pbca*, $P2_12_12_1$, $P\bar{1}$) using experimental conformers of three forms as the input. Atomic point charges were assigned in COMPASS force field. Default options were used throughout with fine search option in Monte Carlo simulation and for clustering of frames to get unique structures. Lattice energy minimization of predicted structures was carried out without any modifications except for the use of Ewald summation of van der Waals interactions at cut-off of 6.0 Å. All calculations were carried out by keeping the conformation fixed during minimization (rigid body method).

Hydrogen bond dimer energy for conformer 1, 2 and 3 were calculated in Spartan 04 by extracting the dimer from the crystal structure of form 1 and minimizing its energy by keeping the heavy atom positions fixed but optimizing H atom positions. Similarly energy of dimer was calculated using molecular conformer 2 and 3 as the

input. Energy of molecule in each conformation was calculated independently in RHF 6-31G**.

5.13 References

1. G. R. Desiraju, *CrystEngComm*, **2002**, *4*, 499.

2. (a) M. C. Etter, *Acc. Chem. Res.*, **1990**, *23*, 120. (b) M. C. Etter, *J. Phys. Chem.*, **1991**, *95*, 4601.

3. G. R. Desiraju, *Angew. Chem. Int. Ed. Engl.*, **1995**, *34*, 2311.

4. (a) F. H. Allen, W. D. S. Motherwell, P. R. Raithby, G. P. Shields and R. Taylor, *New. J. Chem.*, **1999**, 25. (b) J. Chisholm, E. Pidcock, J. van de Streek, L. Infantes, S. Motherwell and F. H. Allen, *CrystEngComm*, **2006**, *8*, 11.

5. A. I. Kitaigorodskii, *Organic Chemical Crystallography*, Consultants Bureau, New York, **1961**.

6. G. R. Desiraju, *Nat. Mater.*, **2002**, *1*, 77.

7. (a) R. K. R. Jetti, R. Boese, J. A. R. P. Sarma, L. Sreenivas Reddy, P. Vishweshwar and G. R. Desiraju, *Angew. Chem. Int. Ed.*, **2003**, *42*, 1963. (b) J. W. Chew, S. N. Black, P. S. Chow, R. B. H. Tan and K. J. Carpenter, *CrystEngComm*, **2007**, *9*, 128. (c) B. Rodríguez-Spong, C. P. Price, A. Jayashankar, A. J. Matzger and N. Rodríguez-Hornedo, *Adv. Drug. Del. Rev.*, **2004**, *56*, 241.

8. A. Gavezzotti, G. Fillippini, *J. Am. Chem. Soc.*, **1995**, *117*, 12299.

9. www.ccdc.cam.ac.uk.

10. (a) E. Weber, K. Skobridis, A. Wierig, L. R. Nassimbeni and L. Johnson, *J. Chem. Soc.*, *Perkin Trans.*, *2*, **1992**, 2123. (b) T. Senju, T. Hoki and J. Mizuguchi, *Acta. Cryst.*, **2005**, *E61*, o1061. (c) T. Senju, N. Nishimura, T. Hoki and J. Mizuguchi, *Acta. Cryst.*, **2005**, *E61*, o2569. (d) H. V. R. Dias and S. Singh, *J. Chem. Soc., Dalton Trans*., **2006**, 1995; (e) A. Bacchi, E. Bosetti, M. Carcelli, P. Pelagatti, G. Pelizzi and D. Rogolino, *CrystEngComm*, **2006**, 233.

11. (a) S. L. Price, *CrystEngComm*, **2004**, *6*, 344; (b) T. C. Lewis, D. A. Tocher and S. L. Price, *Cryst. Growth Des.*, **2005**, *5*, 983.

12. S. Aitipamula and A. Nangia, *Chem. Commun.*, **2005**, 3159.

13. C. R. Ojala, W. H. Ojala, S. Y. Pennamon and W. B. Gleason, *Acta Cryst.*, **1998**, C*54*, 57.

14. (a) S. R. Bryn, R. R. Pfeiffer and J. G. Stowell, *Solid-State Chemistry of Drugs*, SSCI: West Lafayette, IN, **1999**. (b) N. Blagden, R. J. Davey, H. F. Lieberman, L. Williams, R. Payne, R. Roberts, R. Rowe and R. Docherty, *J. Chem. Soc.*, *Faraday Trans.*, **1998**, *94*, 1035. (c) A. L. Bingham, D. S. Hughes, M. B. Hursthouse, R. W. Lancaster, S. Tavener and T. L. Threlfall, *Chem. Commun.*, **2001**, 603. (d) C. P. Price, A. L. Grzesiak and A. J. Matzger, *J. Am. Chem. Soc.*, **2005**, *127*, 5512.

15. J. Bernstein, R. E. Davis, L. Shimoni and N. -L. Chang, *Angew. Chem. Int. Ed. Eng.*, **1995**, *34*, 1555.

16. (a) A. V. Trask, D. A. Hanes, W. D. S. Motherwell and W. Jones, *Chem. Commun.*, **2006**, 51. (b) D. Braga and F. Grepioni, *Angew. Chem. Int. Ed.*, **2004**, *43*, 4002.

17. Powder Cell 2.3. N. Krauss, G. Nolze, Federal Institute for Materials Research and Testing, Berlin, Germany, **2000**.

18. (a) J. D. Dunitz and J. Bernstein, *Acc. Chem. Res.*, **1995**, *28*, 193. (b) J. -O. Henck, J. Bernstein, A. Ellern and R. Boese, *J. Am. Chem. Soc.*, **2001**, *123*, 1834. (c) P. Bombicz, M. Czugler, R. Tellgren and A. Kálmán, *Angew. Chem. Int. Ed.*, **2003**, *42*, 1957.

19. (a) A. Nangia and G. R. Desiraju, *Chem. Commun.*, **1999**, 605. (b) R. Mondal and J. A. K. Howard, *CrystEngComm*, **2005**, *7*, 462.

20. G. R. Desiraju, *Crystal Engineering: The Design of Organic Solids*, Elsevier, Amsterdam, **1989**, pp 179-185.

21. (a) M. Muthuraman, Y. L. Fur, M. Bagieu-Beucher, R. Masse, J. -F. Nicoud, S. George, A. Nangia and G. R. Desiraju, *J. Solid State Chem.*, **2000**, *152*, 221. (b) B. K. Saha and A. Nangia, J. -F. Nicoud, *Cryst. Growth Des.*, **2006**, *6*, 1278. (c) B. K. Saha and A. Nangia, *Cryst. Growth Des.*, **2007**, *7*, 393.

22. (a) M. J. Frisch *et al*, Gaussian 03, Revision B.05. www.gaussian.com (b) *Cerius*[2] suite of software for crystal lattice energy calculation and crystal structure prediction are crystal packer and polymorph predictor www.accelrys.com (c) Spartan 04, Irvine, CA. www.wavefun.com.

23. (a) T. C. Lewis, D. A. Tocher and S. L. Price, *Cryst. Growth Des.*, **2004**, *4*, 979.(b) C. Ouvard and S. L. Price, *Cryst. Growth Des.*, **2004**, *4*, 1119. (c) H. Nowell and S. L. Price, *Acta Cryst.*, **2005**, *B61*, 558.

24. (a) D. Y. Curtin, *Rec. Chem. Prog.*, **1954**, *15*, 111. (b) J. L. Seeman, *Chem. Rev.*, **1983**, *83*, 83. (c) F. A. Carey and R. J. Sandberg, *Advanced Organic Chemistry*, *Part A – Structure and Mechanisms*, 4th Ed., Plenum Press, **2006**, New York, pp. 220-222.

25. G. R. Desiraju, *Acc. Chem. Res.* **2002**, *35*, 565.

26. (a) L. Friedman, R. L. Litle and W. R. Reichle, *Org. Syn., Coll. Vol. V* **1973**,1055 (b) V. P. Miller, D. Yang, T. M. Weigel, O. Han and H. Liu, *J. Org. Chem.* **1989**, *54*, 4175.

27. (a) Bruker, **2000**, SMART (version 5.625) and SHELX-TL (version 6.12), Bruker AXS Inc., Madison, WI, USA; (b) G. M. Sheldrick, **1997**, SHELXS-97 and SHELXL-97, University of Göttingen, Germany.

28. G. M. Sheldrick, **2004**, CELL_NOW, University of Göttingen, Germany.

29. G. M. Sheldrick, **2003**, TWINABS (version 1.05), University of Göttingen, Germany.

30. Bruker, **2003**, SAINT-Plus (version 6.45), Bruker AXS Inc., Madison, WI, USA.

CHAPTER 6

CONCLUSION AND FUTURE PROSPECT

6.1 Lattice and Conformation Energy Compensation

A better understanding of polymorphism will certainly give insight into the mechanism of crystallization and structure property relation of molecules. Molecular structure–crystal structure–crystal energy relationships can be understood clearly through study of different crystalline modifications of the same chemical substance.[1] Energy differences between conformational polymorphs (kinetic and thermodynamic) are very small (0.5-3 kcal mol^{-1}) because intra- and intermolecular energies may cancel each other.[2] This energy compensation was examined in different chemical systems in chapter 2, 3 and 5. In crystal structures of the four conformational polymorphs of 4,4-diphenyl-2,5-cyclohexadienone **1** a compromise between minimization of intramolecular (rotamer) and intermolecular (interaction) energies was noted (Chapter 2). Metastable rotamer A_i exists in the thermodynamically stable form A. But in terms of total energy form A gains stability through better molecular arrangement and packing in the crystal structure compared to forms B and D. In polymorphs of dimethyl fuchsone it was found that α form has both stable conformation and crystal structure (Chapter 3). However β form is found to be thermodynamically stable at higher temperature and phase transition from α, γ forms to β form was observed upon heating. Calculated lattice energy of γ form is almost the same as β form but presence of highly unstable conformer (+9.48 kcal mol^{-1} higher than α conformer) made γ form metastable.
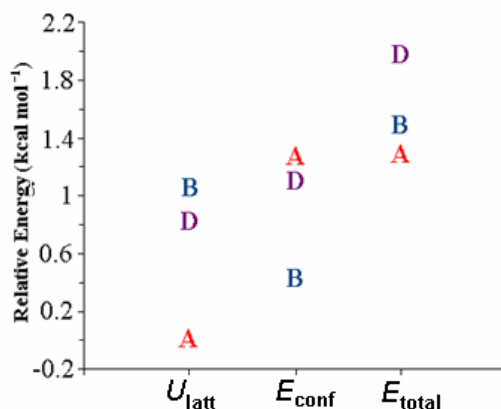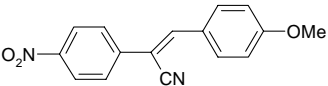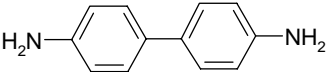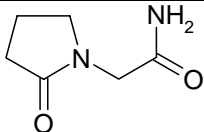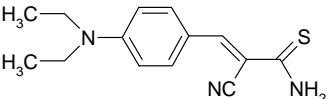
Figure 1. Lattice and conformation energy compensation in the polymorphs of compound **1**.

6.2 Curtin-Hammette Principle in Conformational Polymorphs

Conformational and lattice energy compensation study was further extended by relating to Curtin-Hammette principle[3] in trimorphs of bis(*p*-tolyl)ketone *p*-tosylhydrazone **6**. Metastable conformation present in thermodynamic form 3 was compensated by better close packing arrangement of molecules in the crystal lattice. Experimental and computational findings were consistent with the proposed Curtin–Hammett energy profile for the crystallization of conformational polymorphs 1 and 3 (Chapter 5). To verify this principle for the other systems, 25 conformational polymorphs were taken from the recent literature[4] (see Appendix VIII for molecular diagram). Lattice and conformational energy were calculated for these systems in *Cerius*[2] (COMPASS and DRIEDING 2.21 force field)[5] and Gaussian03[6] (Table 1). Compass values are taken into consideration for comparison because this force field better suited for organic molecules. It has been found that metastable high energy conformation present in stable polymorph and relatively higher energy kinetic form gains stability from the stable conformation in 15 out of 25 polymorph clusters. The energy profile in these systems are represented qualitatively in Figure 2. Extension on Curtin-Hammett principle for conformational polymorphs followed by these 15 systems further validate our proposal in chapter 5.

Table 1. Lattice energy (U_{latt}, Cerius^2, COMPASS), conformation energy (E_{conf}, Gaussian 03, B3LYP/6-31G(d,p)) and total energy ($\Delta E_{\text{total}} = \Delta U_{\text{latt}} + \Delta E_{\text{conf}}$)

Structure	Refcode	Lattice Energy Compass (U_{latt})	Relative conformer energy (ΔE_{conf}) (kcal mol^{-1})	Total energy $\Delta E_{\text{tot}} = U_{\text{latt}} + \Delta E_{\text{conf}}$ (kcal mol^{-1})	Inter- and intramolecular energy balance
	BANHOO01	−38.597	0.000	−38.597	
	BANHOO02	−38.794	1.461	−37.333	Yes
	BANHOO03	−38.705	1.898	−36.807	
	BANJEG	−37.469	3.503	−33.966	
	BENZIE01	−27.272	0.000	−27.272	
	BENZIE02	−31.741	0.507	−31.234	Yes
	BENZIE03	−32.791	0.799	−31.992	
	BENZIE04	−29.848	0.747	−29.101	
	BISMEV	−33.896	0.114	−33.782	
	BISMEV01	−32.856	0.259	−32.596	Yes
	BISMEV03	−33.364	8.631	−24.733	
	BISMEV04	−29.949	0.000	−29.949	
	CELBEA	−33.754	5.944	−27.810	
	CELBEA01	−35.631	0.000	−35.631	No
	CELBEA02	−34.250	5.965	−28.285	

Table 1. *Continued...*
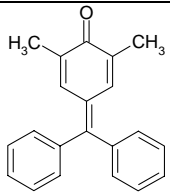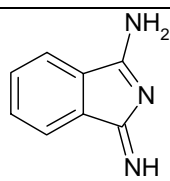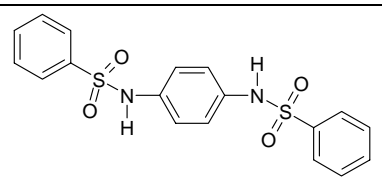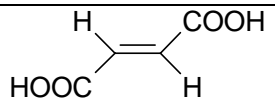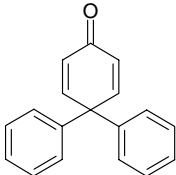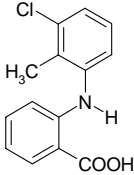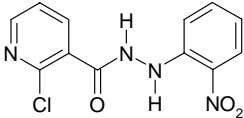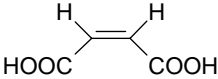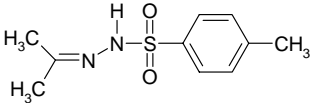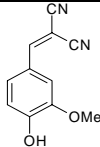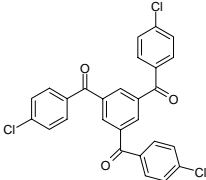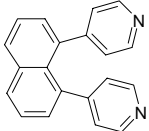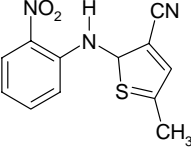
	DMFUSC	−36.716	0.364	−36.352	
	DMFUSC01	−37.174	0.000	−37.174	No
	DMFUSC02	−36.737	9.208	−27.529	
	EXUQAP	−22.067	0.000	−22.067	Yes
	EXUQET	−21.121	2.586	−18.535	
	FIBKUW01	−44.043	1.061	−42.982	Yes
	FIBKUW02	−43.001	0.000	−43.001	
	FUMAAC	−32.572	0.051	−32.521	Yes
	FUMAAC01	−25.073	0.000	−25.073	
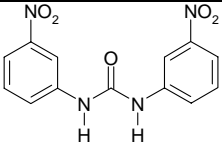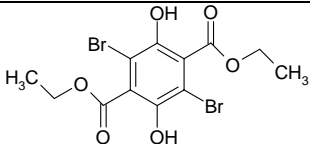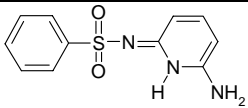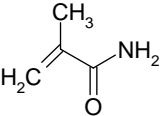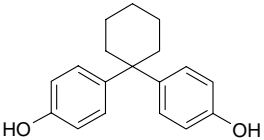
Table 1. *Continued...*

	HEYHUO	−32.573	2.673	−29.900	
	HEYHUO01	−31.652	1.057	−30.595	Yes
	HEYHUO02	−31.639	6.267	−25.372	
	HEYHUO03	−31.874	0.000	−31.874	
	KAXXAI	−36.184	0.000	−36.184	Yes
	KAXXAI01	−37.172	1.725	−35.447	
	KEXYOC	−41.722	2.179	−39.543	
	KEXYOC01	−41.096	3.373	−37.723	No
	KEXYOC02	−42.243	0.000	−42.243	
	MALIAC12	−27.283	0.172	−27.111	No
	MALIAC13	−27.904	0.000	−27.904	
	NAQRIG	−27.026	0.000	−27.026	No
	NAQRIG01	−26.011	0.447	−25.564	
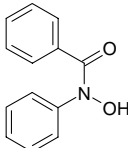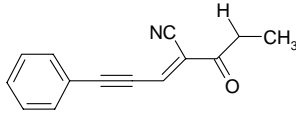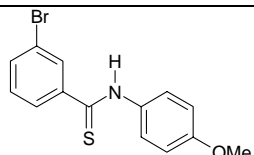
Table 1. *Continued...*

	NEMLOG	−30.314	0.000	−30.314	Yes
	NEMLOG02	−34.539	0.962	−33.577	
	OHIBOW01	−56.758	8.697	−48.061	No
	OHIBOW02	−60.001	0.000	−60.001	
	PEGWII	−39.312	0.432	−38.880	No
	PEGWII01	−40.268	0.000	−40.268	
	QAXMEH	−30.985	0.431	−30.554	
	QAXMEH01	−31.983	1.429	−30.553	
	QAXMEH02	−34.066	0.000	−34.066	
	QAXMEH03	−33.446	0.883	−32.563	No
	QAXMEH04	−33.497	2.236	−31.260	
	QAXMEH05	−32.777	1.919	−30.858	
	QAXMEH12	−32.391	0.820	−31.571	

Table 1. *Continued...*

SILTOW	−50.566	0.696	−49.870	
SILTOW01	−53.205	3.995	−49.210	Yes
SILTOW11	−51.041	0.000	−51.041	
TEHNID	−36.250	0.000	−36.250	Yes
TEHNID01	−40.436	10.552	−29.884	
UJIRIO01	−29.156	0.000	−29.156	Yes
UJIRIO02	−31.892	1.635	−30.256	
WANSAG	−19.713	0.000	−19.713	Yes
WANSAG03	−19.868	0.635	−19.233	
WETFAD	−36.226	0.257	−35.969	No
WETFAD01	−37.112	0.000	−37.112	

Table 1. *Continued...*

	XERSOD	−32.130	0.000	−32.130	Yes
	XETNOA	−36.253	0.229	-36.024	
	YEJRUA	−34.733	3.719	−31.014	No
	YEJRUA01	−35.358	0.000	−35.358	
	α form[a]	−33.427	0.080	−33.347	Yes
	β form[a]	−34.500	1.067	−33.433	
	γ form[a]	−31.971	0.000	−31.971	

[a] Recent report of conformational trimorph N-(4'-methoxyphenyl)-3-bromothiobenzamide: A. Bashkirava, P. C. Andrews, P. Crhoek, *Chem. Asian J.*, **2007**, *2*, 530.
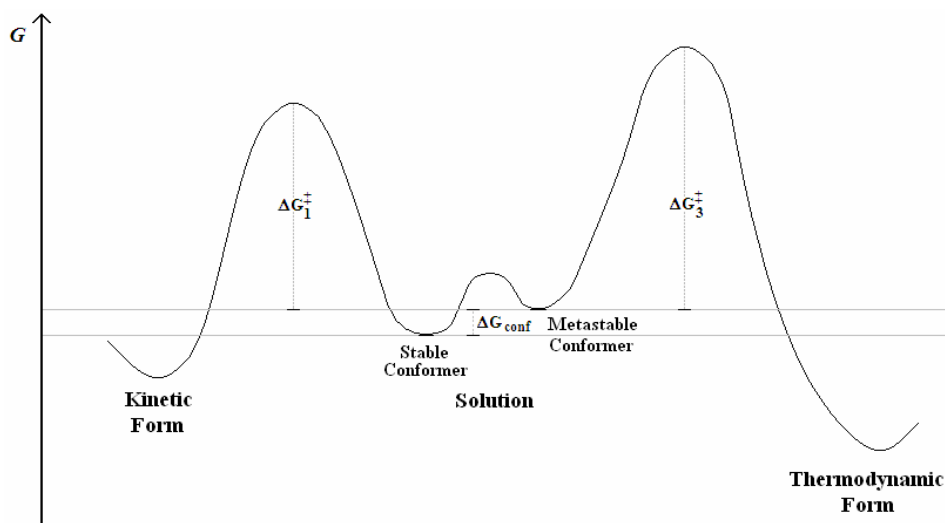
Figure 2. Qualitative representation of Curtin–Hammett principle in the crystallization of conformational polymorphs.

6.3 Thermal Analysis and Variable Temperature Powder X-ray Diffraction in Characterizing Polymorphs

Variable temperature powder diffraction (VT-PXRD) study is found to be very useful in proper characterization of polymorphs. Enantiotropic relationship and the phase transformation of the tetramorphs of 4,4-diphenyl-2,5-cyclohexadienone **1** was studied using VT-PXRD (Chapter 2). It was found that VT-PXRD experiments were more informative in elucidating phase transformation among polymorphs when DSC scan is silent. Transformation of 2,6-dimethyl-4-(α,α-diphenylmethylene)-1,4-benzoquinone **4** polymorphs were observed in VT-PXRD experiments but DSC does not show any phase change upon heating. Use of multiple thermal analysis technique for elucidating the stability relationships between polymorphs is the highlight of studies presented in this thesis.

It is very important in drug substances where metastable more soluble form can easily transform to the stable, less soluble modification during manufacture, formulation and/or storage e.g. ritonavir.[7] Thermochemical relation among polymorphs of a leading anti-depressant drug venlafaxine hydrochloride and phase transformation to a new

polymorph was identified by using multiple thermal analysis techniques (Figure 3). Novel form 6 found in the study is the stable one at higher temperature compared to marketed form 1 and form 2. Moreover once form 6 is formed, it does not show any phase transition even after lowering of temperature up to 100 K. It would not have been possible to characterize new polymorphs unambiguously and assign the kinetic/thermodynamic phase without the use of thermal methods, e.g. DSC, TGA, hot stage microscopy. *In-situ* variable temperature powder X-ray diffraction gave valuable structural and physical information about polymorphic phases.
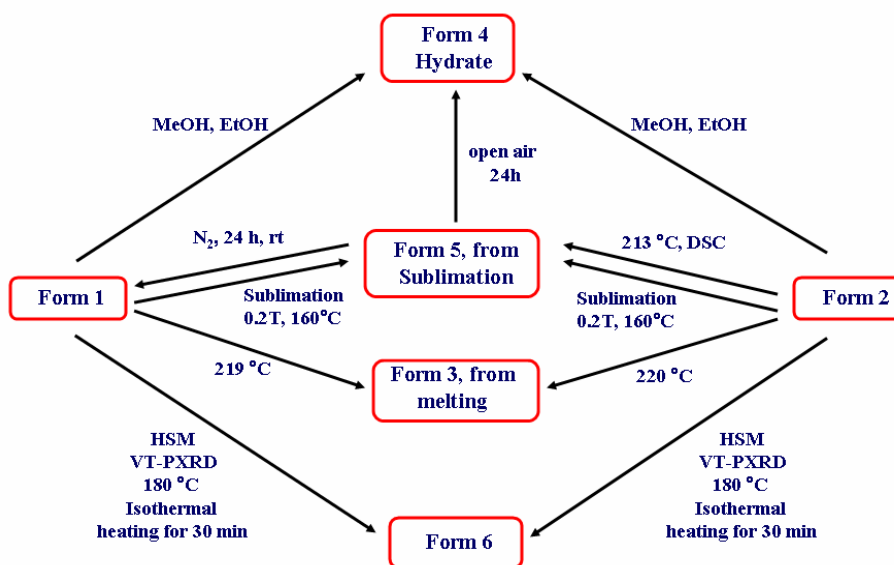
Fugure 3. Phase relationship among the venlafaxine hydrochloride polymorphs 1-6.

6.4 Design of New Polymorphic Systems

The discovery of polymorphism is generally unpredictable, even as it is true that combination of serendipity and subsequent rigorous observation could lead to novel polymorphs. Design of new polymorphic system is encouraged in crystal engineering subject because it results many new findings in structure-property relation and to understand the subject polymorphism more clearly. Phenylogue series approach is one such advancement from our laboratory producing new polymorphic systems.[8] Bis(*p*-

tolyl)ketone *p*-tosylhydrazone **6** studied in chapter 5 is phenylgue extended compound of acetone tosyl hydrazone, which reported as two conformational polymorphs.[9] Compound **6** results in three conformational polymorphs where form 1 have expected dimer synthon whereas form 2 and form 3 are devoid of hydrogen bonding. Thermodynamic and stable form 3 is stabilized by close packing of tolyl–SO_2 and N–tolyl rings in sandwich type structure. From size and packing considerations, the sandwich motif would be stabilized when the two aryl groups are identical, i.e. in tolyl compound **6**, but not for other derivatives discussed in chapter 5 because our concern is tolyl–SO_2–hydrazones only. Phenylsulfonyl diphenyl-hydrazone is a simple molecule to evaluate whether identity of N–aryl and S–aryl groups will lead to polymorphism (Scheme 1, R=R′=H).

Various derivatives of benzophenone hydrazones can be prepared by replacing S–aryl and N–aryl groups (Scheme 1) and can be taken up for screening polymorphism. Aniline–SO_2–hydrazones can produce synthon polymorphism as there will be more than one active donors compete to participate in hydrogen bonding. Similarly other derivatives with halogen groups and different functional group can produce interesting results as these molecules have several torsional degree of freedom.
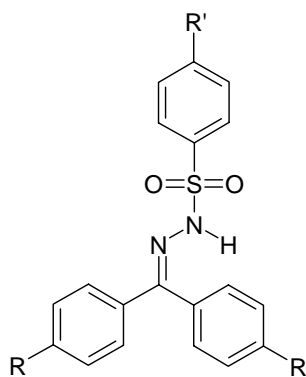
R′= H, F, Cl, Br, I, NH_2, $NHCOCH_3$, NO_2
R = H, F, Cl, Br, I, NH_2, $NHCOCH_3$, NO_2

Scheme 1

6.5 References

1. (a) C. P. Brock, W.B. Schweizer and J. D. Dunitz, *J. Am. Chem. Soc.*, **1991**, *113*, 9811. (b) J. D. Dunitz, *Acta Cryst.*, **1995**, *B51*, 619.

2. (a) C. Ouvrard and S. L. Price, *Cryst. Growth Des.*, **2004**, *4*, 1119. (b) H. Nowell and S. L. Price, *Acta Cryst.*, **2005**, *B61*, 558.

3. (a) D. Y. Curtin, *Rec. Chem. Prog.*, **1954**, *15*, 111. (b) J. L. Seeman, *Chem. Rev.*, **1983**, *83*, 83. (c) F. A. Carey, R. J. Sandberg, *Advanced Organic Chemistry*, *Part A – Structure and Mechanisms*, 4th Ed., Plenum Press, **2006**, New York, pp. 220-222.

4. F. H. Allen and R. Taylor, *Chem. Soc. Re*v., **2004**, *33*, 463. www.ccdc.cam.ac.uk.

5. *Cerius*² suite of software for crystal lattice energy calculation and crystal structure prediction are crystal packer and polymorph predictor www.accelrys.com.

6. M. J. Frisch *et al*, Gaussian 03, Revision B.05. www.gaussian.com

7. S. R. Chemburkar, J. Bauer, K. Deming, H. Spiwek, K. Patel, J. Morris, R. Henry, S. Spanton, W. Dziki, W. Porter, J. Quick, P. Bauer, J. Donaubauer, B. A. Narayanan, M. Soldani, D. Riley and K. McFarland, *Org. Process Res. Dev.*, **2000**, *4*, 413.

8. S. Aitipamula and A. Nangia, *Chem. Commun.*, **2005**, 3159.

9. C. R. Ojala, W. H. Ojala, S. Y. Pennamon and W. B. Gleason, *Acta Cryst.*, **1998**, C*54*, 57

Appendix I

Table 1 CSD refcodes of organic polymorph clusters up to the recent update of the Cambridge Structural Database (May 2007 update).[a]

Heptamorph					
QAXMEH					

Pentamorphs					
GLYCIN		IFULUQ		SUTHAZ	

Tetramorphs			
ADULEQ	BISMEV	KELGEO	SLFNMB
AMBACO	CBMZPN	MABZNA	TPEPHO
BENZIE	CILHIO	PYRZIN	VIPKIO
BEWKUJ	HEYHUO	RUWYIR	VISKAJ
BIXGIY	KAXHAS	STARAC	WUWTOX

Trimorphs[b]					
AMNTPY	DIYJUQ	GEHBAX	MBPHOL	PHBARB	TUHBAZ
AWAKIS	DLABUT	GISRIJ	MBYINO	PNEOSI	UCECAG
AZADAG	DLMSUC	HADKIG	MBZYAN	PHTHCY	TURPYB
BALWEQ	DMANTL	HIMWIJ	MCHTEP	PUBMUU	UDAYUT
BANHOO	DMFUSC	HNIABZ	METHOL	PUPBAD	UJORIU
BIMYAX	DMMTCN	HYQUIN	MEZKEH	QNACRD	UNEWUF
BIYSEH	DOBTUJ	IJETOG	MNIAAN	QOGNEF	WEFKIC
BOPKOG	DPYRAM	IMDIAC	NADQAL	RBTCNQ	WIRXAW
BZCHOL	DUCKOB	IVADUE	NAGHOT	SAMPYM	WUWTIR
CENRIW	DUVFUV	JATFUF	NAPYMA	SIFLOI	XINBEB
COMXAD	DUVZOJ	JIBCIG	NAZLAC	SIKLIH	YACTEC
DATREV	ESTRON	JUSBUU	NIMFOE	SILTOW	YERRUI
DBEZLM	FACRIK	KEXYOC	NOJHEZ	SLFNMA	YUYHIJ
DCBFRO	FAFWIS	KTCYQM	OCHTET	SOBPEE	ZEPFAB

DCLANT	FAWFOY	LAURAC	PARQUI	SULAMD	ZEXREZ
DCLBEN	FOMNEB	LAVMOK	PATSEJ	TAWRIT	ZOGQAN
DEGGEB	FEGWAP	LCYSTN	PATVEM	TELYAK	ZZZHWI
DETBAA	FESKAP	LILXIN	PCBZAM	TEPHTH	ZZZIYE
DHNAPH	FIDYIA	MACCID	PDABZA	THIOUR	ZZZVTY
DIMETH	FILGEM	MALEHY	PEFTIE	TNBENZ	
DIWWEL	GADSIO	MALOAM	PETNEI	TORSEM	

[a]   S. Chen, I.A. Guzei and L. Yu, *J. Am. Chem. Soc.*, **2005**, *127*, 9881.
[b]   Recent report of conformational trimorph N-(4'-methoxyphenyl)-3-bromothiobenzamide: A. Bashkirava, P. C. Andrews, P. C. Junk, E. G. Robertson, L. Spiccia and N. Vanderhoek, *Chem. Asian J.*, **2007**, *2*, 530.

Appendix II

Table 1. 60 predicted frames of crystal structures **1** simulated using full body refinement in six common space groups (*Cerius*[2] platform, COMPASS force field, normalized to per molecule of quinone).

Ranking[a] based on U_{latt}	Cell Volume [Å^3]	Lattice energy [kcal mol^{-1}]	τ_1, τ_2 [°]
		*P*2$_1$	
2	**316.98**	**−92.546**	**32.0, 37.9**
3	**322.45**	**−92.201**	**14.6, 15.9**
23	320.96	−91.184	0.0, 48.9
53	329.67	−90.319	1.2, 54.7
55	333.89	−89.816	5.6, 64.3
56	339.74	−89.730	19.4, 42.5
57	337.01	−89.500	31.8, 29.2
58	337.18	−89.338	23.7, 31.7
59	343.56	−89.284	19.8, 39.8
60	345.28	−89.067	18.8, 33.5
		*P*2$_1$/*c*	
5	**318.19**	**−92.058**	**8.3, 49.8**
11	324.32	−91.854	23.5, 36.2
14	323.40	−91.537	16.7, 42.4
17	321.43	−91.383	2.3, 44.7
18	328.42	−91.359	22.1, 36.4
21	325.11	−91.263	26.6, 31.7
22	325.03	−91.258	17.2, 34.2
26	325.28	−91.015	12.2, 21.4
37	317.95	−90.750	11.7, 16.0
39	334.43	−90.729	25.8, 38.6
		*C*2/*c*	
8	**319.37**	**−91.910**	**25.1, 25.1**
10	**322.38**	**−91.869**	**7.4, 34.5**
16	325.66	−91.497	16.3, 31.5
24	324.58	−91.049	23.0, 32.8
29	322.45	−90.925	31.2, 32.8
34	330.19	−90.818	24.3, 37.2
35	323.84	−90.766	0.7, 45.8
42	325.74	−90.665	2.1, 58.2
46	326.49	−90.498	15.3, 28.2
50	327.77	−90.346	15.6, 44.5

	Pbca		
15	328.16	−91.504	18.7, 29.4
19	332.26	−91.315	21.6, 35.9
20	319.40	−91.273	20.5, 31.8
25	327.05	−91.041	20.5, 23.4
30	327.71	−90.909	27.1, 31.0
31	332.84	−90.855	21.8, 32.2
41	325.13	−90.715	30.4, 36.9
45	332.38	−90.550	26.0, 28.2
47	335.14	−90.479	12.7, 39.8
49	326.90	−90.378	17.7, 49.7
	$P2_12_12_1$		
4	**323.78**	**−92.116**	**29.1, 30.9**
6	**317.63**	**−92.027**	**1.1, 36.9**
12	321.02	−91.651	22.0, 32.2
33	329.11	−90.820	20.0, 39.3
43	327.75	−90.608	25.3, 39.6
44	330.38	−90.594	25.4, 31.3
48	332.18	−90.397	24.8, 38.8
51	318.79	−90.338	19.5, 46.7
52	328.95	−90.326	21.7, 39.9
54	334.51	−90.211	18.1, 32.8
	$P\bar{1}$		
1	**316.70**	**−92.989**	**28.4, 28.6**
7	**321.49**	**−92.016**	**2.7, 51.1**
9	**319.69**	**−91.871**	**27.0, 38.0**
13	321.58	−91.565	6.0, 47.9
27	325.94	−90.965	23.3, 36.4
28	324.22	−90.963	26.7, 26.7
32	325.34	−90.837	12.2, 51.6
36	330.07	−90.765	25.0, 35.6
38	330.51	−90.740	21.3, 39.8
40	321.71	−90.718	0.8, 56.3

[a] Highlighted frames are re-computed by rigid body method and re-ranked based on E_{total}. Frame #3 (= re-ranked frame #1) matches with experimental form A (Tables 5 and 8 in chapter 2).

APPENDIX III

Table 1. Crystallographic data for the structures discussed in this thesis.

	Chapter 4	*Chapter 5*		
	5	**6 (Form 1)**	**6 (Form 1)**[a]	**6 (Form 2)**
Empirical formula	$C_{17}H_{28}NO_2{}^+.Cl$	$C_{22}H_{22}N_2O_2S$	$C_{22}H_{22}N_2O_2S$	$C_{22}H_{22}N_2O_2S$
Formula wt.	313.85	378.48	378.48	378.48
Crystal system	monoclinic	monoclinic	monoclinic	monoclinic
Space group	$P2_1/n$	*C*2/*c*	*C*2/*c*	*C*2/*c*
T [K]	100	100(2)	298(2)	298(2)
a [Å]	5.887(10)	22.0093(13)	22.250(3)	42.043(8)
b [Å]	19.37(3)	11.9763(7)	12.1201(15)	8.0381(16)
c [Å]	31.41(5)	15.1853(9)	15.2891(19)	12.345(3)
α [deg]	90.00	90	90	90
β [deg]	92.16(3)	100.937(1)	100.538(2)	104.08(3)
γ [deg]	90.00	90	90	90
Z	8	8	8	8
Volume [Å^3]	3579(10)	3930.0(4)	4053.5(9)	4046.5(14)
D_{calc} [g/cm^3]	1.165	1.279	1.240	1.242
F (000)	1360	1600	1600	1600
μ [mm^{-1}]	0.218	0.184	0.178	0.179
$2\theta_{\text{max.}}$	1.97-45.00	1.99-52.80	1.99-52.16	1.978-46.68
Range h	-6 to 6	-27 to 27	-27 to 27	-46 to 45
Range k	-20 to 20	-14 to 14	-14 to 14	0 to 8
Range l	-33 to 33	-18 to 18	-18 to 18	0 to 13
N-total	26361	28954	20656	3512
N-independent	4591	4029	4005	3512
N-observed	1315	3771	2936	1514
R_1 [I>2σ(I)]	0.1073	0.0408	0.0501	0.0724
wR_2	0.2029	0.1047	0.1307	0.1405
GOF	0.950	1.072	1.037	0.950

[a] Crystal structure of form 1 of compound **6** was re-determined at 298 K for direct comparison of packing coefficient and crystal density with form 2 and 3.

Table 1. *Continued…*

Chapter 5			
6 (Form 3)	**6•dichloromethane**	**7**	**8**
$C_{22}H_{22}N_2O_2S$	$(C_{22}H_{22}N_2O_2S) \cdot (CH_2Cl_2)_{0.5}$	$C_{20}H_{18}N_2O_2S$	$C_{20}H_{16}F_2N_2O_2S$
378.48	420.94	350.42	386.41
monoclinic	triclinic	monoclinic	monoclinic
$P2_1/c$	$P\bar{1}$	$P\bar{1}$	$P2_1/c$
298(2)	100(2)	298(2)	298(2)
8.2971(5)	7.9174(18)	9.8402(16)	12.3523(16)
39.758(3)	11.701(3)	10.1297(16)	9.2366(12)
5.9349(4)	13.248(3)	10.5669(17)	16.492(2)
90	111.862(4)	117.517(2)	90
97.2940(10)	107.198(4)	95.800(2)	103.942(2)
90	93.619(4)	99.945(2)	90
4	2	2	4
1942.0(2)	1067.1(4)	900.2(3)	1826.2(4)
1.295	1.310	1.293	1.405
800	442	368	800
0.186	0.297	0.195	0.214
1.958 to 52.06	1.862 to 56.78	1.988 to 52.04	1.998 to 46.58
-10 to 10	-10 to 10	-12 to 12	-13 to 13
-49 to 46	-15 to 15	-12 to 12	-10 to 10
-7 to 7	-17 to 17	-13 to 13	-18 to 18
14231	12442	9463	17136
3757	4985	3528	2632
3418	4152	2949	2275
0.0464	0.0579	0.0524	0.0334
0.1128	0.1385	0.1320	0.0855
1.135	1.028	1.030	1.048

Table 1. *Continued...*

Chapter 5			
9	**9•** benzene	**10**	**10•**benzene
$C_{20}H_{16}Cl_2N_2O_2S$	$(C_{20}H_{16}Cl_2N_2O_2S)\cdot$ $(C_6H_6)_{0.5}$	$C_{20}H_{16}Br_2N_2O_2S$	$(C_{20}H_{16}Br_2N_2O_2S)\cdot$ $(C_6H_6)_{0.5}$
419.31	458.36	508.23	547.28
monoclinic	triclinic	orthorhombic	triclinic
*C*2/*c*	$P\bar{1}$	*Pbca*	$P\bar{1}$
100(2)	298(2)	100(2)	298(2)
22.4996(17)	7.9816(16)	11.4666(7)	8.0184(8)
11.4602(7)	11.793(2)	15.5694(9)	11.9872(12)
15.4310(9)	13.501(3)	22.2113(13)	13.5855(13)
90	112.409(3)	90.00	112.826(2)
102.552(2)	106.616(3)	90.00	106.592(2)
90	93.815(3)	90.00	93.964(2)
8	2	8	2
3883.8(4)	1103.5(4)	3965.3(4)	1129.26(19)
1.434	1.380	1.703	1.610
1728	474	546	546
0.460	0.411	3.704	3.704
1.998 to 52.1	1.984 to 52.74	1.988 to 52.06	1.988 to 52.06
-27 to 27	-9 to 9	-9 to 9	-9 to 9
-14 to 14	-14 to 14	-14 to 14	-14 to 14
-19 to 19	-16 to 16	-16 to 16	-16 to 16
19751	11810	11845	11845
3843	4464	4429	4429
3665	3567	3156	3156
0.0317	0.0418	0.0241	0.0391
0.0833	0.1080	0.0589	0.0899
1.057	1.023	1.031	1.030

Appendix IV

Table 1. 93 refcodes of polymorphs with OH/NH functional groups present in the molecule but no strong hydrogen bonds in the crystal structure.

ABEFUJ	CPAHYD01	HAXHET	QQQAXJ01	TOAZOC
ABEFUJ01	DAKXUI	HAXHET01	QQQBVP02	TOAZOC01
AKOVOL	DAWMAP	HORCAS01	SACRET	TOAZOC03
AKOVOL01	DAWMAP01	IMCYLP10	SIFLOI	TPHPOR04
AKOVOL02	DBEZLM	JAWXEK	SIFLOI01	**UCUGOP**
AKOVOL03	DBEZLM01	JEFDON	SIFLOI02	VENTUD
ASEHUB	DBEZLM02	**KUVWON**	TAQCET	VENTUD01
ASEHUB01	DBEZLM04	LANXOO02	TAQCET01	VUSFIY
ATIWOP01	DBEZLM05	LECROB	TEBETU03	VUSFIY01
BTUPTE	DPENAM	LECROB01	THIOUR	**WEFKEY01**
BTUPTE01	DPENAM01	**MAMGUD**	THIOUR03	WULZIM
CASHOT	DPENAM02	MBPHOL01	THIOUR04	YEPHAC
CASHOT01	DUVFUV03	MBPHOL02	THIOUR05	YEPHAC01
CASHOT02	FAJTIT	MBPHOL10	THIOUR08	ZEYBIO
CASHOT03	FAJTIT01	MBPHOL11	THIOUR09	ZEYBIO01
CEBKEZ01	FEFQUD01	MBPHOL12	THIOUR10	ZZZHUW02
CEMDON	GEGGEF	MPYZBD02	THIOUR11	ZZZPLY02
CEMDON01	GEGGEF01	NAJDOS	THIOUR13	
CPAHYD	GEHXEX	PIVIND10	THIOUR14	

Appendix V
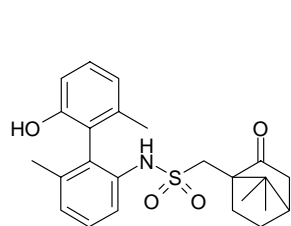
AJALIG
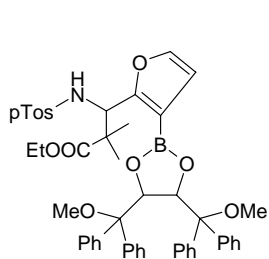
AYEQEA
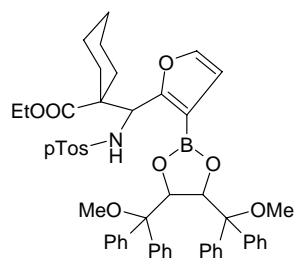
AYEQIE
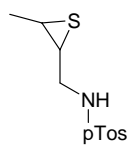
CAZCUC
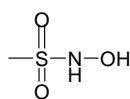
DIRMIA
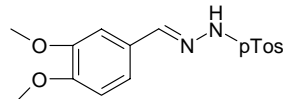
FAKTEQ
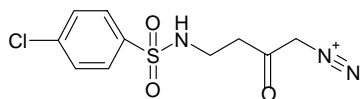
FAYMEX
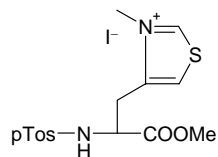
FEPGUD
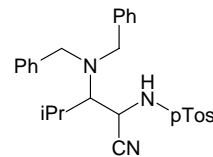
HEHLIP
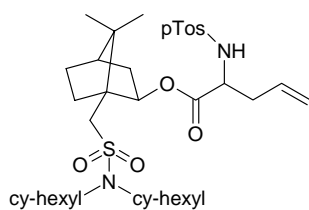
HUKXOA
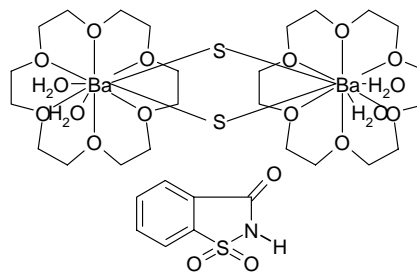
IHEJEK
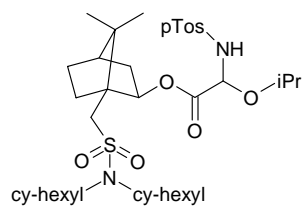
JACWAM
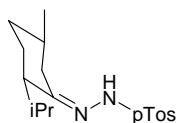
JUNLIN
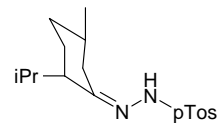
JUNLOT
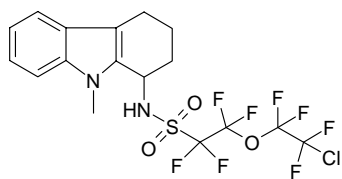
LAXCAP
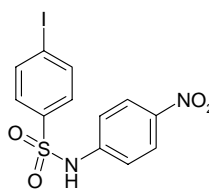
MEZGIH
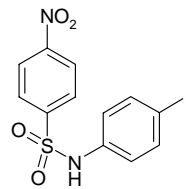
MEZGON
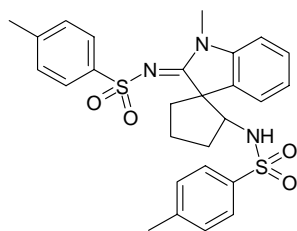
MTSAIN
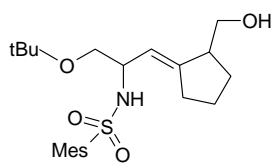
MUBLEA
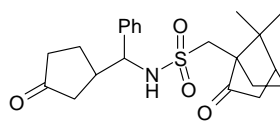
NOVYAY

ODASAO

QUBTOW

SIZLUI

TADMAN

TOFPOT

VATREO

XOGDIG

XOPVED
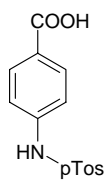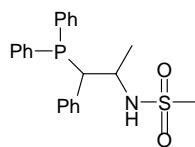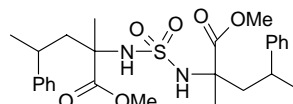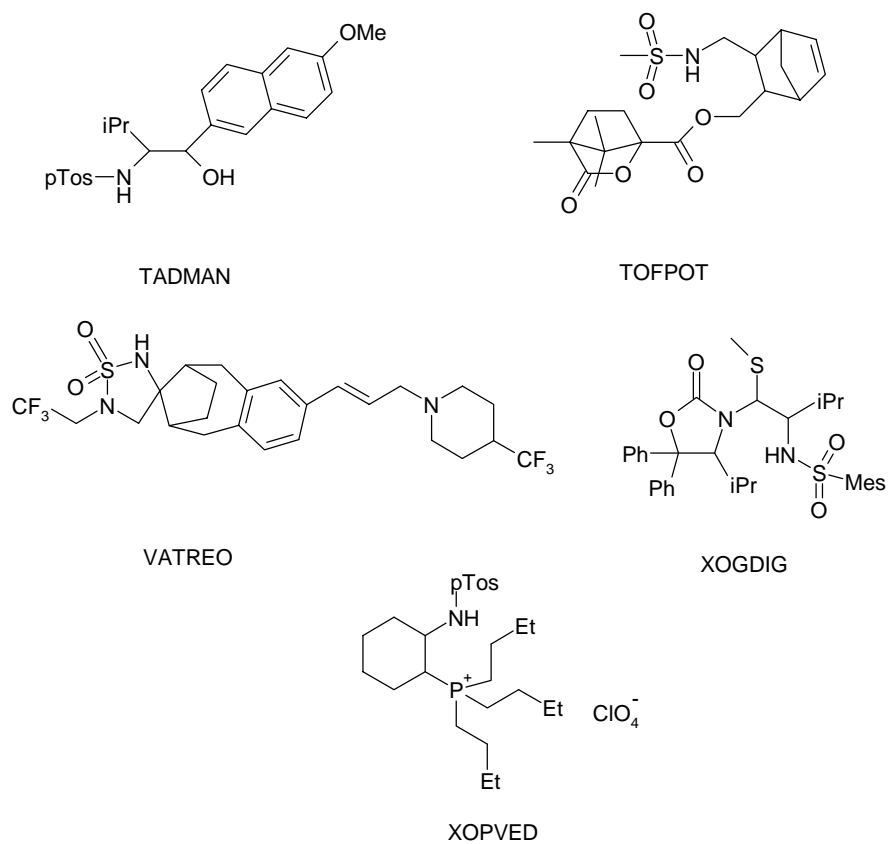
Scheme 1. CSD refcodes of 28 sulfonamide crystal structures (N–H proton located) with no strong N–H···O/N/X⁻ hydrogen bond (> 2.5 Å).

Appendix VI

Table 1: 60 predicted frames of crystal structures **6 (Form 1)** simulated using rigid body minimization in six common space groups (*Cerius*[2], COMPASS force field, normalized to per molecule of **6**).

Frame no	Lattice energy [kcal mol^{-1}]	Net volume [Å^3]	Cell Dimension [Å, °]	N-H…O Bond Dimer/ catemer
			P2$_1$/c	
1	−37.801	477.64	9.697, 12.125, 17.292, 69.88	No H bond
2	−37.470	486.94	13.503, 7.499, 19.239, 89.06	No H bond
3	−37.343	488.87	11.798, 25.784, 6.438, 89.53	No H bond
4	−37.200	495.39	29.695, 10.805, 6.554, 70.43	No H bond
5	−36.723	498.61	12.805, 17.082, 10.498, 119.71	No H bond
6	−36.688	497.72	6.689, 19.549, 15.265, 103.78	No H bond
7	−36.665	488.04	21.725, 9.485, 9.952, 103.73	No H bond
8	−36.588	494.70	9.870, 11.117, 19.584, 67.05	No H bond
9	−36.471	499.75	8.849, 17.713, 12.793, 94.51	No H bond
10	−36.455	485.25	5.640, 30.354, 11.974, 71.22	No H bond
			C2/c	
1	**−41.134**	**467.39**	**21.605, 11.734, 15.027, 101.01**	**Dimer**
2	−38.849	478.36	13.526, 7.532, 42.501, 117.89	No H bond
3	−38.176	481.99	13.520, 7.494, 42.536, 63.47	No H bond
4	−37.389	496.86	23.565, 7.096, 23.996, 97.75	Catemer
5	−37.256	487.46	16.617, 6.514, 40.644, 62.43	No H bond
6	−37.085	493.34	11.631, 13.778, 27.056, 65.56	No H bond
7	−36.445	497.33	23.590, 7.097, 27.934, 96.82	Dimer
8	−36.403	491.55	16.733, 6.516, 39.024, 112.47	No H bond
9	−36.207	505.81	30.770, 7.449, 17.895, 99.42	No H bond
10	−36.137	493.46	22.776, 5.643, 32.032, 105.48	No H bond
			P$\bar{1}$	
1	−40.637	462.50	6.501, 19.257, 8.025, 111.87, 94.10, 93.98	No H bond
2	−38.374	489.55	14.998, 12.328, 6.567, 63.47, 64.51, 76.18	Dimer
3	−38.088	480.56	9.266, 10.166, 11.804, 100.72, 99.68, 113.93	No H bond
4	−38.074	491.97	6.495, 13.725, 13.014, 113.93, 109.64, 90.63	Dimer

5	−38.037	475.22	18.916, 11.137, 5.432, 60.34, 74.14, 76.64	No H bond
6	−37.838	480.53	11.153, 8.625, 11.848, 76.76, 68.65, 83.84	No H bond
7	−37.827	487.29	20.535, 7.557, 6.876, 83.15, 75.13, 71.17	No H bond
8	−37.641	476.16	9.282, 11.722, 10.224, 68.18, 84.81, 67.38	No H bond
9	−37.611	491.49	12.586, 14.141, 6.742, 68.27, 67.32, 66.71	No H bond
10	−37.406	489.88	6.790, 13.233, 12.181, 91.686, 100.32, 113.69	No H bond
			Pbca	
1	−39.690	480.39	15.139, 21.712, 11.693	Dimer
2	−36.927	491.13	19.308, 21.356, 9.529	No H bond
3	−36.720	495.70	23.070, 7.707, 22.303	No H bond
4	−36.445	487.88	21.687, 11.926, 15.090	No H bond
5	−36.172	488.26	12.129, 9.607, 33.524	No H bond
6	−36.153	506.03	5.536, 33.674, 21.716	No H bond
7	−35.826	501.52	17.825, 9.324, 24141	No H bond
8	−35.531	509.96	19.778, 18.636, 11.437	No H bond
9	−35.264	500.64	11.831, 22.475, 15.063	No H bond
			$P2_12_12_1$	
10	−35.975	516.20	18.858, 13.040, 16.794	No H bond
1	−37.528	495.50	6.615, 10.986, 27.272	No H bond
2	−37.349	492.27	5.579, 11.920, 29.612	No H bond
3	−36.802	491.29	29.731, 5.526, 11.960	No H bond
4	−36.696	494.05	9.798, 16.837, 11.979	No H bond
5	−36.552	486.10	11.340, 7.858, 21.819	No H bond
6	−36.018	495.69	5.502, 16.526, 21.807	No H bond
7	−35.819	492.46	14.953, 10.038, 13.124	No H bond
8	−35.422	498.82	13.330, 19.208, 7.793	No H bond
9	−35.194	491.50	11.098, 13.571, 13.054	No H bond
10	−35.052	508.91	11.300, 20.101, 8.962	No H bond
			$P2_1$	
1	−38.015	484.28	5.547, 11.965, 14.596, 91.23	No H bond
2	−37.373	491.25	14.568, 10.712, 6.605, 72.40	No H bond
3	−36.704	497.62	10.752, 6.543, 14.148, 90.58	No H bond
4	−36.344	496.17	17.009, 5.485, 11.456, 68.20	No H bond
5	−36.198	499.90	10.023, 9.509, 10.621, 99.01	No H bond
6	−36.098	501.36	15.061, 5.602, 15.569, 90.27	No H bond
7	−36.094	501.11	11.882, 5.601, 15.659, 89.09	No H bond
8	−35.896	499.71	12.058, 5.488, 15.389, 78.92	No H bond

| 9 | −35.072 | 509.31 | 11.856, 9.952, 9.260, 68.79 | No H bond |
| 10 | −35.039 | 512.83 | 11.937, 9.985, 9.234, 68.74 | No H bond |

Table 1: 60 predicted frames of crystal structures **6 (Form 2)** simulated using rigid body minimization in six common space groups (*Cerius*[2], COMPASS force field, normalized to per molecule of **6**).

Frame no	Lattice energy [kcal mol^{-1}]	Net volume [Å^3]	Cell Dimension [Å, °]	N-H…O Bond
			P2$_1$/c	
1	−41.716	467.01	10.836, 36.943, 4.851, 74.14	No H bond
2	−40.235	468.23	6.469, 20.820, 14.211, 78.10	No H bond
3	−40.173	482.75	5.917, 40.614, 8.095, 96.96	No H bond
4	−40.040	473.07	26.400, 4.778, 16175, 111.969	No H bond
5	−39.167	485.21	5.950, 41.428, 7.942, 82.49	No H bond
6	−39.118	488.15	5.978, 40.530, 8.123, 97.48	No H bond
7	−39.099	474.43	26.471, 16.679, 4.854, 117.69	No H bond
8	−39.033	473.04	25.113, 4.828, 17.126, 114.32	No H bond
9	−38.966	476.61	5.181, 22.155, 17.194, 104.99	No H bond
10	−38.952	478.18	7.953, 17.515, 14.070, 77.41	No H bond
			C2/c	
1	**−41.716**	**467.05**	**42.328, 7.846, 11.874, 71.37**	**No H bond**
2	−40.235	480.83	30.577, 5.878, 21.922, 77.50	No H bond
3	−40.173	465.06	36.923, 4.768, 21.168, 93.34	No H bond
4	−40.050	468.15	36.617, 4.813, 21.273, 87.86	No H bond
5	−39.167	474.23	27.263, 4.774, 31.327, 111.50	No H bond
6	−39.118	475.89	37.422, 4.813, 21.150, 88.15	No H bond

7	−39.099	475.95	9.836, 12.111, 34.884, 113.61	No H bond
8	−39.033	483.72	43.853, 5.396, 16.933, 74.96	No H bond
9	−38.966	485.73	16.865, 5.405, 44.986, 108.63	No H bond
10	−38.952	485.53	16.885, 5.400, 44.388, 106.34	No H bond

$P\bar{1}$

1	−41.056	476.22	6.027, 21.397, 7.932, 102.70, 97.33, 103.60	No H bond
2	−40.531	464.36	7.521, 14.419, 8.843, 95.71, 102.59, 92.91	No H bond
3	−40.506	464.59	16.378, 4.799, 13.543, 98.51, 109.00, 105.50	No H bond
4	−40.100	472.14	13.551, 4.796, 17.163, 107.33, 97.47, 112.63	No H bond
5	−40.057	482.22	23.157, 7.930, 6.080, 82.91, 70.82, 60.05	No H bond
6	−40.051	466.14	7.575, 11.439, 11.936, 101.69, 110.08, 96.46	No H bond
7	−40.023	474.20	5.018, 13.284, 16.492, 67.61, 69.42, 78.14	No H bond
8	−40.016	468.57	4.789, 10.822, 18.521, 86.12, 86.19, 78.52	No H bond
9	−39.994	471.45	7.820, 13.098, 9.886, 74.02, 80.48, 77.05	No H bond
10	−39.898	472.85	16.364, 4.829, 14.046, 92.01, 107.16, 114.89	No H bond

Pbca

1	−40.078	476.11	6.053, 16.372, 38.432	No H bond
2	−39.746	479.02	23.101, 10.955, 15.142	No H bond
3	−39.261	483.13	16.620, 41.452, 5.610	No H bond
4	−38.668	477.92	7.639, 36.179, 13.835	No H bond
5	−38.561	478.12	37.480, 12.850, 7.941	No H bond
6	−38.399	482.72	36.010, 13.991, 7.665	No H bond
7	−38.147	489.03	19.213, 25.634, 7.913	No H bond
8	−37.595	496.22	12.906, 37.751, 8.025	No H bond
9	−37.500	486.41	10.643, 41.204, 8.873	No H bond
10	−37.488	487.00	16.582, 15.417, 15.240	No H bond

$P2_12_12_1$

1	−39.416	481.05	5.055, 13.508, 28.225	No H bond
2	−38.017	482.27	19.562, 4.801, 20.541	No H bond

3	−36.673	515.28	15.698, 22.185, 5.921	No H bond
4	−36.653	502.75	15.347, 13.004, 10.077	No H bond
5	−36.510	510.60	19.164, 22.039, 4.836	No H bond
6	−36.509	510.79	19.161, 22.026, 4.841	No H bond
7	−36.495	487.10	13.148, 18.992, 7.803	No H bond
8	−36.283	498.79	19.062, 21.832, 4.794	No H bond
9	−36.239	498.55	12.820, 4.907, 31.700	No H bond
10	−36.053	514.50	7.046, 13.395, 21.807	No H bond
			$P2_1$	
1	−40.243	473.47	16.843, 12.184, 4.871, 108.72	No H bond
2	−39.863	478.78	13.587, 5.031, 14.738, 71.87	No H bond
3	−39.383	478.96	12.261, 4.888, 15.997, 92.29	No H bond
4	−38.195	490.04	21.268, 8.653, 6.310, 65.01	No H bond
5	−37.308	492.17	11.251, 19.720, 4.774, 111.68	No H bond
6	−37.307	492.29	10.449, 19.771, 4.773, 86.78	No H bond
7	−37.110	497.05	12.351, 4.858, 16.971, 77.49	No H bond
8	−36.380	491.72	10.809, 4.820, 18.899, 92.76	No H bond
9	−36.776	488.45	7.583, 12.523, 11.249, 66.09	No H bond
10	−36.772	500.62	18.879, 10.546, 5.116, 79.45	No H bond

Table 3: 60 predicted frames of crystal structures **6 (Form 3)** simulated using rigid body minimization in six common space groups (*Cerius*[2], COMPASS force field, normalized to per molecule of **6**).

Frame no	Lattice energy [kcal mol^{-1}]	Net volume [Å^3]	Cell Dimension [Å, °]	N-H…O Bond
			$P2_1/c$	
1	**−42.770**	**462.20**	**8.070, 39.466, 5.836, 95.91**	**No H bond**
2	−42.385	467.86	8.049, 40.318, 5.793, 84.54	No H bond
3	−40.240	477.09	43.986, 8.362, 5.631, 112.88	No H bond

4	−40.237	476.84	40.934, 8.369, 5.624, 98.15	No H bond
5	−40.035	482.78	10.039, 20.881, 9.720, 108.62	No H bond
6	−39.200	480.82	13.761, 28.423, 5.121, 106,24	No H bond
7	−39.090	480.56	5.238, 16.205, 23.590, 73.75	No H bond
8	−39.076	479.96	5.215, 34.569, 11.226, 71.54	No H bond
9	−38.603	487.88	10.612, 32.259, 5.798, 79.48	No H bond
10	−38.405	495.90	29.985, 11.752, 6.037, 111.30	No H bond
			C2/c	
1	−40.896	470.72	39.970, 5.809, 16.500, 100.58	No H bond
2	−40.367	468.63	33.860, 11.623, 10.323, 113.57	No H bond
3	−40.289	473.58	30.682, 5.247, 24.584, 106.80	No H bond
4	−40.274	474.19	39.493, 7.984, 12.336, 102.78	No H bond
5	−39.171	477.03	35.752, 5.091, 20.992, 92.83	No H bond
6	−39.003	487.20	47.928, 5.659, 16.523, 119.58	No H bond
7	−38.542	498.19	21.132, 5.767, 33.387, 101.59	No H bond
8	−38.184	486.95	24.787, 5.154, 32.614, 110.78	No H bond
9	−38.184	485.17	30.223, 5.136, 25.305, 98.80	No H bond
10	−38.131	486.52	30.467, 5.126, 26.135, 107.52	No H bond
			$P\,\overline{1}$	
1	−44.535	459.44	21.301, 8.081, 5.787, 84.43, 83.70, 66.60	No H bond
2	−43.575	459.41	19.778, 8.032, 5.887, 95.75, 97.01, 94.94	No H bond
3	−43.160	460.35	7.991, 20.294, 5.918, 80.33, 84.25, 77.20	No H bond
4	−43.060	460.14	8.057, 22.421, 5.837, 116.12, 95.84, 98.33	No H bond
5	−42.921	463.96	8.041, 20.497, 5.815,	No H bond

			88.869, 84.32, 76.63	
6	−40.564	471.94	5.854, 17.139, 11.231, 70.78, 70.93, 65.44	No H bond
7	−40.187	475.69	5.801, 10.784, 16.381, 103.87, 99.77, 100.99	No H bond
8	−39.859	481.98	6.025, 15.929, 11.241, 80.17, 75.08, 68.13	No H bond
9	−39.752	479.13	5.855, 13.671, 13.340, 89.98, 64.62, 84.01	No H bond
10	−39.519	474.98	13.750, 17.11, 5.150, 104.46, 112.00, 110.12	No H bond
			Pbca	
1	−39.201	480.91	12.500, 38.880, 7.917	No H bond
2	−38.615	490.71	20.901, 16.991, 11.054	No H bond
3	−37.948	483.42	39.773, 9.352, 10.397	No H bond
4	−37.888	507.65	21.188, 32.722, 5.858	No H bond
5	−37.027	492.42	35.206, 12.840, 8.714	No H bond
6	−36.963	489.55	40.123, 9.364, 10.423	No H bond
7	−36.635	489.80	16.850, 17.399, 13.366	No H bond
8	−36.409	485.85	16.933, 11.047, 20.778	No H bond
9	−36.318	497.41	11.586, 34.121, 10.650	No H bond
10	−36.029	500.23	10.471, 10.894, 35.080	No H bond
			$P2_12_12_1$	
1	−40.269	484.59	10.146, 5.980, 8.074	No H bond
2	−38.542	494.70	41.645, 5.849, 8.124	No H bond
3	−37.294	500.04	5.234, 12.631, 30.255	No H bond
4	−36.989	517.34	8.550, 11.583, 19.646	No H bond
5	−36.893	490.39	18.215, 20.693, 5.204	No H bond
6	−36.443	502.16	17.580, 21.768, 5.249	No H bond
7	−36.357	517.34	16.017, 5.910, 21.859	No H bond
8	−36.319	503.89	11.886, 6.6621, 25.609	No H bond
9	−36.304	498.61	20.169, 9.294, 10.639	No H bond
10	−35.831	512.83	18.508, 5.128, 21.613	No H bond
			$P2_1$	
1	−41.501	470.75	8.207, 5.710, 20.392, 99.89	No H bond
2	−38.332	489.88	16.262, 12.388, 5.259, 112.35	No H bond
3	−37.481	503.94	16.749, 5.775, 11.376, 113.65	No H bond
4	−36.301	515.16	15.510, 5.786, 11.567, 97.02	No H bond
5	−35.854	511.11	5.150, 19.693, 10.464, 74.43	No H bond

6	−35.387	510.30	10.572, 11.408, 8.648, 78.13	No H bond
7	−34.991	532.23	14.894, 10.118, 7.812, 115.27	No H bond
8	−34.980	517.95	5.327, 10.717, 18.709, 75.91	No H bond
9	−34.975	517.73	18.689, 10.717, 5.328, 103.99	No H bond
10	−34.895	513.52	12.287, 8.384, 10.038, 83.37	No H bond

Appendix VII

Table 1. Ten lowest energy predicted structures of tolyl molecule **6** in six common space groups.

Frame No.	Lattice energy (kcal mol^{-1})	Net volume (Å^3)	N–H···O bonding	H bond energy (kcal mol^{-1})
		P2$_1$/c		
1	26.857	506.07	No H bond	0.000
2	27.645	510.59	No H bond	0.000
3	27.747	523.30	Dimer	–2.740
4	27.880	511.71	No H bond	0.000
5	28.202	512.37	No H bond	0.000
6	28.204	525.96	Dimer	–2.417
7	28.380	528.04	No H bond	0.000
8	28.657	522.94	No H bond	0.000
9	28.899	524.40	No H bond	0.000
10	29.009	536.70	No H bond	0.000
		P $\bar{1}$		
1	23.864	503.53	Dimer	–2.460
2	26.847	499.19	No H bond	0.000
3	26.888	513.48	No H bond	0.000
4	26.892	511.58	Dimer	–2.731
5	26.997	511.99	Dimer	2.814
6	27.216	499.48	No H bond	0.000
7	27.286	511.26	Dimer	–2.729
8	27.374	501.29	No H bond	0.000
9	27.544	508.81	No H bond	0.000
10	27.576	510.86	No H bond	0.000
		P2$_1$2$_1$2$_1$		
1	27.785	516.42	No H bond	0.000
2	27.887	518.86	No H bond	0.000
3	28.244	523.13	No H bond	0.000
4	28.657	524.24	No H bond	0.000
5	28.707	537.77	No H bond	0.000
6	28.722	522.98	No H bond	0.000
7	28.932	508.80	No H bond	0.000
8	29.057	522.32	No H bond	0.000
9	29.075	513.81	No H bond	0.000
10	29.081	528.22	No H bond	0.000
		P2$_1$		
1	28.278	514.36	No H bond	0.000

2	28.456	526.03	No H bond	0.000
3	30.133	514.54	No H bond	0.000
4	30.237	522.27	No H bond	0.000
5	30.376	523.18	No H bond	0.000
6	30.787	538.43	No H bond	0.000
7	30.807	548.54	No H bond	0.000
8	31.653	533.19	No H bond	0.000
9	31.782	523.92	No H bond	0.000
10	31.807	551.57	No H bond	–0.001
		*C*2/*c*		
1	26.337	504.84	No H bond	0.000
2	28.338	525.80	No H bond	0.000
3	29.031	514.45	Dimer	–2.111
4	29.165	525.97	No H bond	0.000
5	29.250	520.23	No H bond	0.000
6	29.268	529.48	Dimer	–3.006
7	29.480	518.90	No H bond	0.000
8	29.576	522.79	Dimer	–2.505
9	29.717	525.06	No H bond	0.000
10	29.753	525.71	Dimer	–2.875
		Pbca		
1	28.166	514.99	No H bond	0.000
2	29.197	532.97	No H bond	0.000
3	29.357	527.16	No H bond	0.000
4	29.505	508.47	No H bond	0.000
5	29.804	511.11	No H bond	0.000
6	29.876	521.05	Dimer	–2.667
7	30.110	539.11	No H bond	0.000
8	30.530	519.40	No H bond	0.000
9	30.612	539.98	No H bond	0.000
10	30.666	525.34	No H bond	0.000

Table 2. Ten lowest energy predicted structures of acetone tosyl hydrazone molecule in six common space groups.

Frame No.	Lattice energy (kcal mol^{-1})	Net volume (Å^3)	N–H···O bonding	H bond energy (kcal mol^{-1})
		*P*2$_1$/*c*		
1	–30.222	286.86	Dimer	–3.086
2	–30.704	308.89	Dimer	–2.653
3	–29.489	300.64	Dimer	–2.180
4	–29.311	307.07	Dimer	–3.184
5	–29.008	305.84	Dimer	–2.547

6	–28.785	311.88	Dimer	–3.107
7	–28.679	295.16	Catemer	–2.189
8	–28.573	298.15	Catemer	–2.743
9	–28.512	299.86	Catemer	–2.252
10	–28.491	316.98	Dimer	–2.845
		$P\bar{1}$		
1	–31.468	286.10	Dimer	–2.841
2	–31.186	298.57	Dimer	–2.959
3	–31.009	295.10	Dimer	–2.916
4	–30.563	296.96	Dimer	–2.614
5	–30.438	291.55	Dimer	–2.996
6	–30.402	297.16	Dimer	–3.096
7	–30.362	297.30	Dimer	–3.054
8	–30.119	297.53	Dimer	–2.467
9	–29.765	302.16	Dimer	–3.161
10	–29.629	288.28	Dimer	–2.503
		$P2_12_12_1$		
1	–28.234	302.88	Catemer	–2.818
2	–27.905	299.25	Catemer	–2.719
3	–27.840	297.53	Catemer	–2.193
4	–27.598	297.50	Catemer	–2.349
5	–27.554	300.80	No H bond	0.000
6	–27.536	304.05	Catemer	–2.248
7	–27.486	300.18	Catemer	–2.603
8	–27.279	303.56	No H bond	0.000
9	–27.275	291.44	No H bond	0.000
10	–27.253	309.90	Catemer	–2.949
		$P2_1$		
1	–27.729	287.44	No Hbond	–0.296
2	–27.771	292.65	Catemer	–1.767
3	–27.730	297.21	No Hbond	–0.106
4	–27.222	302.83	No Hbond	0.000
5	–26.622	299.72	No Hbond	–0.272
6	–26.649	299.95	No Hbond	–0.159
7	–26.478	302.81	No Hbond	0.000
8	–26.421	294.55	No Hbond	–0.281
9	–26.281	298.21	Catemer	–1.801
10	–26.184	294.94	No Hbond	–0.242
		$C2/c$		
1	–29.953	302.63	Dimer	–3.158
2	–29.727	301.65	Dimer	–3.162
3	–29.594	290.01	Dimer	–2.697
4	–29.211	298.46	Dimer	–2.832

5	–29.191	301.29	Dimer	–2.395
6	–28.845	302.66	Dimer	–2.779
7	–28.558	307.12	Dimer	–3.052
8	–28.442	298.52	Dimer	–3.049
9	–28.426	297.13	Dimer	–2.745
10	–28.364	310.39	Dimer	–3.201
		Pbca		
1	–28.927	299.81	Dimer	–2.667
2	–28.886	300.91	Dimer	–2.894
3	–28.834	301.51	Catemer	–2.934
4	–28.360	297.94	Catemer	–2.877
5	–28.005	297.00	Catemer	–2.878
6	–27.794	303.89	Dimer	–2.750
7	–27.711	304.49	Catemer	–2.430
8	–27.558	298.90	Catemer	–2.824
9	–27.460	313.40	Dimer	–2.875
10	–27.303	297.45	Catemer	–1.637

Table 3. Ten lowest energy predicted structures of sulphathizole in six common space groups.

Frame No.	Lattice energy (kcal mol^{-1})	Net volume (Å^3)	N–H···O/ N–H···N bonding	H bond energy (kcal mol^{-1})
		P2$_1$/c		
1	–46.750	294.80	Present	–9.437
2	–46.628	286.47	Present	–7.600
3	–46.419	289.74	Present	–7.122
4	–45.607	287.13	Present	–7.755
5	–45.304	289.25	Present	–7.228
6	–45.239	305.87	Present	–9.384
7	–45.158	277.15	Present	–4.747
8	–44.241	285.59	Present	–5.844
9	–43.946	301.16	Present	–8.197
10	–43.939	299.57	Present	–8.190
		P-1		
1	–45.734	293.32	Present	–8.884
2	–45.505	297.73	Present	–9.861
3	–45.374	291.59	Present	–8.685
4	–45.270	281.33	Present	–6.083
5	–45.263	301.24	Present	–7.940
6	–45.233	277.44	Present	–5.596

7	–45.086	283.99	Present	–7.091
8	–45.026	293.78	Present	–8.205
9	–44.922	282.44	Present	–6.512
10	–44.921	294.81	Present	–8.757
		$P2_12_12_1$		
1	–46.543	295.62	Present	–9.454
2	–45.721	298.28	Present	–9.685
3	–45.345	298.91	Present	–8.980
4	-45.161	304.62	Present	–10.579
5	–44.598	302.03	Present	–6.850
6	–44.581	290.04	Present	–6.176
7	-44.441	297.25	Present	–7.272
8	–44.259	286.81	Present	–4.358
9	–44.236	288.72	Present	–8.287
10	–43.890	284.95	Present	–6.578
		$P2_1$		
1	–47.648	290.22	Present	–10.339
2	–46.840	290.54	Present	–9.493
3	–46.604	286.79	Present	–6.924
4	–46.487	281.43	Present	–7.273
5	–46.397	301.41	Present	–9.773
6	–45.943	290.90	Present	–7.106
7	–45.533	291.95	Present	–9.104
8	–45.141	291.86	Present	–6.817
9	–44.733	284.71	Present	–5.766
10	–44.390	309.68	Present	–9.438
		$C2/c$		
1	–46.849	285.56	Present	–8.298
2	–46.123	285.62	Present	–7.027
3	–45.711	290.28	Present	–6.781
4	–45.698	289.89	Present	–8.536
5	–45.550	291.44	Present	–9.276
6	–45.100	289.43	Present	–7.395
7	–44.905	286.50	Present	–6.946
8	–44.860	285.99	Present	–7.340
9	–44.852	282.24	Present	–7.851
10	–44.625	292.08	Present	–6.667
		Pbca		
1	–45.587	286.66	Present	–7.374
2	–45.026	306.91	Present	–9.470
3	–44.723	304.31	Present	–8.922
4	–44.586	310.76	Present	–7.763
5	–44.278	318.51	Present	–8.853

6	–44.133	283.13	Present	–5.697
7	–44.080	284.81	Present	–4.453
8	–43.985	299.01	Present	–8.511
9	–43.907	291.74	Present	–8.036
10	–43.815	282.05	Present	–4.771

ABOUT THE AUTHOR

Saikat Roy, son of Shyam Sundar Roy and Sabita Roy, was born in Durgapur, a town in Burdwan District of West Bengal, India in 1978. He received his elementary and secondary school education in Gopalmath and Andal High School. After the completion of BSc. And MSc. from Triveni Devi Bhalotia college and Burdwan University, he joined the School of Chemistry, University of Hyderabad for his PhD degree in 2002. He is recipient of UGC-NET fellowship from 2002-2007 (JRF-SRF).

List of Publications

1. Thermochemical analysis of Venlafaxine hydrochloride polymorphs 1-5.
   S. Roy, S. Aitipamula and A. Nangia.
   Cryst. Growth Des., **2005**,*5*, 2268-2276.

2. Conformational, Concomitant Polymorphs of 4,4-Diphenyl-2,5-cyclohexadienone: Conformation and Lattice Energy Compensation in the Kinetic and Thermodynamic Forms.
   S. Roy, R. Banerjee, A. Nangia and G. J. Kruger
   Chem. Eur. J., **2006**, *12*, 3777-3788.

3. Polymorphs of 1,1-bis(4-hydroxyphenyl)cyclohexane and multiple *Z'* crystal structures by melt and sublimation crystallization.
   B. Sarma, **S. Roy** and A. Nangia
   Chem. Commun., **2006,** 4918-4920.

4. Stable Polymorph of Venlafaxine Hydrochloride by Solid-to-Solid Phase Transition at High Temperature.
   S. Roy, P. M. Bhatt, A. Nangia and G. J. Kruger
   Cryst. Growth Des., **2007**, *7*, 476-480.

5. Coupled Thermal Gravimetric and Infrared Spectroscopic Analysis (TG-IR) in Polymorph Charecterization.
   S. Roy, B. Sarma and A. Nangia
   Mettler Toledo Thermal Analysis Newsletter, **2007** (in press).

6. The Curtin–Hammett Principle in Crystallization. Kinetic and Thermodynamic Conformational Polymorphs of bis(*p*-Tolyl)ketone *p*-Tosylhydrazone.
   S. Roy and A. Nangia
   Cryst. Growth Des., **2007**, (In print).

7. Conformational polymorph of 2,6-Dimethyl Fuchsone. Revisited.
   S. Roy, P. M. Bhatt, S. K. Chandran, A. Nangia and G. J. Kruger
   (manuscript under preparation)

8. Modulated Structure of 2,4,6-Tris(2-Bromo-3-Pyridinoxy)-1,3,5-Triazine.
   B. K. Saha, **S. Roy** and A. Nangia
   (manuscript under preparation)